A Molecular Mechanism to Regulate Lysosome Motility for Lysosome Positioning and Tubulation

by

Xinran Li

A dissertation submitted in partial fulfillment
of the requirements for the degree of
Doctor of Philosophy
(Molecular, Cellular, and Developmental Biology)
in the University of Michigan
2016

Doctoral Committee:

Associate Professor Haoxing Xu, Chair
Professor Robert Fuller
Professor Richard Hume
Professor Kristen Verhey
Associate Professor Yanzhuang Wang

“When you have eliminated the impossible, whatever remains, however improbable, must be the truth”

-Sherlock Holmes, “The Sign of the Four” (1890)

To my family
For their love, support, and encouragement

Acknowledgements

A lot of people have helped me through this four-and-half year Ph.D. study, without their help it would not be possible to finish all the work I have completed over this period. I would like to take this opportunity to express my appreciation to them.

First of all, I would like to thank my Ph.D. advisor, Dr. Haoxing Xu. About six and half years ago, Dr. Xu offered me the opportunity to work in his lab as a full time technician, and later lab manager, despite my low GPA from my undergraduate courses. This offer gave me a unique opportunity to be exposed to high-end research in a first-class U.S. university. Later on, Dr. Xu also gave me full support during my application for the Ph.D. program, which was really a crucial factor to my being admitted as a Ph.D. student here. Dr. Xu also helped me along the whole time I spent here, both as a scientific mentor that provides professional and inspiring instructions and advice, and as an experienced wise man who provided me lots of useful information and experiences on career and personal choices. The freedom he gave me and the trust he put on me are also important components towards the fulfillment of my research projects described in this thesis. In summary, I deeply feel fortunate to have Dr. Xu as my Ph.D. mentor.

I would also like to thank my thesis committee members, Dr. Robert Fuller, Dr. Richard Hume, Dr. Kristen Verhey and Dr. Yanzhuang Wang, for their generous help on my thesis project and their invaluable advice and suggestions along the progress of my thesis. Dr. Robert Fuller is an expert on protein trafficking and provided helpful comments about the caveats of my thesis project. Also the Membrane Trafficking Club that he organized was a unique opportunity

for me to get insights in the many aspects of intracellular membrane trafficking from the many great labs in the University of Michigan. Dr. Richard Hume, being the professor working closest to my lab (physically), is the single professor me and my lab-mates sought most help from when we are in need of equipment, reagents, or advice. Dr. Hume also provided great suggestions during the preparation of both manuscripts presented in this thesis. Dr. Kristen Verhey is a real expert on motor proteins, and without her the data I obtained shown in Chapters II and III would not be possible. I am also grateful to her for generously sharing her reagents and constructs about motor proteins that were key to the completion of the project. Dr. Yanzhuang Wang is one of the keenest scientists that I have ever met, providing crucial comments that vastly improved the quality of my manuscript. Dr. Wang's lab also helped my project a lot by providing reagents and experiences on cell culture, cell lines, and antibodies.

I would take this opportunity to thank Mary Carr, the graduate coordinator of our department. She has been a great helper in every aspect of the graduate life, and she is forever so patient and so helpful for the so many troublesome matters that we seek help from her.

I also owe my thanks to my colleagues in the Xu lab, although some of them have already moved on to the next stop in their careers. The first people I met in the United States the day I arrived are Dongbiao Shen and Xiang Wang, two former graduate students of the Xu lab. Dongbiao and Xiang helped me a lot, both personally and scientifically. My first two years of stay in the U.S. relied heavily on their help in a lot of things e.g. finding a living place and getting driver's license. They are now working in California and I wish them bright futures. Dr. Xianping Dong and Dr. Xiping Cheng are two senior postdocs that were in the lab when I arrived. They were the two most experienced members in the lab and were invaluable along my way of maturation into a scientist. Xianping is now a faculty at Dalhousie University in Canada and

Xiping took a position in Regeneron Pharmaceuticals. Mohammad Samie is a former Ph.D. student in the lab that joined the lab just a week ahead of me. He was really talented in many things, and his amiable personality and willingness to help people were greatly appreciated by me and all other lab members. He took a postdoc position at Yale after graduation from the Xu lab. Abigail G. Garrity is also a former Ph.D. student who cooperated with me in my first author review paper published on Journal of Physiology in 2013. She took a position at a consulting company.

Brian Eisinger, Andrew Goschka, Nick Rydzewski, Tony Zhuo, and Megan Lemorie are past lab managers that have supported the progress of the project by maintaining the lab in good conditions. Mingkun Zhao, Dmitry Davydov, Cyrus Tsang, and Kathy Dong are former undergraduates that participated in my projects by doing experiments and data analysis. I deeply appreciate their help.

The current lab members have also helped me a lot. Dr. Xiaoli Zhang is a postdoc joined the lab half a year after me. She cooperated with me all the way along with her expertise in electrophysiology. Dr. Wuyang Wang and Dr. Nirakar Sahoo are great colleagues to work with and provided a lot of comments and suggestions in lab meetings to help improve my projects. I especially thank Nirakar for his company as a golfing friend that hangs out with me to play golf despite his difficult financial situations.

I would like to give my special thanks to Qiong Gao, a Ph.D. student joined the program at the same time as me. She is the person in the lab that is so warm-hearted and lively that makes the everyday dull experimental lab life full of cheering and joys. In my opinion she is the most indispensable member of the lab. I would also give my thanks to Lu Yu, a Ph.D. student in the

lab who is always considerate and eager to help others, and who can always provide great comments on anything we discuss. Additionally, I would like to thank Mingxue Gu and Zhangyuan Yin, although recently joined the lab, are helpful in providing comments and suggestions, and are great friends to hang out with.

I also owe debt to a wonderful undergraduate in the lab, Ahmad Hider, who helped me with most of the data analysis in the manuscript described in Chapters II and III. He has always been curious about the project and has been more than willing to work on the repetitive and dull part of the project, I really appreciate that.

I would like to give thanks to Junsheng Yang, a newly joined lab member that came from my hometown. He is very lively, cheering, and a great friend.

I would also like to thank my friends in Ann Arbor, they made my life here colorful and full of joy.

Lastly, my deepest gratitude goes to my family. They have provided me with their unconditional support and love throughout my life, and the best reason I can deal with all the frustrations and failures in researches is that I know there's always my family to back me up. I would like to thank my father, Bin, for his full support on my choice as a biology scientist despite his original wishes for me to inherit his career. I would like to thank my mother, Guifang, for her ever-present caring for me all through my life. Having said so, I feel like there is no way I can fully express my thanks to my parents without writing a whole book. Additionally, I would like to pay special thanks to my grandfather, who is currently in poor health. He has always been most proud of me and he had taught me so much in my early life. Long has he been looking

towards my graduation as a Doctor, and that is one of the strongest factors that has spurred me to conquer any obstacles I meet in my research and my life.

As always, it is hard to have included everyone deserving thanks in the acknowledgement, as our memories are limited. Therefore, I would like to give thanks to everyone who has helped me in the four and half years that I have missed.

Preface

I joined the Xu lab as a technician in August, 2009, and joined the Ph.D. program directly affiliated to the Xu lab in August, 2011. The data described in this thesis mainly belong to two manuscripts written during my stay at the Xu lab. Chapters II, III, IV are currently under re-submission at Nature Cell Biology, while Chapter V was published in *PNAS, 2013 Dec 24;110(52):21165-70.*

Contents presented in Chapter I (Introduction) partially originated from my first author review paper published in *Journal of Physiology. 2013 Sep 15;591(Pt 18):4389-401*. To be more specific, the main body of sections **1.1.1**, **1.1.2**, parts of the section **1.2.2**, and **Fig. 1.1**, **1.2** are derived from the paper. Abigail G. Garrity contributed to the writing of the paper concerning the small GTPases and the regulation of lysosome trafficking by Ca^{2+}. The other parts of the introduction are generated from my personal understandings about the field.

Contents presented in Chapters II, III, IV are from a manuscript currently (as of December, 2015) under re-submission at Nature Cell Biology with authors listed as Xinran Li, Nicholas Rydzewski, Ahmad Hider, Xiaoli Zhang, Junsheng Yang, Wuyang Wang, Qiong Gao, Xiping Cheng, and Haoxing Xu. All figures from these chapters, except **Fig. 4.3**, were included in the manuscript. **Fig. 4.3** consists of data obtained in the same study, but not included in the finalized manuscript. I designed and carried out most of the experiments. Electrophysiology recordings

were performed by Xiaoli Zhang and Wuyang Wang. Junsheng Yang performed parts of the Co-IP experiments, Qiong Gao performed parts of the western blot experiments. Nicholas Rydzewski and Xiping Cheng participated in the characterization and optimization of several control experiments, while Nicholas also participated in the initiation of the project. Ahmad Hider performed most of the analysis on lysosome distribution and filipin staining.

Contents in Chapter V are originated from the previously published paper "Genetically encoded fluorescent probe to visualize intracellular phosphatidylinositol 3,5-bisphosphate localization and dynamics" on PNAS, with authors listed as Xinran Li, Xiang Wang, Xiaoli Zhang, Mingkun Zhao, Wai Lok Tsang, Yangling Zhang, Richard Gar Wai Yau, Lois S. Weisman, and Haoxing Xu. Xiang Wang participated in the initiation of the project. Xiaoli Zhang carried out the electrophysiology recordings. Mingkun Zhao generated parts of the yeast data, which were not included in the thesis. Wai Lok Tsang participated in western blots and data analysis. Yanling Zhang generated **Fig. 5.4**, and Richard Gar Wai Yau generated parts of the yeast data. Lois Weisman and Haoxing Xu participated in the experiment design, data interpretation and manuscript preparation.

Table of Contents

List of Figures

Abstract

The lysosome is the degradation, recycling, and nutrient sensing center of animal cells. The importance of lysosomes has been shown from lysosomal storage diseases, which are marked with early onset neuron degeneration at the organism level and impaired lysosome functions at cellular level. Additionally, insufficient lysosomal clearance of toxic substances is thought to be one major contributing factor to aging-related diseases such as Alzheimer's disease. Therefore, understanding the pathways regulating lysosomal metabolism is of great importance.

Functions of lysosomes rely heavily on the membrane trafficking. Lysosomes travel directionally in cells to their destinations, where they undergo membrane fusion or membrane fission. The major aim of my doctoral work is to identify major pathways regulating lysosome membrane trafficking. I aimed to investigate regulators of the directional movement and the membrane fission of lysosomes, and identified TRPML1, a lysosomal cation channel, as a major regulator of both processes. I found that TRPML1 is responsible for the perinuclear accumulation of lysosomes under acute conditions such as autophagy induction and cytosolic alkalization. In this process, activation of TRPML1, which requires the lysosomal phosphoinositide $PI(3,5)P_2$, leads to the release of Ca^{2+} into the cytosol. This in turn recruits a Ca^{2+} effector protein, ALG-2, to the lysosomal membrane through its Ca^{2+}-dependent interaction with TRPML1. ALG-2 is associated with the dynactin complex, the adaptor for cytoplasmic dynein, and thus promotes microtubule minus-end directed motility of lysosomes.

My data also showed that hyper-activity and hypo-activity of TRPML1 both lead to the abolishment of lysosome tubulation, a process necessary for the lysosome membrane fission, and suggested that this is due to the disruption of the balance between the plus-end and the minus-end motility of lysosomes. I have also found that one major contributor to the dysfunctional lysosome membrane trafficking in lysosome storage disease cells is the accumulation of lysosomal cholesterol, which constitutively promotes the perinuclear accumulation of lysosomes that disrupts lysosomal membrane trafficking. These findings can greatly advance our understanding about the membrane trafficking mechanisms of lysosomes, and may proof valuable towards the development of treatment for lysosome storage disease patients.

Additionally, I generated and characterized a genetically encode fluorescent probe for $PI(3,5)P_2$, and showed that it could detect the subcellular localization and dynamics of the lipid in living cells. This gives the probe a huge advantage over conventional methods of detecting intracellular $PI(3,5)P_2$ such as HPLC.

CHAPTER I

Introduction[1]

1.1 Overview of Endo-lysosomal membrane trafficking

1.1.1 Introduction to the endocytic membrane trafficking system

Imagine that all modern methods of logistics and transportations are gone: no supermarkets to gather goods from all over the world for you to purchase; no flights and trains to take you to places hundreds or thousands of miles away; no garbage truck to pick up your garbage and you have to deal with trash you generate each day. Feel like being thrown back to Stone Age? That's how important logistics and transportations are to our life.

In eukaryotic cells, the endocytic membrane trafficking system is responsible for the logistics and transportation of things inside the cell. Endocytic vesicles take up nutrients and other substances from outside of the cell, break them down to basic molecules like amino acids and monosaccharides, and release them into the cytosol for energy production or synthesis of cellular components. Endocytic vesicles also transport cellular substances between places inside the cell. Moreover, many unwanted or damaged cellular components are broken down and recycled in endocytic vesicles. All these processes are essential for the cell to maintain its highly

[1] Parts of this Chapter, including Fig. 1.1 and 1.2, were originally published in Journal of Physiology. 2013 Sep 15;591(Pt 18):4389-401. With authors listed as Xinran Li, Abigail G. Garrity, and Haoxing Xu.

organized status. Therefore, the endocytic trafficking system is crucial to the survival of eukaryotic cells.

The endocytic pathway generally begins with a process called endocytosis, in which a piece of membrane from the plasma membrane of the cell gets internalized and forms a membrane-bound vesicle that contains the initial cargo (Marsh and McMahon 1999). Depending on the nature of their generation, newly formed endocytic vesicles can be sorted into three major categories: macropinosomes (which are generated non-specifically and simply take up extracellular fluids) (Lim and Gleeson 2011), endosomes (which are generated through activation of receptors on the plasma membrane by small particles, including clathrin-mediated endocytosis (McMahon and Boucrot 2011) and caveolae (Parton and del Pozo 2013)), and phagosomes (which are generated through activation of receptors on the plasma membrane by large particles such as bacteria or cell debris) (Flannagan, Jaumouille et al. 2012). Among the three types of vesicles, phagosomes are generally only present in immune cells.

After budding off from the plasma membrane, nascent endocytic vesicles quickly mature into early endosomes through the acquisition of early endosome markers and the clearance of plasma membrane markers (the identities of which are to be discussed below). Early endosomes are the first stop in the endocytic pathway. At this stage, endosomes undergo a major sorting process, through which membrane-bound plasma membrane proteins such as receptors are recognized and sorted on tubular structures that protrude out from early endosomes, and recycled back to the plasma membrane through small vesicles called recycling endosomes that bud off from the tubular structures (Grant and Donaldson 2009, Hsu and Prekeris 2010) (**Fig. 1.1**).

The early endosomes, after sorting out the reusable components, now contain cargos destined for delivery to the lysosomes. Endosomes then undergo acidification of the lumen, which is carried by the vesicular ATPase (V-ATPase) that pumps proton from the cytosol to the lumen (Nelson and Harvey 1999). During this period, membrane-bound cargos are sorted into the lumen through the sequential action of a series of protein complexes named ESCRT–0, –I. –II, and –III, respectively (Schmidt and Teis 2012). ESCRT stands for the Endosomal Sorting Complexes Required for Transport, and the protein complexes work together to sort membrane-bound cargos into small inward protrusions of the endosomal membrane, and finally bud the piece of membrane off into the lumen (Schmidt and Teis 2012). This results in small vesicles (known as intraluminal vesicles, or ILV) generated inside the lumen of endosomes. Endosomes carrying multiple ILVs are known as multi-vesicular bodies (MVB) (Babst 2011), also more commonly referred to as late endosomes (**Fig. 1.1**).

Maturation of late endosomes to lysosomes involves further acidification of the lumen (from an average pH of 5.5-6 in late endosomes to pH of 4.5 in lysosomes), as well as the acquisition of the hydrolytic enzymes. Hydrolytic enzymes are acquired from transport vesicles originated from the Golgi complex, or from direct fusion with an existing lysosome (Braulke and Bonifacino 2009) (**Fig. 1.1**). The acidic luminal pH activates the enzymes and breaks down cargo macromolecules to single building blocks (amino acids, monosaccharides, unesterified lipids, etc.) for reutilization.

Finally, lysosomes can undergo a process called exocytosis, during which lysosomes fuse with the plasma membrane, and release their luminal content into the extracellular space. Additionally, lysosomes can undergo a recycling process called lysosome reformation, during which lysosomes, similar to early endosomes, form tubular structures, and small vesicles

containing lysosomal membrane proteins and lipids bud off as “proto-lysosomes” and thus recycle the material from consumed lysosomes (Yu, McPhee et al. 2010) (**Fig. 1.1**).

Aside from the main stem, there are multiple branches on the endocytic pathway involving communication with other intracellular organelles.

Late endosomes and lysosomes (collectively LELs) acquire their luminal enzymes, as well as new supplies of membrane proteins from the Golgi complex. Newly synthesized membrane proteins and luminal enzymes are sorted in Golgi into transport vesicles, and then transported to LELs (Braulke and Bonifacino 2009). Upon arrival, the luminal enzymes are released into the LELs due to the acidic luminal pH.

Lysosomes also retrogradely transport materials back to the Golgi complex through lysosome-derived transport vesicles (Braulke and Bonifacino 2009). These materials include receptors for transporting luminal enzymes, and lipids that are to be processes in the Golgi or ER.

Autophagosomes are a special type of double membrane-bound organelles. During cellular starvation or upon organelle damage, autophagosomes are generated to wrap up the materials (proteins or organelles) destined for degradation, and deliver them to the lysosomes (Mizushima and Komatsu 2011). Besides autophagosomes, cytosolic materials can also be delivered to lysosomes directly through chaperone-mediated autophagy (Kaushik and Cuervo 2012).

1.1.2 Coordination of endocytic trafficking events by phosphoinositides, small GTPases, and Ca^{2+}

Endocytic membrane trafficking, as depicted above, involves multiple steps, and multiple conversions of a vesicle's identity. As there are processes specific to each state, the vesicles must be able to correctly identify themselves to avoid trafficking processes happening on the wrong vesicles. Additionally, endocytic trafficking is a sequential process, in which trafficking events must be coordinated in a temporally sequential way, thus requiring a mechanism through which different steps can be turned on in a sequential manner.

Through the years of evolution, animal cells have developed an efficient system to "shoot two birds with one stone". Two complementary yet cooperating methods are adopted by cells to correctly label the vesicle identities and regulate sequential trafficking steps at the same time.

Firstly, intracellular vesicles, as well as the whole cell, are bound by membrane bilayers. One species of membrane lipid called phosphoinositides localize to the cytosolic side of the membranes and serve as identity marker for the vesicles (Di Paolo and De Camilli 2006). Phosphoinositides are generated by the phosphorylation of phosphatidylinositol at the 3', 4', and 5' positions of the inositol ring. Depending on the position of the phosphorylation, there are seven kinds of phosphoinositides: PI(3)P, PI(4)P, PI(5)P, PI(3,4)P_2, PI(3,5)P_2, PI(4,5)P_2, and PI(3,4,5)P_3.

Different endocytic compartments contain different phosphoinositides to aid their identification. Phosphatidylinositol is phosphorylated in the Golgi complex to PI(4)P, which determines the identity of the secretary vesicles destined for the plasma membrane (Santiago-Tirado and Bretscher 2011). Plasma membrane mainly contains PI(4)P and its derivative, PI(4,5)P_2. Many plasma membrane integral proteins are modulated by PI(4)P and/or PI(4,5)P_2,

and many plasma membrane associated proteins are localized to the plasma membrane through the recognition of PI(4)P or PI(4,5)P_2 (Falkenburger, Jensen et al. 2010).

Upon endocytosis, the membrane PI(4)P and PI(4,5)P_2 are quickly turned over by phosphatases, and PI(3)P is quickly generated through class III phosphatidylinositol-3-kinase (PI3K-III) (Poccia and Larijani 2009). PI(3)P is the major phosphoinositide present on early endosomes, and is required for the rapid recruitment of many early endosome proteins such as EEA1 and *hrs* (Poccia and Larijani 2009). The appearance of PI(3)P on endosomes initiates the maturation of early endosomes. EEA1 is a tethering protein facilitating the fusion between early endosomes (Simonsen, Lippe et al. 1998), and *hrs* is responsible for the initiation of the ESCRT pathway that leads to the generation of ILVs and the progression to late endosomes (Sun, Yan et al. 2003, Hurley 2010). Another protein, PIKfyve, which is the kinase responsible for the conversion from PI(3)P to PI(3,5)P_2, is also recruited to early endosomes by PI(3)P (Sbrissa, Ikonomov et al. 2002).

PIKfyve is a phosphatidylinositol-5-kinase that converts PI(3)P to PI(3,5)P_2, and PI to PI(5)P, two phosphoinositides that mark late endosomes and lysosomes. PI(5)P is less well-studied with very few known effectors (Vicinanza, Korolchuk et al. 2015). PI(3,5)P_2, on the other hand, has been shown to regulate the activity of several proteins important for LEL functions. For example, Vps24p (CHMP3 in mammals) has been shown to be an effector of PI(3,5)P_2 to mediate the last steps of ILV formation (Whitley, Reaves et al. 2003). Also, two LEL cation channels, TRPML1 (Transient Receptor Potential MucoLipin 1) (Dong, Shen et al. 2010) and TPC2 (Two-Pore Channel 2) (Wang, Zhang et al. 2012), are shown to be activated by PI(3,5)P_2.

Similar to endosomes, phagosomes and autophagosomes are both labeled with PI(3)P, and acquire PI(3,5)P_2 as they mature into phagolysosomes or autolysosomes (Poccia and Larijani 2009).

Therefore, phosphoinositides represent a labeling system that serves regulatory functions for endocytic trafficking. Vesicles destined to fuse with the plasma membrane (secretary vesicles and recycling endosomes) are generally labeled with PI(4)P, while vesicles destined to fuse with LELs are generally labeled with PI(3)P. A series of kinases and phosphatases are responsible for the conversion between different phosphoinositide species.

Apart from phosphoinositides, cells have developed a complementary system to coordinate the functions of different organelles along the endocytic trafficking pathway. Ras small GTPases are a superfamily of proteins serving a variety of cellular functions. Among the Ras proteins, several sub-families are known to regulate endocytic trafficking, with the Rab and Arf families being the most studied (Mizuno-Yamasaki, Rivera-Molina et al. 2012). Rab proteins are mainly involved in coordinating sequential endocytic events, while Arf proteins typically regulate vesicle budding. Rab proteins are the largest subfamily of the Ras GTPases, consisting of over 60 members in human (Rojas, Fuentes et al. 2012, Pfeffer 2013).

Small GTPases participate in marking membrane identity and in regulating membrane trafficking events through association with specific membranes (Pfeffer 2013). Small GTPases like Rabs and Arfs transit between two states: a GTP-bound, active state and a GDP-bound, inactive state. Small GTPases acquire the GTP molecule through the action of helper proteins called Guanine nucleotide exchange factors (GEF). When associated with GTP, small GTPases localize onto specific membranes and regulate the activity and/or localization of downstream

effectors (Blumer, Rey et al. 2013). After finishing the job, the GTPase activity of small GTPases can be turned on by GTPase-activating proteins (GAP), and GTP is thus converted to GDP to terminate the action (Stenmark 2009).

The timed association of small GTPases onto the vesicular membranes thus determines a variety of spatiotemporally regulated membrane trafficking events. For example, two tethering factors facilitating vesicular fusion, EEA1 and HOmotypic fusion and Protein Sorting complex (HOPS) are recruited by Rab5 to early endosomes and by Rab7 to late endosomes, respectively (Yu and Hughson 2010).

Ca^{2+} is a versatile regulator for many cellular processes. Ca^{2+} signaling is known to occur on a variety of spatial and temporal manners. The Endoplasmic Reticulum (ER)/Sarcoplasmic Reticulum (SR) has been considered as the major intracellular source of Ca^{2+}, and ER/SR Ca^{2+} release has been shown to signal important cellular functions, including muscle contraction and activation of signaling cascades downstream of G proteins. In recent years, however, the lysosome began to be appreciated as an additional Ca^{2+} store of the cell (Morgan, Platt et al. 2011). After endocytosis, early endosomes gradually lose their luminal Ca^{2+} as they undergo acidification, but then regain high luminal Ca^{2+} as they mature into lysosomes, likely through lysosome-ER contacts (Kilpatrick, Eden et al. 2013, Lopez-Sanjurjo, Tovey et al. 2013).

The importance of lysosomal Ca^{2+} in regulating lysosomal membrane trafficking, especially membrane fusion events, has been suggested in multiple studies (Samie, Wang et al. 2013, Cheng, Zhang et al. 2014, Dayam, Saric et al. 2015). It is generally agreed that Ca^{2+} plays a role in lysosomal membrane fusion events, including lysosome exocytosis, in a manner similar to its role in regulating synaptic vesicle release (**Fig. 1.2**) (Andrews and Chakrabarti 2005,

Cheng, Zhang et al. 2015). In neurons, synaptic vesicles are docked to the plasma membrane at the synapse. Action potential opens voltage gated Ca^{2+} channels at the synapse, leading to a rapid increase (within 1 ms) in the local Ca^{2+}. Synaptotagmin, a class of Ca^{2+}-binding membrane proteins, sense the increased [Ca^{2+}] and trigger the fusion between synaptic vesicle and the plasma membrane through interaction with the Soluble N-ethylmaleimide-sensitive fusion Attachment protein Receptor (SNARE) complex. It has been shown by multiple groups that Synaptotagmin VII, a member of the Synaptotagmin family, is involved in the regulation of lysosome exocytosis (Czibener, Sherer et al. 2006, Idone, Tam et al. 2008, Samie, Wang et al. 2013).

Apart from Synaptotagmin VII, multiple Ca^{2+} sensors have been suggested to regulate endolysosomal signaling events, including calmodulin (Peters and Mayer 1998), calcineurin (Medina, Di Paola et al. 2015), and ALG-2 (Vergarajauregui, Martina et al. 2009). However, most evidences remained inconclusive, leaving the role of Ca^{2+} in regulating endolysosomal membrane trafficking unconsolidated.

1.1.3 The importance of endocytic trafficking to the cell

The endocytic system, as described above, is a complicated network that requires the coordination of many factors and events. Thanks to Darwin, we now know that organisms tend to find the best way over the long years of evolution. Therefore, if the functions of the endocytic trafficking system do not require such a complicated pathway, it would already have been replaced by a much simpler pathway. Throughout the evolution, the components of the endocytic

system remained highly conserved, between organisms as far apart as human and yeasts, suggesting that all these components are required for proper cell functions.

So, why do we need such a complicated system for our cells? Let's take a more detailed look at what the endocytic membrane trafficking system does for the cell.

One of the best defined roles for the endocytic trafficking system is to degrade unwanted materials and recycle them. Lysosomes contain hydrolytic enzymes that are able to hydrolyze molecules delivered to them, including polypeptides, polysaccharides and esterified lipids. The products of the hydrolysis are monomer building blocks (e.g. amino acids) of biomolecules that can be re-utilized by the cell. These small molecules are then released into the cytosol through specific transporters. In this way, the cell recycles much of its waste in a highly efficient manner. Additionally, extracellular macromolecules, or sometimes even larger substances like bacteria or cell debris (in the case of phagocytosis), can also be degraded into building blocks through the endocytic pathway. Therefore, endocytic trafficking not only represents a recycling system at cellular level, but also at the organism level.

In addition to cargo degradation, studies in recent years have shown a central role of lysosomes in nutrient sensing and cellular growth control. The mechanistic Target of Rapamycin (mTOR) is a serine/threonine kinase that serves as the master regulator of cell growth from yeast to humans. mTOR exist in two different complexes, mTORC1 and mTORC2. mTORC1 is the complex responsible for sensing the nutrient availability and extracellular growth signals to control the cellular growth in response to environmental cues.

It has been shown that the activation of mTORC1 requires activation from a small GTPase called Rheb that resides on lysosomal membranes (Buerger, DeVries et al. 2006, Menon,

Dibble et al. 2014). Therefore, mTORC1 needs to translocate to the lysosome for its proper activation. The translocation of mTORC1 onto the lysosome has been shown to require a protein complex named Ragulator (Sancak, Bar-Peled et al. 2010). Rheb is only active when stimuli from growth factors are present (Menon, Dibble et al. 2014), while Ragulator only recruits mTORC1 to lysosome membranes when abundant amino acids are present (Sancak, Bar-Peled et al. 2010). Therefore, the cooperation between Rheb and Ragulator ensures that mTORC1 only activates cellular growth when there is enough material (amino acids) and when it is instructed to do so (growth factors). Interestingly, several studies have shown that the recruitment of mTORC1 onto the lysosome requires amino acids originating from the lysosome lumen, but not from cytosol. When lysosomes have low amino acid contents, mTORC1 does not get activated regardless of cytosolic amino acids (Zoncu, Bar-Peled et al. 2011). Thus, lysosomes not only provide a platform, but also actively participate in regulating cellular growth.

Apart from the roles on cellular recycling and nutrient sensing, endocytic trafficking also plays important roles in other aspects. For example, the activity of multiple plasma membrane receptors and channels/transporters is regulated through endocytosis and exocytosis, through which the amount of protein on the cell surface can be quickly adjusted according to cellular needs. Also, multiple substances, including hydrolytic enzymes and ATP, are shown to be purposely released into the extracellular environment through lysosome exocytosis (Czibener, Sherer et al. 2006, Sivaramakrishnan, Bidula et al. 2012).

The importance of endocytic trafficking, especially the function of lysosomes, has been proved by various lysosome storage diseases (LSDs). Lysosome storage diseases are caused by mutations in endocytic proteins, including lysosomal hydrolytic enzymes, specific transporters, key regulators of vesicle transport/fusion/fission, key regulators of cargo recognition/sorting, etc.

The dysfunction of these proteins leads to the accumulation of substances within the endocytic system, especially in the lysosomes (Pagano, Puri et al. 2000, Yanagawa, Tsukuba et al. 2007, Samie and Xu 2014). More often than not, the accumulation of a substance (e.g. a particular lipid) affects the endocytic pathway, leading to the secondary dysfunction of multiple proteins, and secondary accumulation of other substances. Because of this, most LSDs would end up with accumulation of a similar spectrum of substances (Pagano, Puri et al. 2000, Yanagawa, Tsukuba et al. 2007, Samie and Xu 2014).

A common symptom shared by LSDs is early onset of severe neurodegeneration. The existence of long neurites means that neurons have very high requirement for endocytic transport through long distances. Also, neurons are terminally differentiated, non-dividable cells, therefore rely heavily on cellular clearance systems to maintain their health. Many LSD patients are also accompanied with motor/vision defects. Due to their severe phenotypes, most LSD patients unfortunately face early deaths.

Except for LSDs, which are caused by primary dysfunction of certain genes regulating the endocytic pathway, much more common chronical diseases, including Alzheimer's Disease and Parkinson's Disease, are shown to be related with hypofunction of the lysosomal degradative pathway (Lee, Yu et al. 2010, Follett, Norwood et al. 2014, Erie, Sacino et al. 2015). Normally, intracellular and extracellular toxic materials are degraded through autophagy and phagocytosis, respectively. Under diseases conditions, abnormal amounts of toxic materials accumulate in the body, exceeding the ability of self-clearance. Thus, up-regulation of the endocytic pathway may prove beneficial for common neurodegeneration diseases.

1.2 Lysosomal membrane trafficking: purposes, events, and regulators

1.2.1 Lysosome plays a central role in the endocytic membrane trafficking

Among the many different types of endocytic vesicles, lysosomes play a central role in the coordination of the endocytic membrane trafficking. As described above, the endocytic system contains multiple routes, with vesicles emerging from endocytosis, phagocytosis, or autophagy. Except for recycling endosomes, which contain membrane proteins to be delivered back to the plasma membrane, all endocytic vesicles are eventually delivered to lysosomes. These fusion vesicles are often times named after their origin, such as endolysosomes, phagolysosomes, and autolysosomes.

Lysosomes determine the fate of substances delivered to them. Polypeptides, for example, are broken down to amino acids by cathepsins, and then transported across lysosome membrane into the cytosol through amino acid transporters (Sagne, Agulhon et al. 2001, Boll, Foltz et al. 2002). Digestible polysaccharides are also broken down to monosaccharides, as well as RNA/DNA to single nucleotides. Each of these molecules are thought to be transported out of lysosomes through specific transporters. Lipids, on the other hand, are unesterified by esterases, delivered *onto* the lysosomal membrane, and then transported out of lysosomes (mainly to the Golgi apparatus) on transport vesicles (Pagano, Martin et al. 1991), or through direct membrane contact with other organelles (Chu, Liao et al. 2015).

Except for releasing hydrolysis products, lysosomes can also deliver substances to the extracellular space through exocytosis. This function has been shown to play roles in cell migration (Colvin, Means et al. 2010) and transmitter release (notably ATP) (Shin, Lee et al.

2012). Thus, through accepting materials and redistributing them, lysosomes serve as the recycling and soring center for the cell.

1.2.2 Trafficking events on the lysosome – motility, fusion, and fission

The roles of lysosomes determine that they undergo heavy trafficking in cells. Like other membrane-bound organelles, researches on lysosomal trafficking have been focused on three aspects: the directional movement of lysosomes, and the fusion and fission of lysosome membranes (**Fig. 1.3**).

In order to meet with cargo vesicles, or to fulfill particular purposes such as exocytosis, lysosomes have to travel inside the cells in a directed manner. Such movements are mostly carried out through microtubule-based motor proteins (Rosa-Ferreira and Munro 2011, Tan, Scherer et al. 2011), although actin-based short range movements also contribute to movements close to the plasma membrane (Hissa, Pontes et al. 2013) (**Fig. 1.3, brown arrows**).

Most microtubules inside the cells exhibit a radial pattern, with their minus-ends clustering at the microtubule organizing center (MTOC), which is usually located very close to the cell nucleus, and their plus-ends stretching out to the cell periphery (Brinkley 1985). Therefore, the directional movement of lysosomes along microtubules determines their location inside the cells. The localization of lysosomes is often described as “perinuclear” or “juxta-nuclear” when they are close to the nucleus or “peripheral” when they are away from the nucleus. There is a good reason for such classifications, as researchers have found an interesting relationship between the “perinuclearity” (i.e the degree of proximity to the nucleus) of lysosomes and cellular behaviors. It has been shown that lysosomes undergo somewhat

synchronized perinuclear movement when the cell undergoes acute starvation, i.e. depletion of extracellular nutrient/growth factors (Yu, McPhee et al. 2010, Korolchuk, Saiki et al. 2011). This is hypothesized to promote the fusion between lysosomes and autophagosomes, the generation of the latter triggered by acute starvation (Yu, McPhee et al. 2010, Korolchuk, Saiki et al. 2011). This hypothesis is supported by the finding that the microtubule minus-end directed motor the dynein complex is required for the sufficient delivery of autophagic contents to the lysosomes (Kimura, Noda et al. 2008, Xu, Li et al. 2013). Additionally, it is often noticed that within the same cell, perinuclear lysosomes are generally enlarged compared to peripheral lysosomes, indicating that these lysosomes have merged with other vesicles (Yu, McPhee et al. 2010, Korolchuk, Saiki et al. 2011).

Once reaching the destination, lysosomes will carry out their function, usually through membrane fusion with other vesicles (**Fig. 1.3, green arrows**), or with the plasma membrane (**Fig. 1.3, blue arrow**). As mentioned above (**1.1.2**), Ca^{2+}-regulated, SNARE-mediated membrane fusion machinery has been proposed to be responsible for lysosomal fusion events. To prepare for the fusion event, the lysosome would first get into contact with the target membrane through tethering factors. Tethering factors determine the specificity of membranes in contact, and thus determine the specificity of the membrane fusion.

The lysosomal tethering complex, HOPS (Solinger and Spang 2013), was first characterized in yeast, and best studied for its role in promoting the fusion between yeast vacuoles, the counterpart of lysosomes in yeasts. Loss of HOPS complex components leads to fragmented vacuoles in yeast, suggesting their important roles in vacuole fusion (Wickner 2010). HOPS complex is able to associate with Ypt7 (or in mammals Rab7), as well as members of the SNARE complex (Solinger and Spang 2013). It has been shown that HOPS interacts with

specific trans-SNARE complex to facilitate the vesicle fusion, and inhibits fusion with incorrect SNARE combinations (Collins and Wickner 2007, Starai, Hickey et al. 2008). Therefore, HOPS interacts with the Rab protein to ensure its localization onto the correct membrane, tether the membranes and promote fusion with correct vesicles through specific recognition of the correct SNARE.

The fusion of the membranes is proposed to be carried out in a similar fashion as the synaptic vesicle release. The importance of the SNARE complex and the Ca^{2+} sensor synaptotagmin VII for lysosomal membrane fusion has been shown in studies using knockdown assays as well as dominant negative forms of these proteins (Czibener, Sherer et al. 2006, Idone, Tam et al. 2008, Samie, Wang et al. 2013). The best characterized membrane fusion event involving lysosomes is lysosomal exocytosis. This is mainly due to technical limitations. Where lysosomal exocytosis can be easily monitored through assaying luminal enzyme release, increase of plasma membrane capacitance, or surface labeling of lysosomal membrane proteins on the plasma membrane due to exocytosis, the membrane fusion between lysosomes and other organelles is not directly accessible to extracellular measurements, with the additional complication of the similarities between late endosomes, primary lysosomes (lysosomes not fused with cargo vesicles yet), secondary lysosomes (lysosomes already accepted cargo), etc.

In lysosomal exocytosis, it is now clear that *local* Ca^{2+} plays an important role, i.e. the Ca^{2+} required for the exocytosis comes directly from the lysosomes *per se*, but not from other sources (Czibener, Sherer et al. 2006, Idone, Tam et al. 2008, Samie, Wang et al. 2013). Multiple reports suggest that the Ca^{2+} is released through a lysosomal ion channel called TRPML1 (Transient Receptor Potential MucoLipin 1) (Samie, Wang et al. 2013, Cheng, Zhang et al. 2014). In proposed models, lysosomes are tethered and docked to the target membrane prior to fusion.

When the final signal arrives (e.g. for macrophages, when phagocytosis is initiated), TRPML1 releases Ca^{2+} from lysosome lumen, which is immediately picked up by synaptotagmin VII. Synaptotagmin VII then binds to the SNARE complex and triggers fusion between the lysosome and the plasma membrane (**Fig. 1.2**). The fusion between lysosomes, or between lysosomes and other vesicles, likely occurs in a similar fashion.

After fusion with other vesicles, the total surface area as well as the volume of lysosomes will increase, resulting in enlarged lysosomes. This is most observable during autophagy or phagocytosis. In healthy and fed cells, normal lysosome sizes range from 100 nm to up to 0.5-1 μm as determined by confocal and super-resolution microscopies (**Fig. 1.4**). During active autophagy (e.g. starvation) or phagocytosis, the fusion of lysosomes with much larger cargo vesicles (usually 0.5-3 μm for autophagosomes, and up to 5-10 μm for phagosomes depending on the particle size) results in large secondary lysosomes usually found at the perinuclear region of the cells (Yu, McPhee et al. 2010, Samie, Wang et al. 2013). Recent studies on lysosome reformation regarded these lysosomes as consumed lysosomes, since they are occupied by the large quantities of cargo and are not available for providing more digestive forces (Yu, McPhee et al. 2010, Rong, Liu et al. 2012). As autophagy and phagocytosis require large quantities of lysosomes for digestion, the cell will run short of primary lysosomes very quickly in these circumstances, and accumulate enlarged secondary lysosomes. To ensure the proper homeostasis of lysosome number and size, membrane fission takes place on these lysosomes (Yu, McPhee et al. 2010, Rong, Liu et al. 2012, Chen and Yu 2013).

Not much is known about lysosome membrane fission for many years. Works from the last five years or so demonstrated that lysosome membrane fission resembles that of the budding off of recycling endosomes from sorting tubules on early endosomes (**1.1.1**). Specifically,

lysosomes will generate tubular structures that protrude from the vesicular part, which will be referred to as lysosome tubulation hereafter (Chen and Yu 2013). Membrane fission will take place on these tubules through clathrin-mediated membrane budding, the mechanism used for endocytosis (Rong, Liu et al. 2012). The vesicle that buds off is proposed to serve the purpose of recycling lysosomal membrane lipids and proteins for the generation of new primary lysosomes (**Fig. 1.3, purple arrow**).

Lysosome tubulation and fission (also named lysosome reformation) may happen at a low rate under basal conditions, but is most prominent under conditions of heavy lysosome consumption (Chen and Yu 2013). Interestingly, the phenomenon of lysosome tubulation in macrophages actively undergoing phagocytosis was reported a long time ago (Swanson, Bushnell et al. 1987), but was not linked to lysosome reformation until similar tubulation events were characterized during prolonged starvation conditions. Judged by the similarity between them, lysosome reformation under phagocytosis and prolonged starvation may share the same mechanism. However, as described below, our understandings on both phenomena are insufficient to draw conclusion on this point yet.

Since first characterized in 2010, several aspects of lysosome reformation have been characterized, but more remained unclear. It seems that the reformation process, especially the generation of the tubular structure, is a quite delicate process. Hyper- or hypo-function of many proteins, or even lipids, can lead to the disruption of the reformation process. Conversely, many LSD cells show enlarged lysosomes, an indication of defective lysosome membrane fission.

1.2.3 The key regulators coordinating lysosome membrane trafficking

The coordination of lysosomal trafficking events would require precise regulation. Transport of lysosomes to the right place is a prerequisite for the membrane contact with cargo vesicles, and membrane fission should not take place until after the fusion with the cargo vesicle. The timing of these events, as mentioned above (**1.1.2**), can be coordinated through phosphoinositides, small GTPases, and Ca^{2+}. There are also other important regulators required for different aspects of lysosome trafficking. Below let's take a look at some of the key regulators of lysosomal trafficking events.

Motor proteins

Motor proteins are a class of ATPases that convert energy from ATP hydrolysis to kinetic energy represented as directional movement (Reilein, Rogers et al. 2001). Motor proteins are commonly sorted into three families: dyneins, kinesins and myosins. Among the three families, dyneins and kinesins are microtubule-based, while myosins move along actin filaments. Since most of the directional movements of lysosomes are carried along microtubules, dyneins and kinesins are the main players in lysosome trafficking.

Dyneins are huge protein complexes able of driving cargo movements towards the minus-ends of microtubules, which are usually present at the MTOC close to the cell nucleus. Based on their locations, dyneins are separated into two groups, cytoplasmic dyneins and axonemal dyneins, the latter usually found in neurites, cilia and flagella (King 2000). Two types of cytoplasmic dynein exist, with cytoplasmic dynein 1 responsible for the retrograde transport of most intracellular vesicles, including lysosomes (Schiavo, Greensmith et al. 2013). Cytoplasmic dynein 1 is a protein complex of about 1.5 MDa consisting of a homodimer of two dynein heavy chains (DHC), each of an enormous ~530 kDa size in mammals, a pair of intermediate chains

(DIC), a pair of light-intermediate chains (DLIC), and a total of six light chains (DLC) (Kardon and Vale 2009, Schiavo, Greensmith et al. 2013). Heavy chains are responsible for the association with microtubules, power generation through ATP hydrolysis, and scaffolding intermediate chains and light chains. Intermediate chains are the main site for cargo adaptation, although some cargo adaptors also bind to heavy chains or light chains (Kardon and Vale 2009, Schiavo, Greensmith et al. 2013).

Lysosomes do not recruit the dynein complex directly, but rather through another huge, 1.2 MDa adaptor complex called dynactin (Schroer 2004). Dynactin is a multi-subunit complex, its most obvious structures under electron microscope (EM) feature a ~40 nm long rod-like structure consisting of polymerized actin-related protein Arp1, and a projection arm composed of a dimer of the $p150^{glued}$ protein (Schroer 2004). The Arp1 rod resembles actin filament and is responsible for the interaction with β-spectrin on cargo vesicles, while the $p150^{glued}$ arm associates with the intermediate chain of the dynein complex. Additional proteins, such as dynamitin (p50) and p62, are also present for scaffolding, structure stability, and cargo recognition (Schroer 2004).

Dynactin has been shown to bridge lysosomes and dynein through the recruitment by the Rab7 effector, Rab7-Interacting Lysosomal Protein (RILP) (Jordens, Fernandez-Borja et al. 2001), and the lysosomal cholesterol sensor Oxysterol-binding protein Related Protein 1L (ORP1L) (Johansson, Rocha et al. 2007). RILP interacts with the C-terminal of $p150^{glued}$, while ORP1L is responsible for the association of dynactin to lysosomal spectrin to activate retrograde transport (Johansson, Rocha et al. 2007). Therefore, lysosomes achieve retrograde transport towards the MTOC through the recruitment of dynactin (by lysosomal adaptors), which in turn recruits the dynein complex.

Contrary to dyneins, which exist in huge complexes, the plus-end directed motor proteins, kinesins, are much smaller in size. Kinesins are a large protein family with diverse protein structures, but all containing a kinesin motor domain, and most of them contain coiled-coil domains for dimerization (Verhey and Hammond 2009). 14 kinesin subfamilies have been characterized so far, with most kinesins move the cargo towards the plus-end of microtubules, except for the kinesin-14 subfamily (and a kinesin-5 member Cin8) (Verhey and Hammond 2009, Roostalu, Hentrich et al. 2011).

Kif5B, a member of the kinesin-1 subfamily, is ubiquitously expressed in all tissues and is generally considered as the main kinesin motor responsible for the plus-end motility of endocytic vesicles, including lysosomes (Rosa-Ferreira and Munro 2011). Kif5B is a ~110 kDa protein consisting of an N-terminal motor domain, a long coiled-coil stem and a C-terminal globular domain (Navone, Niclas et al. 1992, Jeppesen and Hoerber 2012). Kif5B associates with the kinesin light chain (KLC) at the C-terminal regions. The globular domain and the KLC cooperate in cargo recognition (Jeppesen and Hoerber 2012). Without cargo binding, Kif5B is autoinhibited through the binding of its C-terminal tail with the motor domain, which arrests the motor domain in an ADP-bound state (Carter and Cross 2006, Verhey and Hammond 2009). Upon cargo recognition, the association with the cargo releases the tail from the motor domain, allowing Kif5B to walk along the microtubule.

Kif5B has been shown to be recruited to the lysosomes through SKIP (SifA and Kinesin Interacting Protein), which is in turn brought to lysosomal surface by a small GTPase Arl8 (ADP-Ribosylation factor Like protein 8) (Rosa-Ferreira and Munro 2011). Therefore, the motility of lysosomes towards different directions inside the cell is mediated through the recruitment of different motor proteins by lysosomal factors.

mTORC1

mTORC1 is a master regulator of cell growth in response to nutrient status and extracellular growth cues. As described above, the activation of mTORC1 is regulated by the lysosomal small GTPase Rheb, and amino acids released from the lysosome lumen. On the other hand, the trafficking of lysosomes is reciprocally regulated by mTORC1.

Inhibition of mTORC1 will activate autophagy, with active generation of autophagosomes (Kim, Kundu et al. 2011). The digestion of autophagosomes requires fusion with lysosomes at the perinuclear region, resulting in enlarged perinuclear autolysosomes. Therefore, inhibition of mTORC1 could result in the retrograde migration of lysosomes towards the nucleus.

Except for an effect on lysosome distribution, mTORC1 is also known to be required for lysosome reformation to take place. During prolonged starvation, in spite of the low level of extracellular nutrient, mTORC1 gets re-activated due to the digestion of autophagic cargo in the lysosome (Yu, McPhee et al. 2010), and the subsequent release of nutrients back to the cytosol. Lysosome reformation is activated at this stage, but inhibition of mTOR would abolish the reformation, and lead to persistence of enlarged vacuoles (Yu, McPhee et al. 2010).

Clathrin

Clathrin is an interesting protein that in cells can coat membranes to form soccer-like structure. Clathrin forms triskelion, in which three clathrin heavy chains form the three legs of the triskelion, and three light chains bound to the inner portion of the heavy chain legs (Pearse 1976, Ford, Pearse et al. 2001, Higgins and McMahon 2002). The heavy chains from different triskelia can assemble together on the membrane in either pentagon or hexagon shapes,

inevitably inducing membrane curvature (Higgins and McMahon 2002). The result of the assembly is part of the membrane curving into the cytosol and, with the help of membrane scission proteins like dynamin, bud off from the original membrane in a soccer ball shaped vesicle (Henley, Cao et al. 1999, Higgins and McMahon 2002, Roux, Uyhazi et al. 2006).

Due to the ability of forming membrane curvature protruding into the cytosol in a regular and well-defined manner, clathrin plays crucial role in membrane fission, and is especially well known for the clathrin-mediated endocytosis (Pearse 1976). Recent evidences have also pointed out that the same clathrin-mediated membrane fission pathway is used for lysosome membrane fission (Rong, Liu et al. 2012), i.e. reformation. Depletion of clathrin or $PI(4,5)P_2$, the phosphoinositide required for the membrane recruitment of clathrin, suppressed the reformation of lysosomes (Rong, Liu et al. 2012).

Cytosolic pH

pH inside the cells is usually tightly regulated, as most proteins require optimized pH for their proper functions. Therefore, on a long term basis, the intracellular and extracellular pH in our body is maintained at a stable level, which is ~7.4 for extracellular environment, and ~7.2 for the cytosol (Deutsch, Taylor et al. 1982).

During acute starvation, the pH of the cytosol is temporarily increased, in some studies as much as from 7.2 to 7.7 (which equals to ~3 times difference in $[H^+]$) (Korolchuk, Saiki et al. 2011). Interestingly, a gross acidification of lysosomes under acute starvation is also reported, proposed to be caused by active v-ATPase pumping protons into the lysosome lumen in compensation to the suddenly increased luminal volume through fusion with autophagosomes (Wong, Li et al. 2012, Mauvezin and Neufeld 2015). The two events are probably correlated, as

rapid acidification of lysosome lumen would lead to a loss of cytosolic protons and thus increased cytosolic pH, but this has not been established yet.

It has been known for many years that cytosolic pH impacts on the positioning of lysosomes inside the cells (Heuser 1989). More acidic cytosolic pH results in a more peripheral distribution of lysosomes, while alkalization of the cytosol results in the accumulation of lysosomes at the perinuclear region (Heuser 1989). This is in accordance with the cytosolic pH observed during starvation, in which lysosomes become more perinuclear with a concurrent alkalization of the cytosol.

TRPML1

TRPML1 is a lysosomal Ca^{2+} permeable cation channel, the malfunction of which causes a severe neurodegeneration disease called mucolipidosis type IV (MLIV) (Bargal, Avidan et al. 2000, Bassi, Manzoni et al. 2000). As the main topic of this thesis, more details about the channel are discussed in the separate section below.

1.3 The lysosomal Ca^{2+}-permeable channel TRPML1

1.3.1 Biophysical properties of the TRPML1 channel

TRPML1 was first mapped in patients with MLIV, and identified as a channel that belongs to the transient receptor potential channel superfamily (Bargal, Avidan et al. 2000, Bassi, Manzoni et al. 2000). Two other channels of the same subfamily, TRPML2 and TRPML3, were later identified from a genomic mapping of the mutations in the Varitint-Waddler mice (Di Palma, Belyantseva et al. 2002). While TRPML1 is ubiquitously expressed in all tissues,

TRPML2 and TRPML3 exhibit more restricted expression patterns (Kim, Li et al. 2007, Cuajungco, Silva et al. 2015).

TRPML1 is a 580 a.a. protein of ~65 kDa size (Bargal, Avidan et al. 2000, Bassi, Manzoni et al. 2000). Like other channels in the TRP family, TRPML1 consists of six transmembrane domains (S1 to S6, supported by experimental and computational evidences, but not structurally confirmed), with the N-terminal and the C-terminal both facing the cytosol. It contains a large luminal loop between S1 and S2, and a pore region spanning between S5 and S6 (Sun, Goldin et al. 2000).

TRPML1 is known to be well co-localized with LEL markers such as Lamp1 when overexpressed (Dong, Cheng et al. 2008). Due to restrictions in specific antibodies, the localization of endogenous TRPML1 on the LEL is not sufficiently visualized, but rather confirmed through electrophysiology recordings (Dong, Cheng et al. 2008, Dong, Shen et al. 2010). Under lysosomal patchclamp, endogenous TRPML1 usually exhibits little or no current at basal conditions, but shows an inwardly-rectifying (ions entering the cytosol from the lysosome lumen) current that is largely non-selective for cations (Dong, Cheng et al. 2008, Dong, Shen et al. 2010).

Two di-leucine motifs facilitate TRPML1's lysosomal localization (Pryor, Reimann et al. 2006). The two motifs are 10 a.a. away from the N-terminal and 2 a.a. away from the C-terminal, respectively. Replacement of the leucines in both motifs to alanines will significantly increase the plasma membrane localization of overexpressed channels, but will not fully exclude lysosomal localization (Pryor, Reimann et al. 2006). TRPML1 can localize to lysosomes either

through direct transport from the Golgi upon protein maturation, or through endocytosis after being delivered to the plasma membrane by secretory vesicles or by lysosome exocytosis.

TRPML1 is shown to be permeable to multiple cations, including Ca^{2+}, Fe^{2+}, Zn^{2+}, Na^{+}, and K^{+}, but not H^{+} (Dong, Cheng et al. 2008). Among all the ions permeable, TRPML1 is most well studies for its role as a Ca^{2+} permeable channel, mainly because of versatile roles Ca^{2+} plays in the cell. To date, Ca^{2+} release from TRPML1 has been shown to be important for several aspects of membrane trafficking around the lysosomes. As a process that requires precise timing, membrane trafficking would require acute mechanisms as triggers. Therefore, the Ca^{2+} release from TRPML1 would require upstream signal cues that allow it to be rapidly turned on or off.

1.3.2 The regulation of TRPML1 through endogenous and artificial molecules

As a lysosomal ion channel, the search for endogenous agonists/antagonists of TRPML1 is much harder compared to plasma membrane channels. It is not until lysosomal patchclamp technique was developed that researchers started to gain knowledge on how the channel activity is modulated.

It was shown from early studies that TRPML1 activity is potentiated by acidic luminal pH (Dong, Cheng et al. 2008), which makes perfect sense since this is a lysosomal ion channel that functions on vesicles with very acidic luminal pH. An endogenous agonist of the channel, though, was not discovered until 2010. Not surprisingly, the late endosome and lysosome localized phosphoinositide, $PI(3,5)P_2$, became the first identified endogenous molecule that could activate the channel with high potency (EC_{50} around 50 nM) (Dong, Shen et al. 2010). $PI(3,5)P_2$ binds to TRPML1 through a stretch of positively charged residues on the cytosolic N-

terminal, as mutations of these residues to Glu (named TRPML1-7Q) could abolish the activation from $PI(3,5)P_2$ (Dong, Shen et al. 2010). A follow-up study showed that two of the residues, $R^{61}K^{62}$, are crucial residues conferring $PI(3,5)P_2$ specificity for activation (Zhang, Li et al. 2012).

Apart from $PI(3,5)P_2$, a recent report showed that mTORC1 phosphorylates TRPML1 under nutrient conditions to inhibit the channel, and that removal of phosphorylation can thus potentiate TRPML1 current (Onyenwoke, Sexton et al. 2015). However, such mechanism likely plays a permissive role, allowing the channel to be activated under de-phosphorylated state, rather than directly activating the channel. Therefore, $PI(3,5)P_2$ remains the only established endogenous molecule that can directly activate the channel.

$PI(4,5)P_2$ is a isomer of $PI(3,5)P_2$, differing only with the position of the phosphate on the inositol ring. $PI(4,5)P_2$ is abundant on the plasma membrane, while $PI(3,5)P_2$ is enriched on lysosomal membranes (Balla and Varnai 2002, Li, Wang et al. 2013). Interestingly, $PI(4,5)P_2$ does not activate TRPML1, but instead inhibits the channel with a sub-micromolar IC_{50} (~0.2 μM) (Zhang, Li et al. 2012). Since opening of the channel on the plasma membrane will cause excessive Ca^{2+} influx into the cell, as well as unwanted changes in the membrane potential, this inhibitory mechanism likely plays a role to prevent channel activation at the wrong place. The residues crucial for the interaction between TRPML1 and $PI(4,5)P_2$ has been mapped to the positively-charged residues $R^{42}R^{43}R^{44}$ through mutagenesis analysis (Zhang, Li et al. 2012).

TRPML1 activity can also be inhibited by a type of luminal lipids, sphingomyelins (Shen, Wang et al. 2012). Sphingomyelins are a class of membrane lipids consisting of a phosphocholine or a phosphoethanolamine head group, and a ceramide tail (consisting of a

sphinosine and a fatty acid). Sphingomyelins are enriched on plasma membrane on the outer layer facing the extracellular space, and can be carried into lysosomes through endocytosis. Sphingomyelins are broken down to ceramide in lysosomes and recycled to the Golgi through lysosome-to-Golgi retrograde transport (Jenkins, Canals et al. 2009, Schuchman 2010). Under normal conditions, sphingomyelins may serve in addition to $PI(4,5)P_2$ to prevent TRPML1 from plasma membrane activation. In disease conditions (e.g. in Niemann-Pick Diseases), however, loss of sphinomyelinase activity, or secondary mechanisms can result in the accumulation of sphingomyelins (Schuchman 2010). The subsequent inhibition of TRPML1 to various degrees (depending on the amount of accumulation) is thought to contribute to the development of disease syndromes (Shen, Wang et al. 2012).

Artificial agonists and antagonists of TRPML1 have been identified through screens of small synthetic molecules. One such screen identified a small molecule SF-51 that is capable of activating TRPML1 in higher-micromolar range (Grimm, Jors et al. 2010). SF-51 was later modified to ML-SA1 (MucoLipin Synthetic Agonist 1, see **Fig. 1.5**), which differs by a single C=C double bound (Shen, Wang et al. 2012). ML-SA1 activated TRPML1 with higher potency than SF-51, and was shown to be able to activate endogenous TRPML1 in cell biology assays (Shen, Wang et al. 2012, Samie, Wang et al. 2013). Newer agonists, named after the ML-SA series, ML-SA3 and ML-SA5, have been identified since, with different structures than ML-SA1 and even higher potency (Wang, Gao et al. 2015).

Artificial antagonists of TRPML1, ML-SI1 and ML-SI3 (**Fig. 1.5**), were identified through similar screens with similar potency to the ML-SA agonists, but instead inhibited the channel (Samie, Wang et al. 2013, Cheng, Zhang et al. 2014). The regions of the channel responsible for the interaction with the agonists/antagonists, however, have not been mapped yet.

1.3.3 TRPML1 has important functions in lysosome membrane trafficking

Indications of TRPML1 in lysosome membrane trafficking came along with the characterization of the symptoms of MLIV, the genetic disease caused by the loss of TRPML1 activity (Nilius, Owsianik et al. 2007, Wakabayashi, Gustafson et al. 2011). MLIV patients exhibit early onset of neurodegeneration and psychomotor defects, which are canonical symptoms for lysosome storage diseases (Wakabayashi, Gustafson et al. 2011). At cellular level, MLIV patient fibroblasts or TRPML1 knockout (ML1KO hereafter) mouse fibroblasts exhibit enlarged LELs, accumulation of autophagosomes, and accumulation of lipids such as cholesterol and lactosylceramide in the lysosomes (Pagano, Puri et al. 2000, Cheng, Shen et al. 2010). These phenotypes are all in line with dysfunctionality in the lysosomal trafficking pathway.

Numerous studies have been done on TRPML1 to figure out the role it plays in regulating lysosomes. Early qualitative analyses have shown phenotypes suggesting delayed lysosome-to-Golgi transport (Pryor, Reimann et al. 2006), delayed autophagosome delivery to the lysosome (Curcio-Morelli, Charles et al. 2010), hyperacidified lysosome lumen (Soyombo, Tjon-Kon-Sang et al. 2006) and accumulation of some ions like Fe^{2+} and Zn^{2+} in the lysosomes (Dong, Cheng et al. 2008, Eichelsdoerfer, Evans et al. 2010). These studies, however, did not provide detailed mechanisms as to how TRPML1 functions to regulate these aspects. For example, delayed lysosome-to-Golgi transport indicates defects in lysosome membrane fission (the generation of retrograde transport vesicles); delayed autophagosome delivery to the lysosome indicates defects in lysosome and autophagosome fusion. But how could TRPML1 regulate the fusion and fission of lysosomes together? And which are the upstream and downstream molecules regarding

TRPML1 in both processes? Questions like these were not answered in early studies, mostly due to the lack of proper tools (such as agonists and antagonists) and insufficient knowledge about the protein *per se*.

More recent studies, especially after the characterization of the artificial agonists and antagonists, were more effective and definitive in dissecting TRPML1's roles. Two notable studies carried out in the Xu lab have identified TRPML1's roles in Ca^{2+} mediated lysosome exocytosis with great detail and also identified some of the downstream targets.

The first paper, published by Samie et al. in 2013 on Developmental Cell (Samie, Wang et al. 2013), reported that TRPML1 regulates lysosome exocytosis during phagocytosis of large particles. The concept is that during phagocytosis, a large part of the plasma membrane is engulfed as phagosome and lost from the plasma membrane. In order to maintain plasma membrane amount, endocytic vesicles would fuse with plasma membrane upon activation of the phagocytosis pathway, right before the actual phagocytosis takes place. It was shown earlier that while endosomes participate in small particle phagocytosis, lysosomes participate in the phagocytosis of large particles (>3 μm).

Samie et al. showed that TRPML1 is required for the phagocytosis to proceed through promotion of Ca^{2+} regulated lysosome exocytosis. It is shown that upon particle recognition, lysosomes are trafficked to the particle contact site and $PI(3,5)P_2$ levels increase, allowing TRPML1 to be activated. Ca^{2+} release from TRPML1 then activated the lysosomal Ca^{2+} sensor synaptotagmin VII (Syt VII) to trigger lysosome exocytosis (**Fig. 1.6**).

This study represents the first report regarding TRPML1's mechanism of action in lysosome membrane trafficking steps. A year later, Cheng et al. published a report on Nature

Medicine (Cheng, Zhang et al. 2014) describing a similar Ca^{2+}- and TRPML1-dependent regulation of lysosome exocytosis that is required in sarcolemma membrane damage repair. The report showed that the muscular dystrophy phenotype observed in ML1KO mice is muscle-primary and is due to the impaired membrane repair upon membrane damage (which happens very often in skeletal muscles). It is shown that TRPML1 is required for this process, promoting lysosome exocytosis after membrane damage to repair the damage site. Boosting up TRPML1 activity through viral infection is also shown to exhibit rescue effects on muscular dystrophy in mdx mice, the mouse model of muscular dystrophy (Cooper 1989).

In 2015, Dayam et al. reported an additional role of TRPML1 in membrane fusion (Dayam, Saric et al. 2015), being required for the phagosome and lysosome fusion after phagocytosis (**Fig. 1.6**). It is shown that in TRPML1 knockdown RAW macrophages, or in these cells treated with the $PI(3,5)P_2$ synthesis inhibitor, Apilimod, as well as the membrane permeable, fast Ca^{2+} chelator, BAPTA-AM, the fusion between phagosomes and lysosomes is significantly delayed. However, no detailed mechanism is tested or speculated.

1.4 The goal of the study

Previous studies, especially the several recent reports described above, have clearly shown that TRPML1 regulates lysosome membrane trafficking, notably the fusion between lysosomal membrane and other intracellular membranes. Some insights about the mechanisms of the TRPML1-Ca^{2+} regulatory pathway of lysosomal membrane fusion have also been provided. These findings, however, cannot fully account for all the phenotypes seen with ML1KO and MLIV patient cells. Especially, the observed phenotype of enlarged late endocytic vesicles seen

in ML1KO and MLIV cells cannot be explained by any of the above findings. The perinuclear localization of the LEL vesicles seen in ML1KO cells, as well as in cells *overexpressing* TRPML1, is also puzzling at this point.

Seeing these apparent blanks in our understandings towards TRPML1's functions, I aim to investigate TRPML1's functions apart from Ca^{2+}-regulated membrane fusion (**Fig. 1.6**). The first goal was to identify TRPML1's role in regulating the motility of lysosomes (Chapter II), and its downstream target(s) along the pathway (Chapter III). The second goal was to examine TRPML1's role in lysosome membrane fission, using the model of lysosome reformation under prolonged starvation or active phagocytosis (Chapter IV). In addition to these main questions, I also developed a genetically encoded $PI(3,5)P_2$ biosensor, which was published and has already been used in multiple studies (Chapter V).

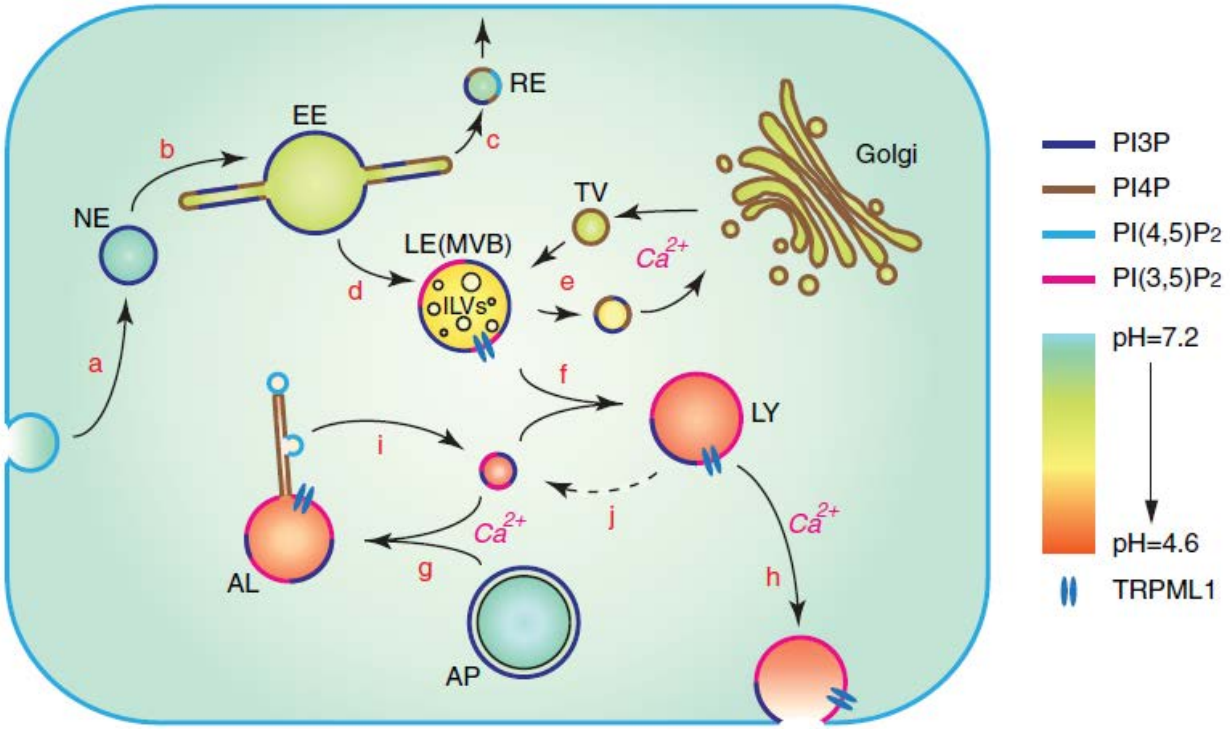

Fig. 1.1 The endocytic trafficking network.

A schematic view of the endocytic trafficking network in animal cells. Luminal pH and dominant phosphoinositides of each compartments are labeled with different colors. During endocytosis, a piece of the plasma membrane is excised and enters the cytosol in the form of a nascent endosome (NE; a). Nascent endosomes fuse with each other (b) and recruit early endosomal proteins to become early endosomes (EE; b). Membrane receptors are sorted and recycled back to the plasma membrane through recycling endosomes (RE; c). Material destined for degradation is passed on to the late endosomes (LE; d), which are also referred to as multi-vesicular bodies (MVB) due to the intraluminal vesicles (ILVs) that contain membrane proteins sorted for degradation. Hydrolytic enzymes are transported to late endosomes through transport vesicles (TV) from Golgi (e). Membrane receptors carrying the enzymes are shuttled back to Golgi through retrograde transport. Late endosomes mature into lysosomes (LY) either through further acidification, or through fusion with existing lysosomes (f). During starvation or when organelles are damaged, lysosomes also accept cargo from autophagosomes (AP) carrying damaged organelles or cytosolic material for degradation (g). The resulting autophagic lysosomes (AL) are usually larger than endocytic lysosomes. Lysosomes can undergo Ca2+-dependent exocytosis (h). Lysosomal membrane proteins are recycled from autophagic lysosomes by fission processes that happen on tubular structures (i). The mechanism of recycling of membrane proteins from endocytic lysosomes has yet to be established (j).

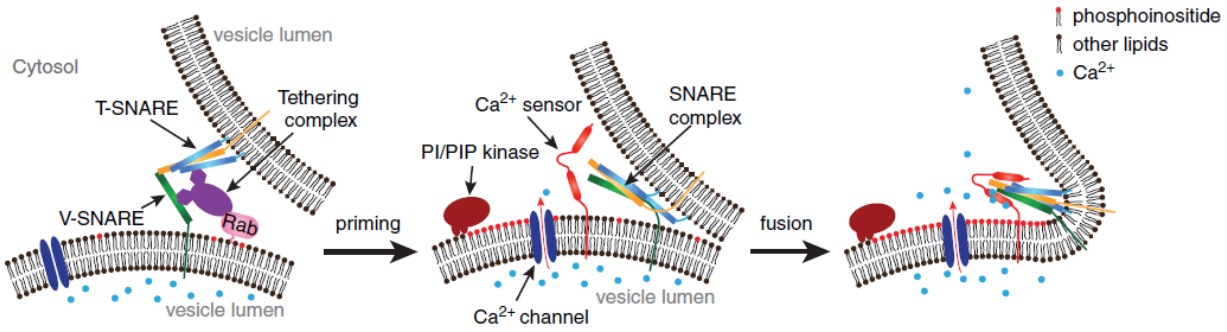

Fig. 1.2 A proposed model of Ca^{2+}-release-regulated lysosomal membrane fusion.

The initiation of vesicle fusion is coordinated by Rab protein and tethering complexes that mediate the assembly of SNAREs (left). After SNARE assembly, lysosome is in a ready-to-fuse state. Upon signaling, $PI(3,5)P_2$ is produced on the lysosomal membrane, leading to Ca^{2+} release (middle), which binds to the Ca^{2+} sensor, likely Synaptotagmin VII, to complete the fusion (right).

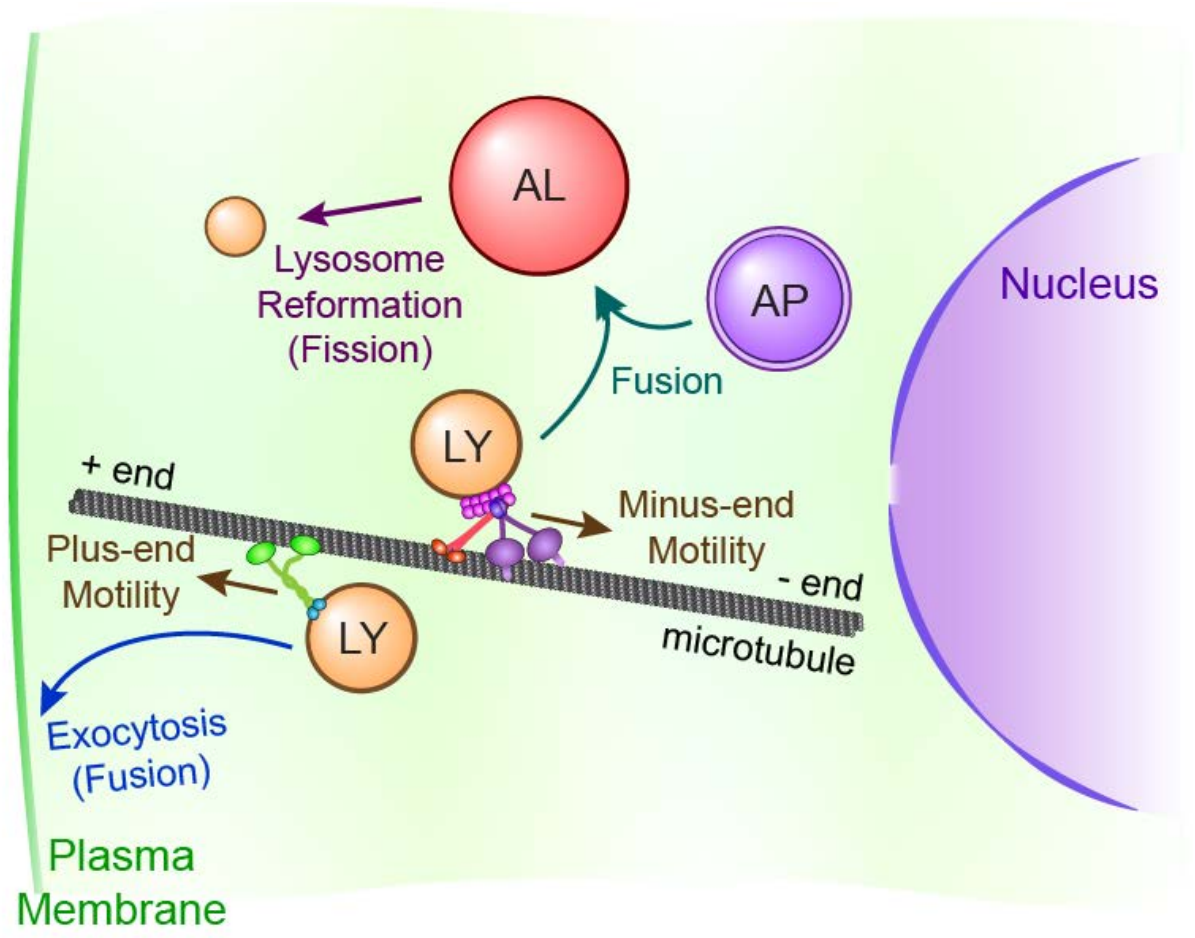

Fig. 1.3 Three major aspects about lysosome membrane trafficking.

In cells, lysosomes undergo microtubule-based directional transport (brown arrows) to their destination, where they can fuse with cargo vesicles (green arrows) or undergo lysosomal exocytosis (blue arrow). After completion of cargo fusion, secondary lysosomes can undergo membrane fission (purple arrow) to recycle membrane components for the generation of new lysosomes. LY: lysosome; AP: autophagosome; AL: autolysosome.

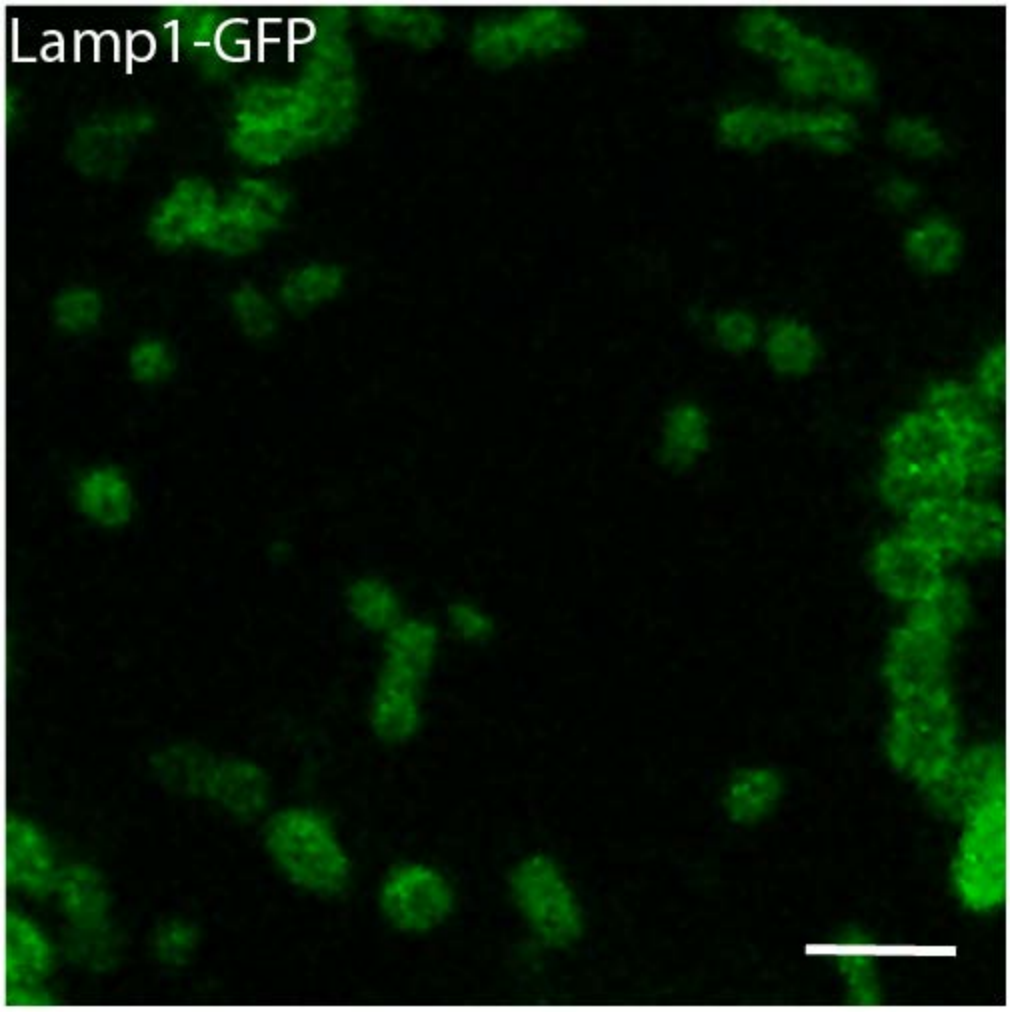

Fig. 1.4 Lysosome size revealed by super-resolution microscopy.

Mouse fibroblast transfected with Lamp1-GFP was subject to live imaging using STED super-resolution microscopy 2 days post-transfection. Lysosomes appeared to be of variable sizes, but generally smaller than 1 μm. Scale bar = 1 μm.

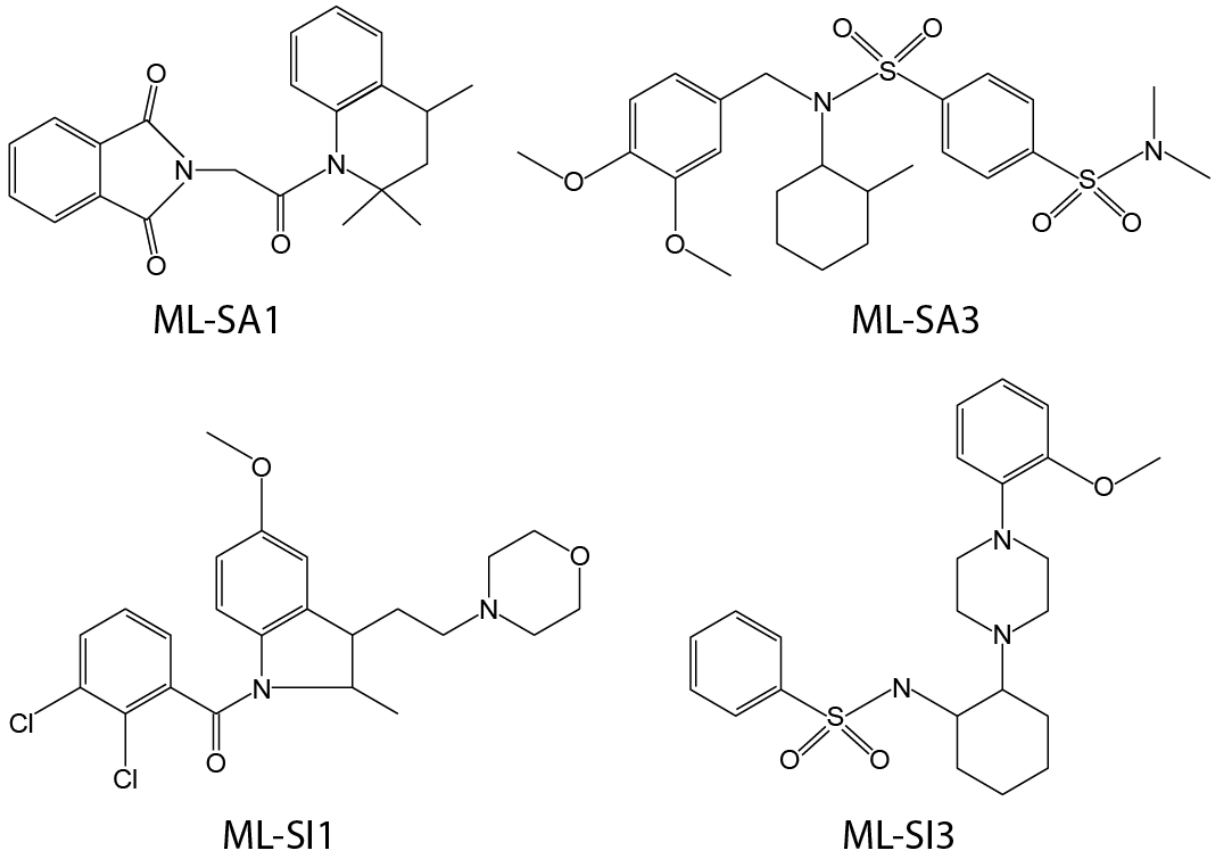

Fig. 1.5 The structures of synthetic agonists and antagonists of TRPML1.

Chemical structures of the ML-SAs and ML-SIs used. Each agonist/antagonist is structurally independent of other molecules.

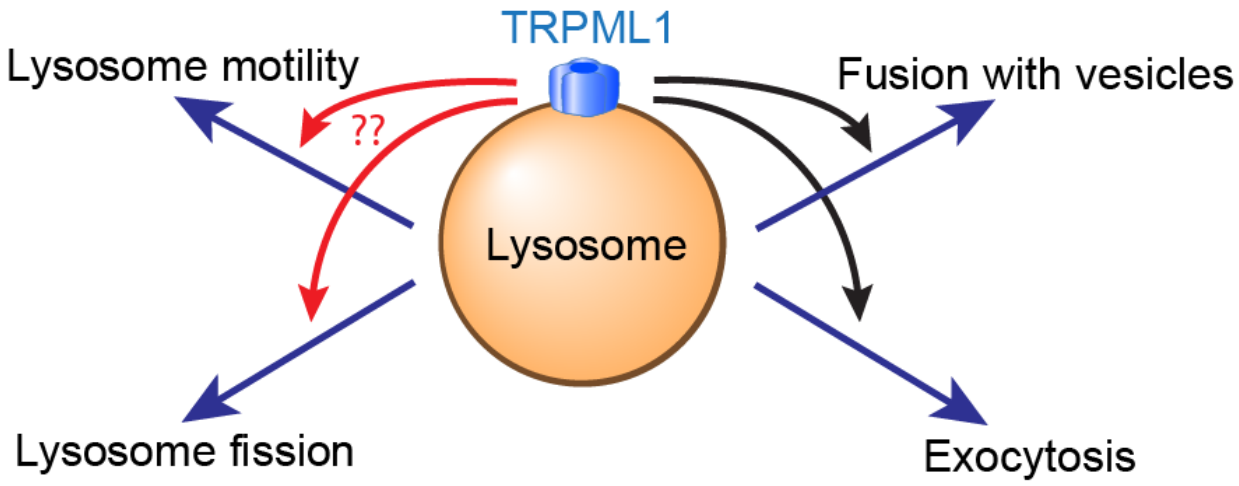

Fig. 1.6 The goal of the study is to identify new roles of TRPML1 in regulating lysosome membrane trafficking.

TRPML1 has been shown to regulate lysosome exocytosis and fusion with phagosomes through its Ca^{2+} release (black arrows). It remains to be tested whether TRPML1 also regulates other aspects of lysosome membrane trafficking, namely lysosome motility and lysosome fission (red arrows).

CHAPTER II

TRPML1 Mediates Retrograde Transport of Lysosomes Independent of the Rab7-RILP-ORP1L Pathway[2]

2.1 Abstract

Lysosome motility is crucial to its functions inside the cell. Directional movement of lysosomes in animal cells is carried out through microtubule-based motor proteins, with kinesin-1 responsible for the plus-end directed movements towards cell peripheral, and cytoplasmic dynein responsible for the minus-end directed movements towards the microtubule-organizing center (MTOC) close to the nucleus. Dynein-mediated minus-end movement of lysosomes has been shown to be mediated by Rab7 and its effector RILP, with the lysosomal cholesterol sensor ORP1L facilitating this process. Here I report an on-demand pathway that drives minus-end directed lysosome movement in response to cellular cues such as acute starvation, mTOR inhibition, or elevated cytosolic pH. TRPML1, a lysosomal Ca^{2+} permeable channel, is shown to mediate this novel retrograde transport of lysosomes independent of the previously described Rab7-RILP pathway.

[2] Originally Submitted in Nature Cell Biology. With authors listed as Xinran Li, Nicholas Rydzewski, Ahmad Hider, Xiaoli Zhang, Junsheng Yang, Wuyang Wang, Qiong Gao, Xiping Cheng, and Haoxing Xu.

2.2 Introduction

Lysosomes serve as the degradation and nutrient sensing center of animal cells. Lysosomes accept cargo through fusion with various cargo-delivery vesicles including endosomes, autophagosomes and phagosomes, and undergo lysosome reformation afterwards. The membrane fusion and fission of lysosomes would require the ability to move directionally inside the cells. Lysosome motility relies on microtubule-based motor proteins, and the direction of the movement is determined by the motor proteins attached to lysosomes (Rosa-Ferreira and Munro 2011, Tan, Scherer et al. 2011).

Previous researches characterized the important functions of Rab7 and its effector protein, RILP, in promoting minus-end (i.e. retrograde) transport of lysosomes (Jordens, Fernandez-Borja et al. 2001, Johansson, Rocha et al. 2007, Rocha, Kuijl et al. 2009, van der Kant, Fish et al. 2013). Rab7 and RILP interact with the dynein adaptor complex dynactin to bring the motor protein to the lysosome surface (Jordens, Fernandez-Borja et al. 2001). Recent researches also showed that this process requires the cooperation from the lysosomal cholesterol sensor ORP1L (Johansson, Rocha et al. 2007, Rocha, Kuijl et al. 2009, van der Kant, Fish et al. 2013).

Consistent with previous findings, the constitutively active Rab7, Rab7-Q67L, which is locked in its GTP-bound state, can induce perinuclearly-localized lysosomes (Bucci, Thomsen et al. 2000). Similar phenotype is observed for RILP overexpression (Cantalupo, Alifano et al. 2001). This perinuclear localization of lysosomes is most likely caused by the excessive recruitment of dynein that outcompetes kinesin and drags all lysosomes towards the MTOC. On the other hand, overexpression of the dominant negative form of Rab7, Rab7-T22N, induces dispersal of lysosomes towards the peripheral areas of the cell (Bucci, Thomsen et al. 2000,

Cantalupo, Alifano et al. 2001). Therefore, manipulation of the activity of the Rab7-RILP pathway can dictate the intracellular distribution of lysosomes.

An important thing to point out, though, is that all previous researches characterizing retrograde transport of lysosomes were carried out with cells under normal, unstressed conditions. It is now known that lysosomes can undergo rapid changes in their distribution facing urgent conditions, e.g. upon deprivation of serum factors or amino acids (Korolchuk, Saiki et al. 2011). Under such conditions, lysosomes very rapidly (within an hour) get recruited to the perinuclear region where they fuse with autophagosomes to complete autophagy. Under such acute conditions, it is unlikely that lysosome cholesterol levels, therefore ORP1L levels, would undergo dramatic changes. Therefore, it remains unclear whether such shifts in lysosome distribution are mediated through the same regulatory machinery.

Prior to this study, there were already indications that TRPML1 might play a role in regulating lysosome positions. It was noticed that in both ML1KO cells and TRPML1 overexpressing cells, lysosomes appeared to be perinuclear (Vergarajauregui, Martina et al. 2009, Wakabayashi, Gustafson et al. 2011). However, such contradictory results were hard to analyze or come up with a model to explain. Due to the recent characterization of small molecule agonists and antagonists of TRPML1, I now possess the tools for us to determine the role of TRPML1 in regulating lysosome positioning through acute manipulation of its activity.

2.3 Results

2.3.1 TRPML1 is necessary for the on-demand retrograde transport of lysosomes towards microtubule organizing center

To investigate the role of TRPML1 in lysosome positioning, I utilized a wide variety of mammalian cells, including Cos1, HeLa, and primary mouse fibroblasts. This is to check if the phenomena I observe are due to cell type-specific effects or represent a more general function. To monitor the distribution of late endosomes and lysosomes (LEL, hereafter all referred to as lysosomes for simplicity), I utilized multiple methods of labeling including lysotracker, fluorescently-labeled dextran, and GFP/mCherry fused to the cytosolic C-terminal of Lamp1, a canonical lysosome marker (**Fig. 2.1a, 2.1b**). Lysotracker is a dye that is membrane permeable under normal pH, but becomes membrane impermeable when protonated under acidic pH, producing concentrated fluorescence in very acidic organelles (see Materials and Methods). Fluorescently-labeled dextrans (Oregon-green or tetramethylrhodamine for green and red colors, respectively) are non-digestible polysaccharides that enter the lysosomes through endocytosis. Since lysotracker fluorescence is dependent on luminal pH, while dextran labeling requires active endocytosis and efficient delivery of endocytic vesicles to the lysosomes, both of which are not ensured under experimental conditions that I study, I choose to use Lamp1 as the lysosome marker in the majority of the experiments.

Under normal conditions, lysosomes were scattered throughout the cytoplasm, showing a dispersed pattern (**Fig. 2.1 & 2.2**). Upon serum starvation, autophagy is triggered, indicated by the generation of autophagosomes that are labeled with LC3 (**Fig. 2.3a**). LC3 (ATG8 in yeast) is a small protein that attaches to the autophagosome membrane during autophagosome elongation (Olivier, Proulx et al. 1989). The attachment of LC3 to the autophagosome membrane requires a cleavage on its C-terminal by ATG4 to expose its Glycine residue, which is used to conjugate to phosphatidylethanolamine on the autophagosome membrane (Ichimura, Kirisako et al. 2000). Therefore, mature LC3 (LC3-II) shows a smaller apparent protein mass in western blots than

immature LC3 (LC3-I) (usually from ~16 kDa to ~14 kDa). When attached to tandem fluorephores of GFP and RFP, LC3 can also serve as an indicator of autophagosomes versus autolysosomes (Kimura, Noda et al. 2007), with autophagosomes showing fluorescence in both green and red channels, while autolysosomes showing only red fluorescence due to the quench of GFP signal by acidic pH.

The accumulation of autophagosomes is most prominent at the perinuclear regions (**Fig. 2.3a**). Consistent with recent reports (Thoreen, Kang et al. 2009, Korolchuk, Saiki et al. 2011), upon starvation, a rapid redistribution of lysosomes towards the perinuclear regions was seen (**Fig. 2.1b, 2.2a-c, 2.2f**). More specifically, the lysosomes were recruited close to the MTOC (**Fig. 2.3b**). The redistribution of lysosomes is thought to promote the fusion between lysosomes and autophagosomes. This is supported by the fact that the perinuclear Lamp1-positive vesicles seen in starved cells were of a larger size compared to fed cells (**Fig. 2.2a, 2.2b, insets**), suggesting that these vesicles were secondary lysosomes, most likely autolysosomes.

Torin-1 is a potent ATP-competitive mTOR inhibitor that can trigger autophagy through inhibition of mTORC1 (Thoreen, Kang et al. 2009). Under Torin-1 treatment, lysosomes also underwent a redistribution to the perinuclear region (**Fig. 2.2e, 2.2g**), consistent with the hypothesis that the redistribution is for the fusion between lysosomes and autophagosomes.

To better understand the kinetics of the redistribution of lysosomes, I proceeded to analyze the directional movement of lysosomes using fluorescence recovery after photobleaching (FRAP). Under normal conditions, the amount of lysosomes traveling towards the plus-end or towards the minus-end of microtubules showed no significant differences, although generally slightly more lysosomes were moving towards the minus-end (**Fig. 2.4a, 2.4d**). Acute starvation

(within 30 minutes) triggered a selective increase of lysosomes trafficking towards the minus-end (i.e. MTOC), without affecting the amount of lysosomes trafficking to the other direction (**Fig. 2.4b, 2.4d**). This result clearly suggests that starvation promotes perinuclear migration of lysosomes through the up-regulation of the minus-end motility, but not the suppression of the plus-end motility.

The motility of lysosomes trafficking towards both directions was greatly reduced under BAPTA-AM treatment, a fast, membrane permeable Ca^{2+} chelator (Data not shown). Thus, Ca^{2+} is important in regulating lysosome motility. TRPML1 is a Ca^{2+} release channel on the lysosome. I therefore tested whether TRPML1 plays specific roles in the regulation of lysosome motility utilizing synthetic agonists/antagonists to acutely manipulate TRPML1 activity (**Fig. 2.5a**). The benefit of using synthetic molecules, compared to the traditional ML1KO/shRNA/RNAi methods, is to get rid of the interference of secondary effects, such as accumulation of lysosome lipids, caused by the chronic inhibition of TRPML1.

To test whether TRPML1 plays a role in the promotion of perinuclear migration of lysosomes under acute starvation, I used two structurally unrelated TRPML1 inhibitors, ML-SI1 and ML-SI3 (Samie, Wang et al. 2013). Both inhibitors were able to block the perinuclear accumulation of lysosomes under starvation (**Fig. 2.2a, 2.2b, 2.2d, 2.2f**), suggesting that TRPML1 activity is required for the process. Likewise, the perinuclear migration of lysosomes under Torin-1 treatment was also suppressed through TRPML1 inhibition (**Fig. 2.2e, 2.2g**). Interestingly, inhibition of TRPML1 during short term starvation also led to the accumulation of autophagosomes not fused with lysosomes, indicated by GFP-RFP-LC3 (**Fig. 2.6**). This would suggest that TRPML1 activity is also required for the sufficient delivery of autophagosomes to lysosomes.

Consistent with the effects on lysosome distribution, FRAP analysis showed that the elevated retrograde transport of lysosomes under starvation was blocked by TRPML1 inhibition (**Fig. 2.4c, 2.4d**). Therefore, TRPML1 activity might be selectively required for the up-regulation of the minus-end directed motility of lysosomes. It is worth noting, however, that inhibition of TRPML1 under normal conditions had only a subtle effect on lysosome distribution (**Fig. 2.2d, 2.2f**). Moreover, FRAP assay showed that inhibition of TRPML1 did not suppress all lysosome movements towards the minus-end under starvation, but rather only brought it down to pre-starvation levels (**Fig. 2.4d**). This suggests that TRPML1 is only responsible for the on-demand up-regulation of the minus-end motility of lysosomes, but plays little role in regulating housekeeping retrograde transport of lysosomes.

Starvation is shown to cause a quick elevation in cytosolic pH, reportedly from 7.1 to 7.7 within 45 minutes in HeLa cells (Korolchuk, Saiki et al. 2011). Alkalization of the cytosol is sufficient to induce perinuclear migration of lysosomes (Heuser 1989). Whole-endolysosomal TRPML1 currents were also facilitated by alkaline cytosolic pH and inhibited by acidic cytosolic pH (**Fig. 2.5b**). TRPML1 inhibition also suppressed the migration of lysosomes towards the perinuclear region under cytosolic alkalization (**Fig. 2.7a-c**), driven by the treatment of Ammonia Ringer's solution (see Methods part for the recipe). Despite the apparent starvation caused by switching to the Ammonia Ringer's, mTORC1 activity remained relatively unaffected during the treatment period (30 min), suggesting that the process is not mediated through mTOR inhibition (**Fig. 2.7d**).

Collectively, the above data suggest that TRPML1 activity is required to drive the on-demand retrograde migration of lysosomes in response to acute conditions such as autophagy induction or cytosolic alkalization.

2.3.2 TRPML1 activation is sufficient to promote Ca^{2+}-dependent retrograde transport of lysosomes

Having confirmed the necessity of TRPML1 in the process, I proceeded to test whether artificial activation of TRPML1 is sufficient to up-regulate the retrograde transport of lysosomes. When HeLa cells, Cos1 cells, or WT mouse fibroblasts were treated with a synthetic TRPML1 agonist, ML-SA1, lysosomes were apparently much more perinuclear (**Fig. 2.8a-c, 2.8g**). Similar perinuclear localization was observed in fibroblasts treated with two other structurally-unrelated TRPML1 agonists, ML-SA3 and ML-SA5 (Wang, Gao et al. 2015) (**Fig. 2.9a**), suggesting that the effect seen with ML-SA1 was specific to TRPML1 activation. Overexpression of TRPML1, but not the other two TRPML family members TRPML2 and TRPML3, also resulted in the perinuclear accumulation of lysosomes (**Fig. 2.8d, 2.8g, 2.9b-e**). Therefore, activation of TRPML1 is already sufficient to induce perinuclear localization of lysosomes. The effects of TRPML1 overexpression on lysosome re-distribution can be reversed by either the application of BAPTA-AM, or by the TRPML1 inhibitors (**Fig. 2.8e, 2.8f, 2.8i**).

In FRAP analyses, as well as time-lapse imaging, acute application of ML-SA1 (within 30 minutes) increased the minus-end directed migration of lysosomes selectively and significantly (**Fig. 2.10a-c**). Conversely, time-lapse imaging showed that ML-SI3 resulted in the dispersal of lysosomes in TRPML1 overexpressing fibroblasts, an effect opposite to ML-SA1 (**Fig. 2.10d**). To test organelle specificity, the distribution of mitochondria was compare with or without ML-SA1 application, which showed no difference (**Fig. 2.11**). Collectively, these results

suggest that TRPML1 activation is sufficient to up-regulate retrograde transport and the perinuclear accumulation of lysosomes.

2.3.3 Chronic effects of cholesterol accumulation on lysosome distribution

It is known that lysosomes are distributed perinuclearly in many LSD cells (Samie and Xu 2014, Xu and Ren 2015). ML1KO mouse fibroblasts display similar perinuclear lysosome localization (**Fig. 2.12**). This distribution, however, is opposite to that seen with transient inhibition of TRPML1 shown above. To mimic the chronic loss of TRPML1 activity in ML1KO cells, we treated WT fibroblasts with increased lengths of TRPML1 inhibitors under complete medium. Within 6 hours, inhibition of TRPML1 did not result in significant difference in lysosome distribution compared to untreated cells. Longer treatments (from 18 hours up to 48 hours) resulted in progressively more perinuclear lysosome distribution (**Fig. 2.13a-c**). Therefore, some properties must be different between transient and long-term inhibition of TRPML1 that lead to the differences in the lysosome distribution.

One thing that is different between short term inhibition of TRPML1 and long term loss of TRPML1 activity is the secondary accumulation of lysosomal substances due to defective trafficking (Pagano, Puri et al. 2000, Samie and Xu 2014). Importantly, a variety of membrane lipids including cholesterol are known to accumulate in lysosomes in ML1KO cells. Given the established role of lysosomal cholesterol and its sensor ORP1L in promoting minus-end motility of lysosomes in cooperation with Rab7 and RILP (Johansson, Rocha et al. 2007, Rocha, Kuijl et al. 2009), I designed experiments to test whether cholesterol accumulation could account for the abnormal lysosome distribution observed in ML1KO cells and other LSD cells.

First of all, using filipin staining, which stains unesterified free cholesterol, I confirmed that significant elevation of lysosomal cholesterol was observed in ML1KO fibroblasts, as well as in WT fibroblasts that were treated with the TRPML1 inhibitor ML-SI3 for a long period (1 day), but not in WT fibroblasts treated with a short period (1 hour) of ML-SI3 (**Fig. 2.14a, 2.14b, 2.14d**). Hence, the degree of cholesterol accumulation in these cells corresponds well with the degree of perinuclear distribution of lysosomes observed. Fibroblasts from NPC1 (Niemann-Pick type C1 protein) knockout mouse, the mouse model for the human cholesterol storage disease Niemann-Pick type C (Reid, Sugii et al. 2003, Kwiatkowska, Marszalek-Sadowska et al. 2014), were used as a positive control for cholesterol accumulation (**Fig. 2.14c, 2.14d**). It is noticeable that the accumulated cholesterol, which co-localize well with Lamp1 (**Fig. 2.14f**), showed primarily perinuclear distribution in these conditions (**Fig. 2.14**).

Intracellular accumulation of cholesterol can be reduced using the statin class drugs to inhibit cholesterol synthesis, while depleting extracellular cholesterol. I utilized one of such drugs, simvastatin (Rocha, Kuijl et al. 2009), in combination with serum depletion (because Fetal Bovine Serum used in cell culture contains liposomes positive for cholesterol) to remove lysosomal cholesterol. Filipin staining in cells treated with simvastatin clearly showed a significant decrease in cholesterol levels in ML1KO, NPCKO, but not in WT fibroblasts (**Fig. 2.14a-c, 2.14e**). The reduction of cholesterol resulted in more peripherally-localized lysosomes in ML1KO fibroblasts and NPCKO fibroblasts (**Fig. 2.12a-d**). In NPCKO fibroblasts, co-application of ML-SI3 resulted in a further shift of lysosomes to the peripheral, due to the activation of TRPML1 under serum starvation conditions I used for cholesterol depletion (**Fig. 2.12c, 2.12d**). In contrast, cholesterol depletion in WT fibroblasts did not result in significant changes in the lysosome distribution under starvation (**Fig. 2.12e, 2.12f**). These results suggest

that the perinuclear lysosome distribution in ML1KO, NPCKO, and probably in other LSD cells is caused by the excessive accumulation of cholesterol independent of TRPML1. The data also suggest that the lysosome distribution under starvation, on the other hand, is mainly dependent on TRPML1 activation, but not cholesterol.

2.3.4 TRPML1 promotes retrograde trafficking of lysosomes independent of the Rab7-RILP pathway

Cholesterol is known to promote retrograde transport of lysosomes through ORP1L's cooperation with Rab7 and RILP (Johansson, Rocha et al. 2007, Rocha, Kuijl et al. 2009). To further test the relationship between TRPML1's role in lysosome motility and the Rab7-RILP pathway, I manipulated the activity of the two pathways to observe their influence on each other. In WT fibroblasts, overexpression of the constitutively active form of Rab7, Rab7-Q67L (Spinosa, Progida et al. 2008), as well as overexpression of the Rab7 effector RILP (Cantalupo, Alifano et al. 2001), resulted in perinuclear accumulation of lysosomes (**Fig. 2.15a-d**). This lysosome distribution was unaffected with the inhibition of TRPML1 through ML-SI3 (**Fig. 2.15a-d**), suggesting that TRPML1 is not downstream of either Rab7 or RILP.

The dominant negative form of Rab7, Rab7-T22N, is known to cause dispersal of lysosomes to the peripheral of cells by inhibition of the Rab7-RILP pathway (Bucci, Thomsen et al. 2000, Cantalupo, Alifano et al. 2001). Overexpression of the Rab7-T22N construct in ML1KO fibroblasts (**Fig. 2.16c, 2.16d**), or in WT fibroblasts treated with ML-SI3 for 18 hours (**Fig. 2.13d**) redistributed the lysosomes to the peripheral, confirming that the perinuclear distribution of the lysosomes in these cells is caused by the Rab7 pathway. Overexpression of

Rab7-T22N, however, did not suppress the retrograde migration of lysosomes under acute starvation, or short-term application of ML-SA1 (**Fig. 2.16a, 2.16b**). These data suggest that the Rab7-RILP pathway is also not downstream of TRPML1. Therefore, TRPML1 regulates lysosome motility independent of the Rab7-RILP pathway.

2.4 Discussion

Lysosome motility is important for the functions of lysosomes in cargo degradation, lysosome exocytosis, and nutrient sensing. The canonical Rab7-RILP pathway demonstrates how lysosomes are transported along the microtubule towards the minus-end, i.e. retrograde transport, under normal conditions. It remained to test whether lysosomes adopt the same mechanism for their retrograde movement under acute situations like starvation.

In the first part of my study, I showed that the lysosomal Ca^{2+} release channel, TRPML1, participates in the up-regulation of retrograde motility of lysosomes under acute starvation, mTOR inhibition and cytosolic alkalization. To be specific, TRPML1 activity is required for the additional retrograde transport of lysosomes under the described conditions, and artificial activation of TRPML1 itself is sufficient to accumulate lysosomes at the perinuclear region. I have also showed that TRPML1 regulates this process through its role as a Ca^{2+} release channel.

The conclusion that TRPML1 up-regulates retrograde transport of lysosomes to promote perinuclear accumulation of lysosomes is mainly based on the FRAP assay. Although the data are clear and strong, similar to most assays, this assay is not 100% conclusive. One thing to note is that although microtubules often have their minus ends close to the MTOC, and their plus ends reaching out to the peripheral, they sometimes do wind and/or turn backwards. This means that

occasionally a lysosome may travel towards the plus end, but retrogradely towards the nucleus, or vice versa. Co-expression of fluorescently-tagged tubulins may solve this uncertainty. However, this complexity does not impact on the conclusion that TRPML1 promotes retrograde transport of lysosomes, since retrograde transport is defined as the transport towards the perinuclear region irrelevant to the polarity of the microtubules.

One thing that I noticed during the FRAP assay, is that under all experimental conditions tested, the majority of the lysosomes remained immotile, moving very little distances towards any direction. Therefore, it is worthy to test whether the activation of TRPML1 turns immotile lysosomes into motile lysosomes, or switches the direction of movement of those already motile lysosomes, or both? The data of the FRAP assay show an increase of the net number of moving lysosomes under TRPML1 activation or under starvation (**Fig. 2.4 & 2.10**), apparently suggesting that TRPML1 activation is able to turn immotile lysosomes into motile, retrogradely moving lysosomes, but is not sufficient to tell whether TRPML1 activation can switch the direction of the already moving lysosomes. One follow-up experiment available to test this is to use photo-convertible fluorescent protein tagged markers to label lysosomes. This would allow tracking of single lysosomes' trafficking status, thus enable us to monitor if there's direction switch of lysosomes under TRPML1 activation.

It remains an interesting question whether starvation, mTOR inhibition and cytosolic alkalization converge and share the same mechanism to activate the TRPML1 pathway. It is known that cytosolic pH is elevated under acute starvation, likely caused by the acidification of autolysosomes which requires a lot of protons (Korolchuk, Saiki et al. 2011, Mauvezin and Neufeld 2015). If this is true, mTOR inhibition should have a similar effect to starvation in causing elevation of cytosolic pH. Therefore, starvation and mTOR inhibition may affect

lysosome motility through cytosolic alkalization. However, one drawback of this hypothesis is that luminal acidification of autolysosomes does not occur until the fusion between lysosomes and autophagosomes happen, which in the current understanding is the purpose of retrograde transport of lysosomes *per se*. It is also possible that starvation or mTOR inhibition use other mechanisms to initiate the retrograde transport of lysosomes, and the cytosolic alkalization generated after the formation of autolysosomes serves as a positive feedback.

Perinuclear lysosome distribution, as mentioned above, is observed in many LSD cells, including ML1KO (Samie and Xu 2014, Xu and Ren 2015). I have shown here that this phenotype is likely caused by cholesterol accumulation in the LSD cells, and that this perinuclear distribution of lysosomes is caused by the activation of the Rab7-RILP pathway, independent of TRPML1.

On top of the above finding, I characterized the relationship between TRPML1 and the Rab7-RILP pathway. Through experiments with constitutively active and dominant negative constructs, I found that the TRPML1 pathway and the Rab7-RILP pathway are independent of each other, and my data suggest a model where they form complementary pathways. Under normal conditions, TRPML1 remains mainly inactive. Endocytic vesicles acquire cholesterol from the plasma membrane or endocytosed liposomes that aid the Rab7-RILP pathway to transport the lysosomes towards MTOC in a constitutive manner. Under urgent needs, cells use the other pathway, through TRPML1 activation, to cause rapid retrograde transport of lysosomes.

2.5 Materials and Methods

DNA subcloning

GFP-TRPML1, Lamp1-GFP and Lamp1-mCherry constructs were generated as described previously (Li, Wang et al. 2013). RILP-GFP was provided by Dr. Roberto Botelho (Ryerson University, Toronto). Rab7-T22N-GFP and Rab7-Q67L-GFP mutants were generated with a site-directed mutagenesis kit. All constructs were verified with sequencing.

Mouse lines

Characterizations of TRPML1 and NPC1 KO mice were described previously (Venugopal, Browning et al. 2007, Shen, Wang et al. 2012). Animals were used under approved animal protocols and the Institutional Animal Care Guidelines of the University of Michigan.

Mammalian cell culture and transfection

Mammalian cells were cultured in a 37 °C, 5% CO_2 incubator. Mouse fibroblasts were isolated and cultured as previously described (Li, Wang et al. 2013). Immortalized cell lines (Cos1 and HeLa) were originated from ATCC and cultured following standard tissue culture protocols. Unless indicated, all cells were cultured in Dulbecco's Modified Eagle Medium (DMEM, Invitrogen) supplemented with 10% FBS (Gemini and Sigma). For fibroblasts, transfection was performed using the Neon electroporation kit (Invitrogen). All other cells were transfected with Lipofectamine 2000 (Invitrogen). Culture media were refreshed 18-24 hours after transfection, and cells were imaged around 48 hours post transfection to allow sufficient recovery from transfection stress (lysosomes in transfected cells generally exhibited perinuclear localization pattern within 1 day post transfection likely due to cell stress).

Ammonia Ringer's solution

The formula of Ammonia Ringer's was adapted from that of Acidic Ringer's solution (Durchfort, Verhoef et al. 2012, Li, Wang et al. 2013). Specifically, acetic acid was replaced by ammonia chloride to alkalize the cytosol. The solution contained (in mM) 130 HCl, 20 NH_4Cl, 5 KCl, 2 $CaCl_2$, 1 $MgCl_2$, 2 NaH_2PO_4, 10 HEPES, and 10 glucose; after mixing the solution was adjusted to a pH of 7.9 with NaOH. To prevent precipitation, NaH_2PO_4 was made separately as a 100× stock solution and added fresh right before use.

Starvation

For starvation, complete medium was replaced with DMEM without supplements through four careful, extensive washes. For drug treatments under starvation conditions, drugs were mixed into the starvation medium directly.

Immunolabeling

Lamp1-GFP transfected cells were rinsed with phosphate-buffered saline (PBS) and fixed in 4% paraformaldehyde for 20 min at room temperature (RT). Fixed cells were washed and blocked with 2% bovine serum albumin in PBS for 2 hous, and then incubated overnight with primary antibodies in the blocking solution. Cells were then washed and incubated with secondary antibodies for 1 hour before being subjected to fluorescent imaging.

Filiin staining and quantification

Filipin staining was performed as described previously. Briefly, filipin was dissolved in DMSO at 25 mg/mL as a stock solution. The working solution (0.05 mg/mL) was prepared fresh in PBS with 10% FBS. To stain intracellular cholesterol, cultured cells were rinsed with PBS, and then fixed with 3% paraformaldehyde in PBS at RT for 1 h. Fixed cells were washed with

PBS and then incubated with 1.5 mg/mL glycine in PBS at RT for 10 min to quench the paraformaldehyde. Finally, the cells were incubated with filipin working solution at RT for 2 h, and washed with PBS four times before imaging. All manipulations involving Filipin were kept strictly in dark until imaging

ImageJ was used to analyze the staining results. For each individual cell, the fluorescence intensities of three randomly selected areas close to the cell border were averaged, subtracted with the image background noise (intensity of void areas), then multiplied by the cell area, and considered intracellular background intensity. Lysosomal intensity, representing the net intensity of the brighter puncta filipin signal inside the cells, was taken as the total fluorescence intensity of the cell minus intracellular background intensity. Note that because lysosomes are the primary storage sites of unesterified cholesterol under cholesterol storage conditions (see **Fig. 2.14f**), the puncta filipin signal was presumed to be originated from lysosomal cholesterol. Lysosomal cholesterol was then normalized as 100 x lysosomal intensity/intracellular background intensity.

Cholesterol depletion

Depletion of cholesterol was performed as described previously (Rocha, Kuijl et al. 2009). Briefly, 50 μM of activated simvastatin was applied to DMEM without FBS, and then supplemented with 230 μM mevalonate (to supply essential nonsterol isopreniods) in the absence of cholesterol. Cells were washed extensively and incubated in the cholesterol-depleting medium for 3 hours before imaging.

Fluorescence imaging and image analysis

Live imaging was performed with an Olympus Spindisk Confocal microscope equipped with a heated chamber to maintain the specimen temperature at ~37 °C. Except for FRAP experiments, which were carried out using a 3x1 μm z-stack setting for fast speed, all live imaging were taken using a 0.3 μm step size z-stack setting from top to the bottom of the cells. GFP-tagged proteins were visualized with a 488/515 (excitation/emission in nm) filter set; mCherry-tagged proteins were visualized with a 561/607 filter set. Quantification was performed in ImageJ.

Photobleaching and quantification of lysosome movements.

Photobleaching experiments were performed with the FRAP function of Metamorph software in an Olympus spindisk confocal system. Briefly, after cells were incubated at ~37 °C for 10 min, a region (10 μm × 25-30 μm, corresponding to 42 pixels × 106–127 pixels at 60× magnification) was selected in which anterograde and retrograde movement could be distinguished easily and unambiguously. Each selected area had at least 100 lysosomes immediately adjacent to each side. The selected area was photobleached with an 800 ms/pulse protocol (561 nm excitation) and then live-imaged for 5 min (1 frame/s) with a z-stack of three 1-μm steps using a 561/607 filter set. The frames were converted to a movie in Metamorph. The midline of each bleached area was drawn, and the number of lysosomes crossing the midline in each direction during the 5-min imaging time was counted. If the same lysosome re-crossed the midline in the opposite direction without first exiting the bleached area it was not multi-counted.

Quantification of lysosome distribution

For an illustration of the quantification please see **Fig. 2.17**. Specifically, lysosome distribution was analyzed in fibroblasts with cell areas in the range of 2,500-7,500 μm^2, and in

HeLa cells ranging 800-2,500 μm^2. The nuclear area was excluded during quantification. Average Lamp1 intensities were measured for the whole cell (I_{total}), the area within 10 μm of the nucleus ($I_{perinuclear}$), and the area >15 μm from the nucleus ($I_{peripheral}$). For HeLa cells, the latter two areas were within 5-10 μm of the nucleus, respectively. The perinuclear and peripheral normalized intensities were first calculated and normalized as $I<10 = I_{perinuclear}/I_{total} - 100$ and $I>15 = I_{peripheral}/I_{total} - 100$, respectively (I<5 and I>10 for HeLa cells). The perinuclear index was defined as I<10 – I>15 (I<5 – I>10 for HeLa cells). Quantifications were done by researchers blind to the experimental groups presented.

Endolysosomal electrophysiology

Endolysosomal electrophysiology was performed in isolated enlarged endolysosomes with a modified patch-clamp method as described previously (Dong, Shen et al. 2010, Wang, Zhang et al. 2012, Zhang, Li et al. 2012). Briefly, cells were treated with 1 μM vacuolin-1 for 1–12 hours. Enlarged vacuoles (up to 5 μm) were isolated manually with a patch pipette, and then whole-endolysosome voltage clamp recordings were performed. The vacuolar membrane was ruptured with a series of voltage steps. Whole-endolysosome configuration was verified by the re-appearance of capacitance transients after break-in. Whole-endolysosomal currents were elicited by repeated voltage ramps from -120 to 120 mV (400 ms) with an inter-ramp interval of 2 s. The pipette (luminal) solution was modified Tyrode's, including (in mM) 145 NaCl, 5 KCl, 2 $CaCl_2$, 1 $MgCl_2$, 10 HEPES, 10 MES, 10 glucose (pH adjusted with NaOH to pH 4.6). The bath (internal/cytoplasmic) solution contained (in mM) 140 K-gluconate, 4 NaCl, 1 EGTA, 2 $MgCl_2$, 0.39 $CaCl_2$, 20 HEPES (pH adjusted with KOH to 7.2; free $[Ca^{2+}]_i$ ~ 100 nM estimated using MaxChelator software). Bath solutions were applied via a perfusion system that allowed a complete solution exchange within a few seconds. Data were collected using an Axopatch 2A

patch clamp amplifier, Digidata 1440, and pClamp 10.2 software (Axon Instruments). Whole-endolysosome currents were digitized at 10 kHz and filtered at 2 kHz. All experiments were conducted at RT (21–23 ºC), and all recordings were analyzed with pClamp 10.2, and Origin 8.0 (OriginLab, Northampton, MA)

Chemicals and reagents

The following chemicals were obtained from vendors indicated in parentheses after each name: ML-SA1 (Princeton BioMolecular Research), ML-SI1, Filipin, Simvastatin (Sigma), PI(3,5)P_2 (Echelon), ML-SI3 (AKOS), BAPTA-AM, tetramethylrhodamine-dextran, and Mitotracker (Invitrogen). γ-tubulin antibody was purchased from Sigma (T5326).

Statistical analysis

Statistical data are presented as means ± standard error of the mean (SEM). Comparisons between the experimental groups were made using analyses of variance (ANOVAs). All data are generated from at least three biologically independent experiments.

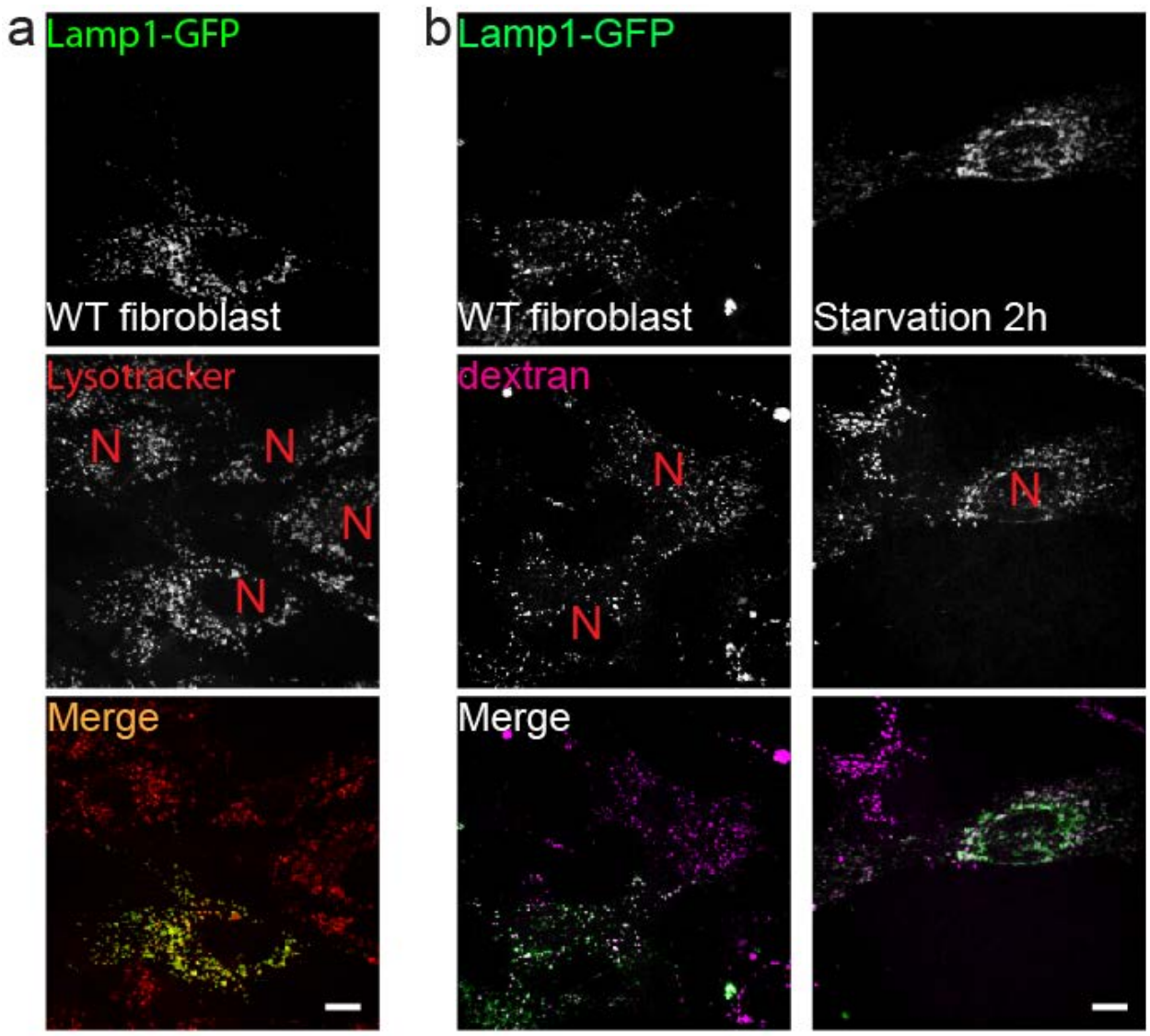

Fig. 2.1 Distribution of lysosomes under normal or starved conditions with different labeling methods.

WT fibroblasts were transfected with Lamp1-GFP and co-labeled with either lysotracker (**a**), or with tetramethylrhodamine-dextran (**b**). Nuclei are labeled with "N". Scale bars = 10 μm.

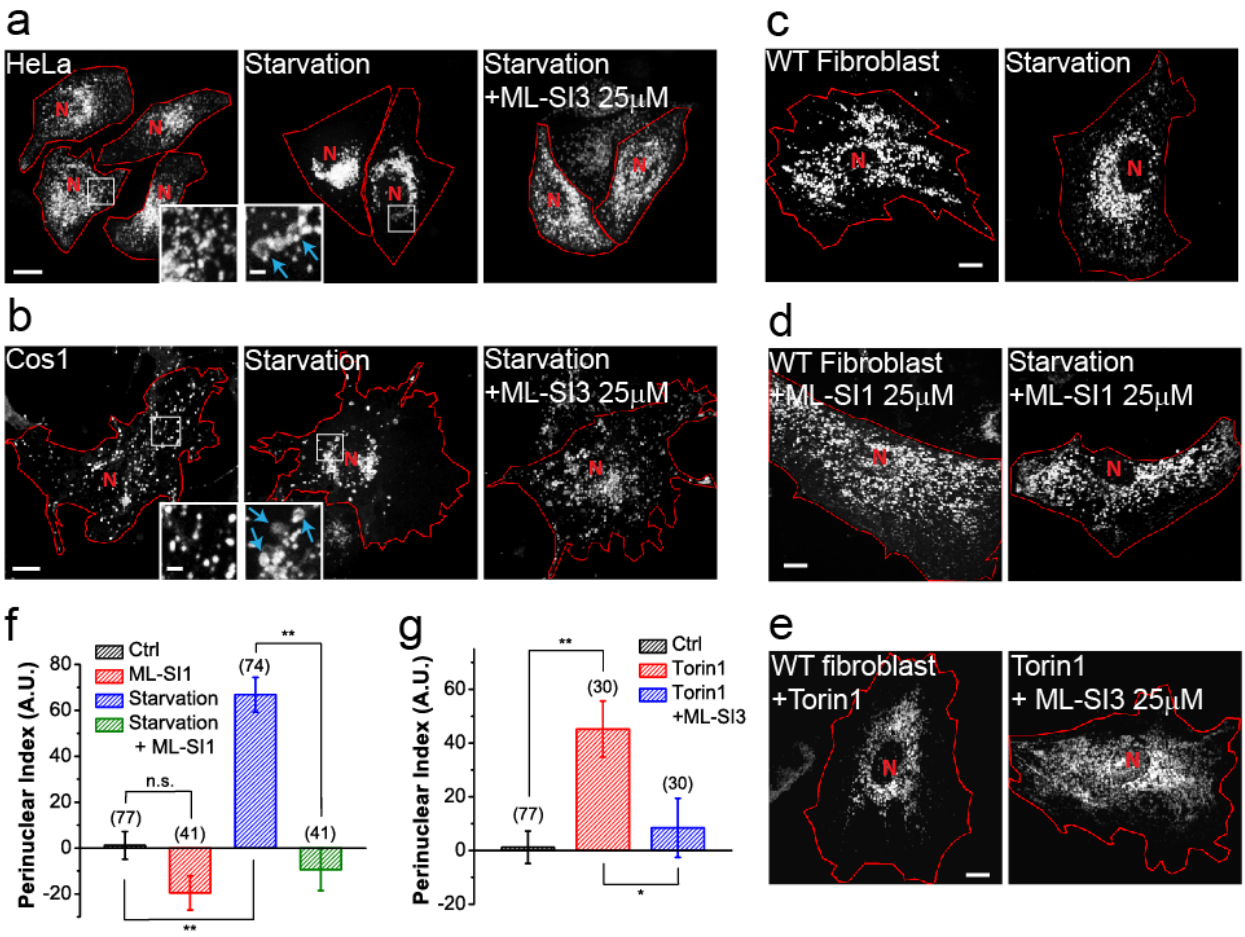

Fig. 2.2 TRPML1 activity is required for the starvation- and Torin-1-driven perinuclear accumulation of lysosomes.

(**a, b**) Representative HeLa cells (**a**) and Cos1 cells (**b**) transfected with the late-endosome and lysosome marker Lamp1-mCherry under 2 hours serum starvation with (right) or without (middle) the TRPML1 inhibitor ML-SI3 (25 μM). Insets illustrate the size of lysosomes with and without starvation (same magnification, blue arrows indicate enlarged lysosomes). (**c**) Representative WT mouse fibroblasts transfected with Lamp1-mCherry in 2 hours starvation condition (right). (**d**) Lysosome (labelled with Lamp1) distribution in WT fibroblasts in the presence of the TRPML1 inhibitor ML-SI1 (25 μM) with (right) or without (left) starvation. (**e**) Lysosome distribution in WT fibroblasts treated with mTOR inhibitor Torin 1 (1 μM) or together with ML-SI3 (25 μM) for 2 h. (**f**) Quantitative analyses of lysosome distribution in the experiments shown in (**c**) and (**d**). The intracellular distribution of Lamp1-positive vesicles was quantified as described in Materials & Methods. Fibroblasts were chosen for most quantification analyses for their large cell area, regular shape, and ML1 KO availability. (**g**) Quantification of groups shown in (**e**). Red lines in images outline cell boundaries and the red "N" marks the nucleus. Graphed data are presented as means ± SEM, number of cells used for quantification are shown in the brackets. *p < .05, **p < .01 in ANOVA. Scale bars = 10 μm, and 2 μm for insets.

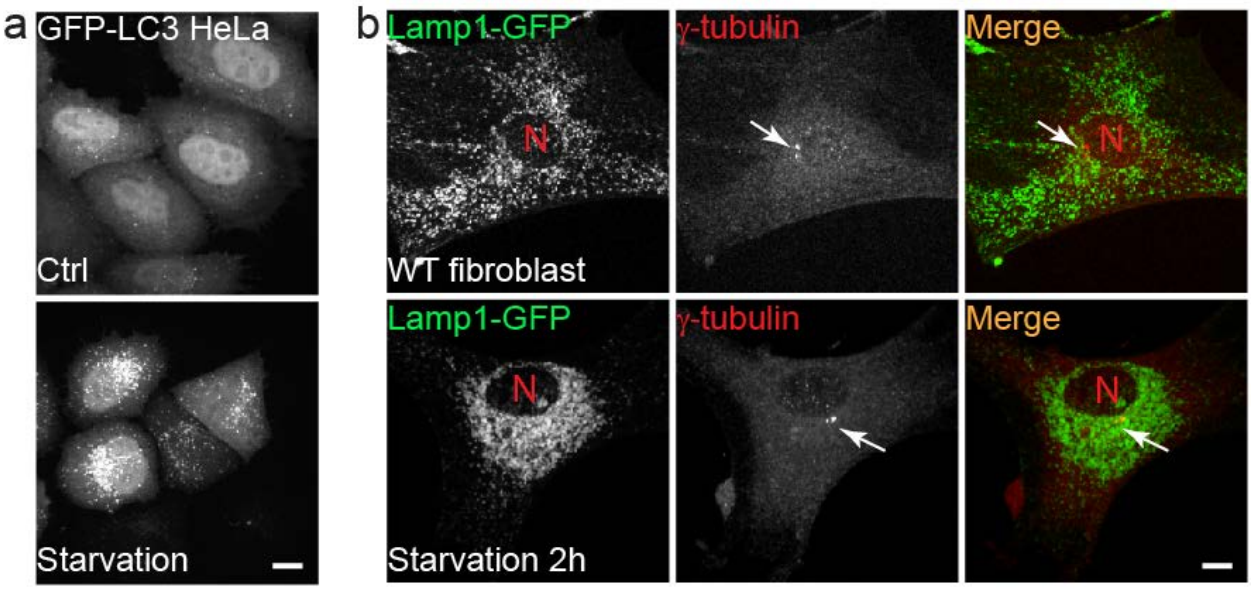

Fig. 2.3 Concurrent accumulation of autophagosomes and lysosomes towards the perinuclear region under acute starvation.

(**a**) HeLa cells stably expressing GFP-RFP-LC3 were subjected to starvation for 2 hours (lower panel). The GFP channel shows puncta that label autophagosomes specifically, but not autolysosomes. (**b**) WT fibroblasts were transfected with Lamp1-GFP and left untreated (top), or starved for 2 hours (bottom), then fixed and immunolabelled for γ-tubulin to visualize centrosomes (MTOC, white arrows). Nuclei are labeled with "N". Scale bars = 10 μm.

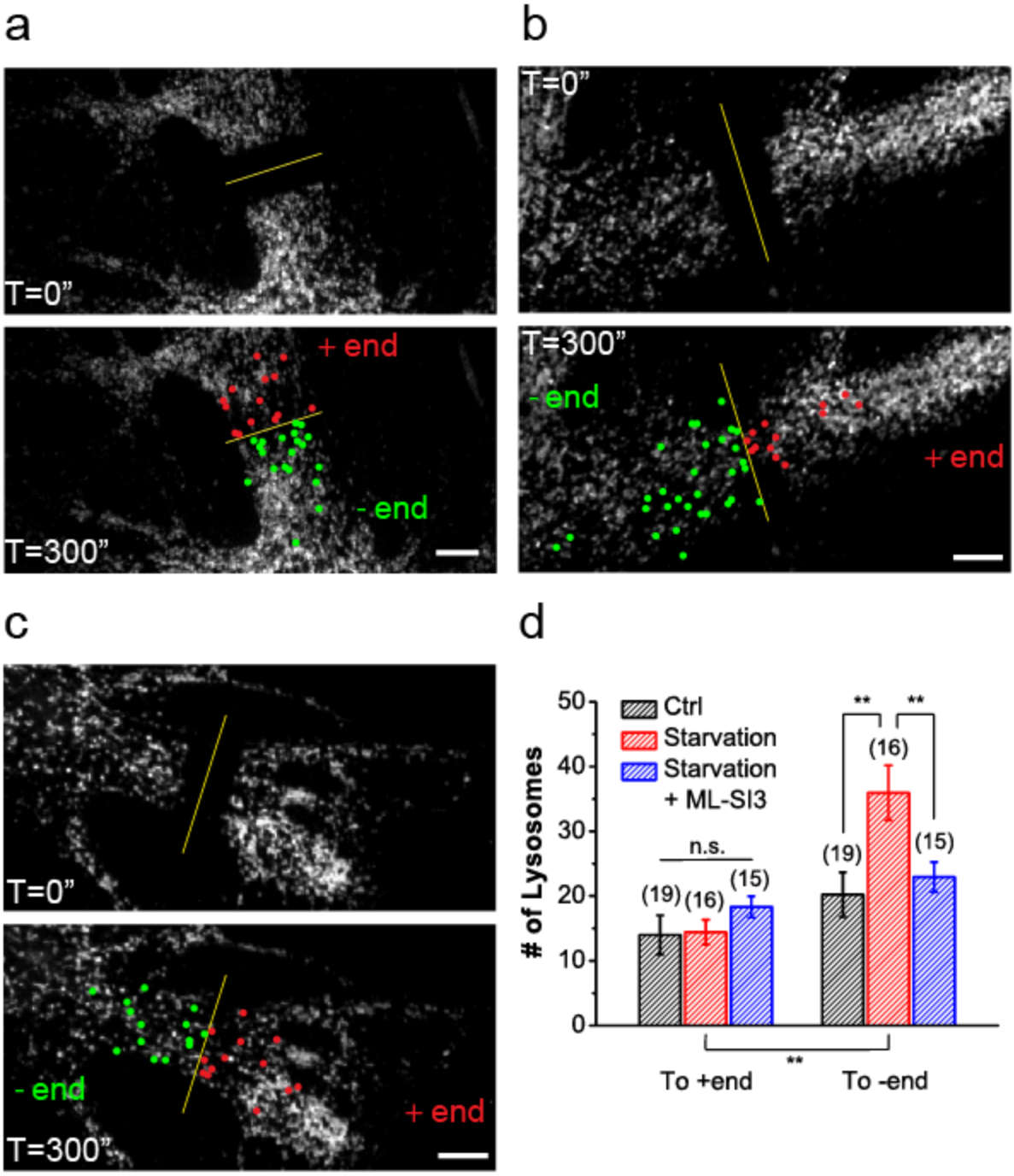

Fig. 2.4 FRAP analysis reveals that TRPML1 is responsible for the increased retrograde transport of lysosomes under starvation.

(**a-c**) FRAP analysis of lysosome movement in WT fibroblasts without any treatment (**a**), with 15–30 min starvation (**b**), or with starvation in the presence of 25 μM ML-SI3 (**c**). Snap images immediately after (top panels) or 5 min (bottom panels) after photobleaching are shown. Lysosomes that traveled across the midline of the photobleached region (yellow line) towards the nucleus (retrograde) are labeled green; those moving away from the nucleus (anterograde) are

labeled red. (**d**) Quantification of lysosomes in (**a-c**) undergoing retrograde or anterograde transport. Graphed data are presented as means ± SEM, number of cells used for quantification are shown in the brackets. *p < .05, **p < .01 in ANOVA.

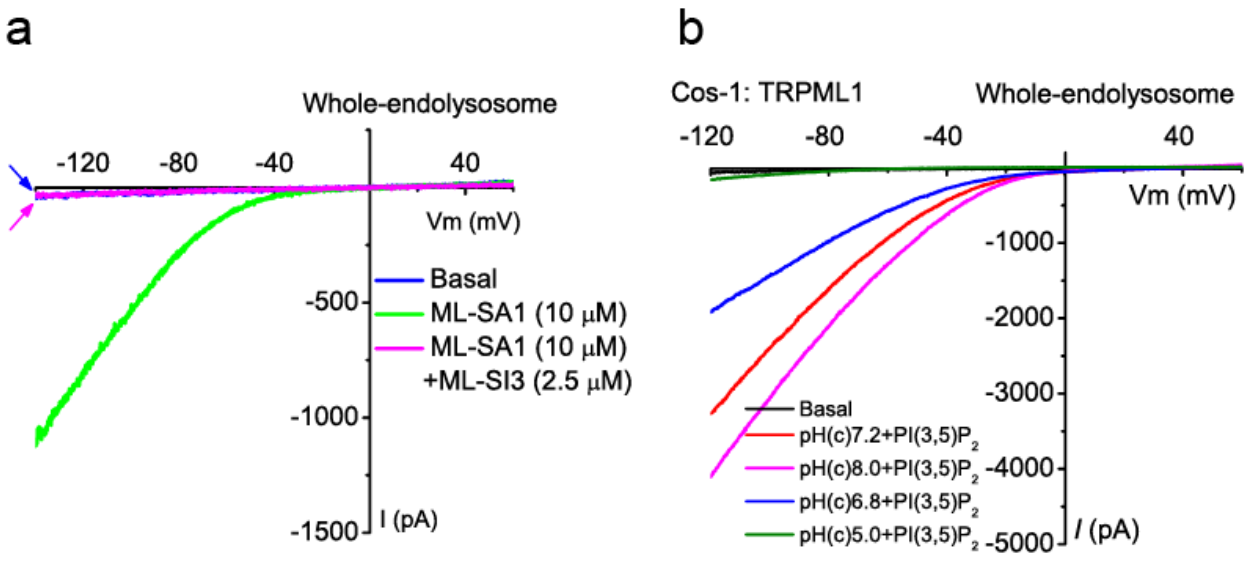

Fig. 2.5 Effect of synthetic agonists/antagonists and cytosolic pH on TRPML1 activity.

(**a**) ML-SA1 (10 μM)-activated whole-lysosome TRPML1 currents were inhibited potently by the TRPML1 inhibitor ML-SI3 (2.5 μM). (**b**) PI(3,5)P_2-activated whole-endolysosome TRPML1 currents were modulated by cytosolic pH.

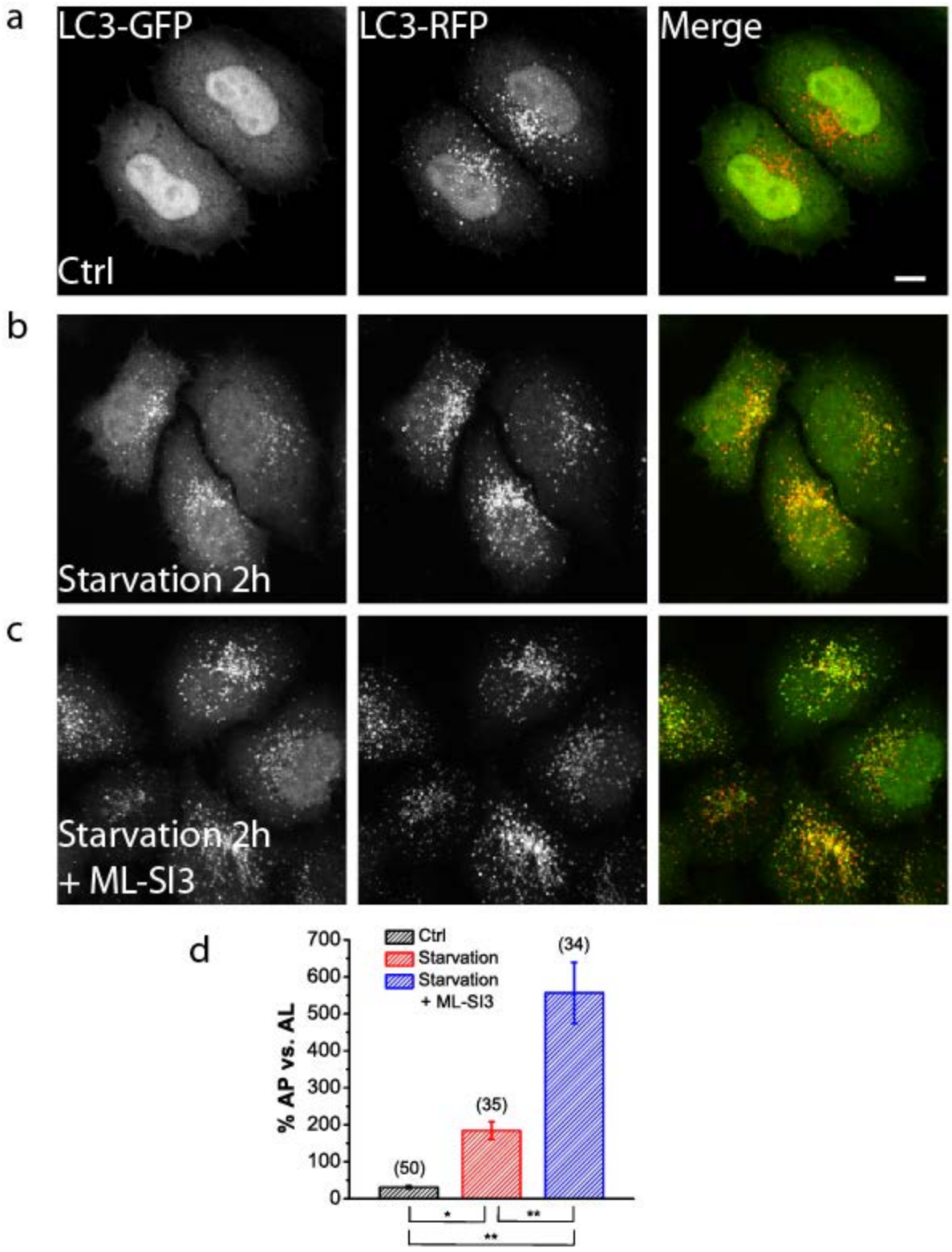

Fig. 2.6 Inhibition of TRPML1 suppresses autolysosome formation

(**a-c**) HeLa cells stably expressing GFP-RFP-LC3 were left untreated (**a**), starved for 2 hours (**b**), or starved for 2 hours in the presence of 25 μM ML-SI3 (**c**). (**d**) Quantification of the number of

puncta that were GFP- and RFP-positive (autophagosomes, AP) over the number of puncta that were only RFP-positive (autolysosomes, AL) for groups shown in (**a-c**). Graphed data are presented as means ± SEM, number of cells used for quantification are shown in the brackets. *p < .05, **p < .01 in ANOVA. Scale bar = 10 μm.

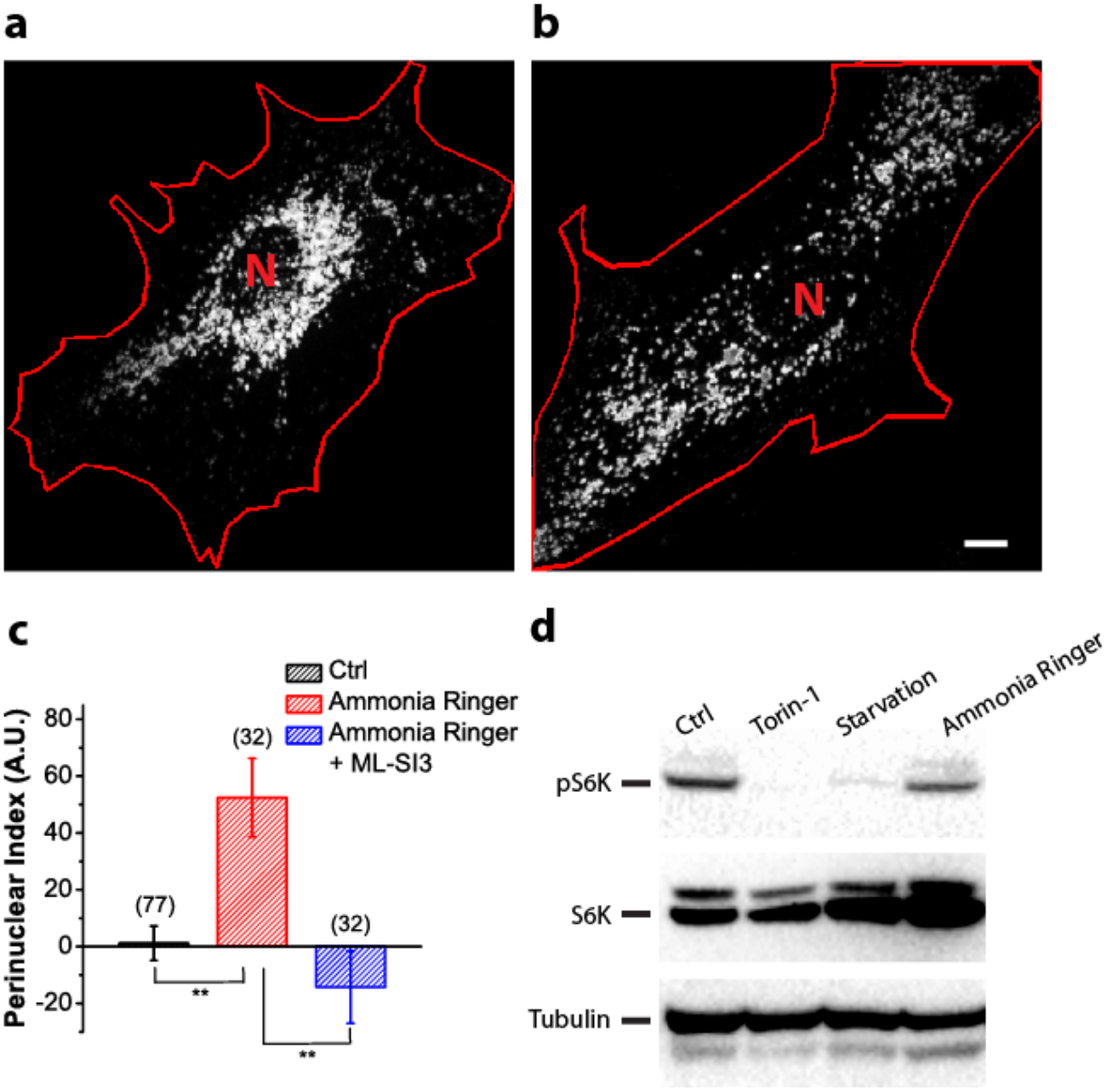

Fig. 2.7 TRPML1 activity is required for alkalization-induced lysosome retrograde migration

(a, b) Lamp1-mCherry-transfected WT fibroblasts were treated with 30 min ammonia Ringer's solution in the presence (**b**) or absence (**a**) of 25 μM ML-SI3. (**c**) Quantification of groups shown in (**a**) and (**b**). (**d**) Western blot showing the phosphorylated form of S6K (pS6K) in HeLa cells starved for 2 hours, treated with 1 μM Torin-1 for 2 hours, or treated with ammonia Ringer's for 30 min. Red lines outline cell boundaries and nuclei are marked with a red "N". Graphed data are presented as means ± SEM, number of cells used for quantification are shown in the brackets. *$p < .05$, **$p < .01$ in ANOVA. Scale bar = 10 μm.

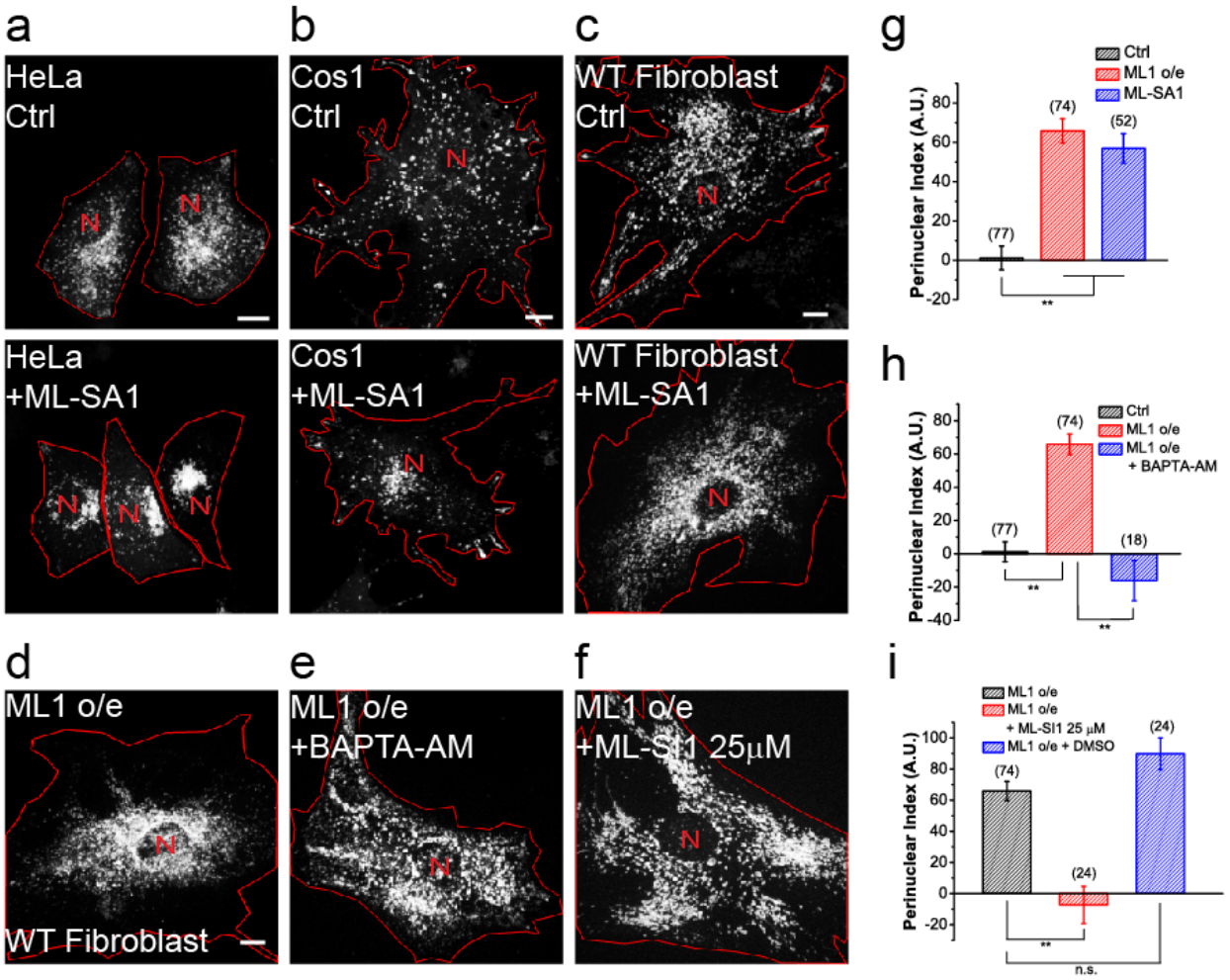

Fig. 2.8 Activation of TRPML1 is sufficient to promote Ca^{2+}-dependent retrograde migration of lysosomes.

HeLa cells (**a**) Cos1 cells (**b**) and WT fibroblasts (**c**) with (bottom) and without (top) 25 μM ML-SA1 for 2 hours. (**d-f**) Lysosome distribution in TRPML1-overexpessing WT fibroblasts (**d**) treated with 10 μM BAPTA-AM for 1 hour (**e**) or 25 μM ML-SI1 for 2 hours (**f**). (**g**) Quantification of lysosome distribution in the experiments shown in (**c**) and (**d**). (**h**) Quantification of experimental group shown in (**e**). (**i**) Quantification of experimental group shown in (**f**).

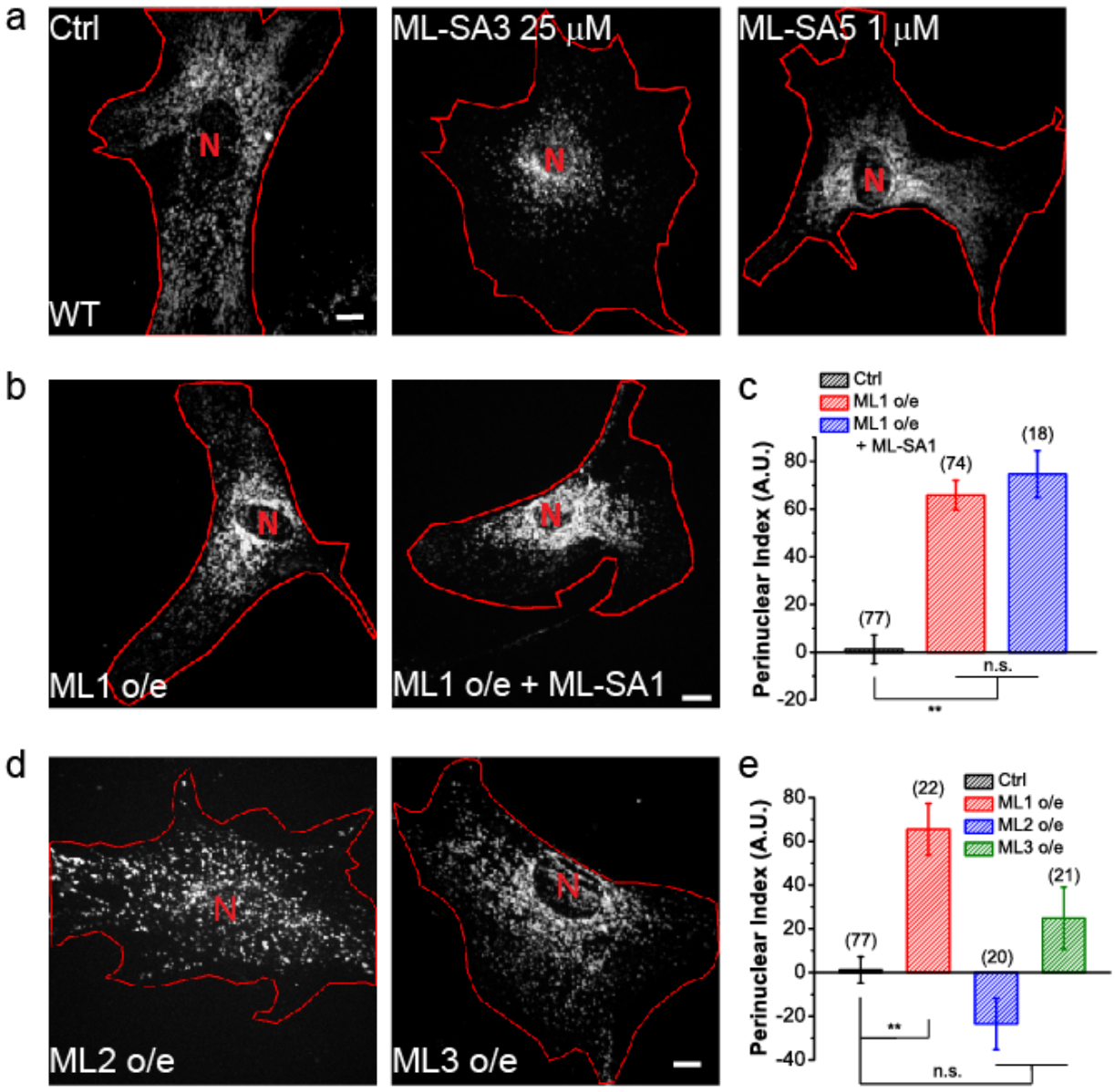

Fig. 2.9 Retrograde migration of lysosomes is specifically promoted by TRPML1 hyperactivity.

(**a**) WT fibroblasts treated with ML-SA3 (25 μM) or ML-SA5 (1 μM), two structurally-independent TRPML1 agonists, for 1 hour. (**b**) In TRPML1-overexpressing cells, the majority of lysosomes were localized in the perinuclear region in the presence or absence of 25 μM ML-SA1. (**c**) Quantifications of groups shown in (**b**). (**d**) Representative images showing WT fibroblasts overexpressing TRPML2 or TRPML3. (**e**) Quantification of groups shown in (**d**). Red lines outline cell boundaries and nuclei are marked with a red "N". Graphed data are presented as means ± SEM, number of cells used for quantification are shown in the brackets. *p < .05, **p < .01 in ANOVA. Scale bars = 10 μm.

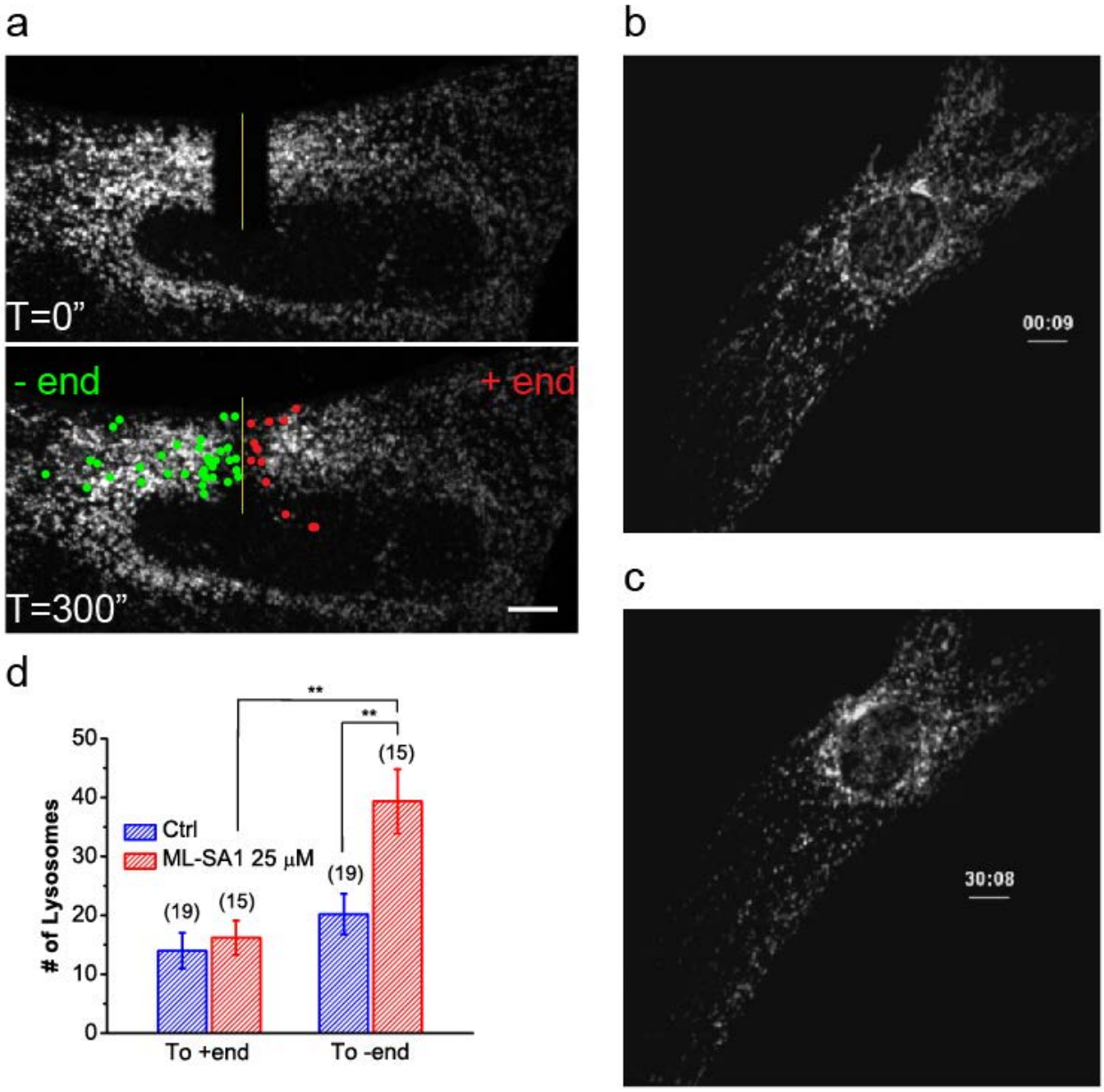

Fig. 2.10 Activation of TRPML1 promotes retrograde transport of lysosomes shown by FRAP and time-lapse imaging.

(**a**) FRAP analysis of lysosome retrograde transport upon 25 μM ML-SA1 application. (**b, c**) The same WT fibroblast expressing Lamp1-mCherry, and right before (**b**) or after 30 minutes (**c**) of 25 μM ML-SA1 treatment. (**d**) Quantification of lysosomes shown in (j) undergoing retrograde and anterograde transport after photobleaching. Graphed data are presented as means ± SEM, number of cells used for quantification are shown in the brackets. *p < .05, **p < .01 in ANOVA. Scale bars = 10 μm.

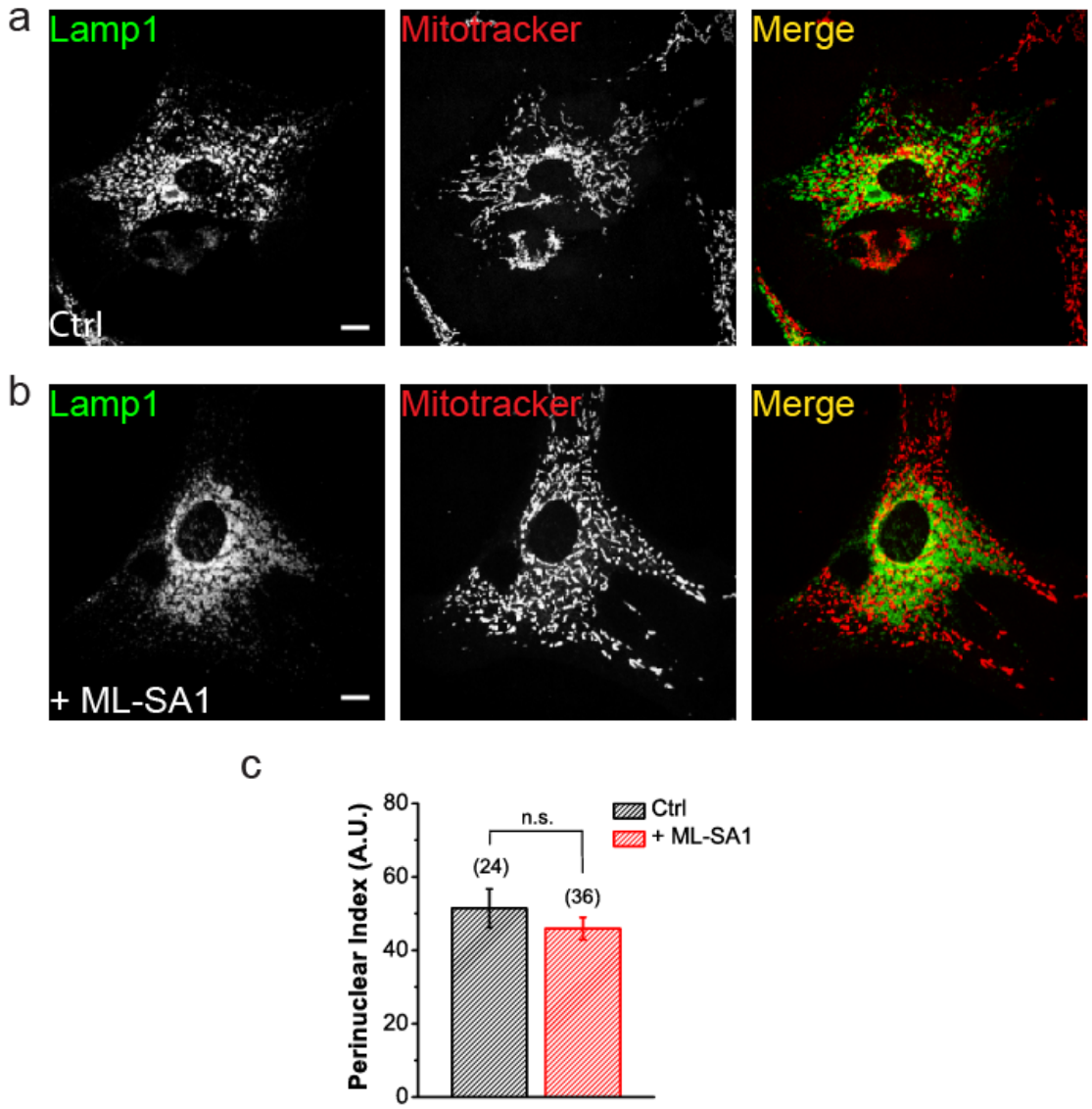

Fig. 2.11 TRPML1 activation increases the retrograde transport of lysosomes selectively, but not mitochondria.

(**a**) Representative images of Lamp1-GFP-transfected fibroblasts stained with MitoTracker (100 nM) for 1 hour. (**b**) MitoTracker in the presence of 25 μM ML-SA1. (**c**) Quantification of groups shown in (**a**) and (**b**). Upon ML-SA1 treatment, lysosomes became more perinuclear, while the distribution of mitochondria was not altered. Scale bars = 10 μm. Data are means ± SEM.

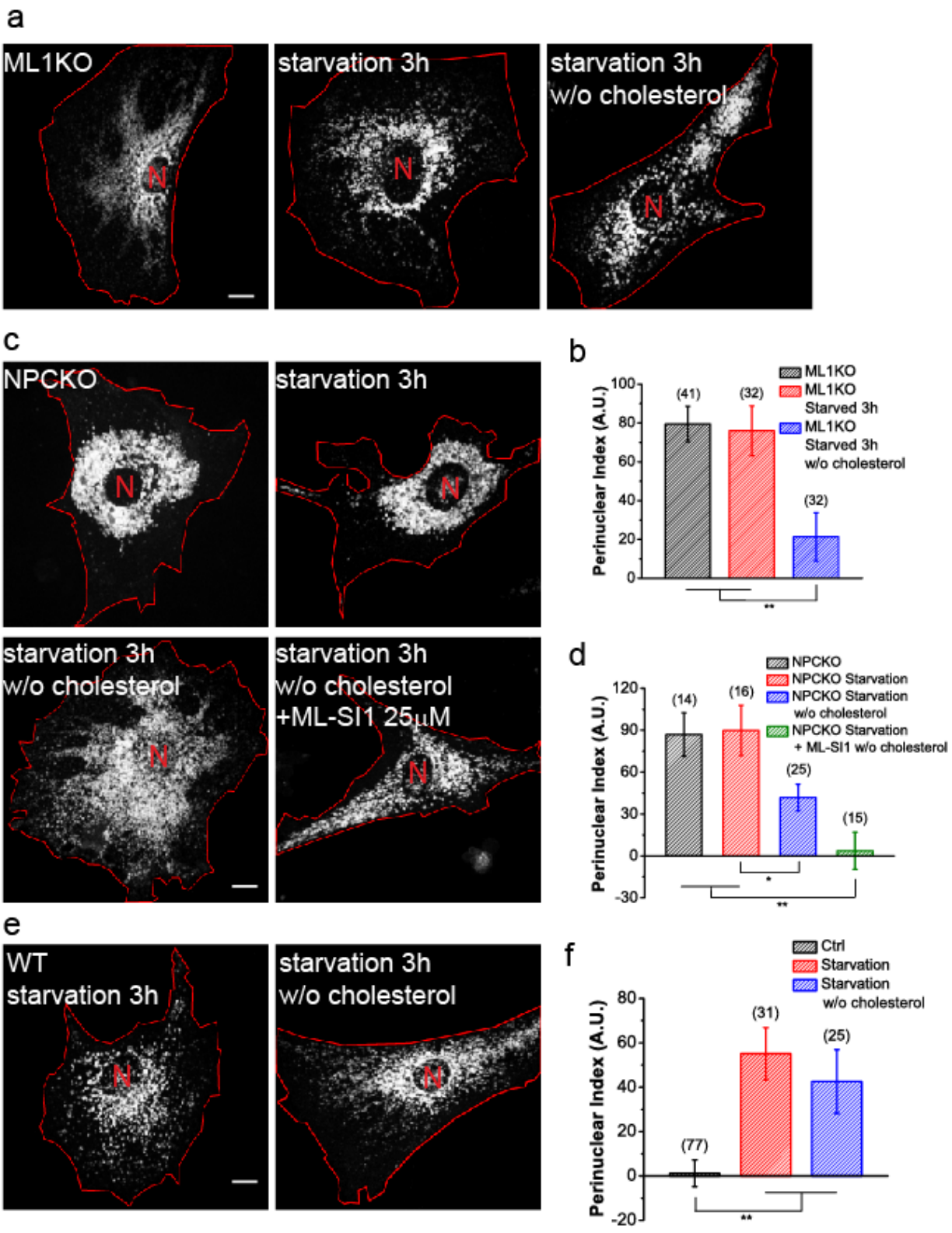

Fig. 2.12 Cholesterol mediates the perinuclear lysosome pattern in LSD cells.

(**a**) Representative images showing Lamp1-mCherry-transfected ML1 KO fibroblasts in starved cells that were treated with simvastatin and mevalonolactone to deplete cholesterol. (**b**) Quantification of groups shown in (**a**). (**c**) Representative images showing Lamp1-mCherry transfected NPC1 KO fibroblasts (upper left), starved for 3 hours (upper right), starved with cholesterol depletion (bottom left), or starved with cholesterol depletion in the presence of 25 μM ML-SI1 (bottom right). (**d**) Quantification of groups shown in (**c**). (**e**) Effect of cholesterol depletion on starvation-induced lysosome redistribution in WT fibroblasts. (**f**) Quantification of observations shown in (**e**). Red lines outline cell boundaries and nuclei are marked with a red "N". Graphed data are presented as means ± SEM, number of cells used for quantification are shown in the brackets. *$p < .05$, **$p < .01$ in ANOVA. Scale bar = 10 μm.

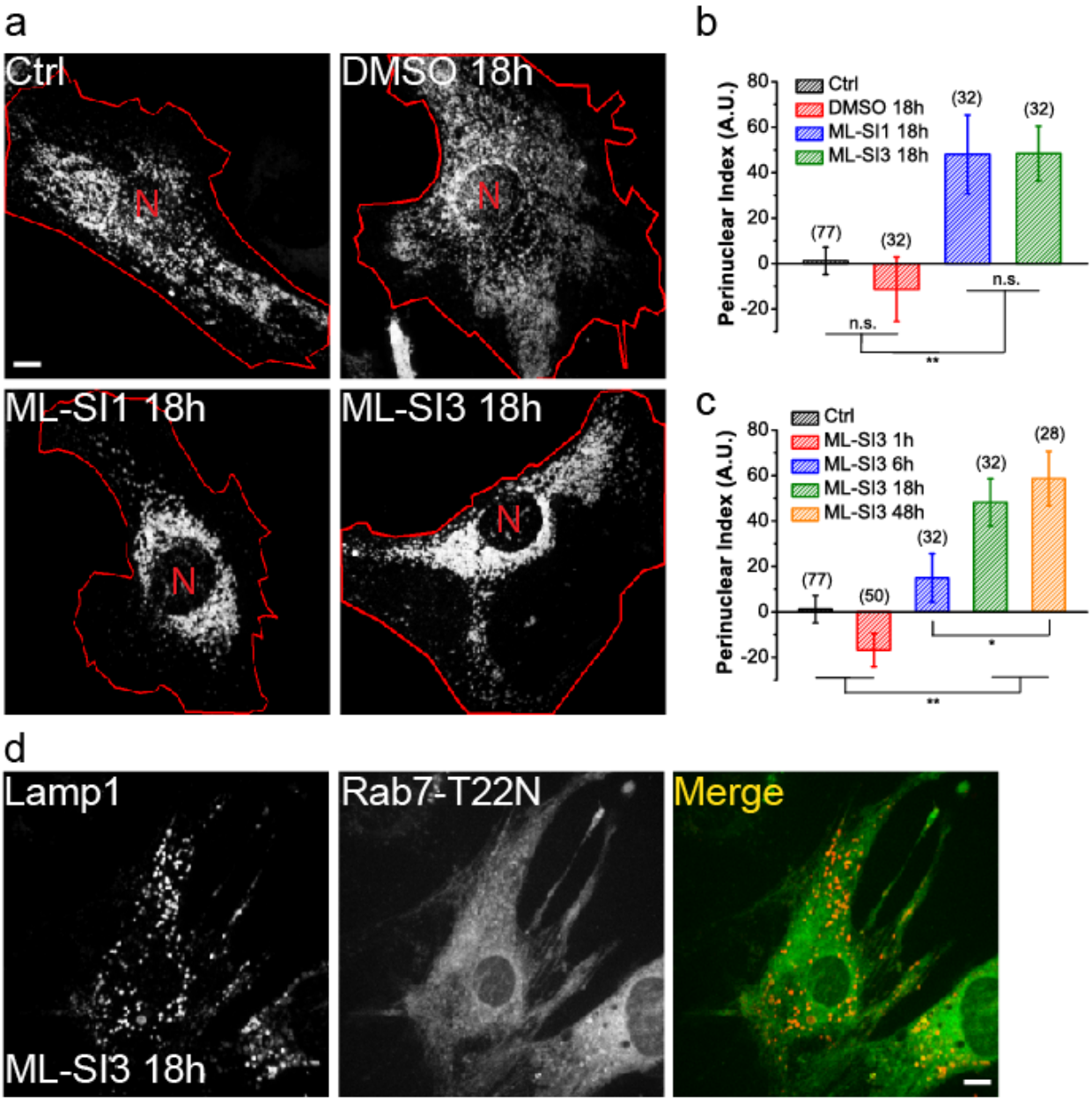

Fig. 2.13 Effect of prolonged, pharmacological inhibition of TRPML1 on lysosome distribution.

(**a**) Lysosome distribution in WT fibroblasts treated with vehicle (0.1% DMSO) (upper right), ML-SI1 25 μM for 18 hour (bottom left), or ML-SI3 25 μM for 18 hour (bottom right) in complete medium. (**b**) Quantification of the groups shown in (**a**). (**c**) Time-dependence of TRPML1 inhibition of lysosome distribution in WT fibroblasts in complete medium. (**d**) Representative images showing lysosome distribution in Rab7-T22N-expressing cells in the presence of ML-SI3 (25 μM) for 18 hours. Red lines outline cell boundaries and nuclei are marked with a red "N". Graphed data are presented as means ± SEM, number of cells used for quantification are shown in the brackets. *p < .05, **p < .01 in ANOVA. Scale bar = 10 μm.

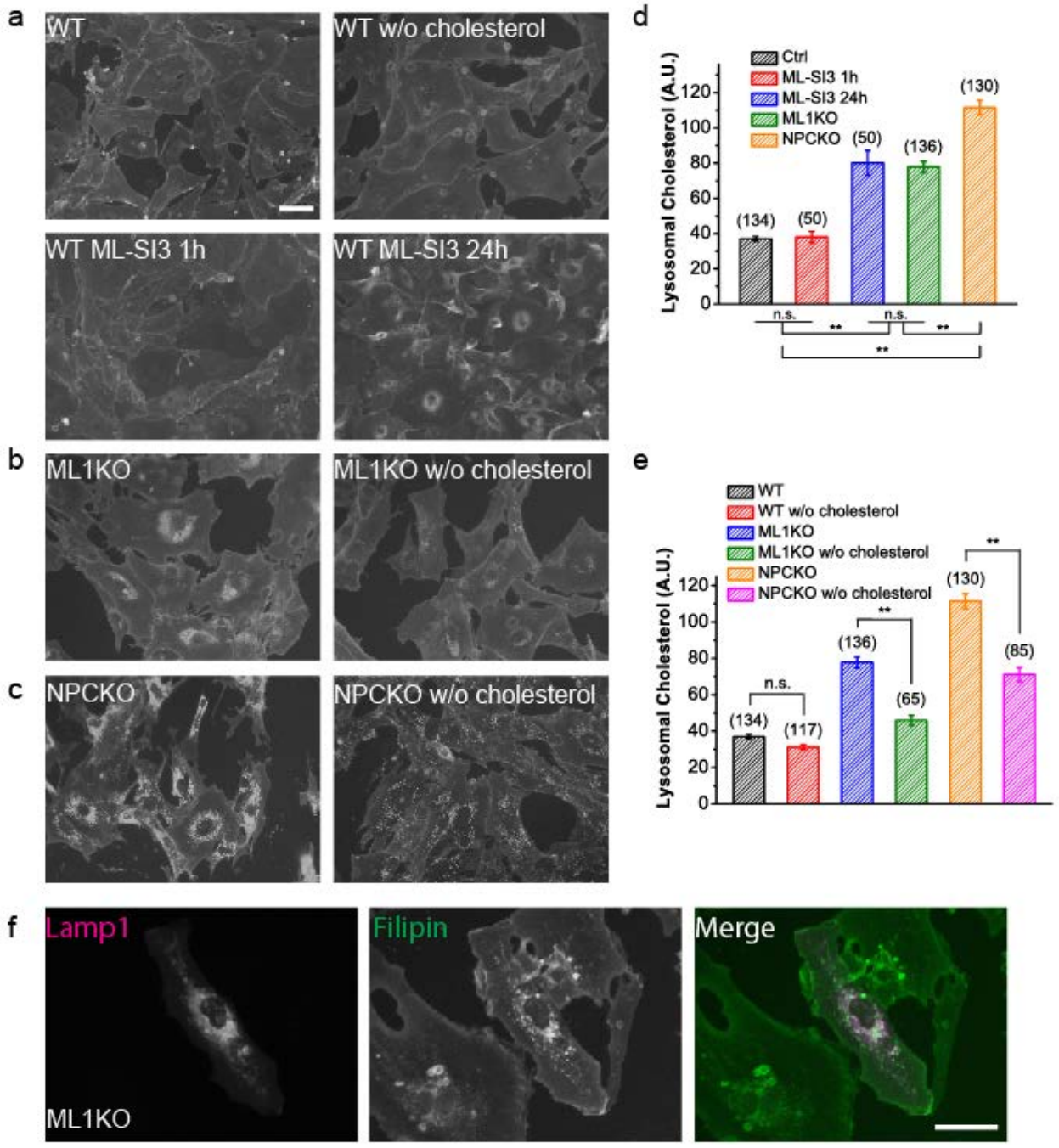

Fig. 2.14 Characterization of the cholesterol accumulation under prolonged TRPML1 inhibition or in LSD model cells.

(**a**) Filipin staining of WT fibroblasts (upper left) and WT fibroblasts depleted of cholesterol with simvastatin (upper right), WT fibroblasts treated with 25 μM ML-SI3 for 1 hour (bottom left) or 24 hours (bottom right). (**b**) ML1 KO fibroblasts with (right) or without (left) cholesterol depletion. (**c**) NPC1 KO fibroblasts with (right) or without (left) cholesterol depletion. (**d**) Quantitative comparison of filipin staining in WT fibroblasts treated with different durations of ML-SI3 versus ML1 KO and NPC1 KO fibroblasts. (**e**) Quantification of filipin stating in WT,

ML1 KO, NPC1 KO fibroblasts with or without cholesterol depletion. (**f**) Representative images showing ML1 KO fibroblasts transfected with Lamp1-mCherry, and stained with filipin. Intracellular puncta filipin staining co-localized well with Lamp1. Graphed data are presented as means ± SEM, number of cells used for quantification are shown in the brackets. *$p < .05$, **$p < .01$ in ANOVA. Scale bars = 50 μm.

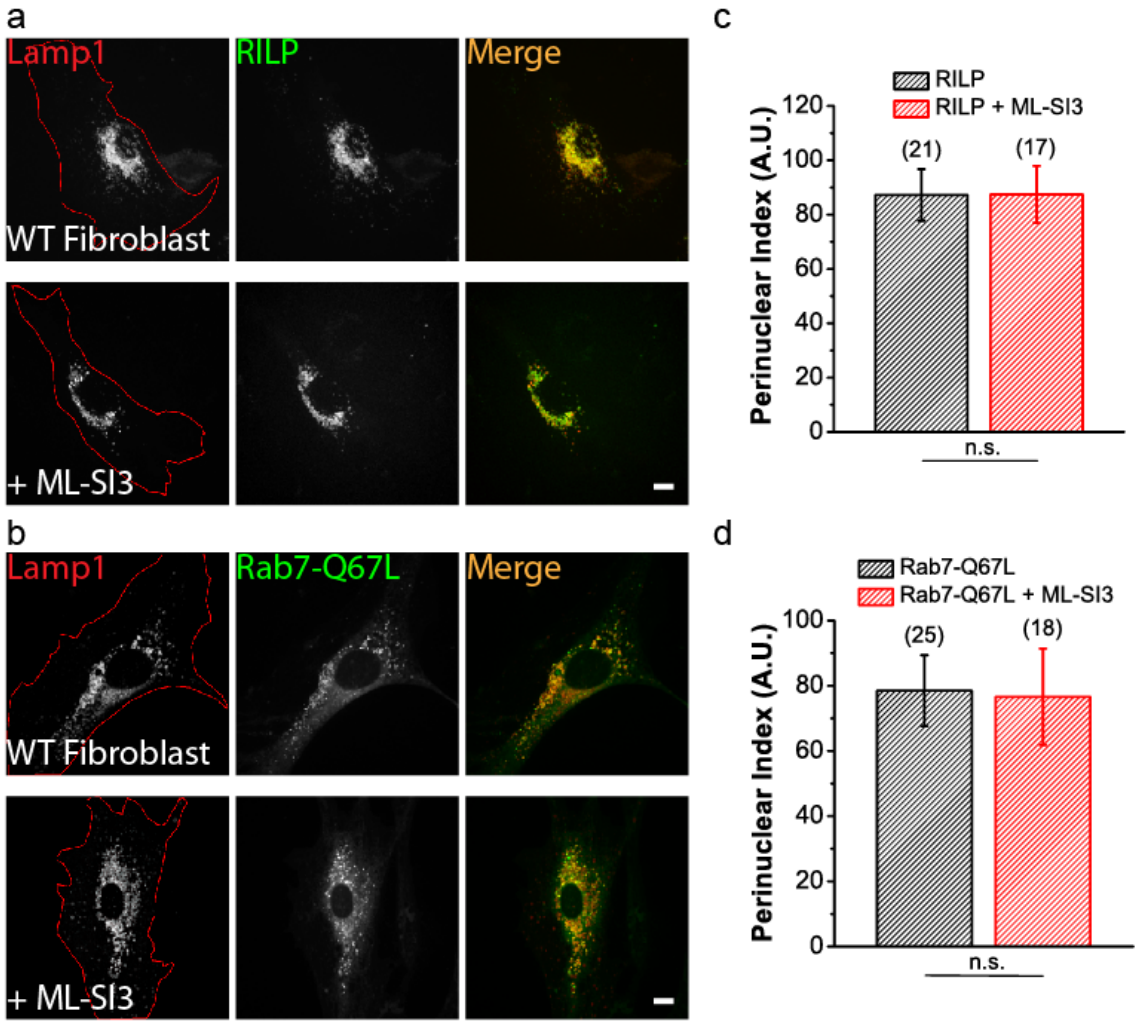

Fig. 2.15 TRPML1 is not downstream of Rab7 and RILP in promoting retrograde migration of lysosomes.

(**a, b**) Representative images showing WT fibroblasts overexpressing Lamp1-mCherry and RILP-GFP (**a**) or Rab7-Q67L-GFP (b) in the presence or absence of 25 μM ML-SI3 for 2 hours. (**c**) Quantification of groups shown in (**a**). (**d**) Quantification of groups shown in (**b**). Red lines outline cell boundaries. Graphed data are presented as means ± SEM, number of cells used for quantification are shown in the brackets. *p < .05, **p < .01 in ANOVA. Scale bars = 10 μm.

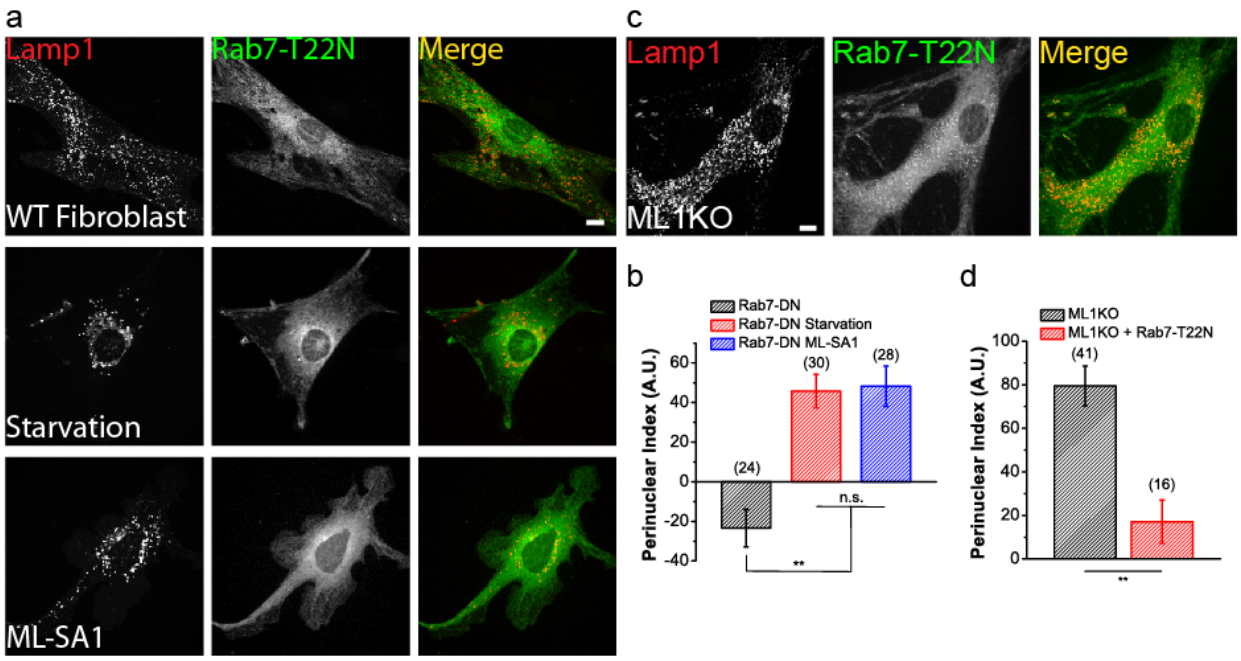

Fig. 2.16 The Rab7-RILP pathway does not work downstream of TRPML1.

(**e**) Representative images showing WT fibroblasts transfected with Lamp1-mCherry and Rab7-T22N-GFP, then left untreated (upper panels), serum starved for 2 hours (middle panels), or incubated with 25 μM ML-SA1 for 2 hours (bottom panels). (**f**) Representative images showing ML1 KO fibroblasts overexpressing Lamp1-mCherry and Rab7-T22N-GFP. (**g**) Quantification of groups shown in (**e**). (**h**) Quantification of the group shown in (**f**). Graphed data are presented as means ± SEM, number of cells used for quantification are shown in the brackets. *p < .05, **p < .01 in ANOVA. Scale bars = 10 μm.

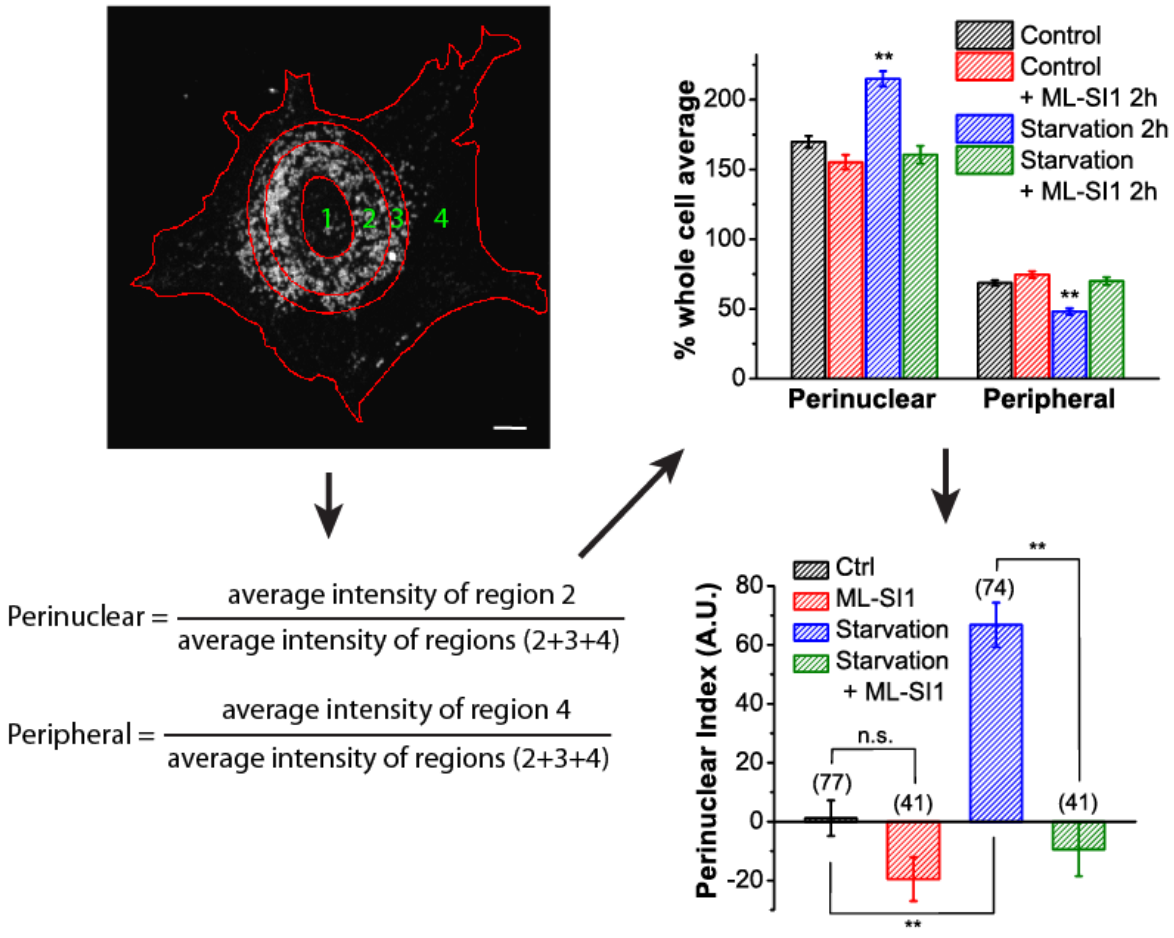

Fig. 2.17 Quantification of the perinuclear index.

To quantify the distribution of lysosomes, cells were divided into four regions: the nucleus (region 1); the perinuclear region (region 2, within 10 μm to the nucleus in fibroblasts or within 5 μm to the nucleus in HeLa cells); the intermediate region (region 3, between 10-15 μm to the nucleus in fibroblasts or 5-10 μm to the nucleus in HeLa cells); the peripheral region (region 4, further than 15 μm to the nucleus in fibroblasts or 10 μm to the nucleus in HeLa cells), as illustrated by the top-left image. The fluorescence intensity of the perinuclear region and the peripheral region were calculated using equations at bottom-left. The resulting normalized fluorescence intensity shown in the top-right graph was further combined together as described in the Methods to form the final perinuclear index shown in the bottom-right graph.

CHAPTER III

Identification of the Upstream and Downstream Players in the TRPML1-Mediated Lysosome Retrograde Trafficking Pathway[3]

3.1 Abstract

Experiments described in Chapter II identified TRPML1 as a novel regulator of the retrograde transport of lysosomes in an on-demand manner, independent of the previously established Rab7-RILP pathway. The next step is to identify the upstream and downstream molecules of the TRPML1 pathway, so that the mechanism of action can be deduced. Here I show that $PI(3,5)P_2$ is required for TRPML1 activation in the retrograde transport, while a TRPML1-interacting calcium sensor, ALG-2, serves as the downstream target of TRPML1. ALG-2 bridges Ca^{2+} signaling from TRPML1 and the dynein adaptor complex dynactin, while the motor protein dynein serves as the final effector of the pathway.

3.2 Introduction

[3] Originally Submitted in Nature Cell Biology. With authors listed as Xinran Li, Nicholas Rydzewski, Ahmad Hider, Xiaoli Zhang, Junsheng Yang, Wuyang Wang, Qiong Gao, Xiping Cheng, and Haoxing Xu.

Ca^{2+} is a versatile regulator of cellular processes. One reason for its versatility is due to the many kinds of Ca^{2+} sensor proteins sensing Ca^{2+} signals in different pathways.

Data in Chapter II suggest that TRPML1 regulates retrograde transport of lysosomes through its Ca^{2+} release. Therefore, a Ca^{2+} sensor must be downstream of TRPML1 to pass on the signal. Multiple Ca^{2+} sensor proteins are known to interact with TRPML1, or play a role downstream of TRPML1. Among these proteins, synaptotagmin VII (Syt VII) is shown to be involved in regulating lysosome exocytosis in macrophages downstream of TRPML1 (Samie, Wang et al. 2013). This protein contains two C2 domains that are responsible for the binding to Ca^{2+} and the interaction with membrane lipids, especially $PI(4,5)P_2$ (Bai and Chapman 2004). It is hypothesized that Syt VII regulates lysosome exocytosis similar to Syt I in regulating synaptic vesicle release, where the Ca^{2+}-binding induces a conformational change of Syt I, leading to the structural change of the SNARE complex that allows membrane mixture of the vesicle and the plasma membrane.

Calcineurin is another Ca^{2+} sensor that was recently reported (Medina, Di Paola et al. 2015) to be downstream of TRPML1 in the signaling of the master regulator of lysosome biogenesis, Transcription Factor E-Box (TFEB). TFEB has been shown to be phosphorylated by mTOR under normal conditions, retaining it in the cytosol through the recognition by 14-3-3 (Pena-Llopis, Vega-Rubin-de-Celis et al. 2011). Under starvation or stressed conditions, TRPML1 activates the Ca^{2+}-regulated phosphatase calcineurin, which de-phosphorylates TFEB, allowing it to dissociate from 14-3-3 and enter the nucleus, promoting transcription of a variety of lysosomal genes (Medina, Di Paola et al. 2015).

Another Ca^{2+} sensor shown to interact with TRPML1 is the penta-EF hand protein Apoptosis-Linked Gene-2 (ALG-2). ALG-2 is a small, 190 a.a. protein that mainly consists of five EF hands for Ca^{2+} binding, although two of the EF hands (EF1 and EF3) were shown to be more critical for its Ca^{2+} sensor role (Vergarajauregui, Martina et al. 2009). ALG-2 has been shown to be able to physically interact with TRPML1 in a Ca^{2+}-dependent manner, i.e. Ca^{2+} binding of ALG-2 is required for its interaction with TRPML1 (Vergarajauregui, Martina et al. 2009). ALG-2 has been shown to be involved in multiple membrane trafficking steps, being able to interact with Sec31A (Shibata, Suzuki et al. 2007, Helm, Bentley et al. 2014) and ALIX (Inuzuka, Suzuki et al. 2010, Okumura, Katsuyama et al. 2013), two proteins involved in ER-to-Golgi vesicle transport and ESCRT-mediated late endosomal membrane abscission, respectively (Shibata, Suzuki et al. 2007, Helm, Bentley et al. 2014, Scheffer, Sreetama et al. 2014). The role for its interaction with TRPML1, however, remained unidentified.

In this chapter, I show experimental results that suggest ALG-2 as the downstream Ca^{2+} sensor of the TRPML1 pathway. I also show that the upstream activator of TRPML1, $PI(3,5)P_2$, is required for the process, and that ALG-2 serves as the bridge linking TRPML1's Ca^{2+} release to the dynein adaptor complex dynactin.

3.3 Results

3.3.1 The role of $PI(3,5)P_2$ in retrograde trafficking of lysosomes

$PI(3,5)P_2$ is a lysosome-localized phosphoinositide (Li, Wang et al. 2013) that regulates autophagy during nutrient deprivation (Vicinanza, Korolchuk et al. 2015) and is the only known endogenous agonist of TRPML1. $PI(3,5)P_2$ binds directly to a stretch of positively-charged

residues on the N-terminal of TRPML1 (Dong, Shen et al. 2010). Mutation of these residues to glutamine (TRPML1-7Q) completely abolishes the sensitivity to $PI(3,5)P_2$, while retaining its sensitivity to synthetic agonists like ML-SA1 (Dong, Shen et al. 2010). Therefore, as the only known candidate for upstream signaling to TRPML1, I investigated the role of $PI(3,5)P_2$ in regulating retrograde trafficking of lysosomes.

Prolonged depletion of $PI(3,5)P_2$ leads to severely enlarged lysosomes that can occupy the majority of the cellular space. Therefore, only short-term depletion of $PI(3,5)P_2$ was applied. Under 1 hour treatment with 1 μM YM 201636 or Apilimod, two well-established synthetic inhibitors of the $PI(3,5)P_2$ and PI(5)P synthesizing enzyme PIKfyve (Jefferies, Cooke et al. 2008, Cai, Xu et al. 2013, Martin, Harper et al. 2013, Ho, Choy et al. 2015), lysosome distributions were slightly, but significantly more peripheral (**Fig. 3.1a, 3.1b**). The depletion of $PI(3,5)P_2$ also effectively suppressed the retrograde migration of lysosomes under acute starvation or mTOR inhibition by Torin-1 (**Fig. 3.1c-f**). These results suggest that $PI(3,5)P_2$ or PI(5)P plays a critical role in the regulation of retrograde motility of lysosomes.

$PI(5)P/PI(3,5)P_2$ depletion was unable to affect the perinuclear accumulation of lysosomes under ML-SA1 treatment, suggesting that TRPML1 might be the downstream target of the phosphoinositides (**Fig. 3.1a, 3.1b**). Consistently, overexpression of the $PI(3,5)P_2$ insensitive mutant TRPML1-7Q did not result in significant change of lysosome distribution as overexpression of the WT channel (**Fig. 3.1g, 3.1h**). ML-SA1 treatment increased the perinuclear localization of lysosomes reliably in TRPML1-7Q-overexpressing cells (**Fig. 3.1g, 3.1h**). Taken together, these results suggest that $PI(3,5)P_2$ is essential for the TRPML1-regulated lysosome transport under physiological conditions, and that synthetic agonists can be used to substitute $PI(3,5)P_2$'s function.

3.3.2 TRPML1-dependent retrograde migration of lysosomes is through cytoplasmic dynein

In animal cells, microtubules-based motor proteins are responsible for the long-range transport of vesicles (Schroer 2004, Verhey and Hammond 2009, Akhmanova and Hammer 2010). Kif5B and cytoplasmic dynein I are shown to be responsible for the transport of lysosomes in mammalian cells (Tanaka, Kanai et al. 1998, Jordens, Fernandez-Borja et al. 2001, Johansson, Rocha et al. 2007, Rosa-Ferreira and Munro 2011). Overexpression of dominant-negative Kif5B (Kif5B-DN) (Silver and Harrison 2011) in mouse fibroblasts produced a very strong clustering of lysosomes at the perinuclear region, whereas overexpression of the dominant negative dynein intermediate chain 2 (DynCI2-DN) (King, Brown et al. 2003) resulted in a predominantly peripheral localization of lysosomes (**Fig. 3.2a, 3.2b, 3.2e**). As expected, starvation or ML-SA1 did not result in any significant changes in the peripheral localization pattern of lysosomes with DynIC2-DN overexpression (**Fig. 3.2b-d, 3.2f**). The overexpression of DynIC2-DN also shifted filipin-positive puncta structure in ML1KO fibroblasts to the cell periphery, without correcting the cholesterol accumulation phenotype (**Fig. 3.2g**). Treatment of the dynein inhibitor Ciliobrevin D (Sainath and Gallo 2015) for 2 hours also reversed the perinuclear distribution of lysosomes caused by ML-SA1 or TRPML1 overexpression in WT fibroblasts (**Fig. 3.2 h-k**). Collectively, these results suggest that cytoplasmic dynein is responsible for the TRPML1-dependent retrograde transport of lysosomes.

3.3.3 ALG-2 acts as the downstream effector of TRPML1 to promote minus-end motility of lysosomes through interaction with the dynactin complex

As a Ca^{2+} dependent TRPML1 interacting protein, I tested whether ALG-2 can serve as the downstream effector of TRPML1 in regulating lysosome motility. Indeed, ALG-2 overexpression in fibroblasts resulted in the perinuclear accumulation of lysosomes similar to TRPML1 hyperactivation (**Fig. 3.3a, 3.3e, 3.4a**). In contrast, overexpression of another lysosomal Ca^{2+} sensor, Syt VII, did not affect lysosome distribution (**Fig. 3.5**). In accordance with the Ca^{2+}-dependence of the interaction between TRPML1 and ALG-2, overexpression of a Ca^{2+}-binding defective EF-hand mutant of ALG-2 (ALG-2 $E^{47}A/E^{114}A$, or ALG-2-EEAA) (Vergarajauregui, Martina et al. 2009) had no effect on lysosome distribution (**Fig. 3.3c, 3.3e**). TRPML1 inhibition also abolished the effect of ALG-2 overexpression (**Fig. 3.3b, 3.3e**). On the other hand, activation of TRPML1 with ML-SA1 increased the co-localization of GFP-ALG-2 with Lamp1-mCherry (**Fig. 3.4**), consistent with the previous reports. Therefore, ALG-2 may serve as a Ca^{2+} effector of TRPML1 to promote retrograde migration of lysosomes.

TRPML1 interacts with ALG-2 through a stretch of three amino acids (R^{44}, L^{45} and K^{46}) on the N-terminal of TRPML1 (Vergarajauregui, Martina et al. 2009). Mutations of these residues (e.g. TRPML1-R^{44}/A or TRPML1-R^{44}LK/AAA) greatly decreases or abolishes the interaction between ALG-2 and TRPML1 (Vergarajauregui, Martina et al. 2009). TRPML1-R^{44}LK/AAA showed much smaller currents in electrophysiology recordings compared with WT channel, while TRPML1-R^{44}/A showed similar activation properties as the WT channel (**Fig. 3.6a-c**). Therefore, I used TRPML1-R^{44}/A as a control for the study. As mentioned in Chapter II, lysosomes in ML1KO fibroblasts displayed a perinuclear pattern likely caused by excessive accumulation of cholesterol that activates the Rab7-RILP pathway (**Fig. 2.12**). Overexpression of either WT TRPML1 or the ALG-2 binding deficient mutant TRPML1-R^{44}/A in ML1KO fibroblasts rescued the cholesterol accumulation (**Fig. 3.6f, 3.6g**). Overexpression of the WT

channel did not suppress the perinuclear distribution of lysosomes but rather resulted in a lysosome distribution similar to that produced by overexpression of the channel in WT cells due to the constitutive activity of TRPML1 under overexpression (**Fig. 3.6d, 3.6e**). In contrast, overexpression of TRPML1-R^{44}/A reversed the perinuclear distribution of lysosomes in ML1KO fibroblasts (**Fig. 3.3d, 3.3f**). Hence, physical interaction between TRPML1 and ALG-2 is required for the retrograde transport of lysosomes under physiological conditions.

It is known that cytoplasmic dynein does not interact with lysosomes directly, but through the dynactin complex, which in turn interacts with lysosomal proteins for its recruitment. In co-immunoprecipitation experiments (Co-IP), ALG-2-mCherry was able to pull down dynamitin, a member of the dynactin complex (Schroer 2004), with specificity (**Fig. 3.7**). Overexpression of dynamitin causes the dynactin complex to disassemble. However, ALG-2-mCherry pulled down both overexpressed dynamitin and endogenous dynamitin (**Fig. 3.7a, 3.7b**). This suggests that dynamitin, but not other members of the dynactin complex, might be the protein responsible for the interaction with ALG-2. Interestingly, ALG-2 pulled down dynamitin in a Ca^{2+}-independent manner (**Fig. 3.7a**), suggesting a model where ALG-2 is constitutively associated with the dynactin complex, and recruits the complex to lysosome surface upon Ca^{2+} release from TRPML1.

To further investigate the role of ALG-2 in retrograde transport of lysosomes, I generated and characterized ALG-2 KO HeLa cells using the CRISPR-Cas9 system (Cong and Zhang 2015) (**Fig. 3.8a, 3.8b**). At resting conditions, ALG-2 KO cells displayed a dispersed lysosome pattern that is not significantly different from the WT (although slightly more peripheral) (**Fig. 3.8c, 3.8h**). Under acute starvation or ML-SA1 application, however, these cells showed a sharp contrast to WT cells by not responding to these treatments in regard to lysosome positions (**Fig.**

3.8d, 3.8e, 3.8h). These data strongly suggest that ALG-2 is required for the retrograde migration of lysosomes under TRPML1 activation or acute starvation. Consistent with results described in Chapter II, perinuclear accumulation of lysosomes caused by RILP overexpression was not blocked by ALG-2 KO (**Fig. 3.8f, 3.8g**), suggesting that ALG-2 is responsible specifically for the TRPML1 pathway, but not for the Rab7-RILP pathway. Additionally, in ALG-2 KO HeLa cells, basal LC3-II levels were dramatically elevated compared to WT cells, and starvation did not induce further increase in LC3-II/LC3-I ratio (**Fig. 3.8i, 3.8j**). Collectively, these results suggest that the TRPML1-ALG-2-dependent retrograde transport is required for efficient autophagic clearance.

3.4 Discussion

In this Chapter I showed data that support a model on how TRPML1 regulates retrograde transport of lysosomes. In this model, $PI(3,5)P_2$ is required to activate TRPML1 under acute trafficking cues. When TRPML1 is activated, ALG-2 senses the Ca^{2+} elevation, and brings the dynactin complex to the lysosome through interacting with TRPML1. Dynactin complex recruits cytoplasmic dynein to allow the final transport of lysosomes in the minus-end direction.

As the only known endogenous agonist of TRPML1 (Dong, Shen et al. 2010), it is not surprising to find that $PI(3,5)P_2$ is required for TRPML1's function in retrograde transport of lysosomes. However, upon starvation, bulk cellular $PI(3,5)P_2$ levels reportedly drop to about 40% of the pre-starvation levels (Zolov, Bridges et al. 2012, Li, Wang et al. 2013). Therefore, activation of TRPML1 under starvation is unlikely caused through a direct increase in the $PI(3,5)P_2$ levels, and $PI(3,5)P_2$ may only play a permissive role in this process, allowing the

channel to open in its presence, simply serving as the location identifier to ensure the activation of TRPML1 is at the correct place.

Starvation is shown to cause mTOR inhibition and cytosolic alkalization, the latter shown in Chapter II to directly trigger retrograde migration of lysosomes. However, TRPML1 channel activity is only slightly increased upon cytosolic alkalization. mTOR was reported recently to suppress TRPML1 function through phosphorylation (Onyenwoke, Sexton et al. 2015), and may also regulate the subcellular localization of endogenous TRPML1, as suggested by studies on Drosophila TRPML (Wong, Li et al. 2012). Additionally, unidentified endogenous TRPML1 agonists may be produced during acute starvation and autophagy induction. It is likely multiple mechanisms mentioned above may locally activate TRPML1 in lysosomes during acute conditions.

The finding that the ALG-2 non-binding TRPML1-R^{44}/A can rescue the lysosome distribution phenotype as well as the cholesterol accumulation in ML1KO fibroblasts is very interesting. This would suggest that firstly, TRPML1 plays a role in clearing cholesterol out of lysosomes, which has been implied through previous studies (Pagano, Puri et al. 2000, Samie and Xu 2014, Wang, Gao et al. 2015). Secondly, the clearance of cholesterol from lysosomes is independent of TRPML1's interaction with ALG-2 and the downstream pathway. Therefore, other downstream effectors of TRPML1 have to be responsible for the clearance of cholesterol from the lysosomes. This would be an interesting topic for future studies.

ALG-2 has been shown to be involved in several vesicular trafficking steps, including ER-to-Golgi transport (Shibata, Suzuki et al. 2007, Helm, Bentley et al. 2014). It is known that Golgi is the organelle that normally resides closest to the MTOC, and may even play a role itself

in organizing microtubules (Rios 2014). Therefore, any transport towards the Golgi likely requires retrograde motility. Since ALG-2 associates with the dynactin complex, can it also regulate ER-to-Golgi transport through recruiting the dynactin complex to those transport vesicles? This would be a very interesting question to test.

Previous studies showed that TRPML1 has multiple downstream Ca^{2+} effectors, such as Synaptotagmin VII for lysosome exocytosis (Samie, Wang et al. 2013), and calcineurin for TFEB activation (Medina, Di Paola et al. 2015). How could TRPML1 regulate diverse downstream Ca^{2+} signaling pathways without messing them up? There are multiple possible mechanisms to ensure the specificity of the Ca^{2+} signaling. First, subcellular localization of the lysosome may have a direct impact on the availability of the downstream pathways. For example, it would not be possible to have lysosome exocytosis if the lysosome is away from the plasma membrane. Second, the downstream signaling pathway may require the presence of additional cofactors/substrates, or the absence of blockers. For example, activation of TRPML1 under fed conditions is unlikely going to cause TFEB translocation, due to the active mTORC1 complex present to re-phosphorylate TFEB. Therefore, TFEB translocation only happens when TRPML1 is active, and mTORC1 is inactive.

3.5 Materials and Methods

DNA subcloning

Dominant-negative Kif5B (human Kif5B a.a. residues 592-963) was subcloned to pmCherry-C1 (Clontech) using Kif5B cDNA as the template with the following pair of primers: forward, CCG GAA TTC ACT CTA CAT TAG CAA AAT G; and reverse, GTC GGA TCC

TTA CAC TTG TTT GCC TC. Dominant-negative dynein intermediate chain 2 (GFP-DYNIC2-DN) and GFP-dynamitin (both gifts from Dr. Kristen Verhey at the University of Michigan) have been characterized previously. mCherry-ALG-2 and GFP-TRPML1-R^{44}LK/AAA were provided by Dr. Rosa Puertollano (NHLBI, NIH). mCherry-ALG2-$E^{47}E^{114}$/AA, GFP-TRPML1-R^{44}/A mutants were generated with a site-directed mutagenesis kit. Other constructs are described in Chapter II. All constructs were verified with sequencing and confirmed with western blotting

Mouse lines; mammalian cell culture and transfection; starvation; fluorescence imaging and image analysis; quantification of lysosome distribution; endolysosomal electrophysiology, and statistical analysis

Same materials and protocols as described in Chapter II were applied.

Generation of ALG-2 KO HeLa cells using CRISPR/Cas9

A SpCas9 plasmid was obtained from Addgene (#48139). Primers for guide RNA generation are as following:

#1 forward: CACCGAGGGCCGGGGCGGTAAGAGT;

#1reverse: AAACACTCTTACCGCCCCGGCCCTC;

#2 forward: CACCGCTCTTACCGCCCCGGCCCTG;

#2 reverse: AAACCAGGGCCGGGGCGGTAAGAGC.

ALG-2 KO HeLa cells were generated using protocols established previously (Cong and Zhang 2015). Briefly, primers were annealed and incorporated onto the plasmid using the BpiI site. WT HeLa cells were transfected with the plasmid and followed by a 2-day puromycin selection after transfection for 24h. The cells were then plated on 96-well plates with an average

density of 0.5 cell per well. Single colonies were selected and sequenced. Identified mutant lines were confirmed by western blotting using anti-ALG-2.

Co-immunoprecipitation

Transfected cells (Cos1 cells for double-overexpression and HEK 293 cells for Co-IP with endogenous protein) from 10 cm dishes were incubated with 1 mL of lysis buffer (1% NP-40, 0.25% Na-deoxycholate, 1 mM Na_3VO_4, 1 mM NaF, 150 mM NaCl, 0.5 mM $CaCl_2$ in 50 mM Tris-HCl, adjusted to pH 7.4) for 30 min at 4 °C with occasional vortex. Lysates were centrifuged at 16,000 ×g for 10 min, and supernatants were incubated with 3 μg of primary antibodies at 4 °C for 1 hour. After addition of 30 μl of protein A/G plus-agarose, lysates were incubated at 4 °C overnight with gentle shaking. Agarose beads were then collected through centrifuge at 500 ×g for 5 min. Beads were washed four times in lysis buffer, then heated to 60 °C for 10 min in NuPAGE loading buffer. Proteins were blotted with anti-GFP/mCherry (1:5000), or anti-Dynamitin (1:1000).

Chemicals and reagents

Chemicals additional to those described in Chapter II are as follows: YM 201636 (Symansis), Ciliobrevin D (EMD Millipore), Apilimod (Axon Medchem BV). Dynamitin antibody was purchased from BD Biosciences (611002), and ALG-2 antibody was purchased from Novus Biologicals (H00010016-M01).

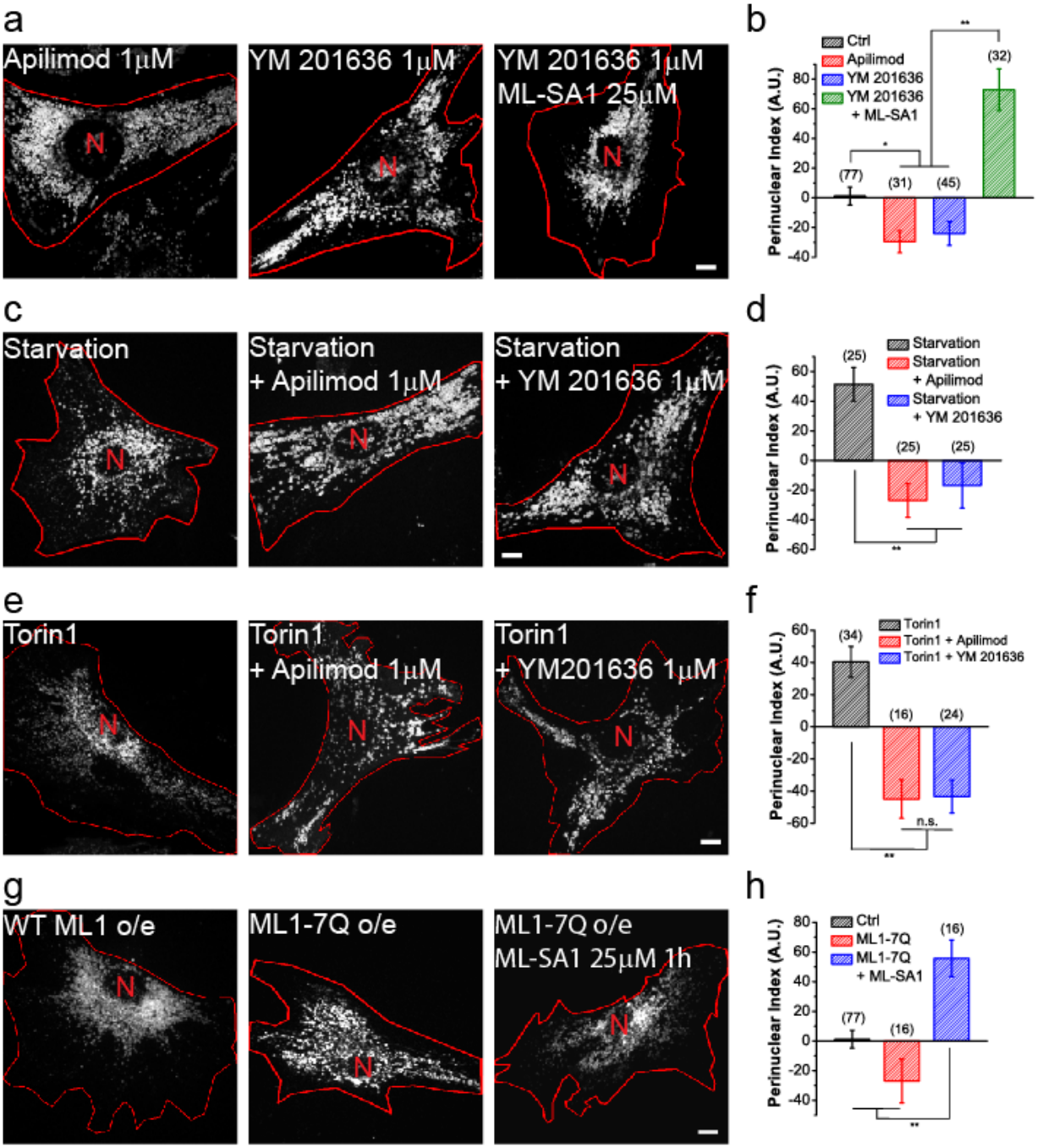

Fig. 3.1 PI(3,5)P_2 is required as an agonist of TRPML1 to promote perinuclear migration of lysosomes.

(**a**) Lysosome distribution in WT fibroblasts treated with 1 μM apilimod for 1 hour (left), 1 μM YM 201636 for 1 hour (middle), or 1 μM YM 201636 plus 25 μM ML-SA1 (right). (**b**) Quantification of groups shown in (**a**). (**c**) Lysosome distribution in WT fibroblasts starved for 1 hour (left), or starved for 1 hour in the presence of 1 μM apilimod (middle) or YM 201636 (right). (**d**) Quantification of groups shown in (**c**). (**e**) Lysosome distribution in WT fibroblasts

treated with 1 μM Torin-1 for 1 hour in the presence of 1 μM apilimod (middle) or YM 201636 (right). (**f**) Quantification of groups shown in (**e**). (**g**) Lysosome distribution in TRPML1-7Q-transfected cells in the presence (right) or absence (middle) of 25 μM ML-SA1 for 1 hour. (**h**) Quantification of groups shown in (**g**), compared to cells expressing Lamp1 alone. Red lines outline cell boundaries and nuclei are marked with a red "N". Graphed data are presented as means ± SEM, number of cells used for quantification are shown in the brackets. *$p < .05$, **$p < .01$ in ANOVA. Scale bar = 10 μm.

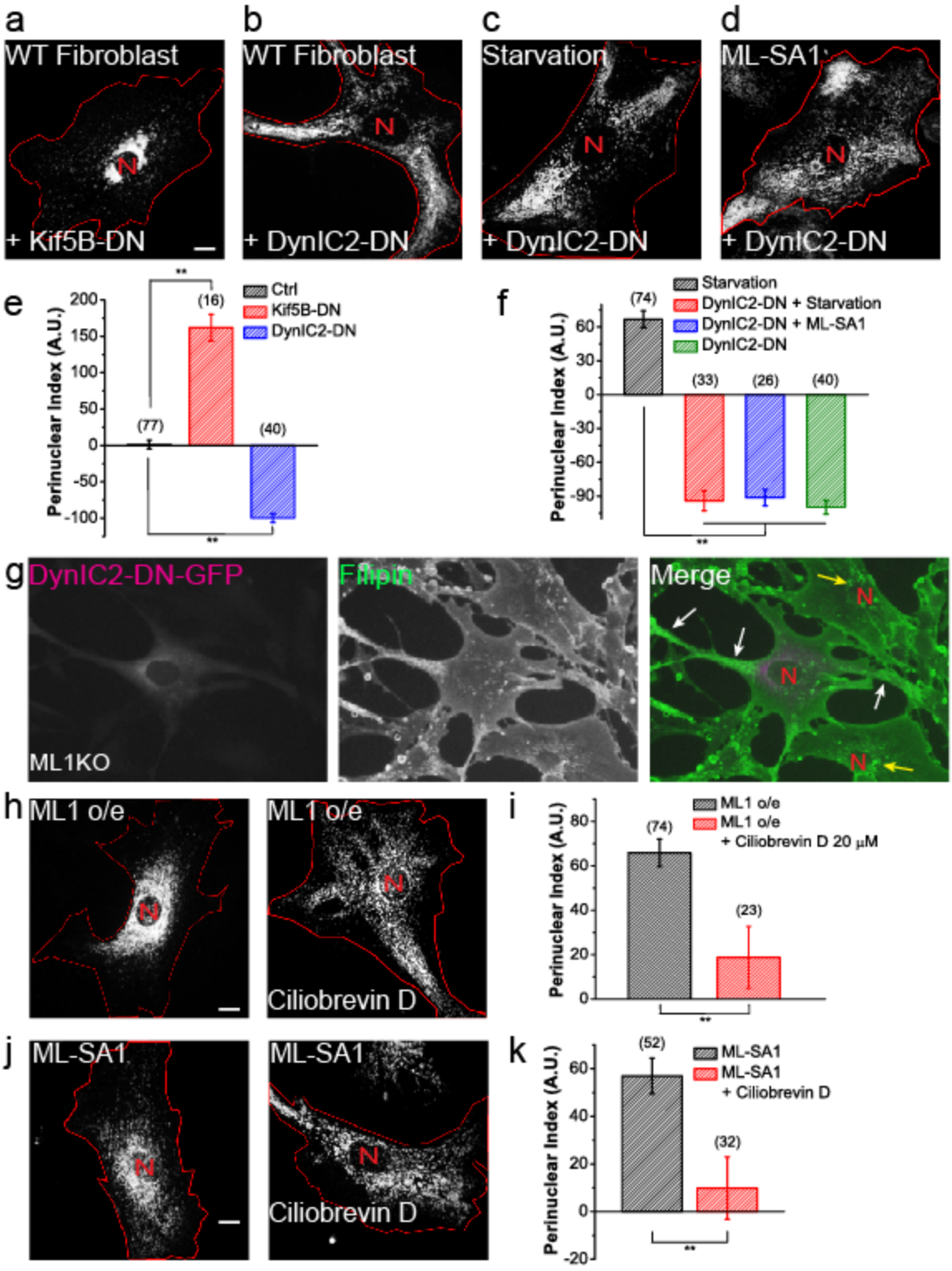

Fig. 3.2 TRPML1 promotes retrograde migration of lysosomes through cytoplasmic dynein.

(**a**) Lysosome (labeled with Lamp1-EGFP) distribution in WT fibroblasts transfected with mCherry-tagged dominant-negative Kif5B (Kif5B-DN). (**b-d**) Lysosome (labeled with Lamp1-

mCherry) distribution in WT fibroblasts transfected with GFP-tagged dominant-negative cytoplasmic dynein intermediate chain 2 (DynIC2-DN), then left untreated (**b**), starved for 2 hours (**c**), or treated with 25 μM ML-SA1 for 2 hours (**d**). (**e**) Quantification of lysosome distribution in groups shown in (**a**) and (**b**). (**f**) Quantification of lysosome distribution in groups shown in (**b-d**). (**g**) Representative images showing ML1KO fibroblasts transfected with DynIC2-DN-GFP, and stained with filipin. White arrows indicate lysosomal cholesterol in DynIC2-DN overexpression cells, while yellow arrows indicate lysosomal cholesterol in non-transfected cells. (**h**) Effect of dynein inhibitor ciliobrevin D (20 μM, 2 hours) on lysosome distribution in TRPML1-expressing fibroblasts. (**i**) Quantification of lysosome distribution in cells shown in (**h**). (**j**) WT fibroblasts treated with ML-SA1 (25 μM) or together with ciliobrevin D (20 μM) for 2 hours. (**k**) Quantification of lysosome distribution in cells shown in (**j**) Red lines outline cell boundaries; "N" marks nuclei. Graphed data are presented as means ± SEM, number of cells used for quantification are shown in the brackets. *$p < .05$, **$p < .01$ in ANOVA. Scale bars = 10 μm.

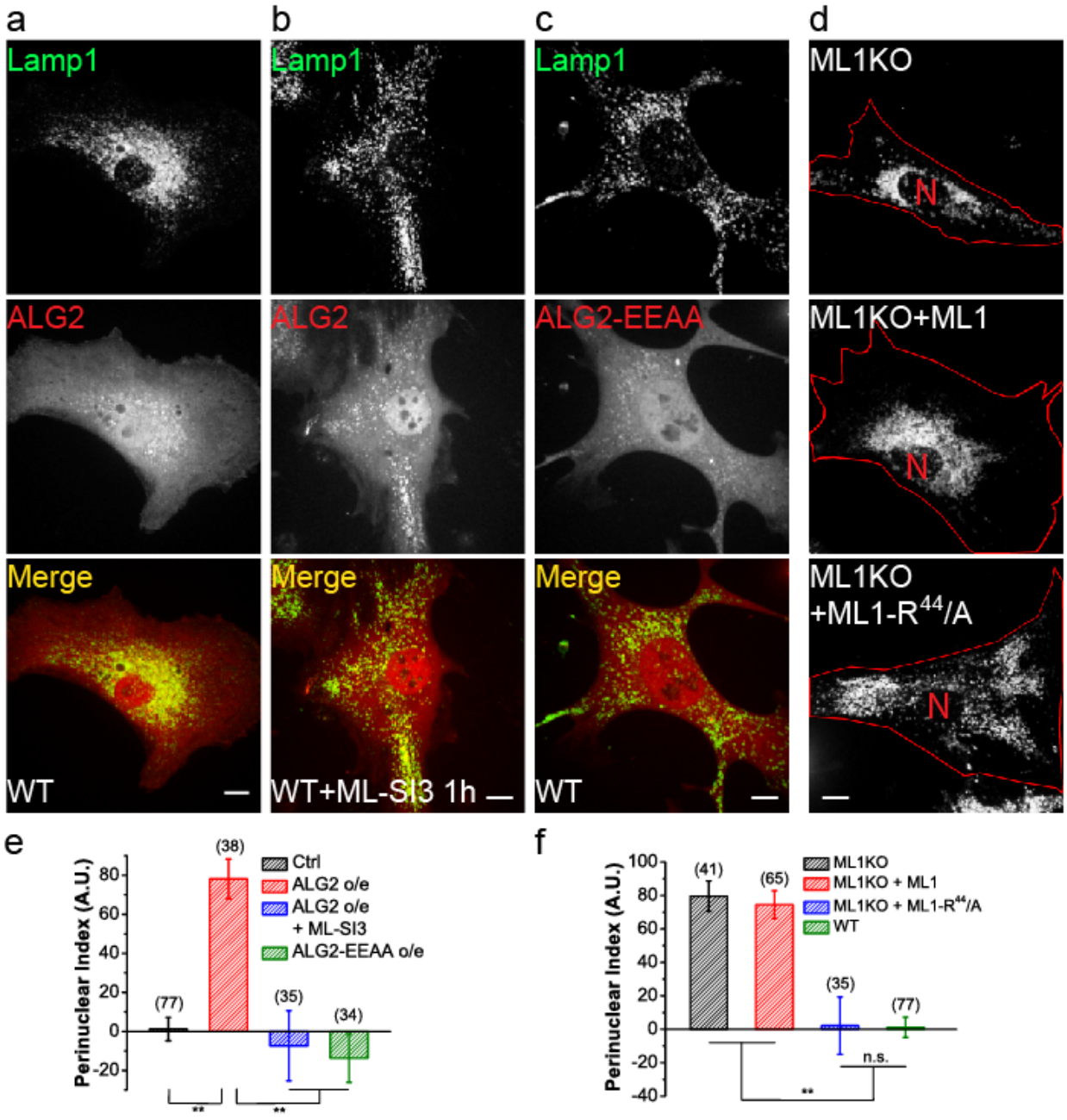

Fig. 3.3 ALG-2 mediates TRPML1-dependent minus-end directed transport of lysosomes.

(**a**) Lysosome distribution in WT fibroblasts co-transfected with Lamp1-GFP and mCherry-ALG-2. (**b**) Lysosome distribution in mCherry-ALG-2-transfected cells treated with ML-SI3 (25 μM) for 1 hour. (**c**) Lysosome distribution in WT fibroblasts co-transfected with Lamp1-GFP and mCherry-ALG-2-EEAA ($E^{47}A/E^{114}A$). (**d**) Lysosome distribution in ML1 KO fibroblasts transfected with Lamp1-mCherry alone (top), Lamp1-mCherry + GFP-TRPML1 (middle), or Lamp1-mCherry + GFP-TRPML1-R^{44}/A (bottom). (**e**) Quantification of lysosome distribution in experiments shown in (**a-c**). (**f**) Quantification of groups shown in (**d**). Red lines in images outline cell boundary and the red "N" marks the nucleus. Graphed data are presented as means ±

SEM, number of cells used for quantification are shown in the brackets. *$p < .05$, **$p < .01$ in ANOVA. Scale bars = 10 μm.

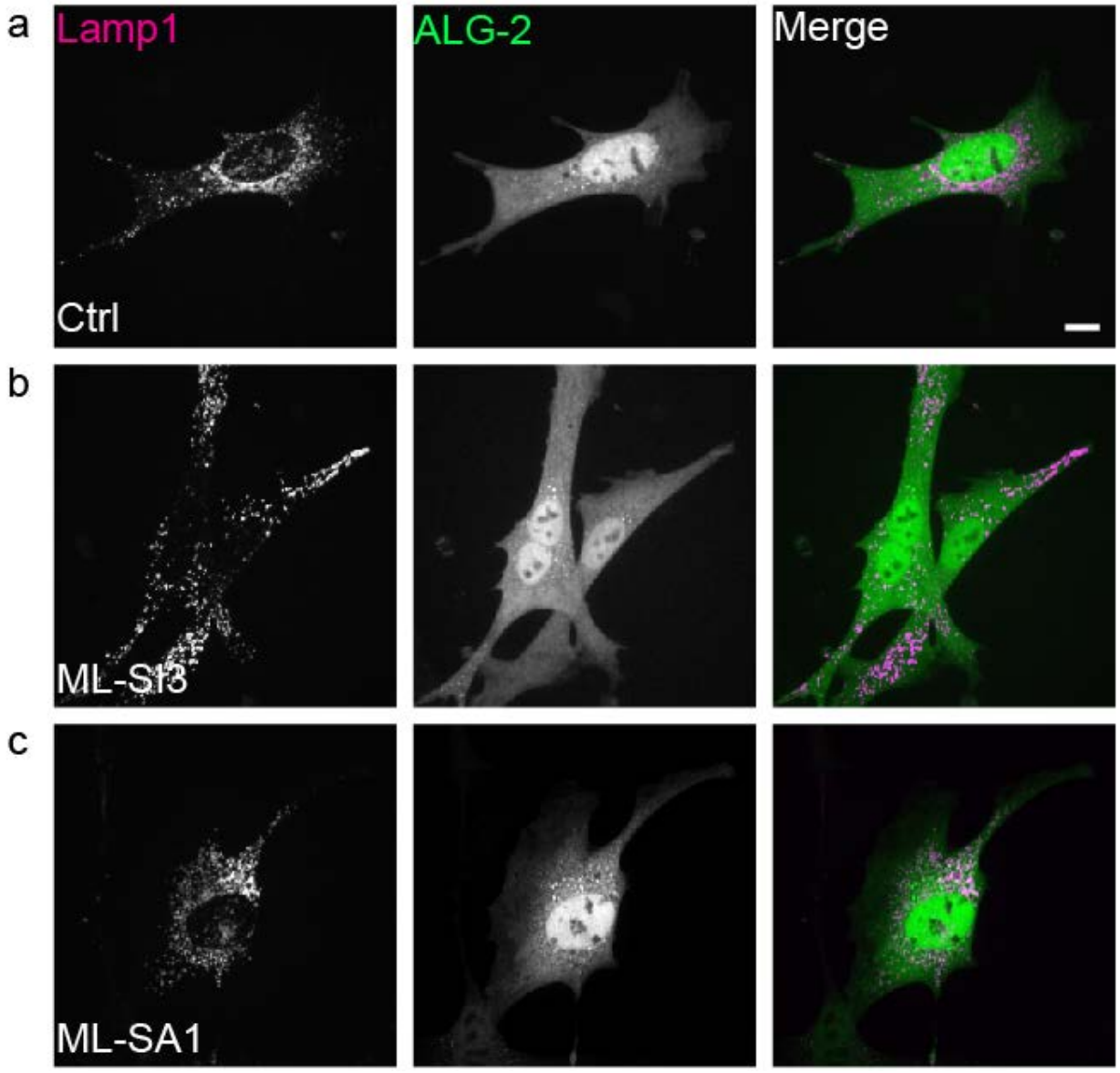

Fig. 3.4 Co-localization of overexpressed ALG-2-GFP and Lamp1-mCherry.

(**a-c**) WT fibroblasts co-transfected with ALG-2-GFP and Lamp1-mCherry, then left without treatment (**a**), treated with 25 μM ML-SI3 for 2 hours (**b**), or treated with 25 μM ML-SA1 for 2 hours (**c**). Some perinuclear bright dots of ALG-2 not co-localized with Lamp1 were seen in all treatment conditions. Treatment of ML-SI3 and ML-SA1 resulted in less (ML-SI3) or more (ML-SA1) co-localization with Lamp1 compared to non-treated control cells, respectively. Scale bar = 10 μm.

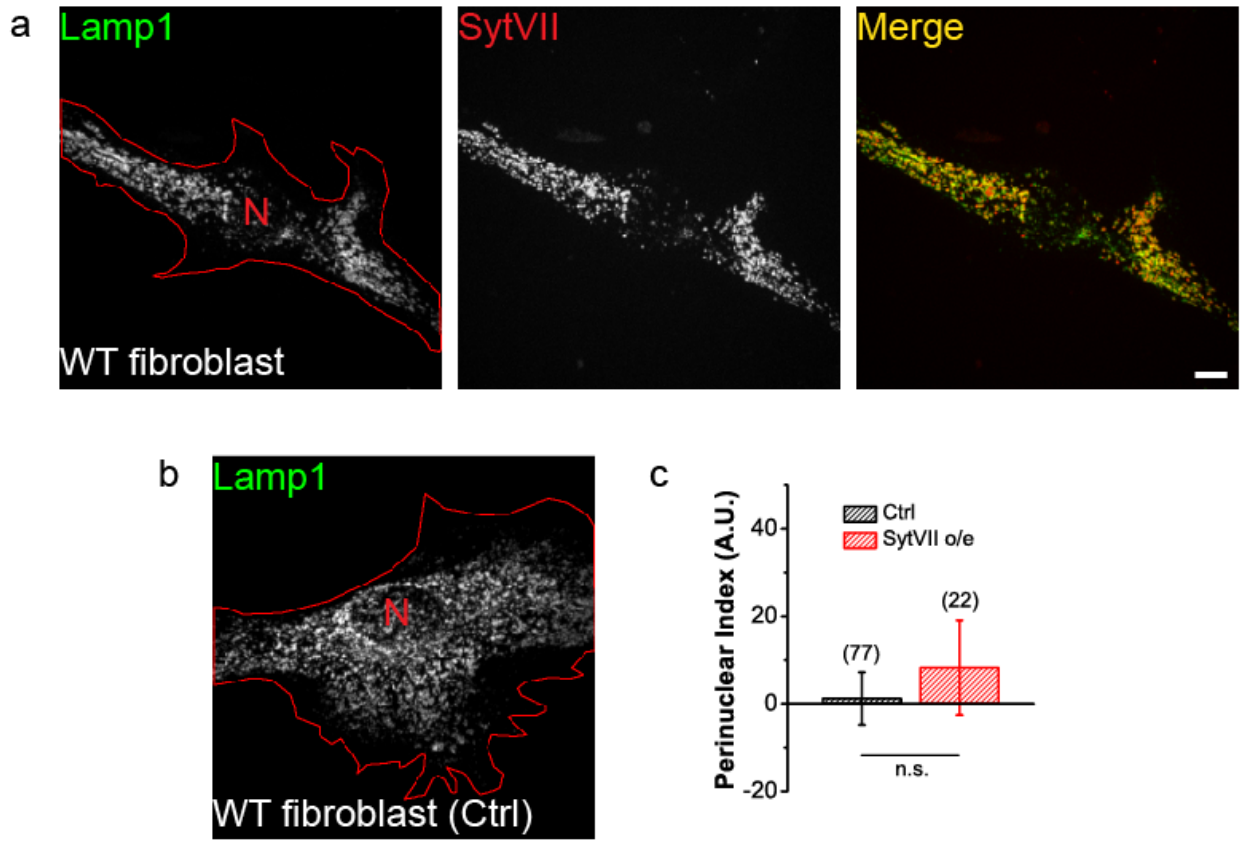

Fig. 3.5 Overexpression of lysosomal Ca^{2+} sensor Synaptotagmin VII does not affect lysosome distribution.

(**a, b**) WT fibroblasts overexpressing Lamp1-mCherry with (**a**) or without (**b**) Syt VII co-expression. (**c**) Quantification of groups shown in (**a, b**). Red lines outline cell boundaries and nuclei are marked with red "N". Graphed data are presented as means ± SEM, number of cells used for quantification are shown in the brackets. *p < .05, **p < .01 in ANOVA. Scale bar = 10 μm.

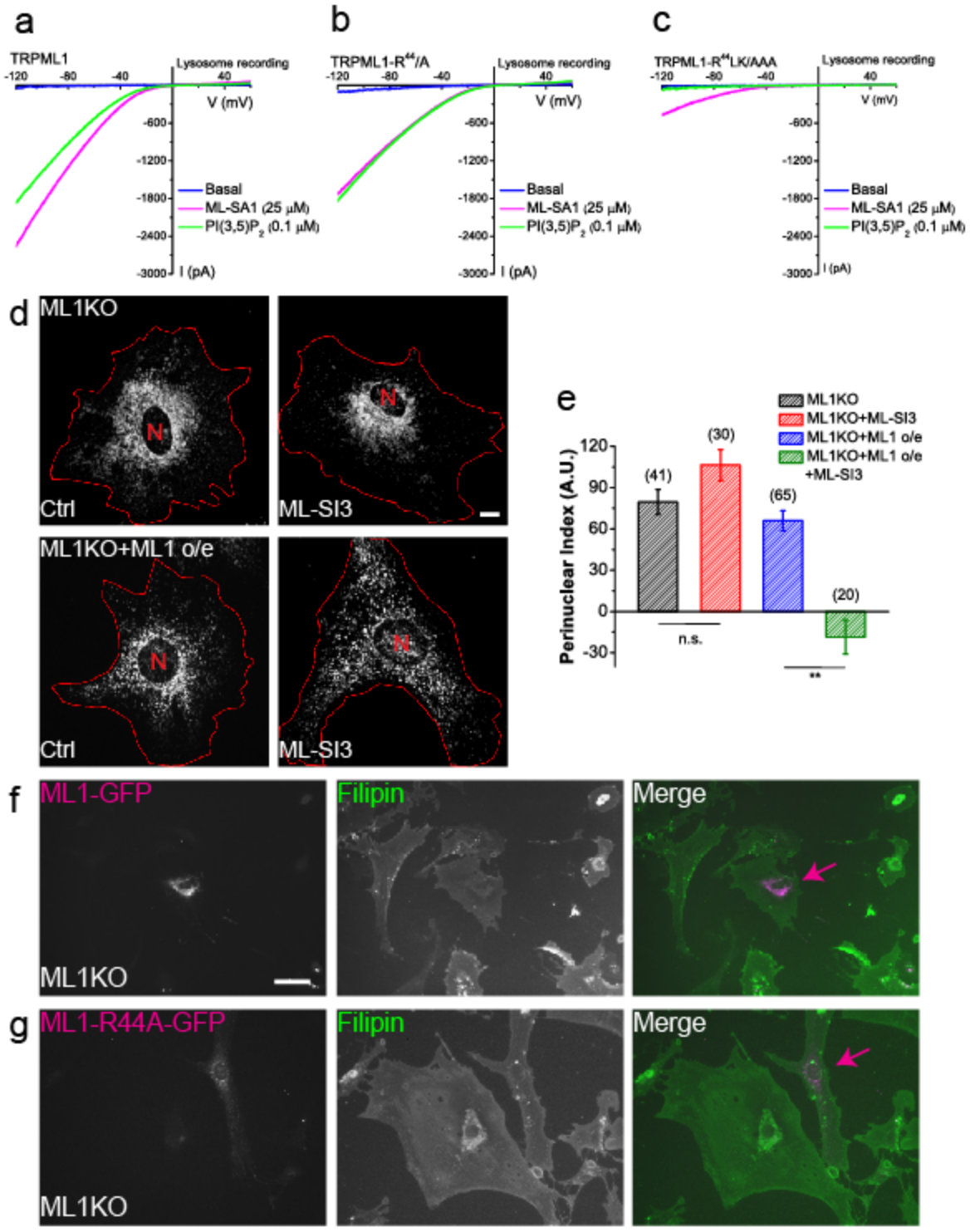

Fig. 3.6 Different rescue effects of TRPML1 and TRPML1-R^{44}/A overexpression in ML1KO fibroblasts.

(**a-c**) Representative whole-lysosome currents in cells overexpressing WT TRPML1 (**a**), TRPML1-R^{44}/A (**b**), or TRPML1-R^{44}LK/AAA (**c**). Whole-lysosome currents were elicited by the endogenous agonist PI(3,5)P_2 or the synthetic agonist ML-SA1. (**d**) Overexpression of

TRPML1 in ML1 KO fibroblasts causes perinuclear accumulation of lysosomes, but contrary to ML1 KO fibroblasts without TRPML1 expression, was reversible through application of 25 μM ML-SI3 for 2 hours. (**e**) Quantification of groups shown in (**d**). (**f, g**) Filipin staining of ML1 KO fibroblasts overexpressing TRPML1 (**f**) or TRPML1-R^{44}/A (**g**). Purple arrows indicate cells with overexpression. Red lines outline cell boundaries and nuclei are marked with a red "N". Graphed data are presented as means ± SEM, number of cells used for quantification are shown in the brackets. *$p < .05$, **$p < .01$ in ANOVA. Scale bars = 10 μm for (**d**), and 50 μm for (**f, g**).

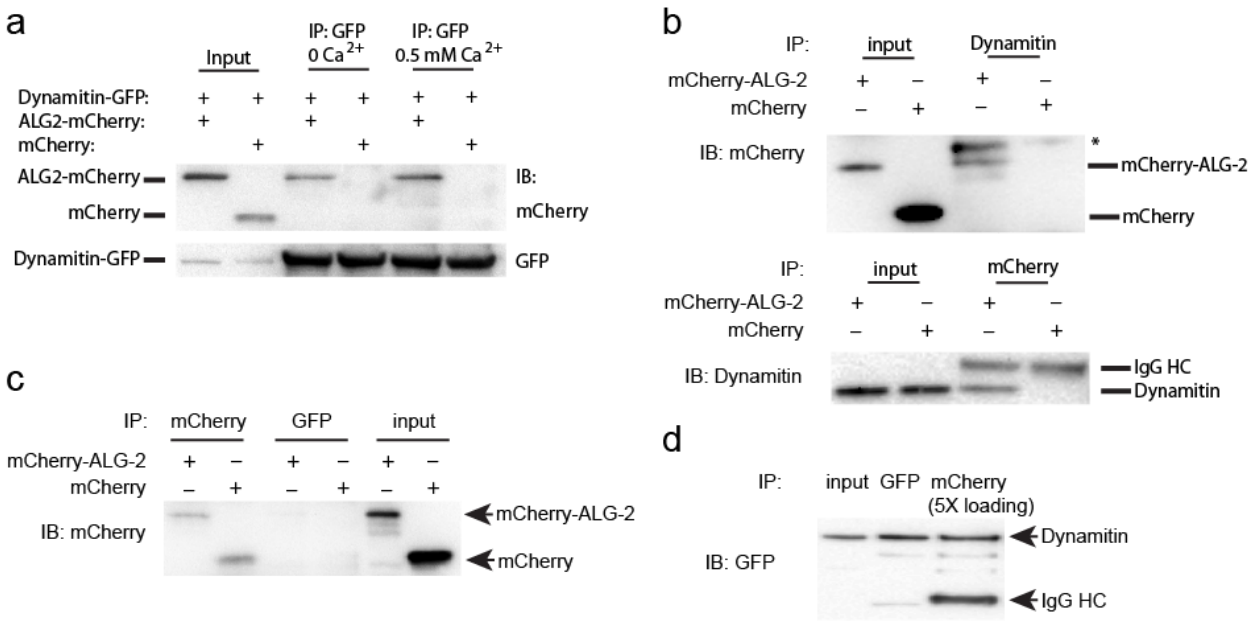

Fig. 3.7 Direct interaction between ALG-2 and dynamitin.

(**a**) Co-immunoprecipitation of ALG-2 and dynamitin in Cos-1 cells doubly transfected with mCherry-ALG-2 and GFP-Dynamitin, in the absence or presence of 0.5 mM Ca^{2+} in the lysis buffer. Cell lysates were directly loaded (input), or immunoprecipitated with either anti-GFP or anti-mCherry antibody, and then blotted against GFP. (**b**) Cells expressing mCherry or mCherry-ALG-2 were subject to Co-IP with either anti-mCherry or anti-Dynamitin, then blotted against mCherry (top) or Dynamitin (bottom). Asterisk indicates a non-specific band seen with HEK293 lysates. (**c**) Cos1 cells expressing either mCherry or mCherry-ALG-2 were subject to Co-IP with either anti-mCherry or anti-GFP antibodies, then blotted against mCherry. (**d**) Cos1 cells co-expressing GFP-dynamitin and mCherry-ALG-2 were subject to Co-IP with either anti-mCherry or anti-GFP antibodies, then blotted against GFP.

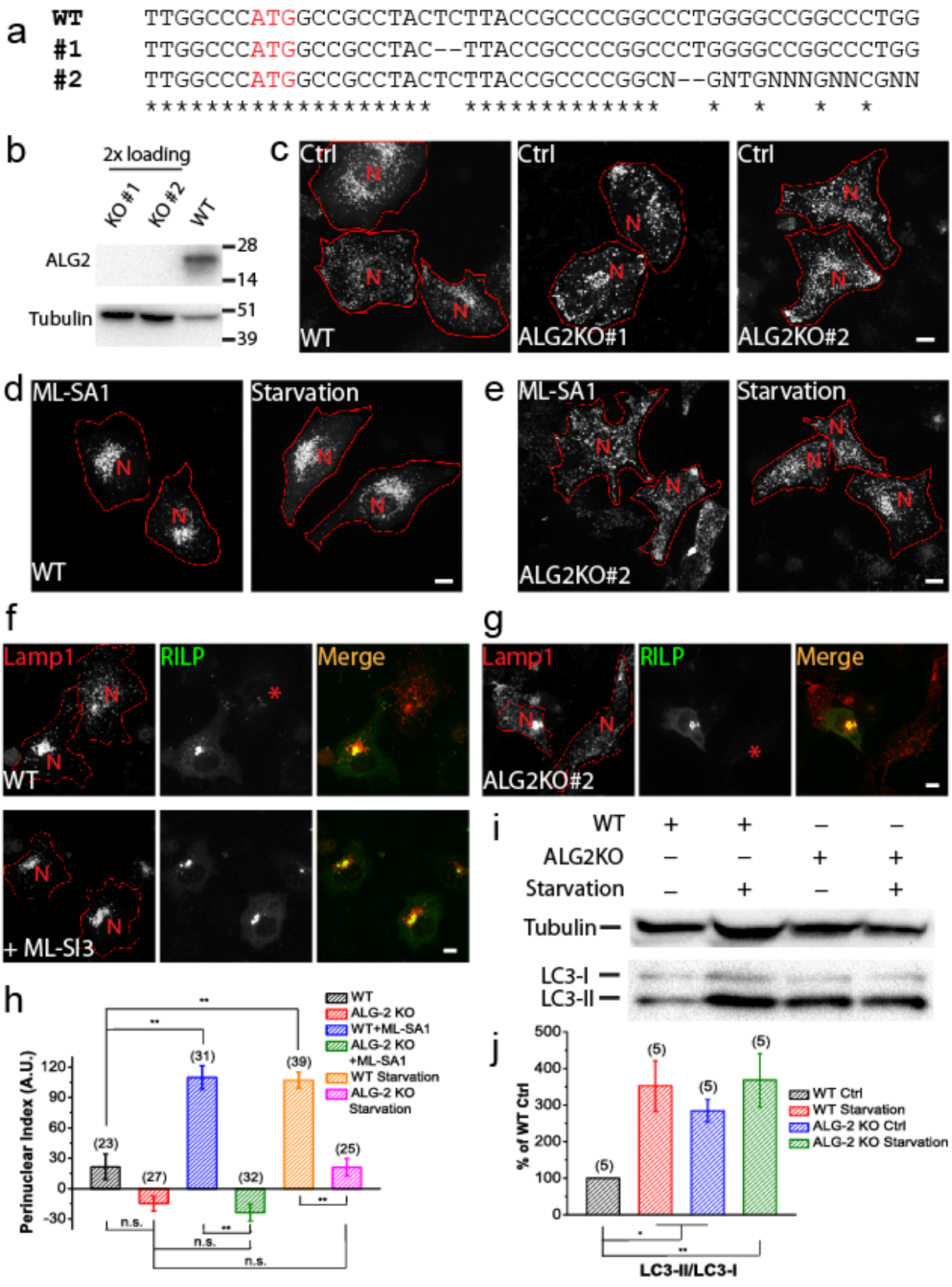
a
WT TTGGCCCATGGCCGCCTACTCTTACCGCCCCGGCCCTGGGGCCGGCCCTGG
#1 TTGGCCCATGGCCGCCTAC--TTACCGCCCCGGCCCTGGGGCCGGCCCTGG
#2 TTGGCCCATGGCCGCCTACTCTTACCGCCCCGGCN--GNTGNNNGNNCGNN
b
2x loading
KO#1
KO#2
WT
ALG2
Tubulin
28
14
51
39
c
Ctrl
WT
ALG2KO#1
ALG2KO#2
d
ML-SA1
Starvation
WT
e
ML-SA1
Starvation
ALG2KO#2
f
Lamp1
RILP
Merge
WT
+ ML-SI3
g
Lamp1
RILP
Merge
ALG2KO#2
h
Perinuclear Index (A.U.)
WT
ALG-2 KO
WT+ML-SA1
ALG-2 KO +ML-SA1
WT Starvation
ALG-2 KO Starvation
(23)
(27)
(31)
(32)
(39)
(25)
n.s.
i
WT
ALG2KO
Starvation
Tubulin
LC3-I
LC3-II
j
% of WT Ctrl
WT Ctrl
WT Starvation
ALG-2 KO Ctrl
ALG-2 KO Starvation
LC3-II/LC3-I

Fi.g 3.8 ALG-2 is required for the TRPML1-promoted acute retrograde migration of lysosomes.

(**a**) DNA sequencing results of the two ALG-2 CRISPR KO HeLa cell lines, the red "ATG" indicates start codon. Mutant #1 had a 2bp deletion on all chromosomes, while mutant #2 had various lengths of out-of-frame deletions. (**b**) Western blot confirmation of the ALG-2 KO. (**c**) Representative images showing Lamp1-mCherry distribution of WT (left) and the two mutant lines in complete medium without any treatment. (**d, e**) WT (d) and ALG-2 KO (e) cells under 2 hours of 25 μM ML-SA1 treatment (left), or under 2 hours of serum starvation (right). Mutant #2 was chosen for further studies based on their more extended morphology. (**f, g**) WT (**f**) and ALG-2 KO (**g**) cells overexpressing Lamp-mCherry and RILP-GFP in the presence of 25 μM ML-SI3 for 2hours. Red asterisks in RILP panels indicate cells not expressing RILP-GFP. (**h**) Quantification of the groups shown in (**c-e**). (**i, j**) Western blot analysis of endogenous LC3 in WT or ALG-2 KO HeLa cells upon 2 hours starvation. LC3-II over LC3-I ratio normalized to WT control cells from 5 independent experiments were quantified in (**j**). Red lines in images outline cell boundary and the red "N" marks the nucleus. Graphed data are presented as means ± SEM, number of cells used for quantification are shown in the brackets. *$p < .05$, **$p < .01$ in ANOVA. Scale bars = 10 μm.

CHAPTER IV

TRPML1 Regulates Lysosome Tubulation through Tuning of the Minus-end Pulling Force[4]

4.1 Abstract

Lysosome tubulation is a process in which tubular structure protrude from the vesicular part of lysosomes. Lysosome tubulation serves as a platform for lysosome reformation, and is most prominent during heavy lysosome consumptions, e.g. under prolonged starvation or during active phagocytosis. Current knowledge on the mechanisms of lysosome tubulation is quite limited, although the functions of various proteins have been found to be required for proper lysosome tubulation to take place. I show here that TRPML1 activity is required for lysosome tubulation in a bell-shaped manner, where too high or too low activity would both lead to the abolishment of lysosome tubulation. I have thus proposed a model in which TRPML1 regulates lysosome tubulation through the tuning of pulling forces between plus-end and minus-end motor proteins.

4.2 Introduction

[4] Originally Submitted in Nature Cell Biology. With authors listed as Xinran Li, Nicholas Rydzewski, Ahmad Hider, Xiaoli Zhang, Junsheng Yang, Wuyang Wang, Qiong Gao, Xiping Cheng, and Haoxing Xu.

Lysosome tubulation is a process long observed (Swanson, Bushnell et al. 1987), but only recently characterized (Yu, McPhee et al. 2010). It has been proposed that lysosome tubulation serves as a platform for lysosome reformation, in which "protolysosomes" bud off from the tubular structures to recycle lysosomal membrane and proteins for the generation of new functional lysosomes (Yu, McPhee et al. 2010, Chen and Yu 2013). This is thought to replenish the pool of lysosomes during heavy consumption periods like prolonged starvation and active phagocytosis.

Lysosome tubulation seems to be a quite delicate process, because the disruption of the function of many lysosomal proteins or nutrient-sensing proteins can lead to abnormal lysosome tubulation, in most cases the loss of tubulation (Rong, McPhee et al. 2011, Mrakovic, Kay et al. 2012, Rong, Liu et al. 2012, Sridhar, Patel et al. 2013). mTORC1 is the first regulator identified for lysosome tubulation during prolonged starvation (Yu, McPhee et al. 2010). It was shown that while inactivated during acute starvation, mTORC1 gets reactivated under prolonged starvation because of the release of amino acids from lysosomes through digestion of autophagic materials. This reactivation of mTORC1 is somehow required for the reformation of lysosomes under prolonged starvation (Yu, McPhee et al. 2010).

Apart from mTOR, the clathrin-mediated membrane fission pathway is also identified to be important for lysosome tubulation and reformation (Rong, Liu et al. 2012). It was shown that $PI(4,5)P_2$, which is responsible for the membrane recruitment of clathrin, is required to be present on lysosomes during lysosome reformation. Clathrin and clathrin adaptor complex AP2, obviously, were also shown to be necessary for the process (Rong, Liu et al. 2012). PI4KIII and PI4P5K1A/1B, which are phosphoinositol-kinases responsible for the generation of PI(4)P and

$PI(4,5)P_2$, respectively, were also shown to be involved in the regulation of lysosome tubulation and reformation in quite complicated manners (Rong, Liu et al. 2012, Sridhar, Patel et al. 2013).

Motor proteins kinesin and dynein were suggested to be necessary for lysosome tubulation using macrophage phagocytosis as the model (Mrakovic, Kay et al. 2012). This is not surprising because the generation of tubular structures on lysosomes inevitably requires the pulling force from two opposite directions, and microtubule-based motor proteins are well fit for this purpose. The same study also identified Rab7-RILP and Arl8-SKIP as compulsory regulators of the tubulation process, being responsible for the recruitment of dynein and kinesin, respectively (Mrakovic, Kay et al. 2012).

Although many proteins are identified to regulate the lysosome tubulation process, more questions remain to be answered. It remains a question as to the mechanism of the generation of lysosomal tubules, as well as tubule extension. The mechanism through which the loss of activity of some of the regulators e.g. mTORC1 (Yu, McPhee et al. 2010) and the lysosomal transporter spinster (Rong, McPhee et al. 2011) can lead to the failure of lysosome tubulation is also unknown. In summary, systematic explanations to the regulation of lysosome tubulation, and to the question of how lysosome tubulation is affected in such a variety of different conditions, are still lacking. Therefore, I proceeded to test the functions of TRPML1 in lysosome tubulation and sought a more general model underlying the failure of lysosome tubulation.

4.3 Results

4.3.1 TRPML1 and lysosomal Ca^{2+} are required for lysosome tubulation

My results shown in Chapters II and III showed that TRPML1 regulates the minus-end motility of lysosomes through ALG-2's recruitment of dynein complex. Provided the previous report that motor proteins are required for the tubulation (Mrakovic, Kay et al. 2012), I examined whether TRPML1 is required for lysosome tubulation.

First of all, I confirmed the necessity of motor proteins in regulating lysosome tubulation through the overexpression of dominant negative motor protein constructs. I found that the loss of activity of either Kif5B or dynein abolished lysosome tubulation during autophagic lysosome reformation (**Fig. 4.1a**). As the previous report was done in macrophages using phagocytosis as the model, this result would suggest that motor proteins are likely required for lysosome tubulation regardless the circumstances under which lysosome tubulation happen.

I then investigated the role of TRPML1 in lysosome tubulation under various conditions in different cell types, including tubulation in prolonged starvation in fibroblasts (**Fig. 4.2a, 4.2b**) and NRK cells (**Fig. 4.1b, 4.1c**), tubulation after LPS activation of phagocytosis in macrophages (**Fig. 4.2c, 4.2d**), and the previously unreported constitutive tubulation in CV1 cells (**Fig. 4.2e, 4.2f**). In all conditions, ML1KO or acute inhibition of TRPML1 abolished lysosome tubulation (**Fig. 4.1 and 4.2**). The Ca^{2+} chelator BAPTA-AM inhibited tubulation potently in CV1 cells (**Fig. 4.2e, 4.2f**), and a strong temperature dependence of tubulation was observed (**Fig. 4.3**). It is worth noting that tubulation in macrophages also required mTOR activity (**Fig. 4.4**).

4.3.2 $PI(3,5)P_2$ is required for TRPML1-dependent lysosome tubulation

$PI(3,5)P_2$ was shown to be required for TRPML1-mediated retrograde transport of lysosomes (Chapter III). Inhibition of the $PI(3,5)P_2$ and PI(5)P synthesis enzyme PIKfyve through YM 201636 inhibited lysosome tubulation in prolonged starvation (**Fig. 4.5a, 4.5c**). The

requirement for $PI(3,5)P_2$ is further confirmed through genetic approaches using Vac14KO fibroblasts. Knocking-out of Vac14, a scaffold protein required for PIKfyve activity, results in ~50% reduction in cellular $PI(3,5)P_2$ levels (Jin, Chow et al. 2008). During prolonged starvation, Vac14KO fibroblasts showed moderately reduced lysosome tubulation, but can be rescued with acute application of ML-SA1 (**Fig. 4.5a, 4.5c**). Furthermore, although overexpression of TRPML1-7Q, which is insensitive to $PI(3,5)P_2$, failed to rescue the lysosome tubulation phenotype in ML1KO fibroblasts, delivery of a low dose of ML-SA1 in TRPML1-7Q transfected ML1KO cells restored lysosome tubulation to near normal levels (**Fig. 4.5b, 4.5d**).

4.3.3 TRPML1 regulates lysosome tubulation by tuning the balance between minus-end and plus-end motility of lysosomes

Normally, if the activation of a protein is required for a certain process, then more activity of the protein would boost up the process it regulates. Interestingly, while loss of TRPML1 activity abolished lysosome tubulation, hyper-activation of TRPML1 through TRPML1 overexpression or through ML-SA1 application also abolished lysosome tubulation (**Fig. 4.6a-c, 4.6f**). This observation led to a hypothesis where a balance between the plus- and the minus-end motility of the lysosome may be important for the generation of tubular structures on lysosomes (**Fig. 4.6g**). In this case, hyper or hypo activation of TRPML1 would disrupt the balance, resulting in an inverted U-shape relationship between TRPML1 activity and lysosome tubulation.

Consistent with the hypothesis, I found that in TRPML1 overexpressing fibroblasts, low concentration of TRPML1 inhibitors restored lysosome tubulation (**Fig. 4.6d, 4.6f**), while high concentrations of the inhibitor blocked lysosome tubulation (**Fig. 4.6e, 4.6f**). Likewise, in ALG-2

overexpressing fibroblasts, a slightly elevated degree of tubulation was observed under complete medium, but tubulation was inhibited during prolonged starvation (**Fig. 4.1d**).

4.4 Discussion

Lysosome motility is required for many lysosome functions including lysosome tubulation (Mrakovic, Kay et al. 2012). Under heavy consumption of lysosomes, lysosome tubulation is triggered to allow the recycling of lysosomal proteins and lipids to replenish the pool of functional lysosomes. Dysfunction of many lysosome-related proteins can lead to the loss of lysosome tubulation, but underlying mechanisms for most of their effects have not been characterized.

My results shown in this chapter demonstrate a possible common mechanism leading to the loss of lysosome tubulation in many dysfunctional conditions. A shared characteristic of most LSDs or other lysosome-related dysfunctions is the storage of various substances in the lysosomes, including cholesterol (Pagano, Puri et al. 2000, Yanagawa, Tsukuba et al. 2007, Samie and Xu 2014). My data suggest that the balance between the plus-end motility and the minus-end motility of lysosomes is important for the elongation and/or maintenance of the tubular structures. Therefore, disruption of this balance will likely disrupt lysosome tubulation regardless of the circumstance under which tubulation is triggered. Since cholesterol accumulation, as shown in Chapter II, can lead to elevated minus-end transport of lysosomes, it is likely that cholesterol storage will disrupt the balance between opposite directions' pulling forces. This would in turn lead to the destabilization of the tubular structure, or failure for the generation of tubular structures. Accordingly, in many disease models, the restoration of

lysosome tubulation may be accomplished simply by tuning the balance between plus-end and minus-end motilities.

4.5 Materials and Methods

DNA subcloning; Mammalian cell culture and transfection; Starvation; Fluorescence imaging and image analysis; Statistical analysis

Same materials and protocols described in Chapter II and Chapter III were applied.

Mouse lines

Characterizations of TRPML1 and Vac14 KO mice were performed as described previously (Venugopal, Browning et al. 2007, Zhang, Zolov et al. 2007, Jin, Chow et al. 2008). Animals were used under approved animal protocols and the Institutional Animal Care Guidelines of the University of Michigan.

Quantification of lysosome tubulation

Cells were chosen randomly with the criterion that their fluorescence was strong enough to visualize tubular structures. Only tubules longer than 2 μm were included in the analysis to reduce false-positive hits (see **Fig. 4.7**). Quantifications were done by researchers blind to the experimental groups presented.

Chemicals and reagents

Chemicals additional to those described in Chapters II and III are as follows: LPS (Sigma), murine GM-CSF (peprotech).

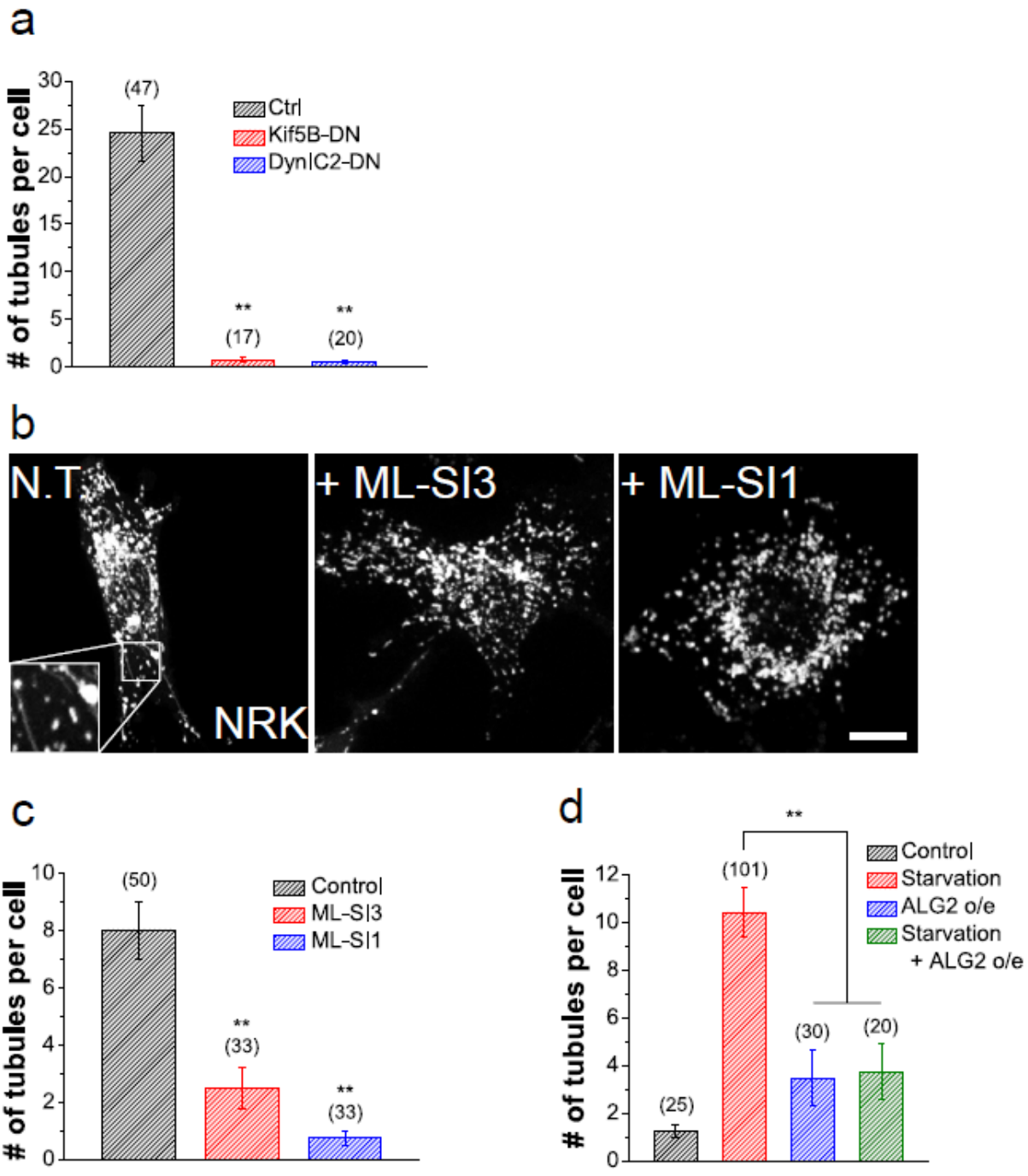

Fig. 4.1 Regulation of lysosome tubulation by TRPML1 and ALG-2.

(**a**) Quantification of lysosome tubulation in CV-1 cells. Dominant-negative constructs of Kif5B and DynIC2 eliminated spontaneous tubulation in Lamp1-GFP-expressing CV1 cells almost completely. (**b**) Representative images of Lamp1-mCherry-transfected NRK cells starved for 16 hours (left), or starved for 16 hours with the last 2 hours in the presence of 25 μM ML-SI3 (middle) or ML-SI1 (right). (**c**) Quantification of groups shown in (**b**). (**d**) Quantification of lysosome tubulation in WT fibroblasts transfected with Lamp1-GFP, or Lamp1-GFP plus ALG-

2-mCherry, with or without starvation for 24 hours. ALG-2 expression inhibited lysosome tubulation strongly in starved cells. Graphed data are presented as means ± SEM, number of cells used for quantification are shown in the brackets. *$p < .05$, **$p < .01$. Scale bars = 10 μm.

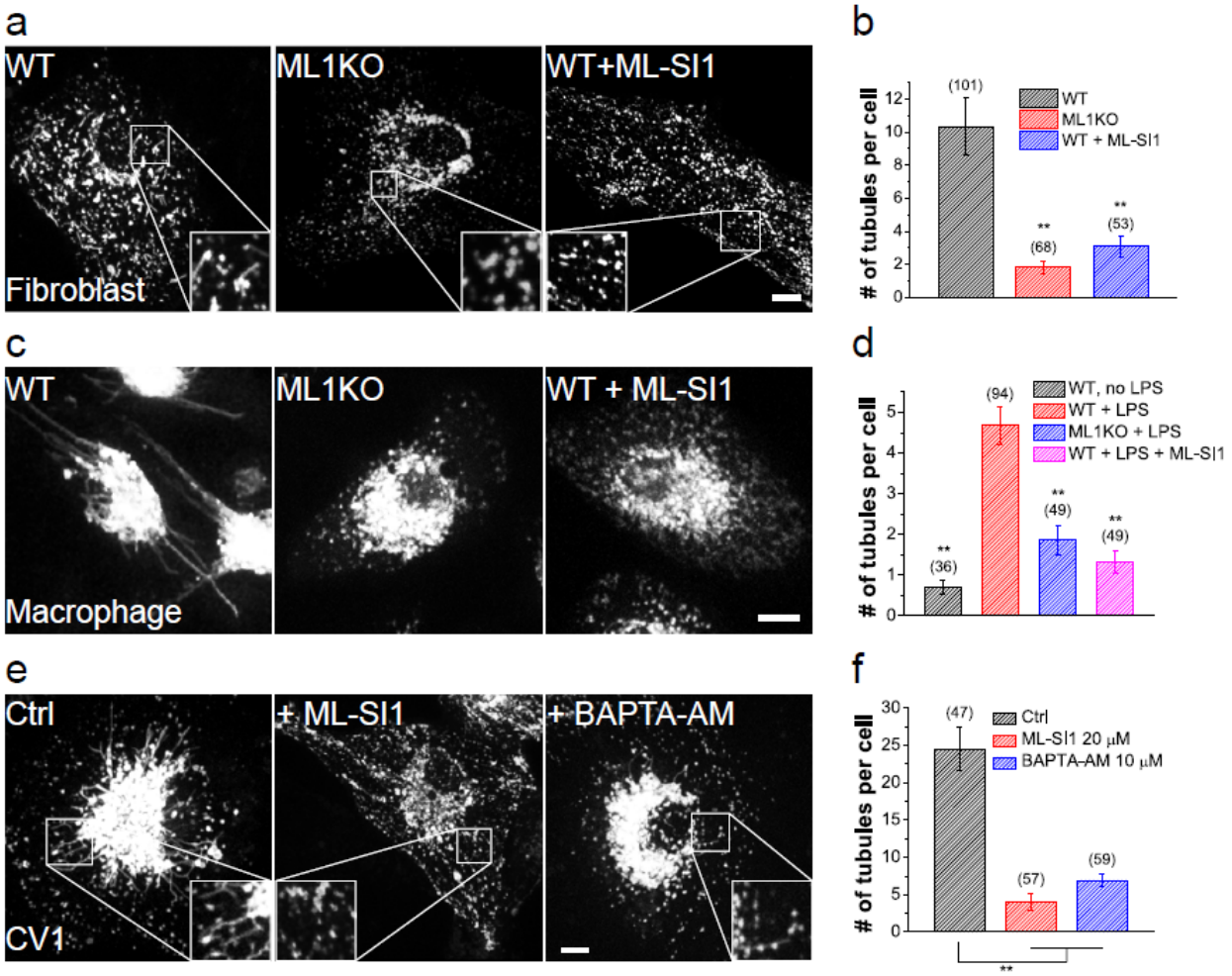

Fig. 4.2 TRPML1 and Ca^{2+}-dependent lysosome tubulation in various cell types and conditions.

(**a**) Lamp1-mCherry-transfected fibroblasts were starved for 24 hours. A high level of lysosome tubulation was seen in WT fibroblasts, but not in ML1 KO fibroblasts or in WT fibroblasts treated with ML-SI1 (25 μM) during the last hour of starvation. (**b**) Quantification of lysosome tubules in the groups shown in (**a**). (**c**) Lysosome tubulation in macrophages loaded with tetramethylrhodamine-dextran (1 hour loading, 2 hours chase) and activated with lysopolysaccharides (LPS) for 3 hours. Lysosome tubulation was prominent in WT macrophages (left), but not in ML1 KO macrophages (middle) or WT macrophages treated with ML-SI1 (25 μM, 30 min; right). (**d**) Quantification of the groups shown in (**c**). (**e**) Effects of ML-SI1 (25 μM, 1 hour) or BAPTA-AM (10 μM, 1 hour) on spontaneous lysosome tubulation in Lamp1-GFP-expressing CV1 cells. (**f**) Quantification of groups shown in (**e**). Graphed data are presented as means ± SEM, number of cells used for quantification are shown in the brackets. *p < .05, **p < .01 in ANOVA. Scale bars = 10 μm.

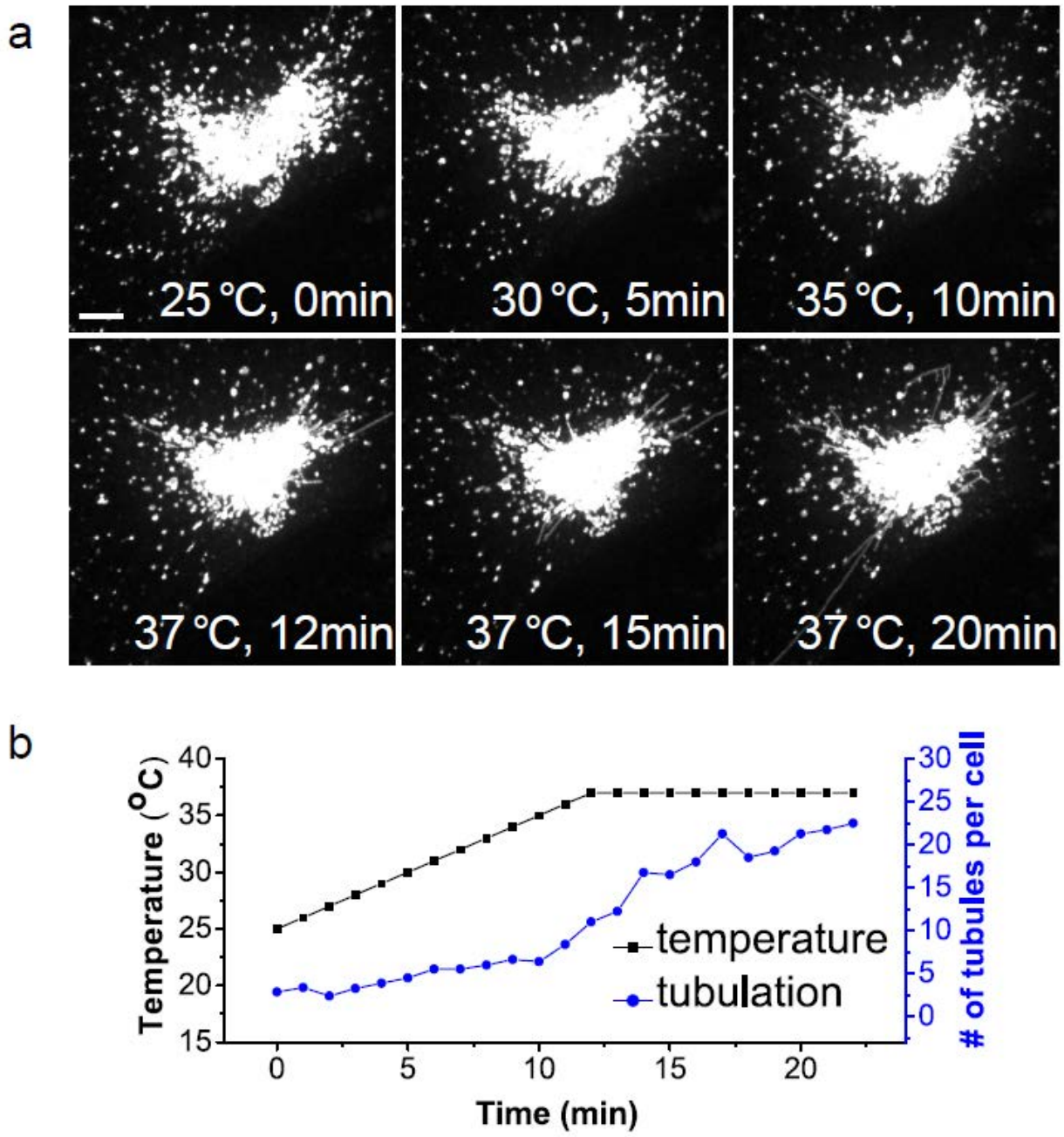

Fig. 4.3 Lysosome tubulation exhibits a strong temperature dependence.

(**a**) Time-lapse images showing a CV1 cell overexpressing Lamp1-EGFP, and treated with a temperature protocol shown in (**b**). (**b**) Quantifications of lysosome tubulation in CV1 cells under different temperatures. Quantifications are the average of four cells. Scale bar = 10 μm.

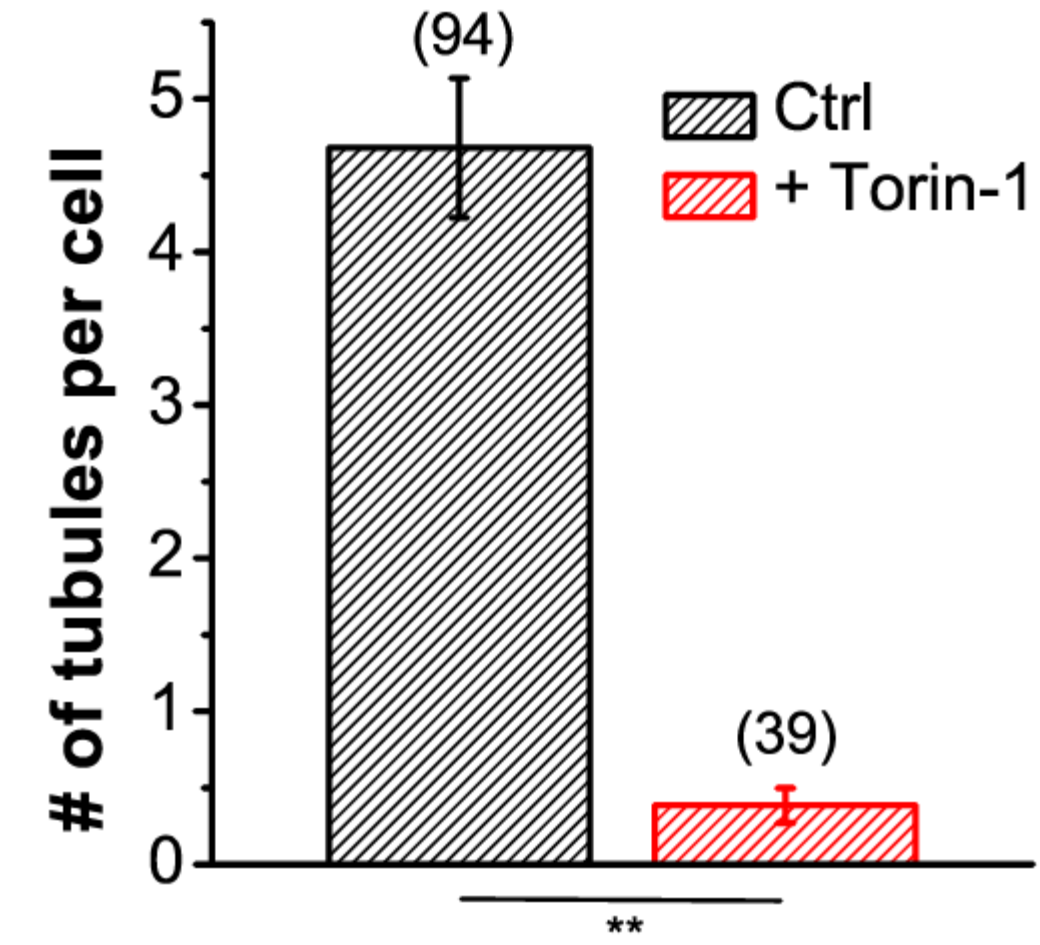

Fig. 4.4 Lysosome tubulation in macrophages requires mTOR activity.

Quantification of the average tubulation per cell in WT macrophages loaded with tetramethylrhodamine-dextran (1 hour loading, 2 hours chase) and activated with lysopolysaccharides (LPS) for 3 hours (Ctrl), or co-applied with 400 nM Torin-1 together with LPS. Graphed data are presented as means ± SEM, number of cells used for quantification are shown in the brackets. **p < .01 in ANOVA.

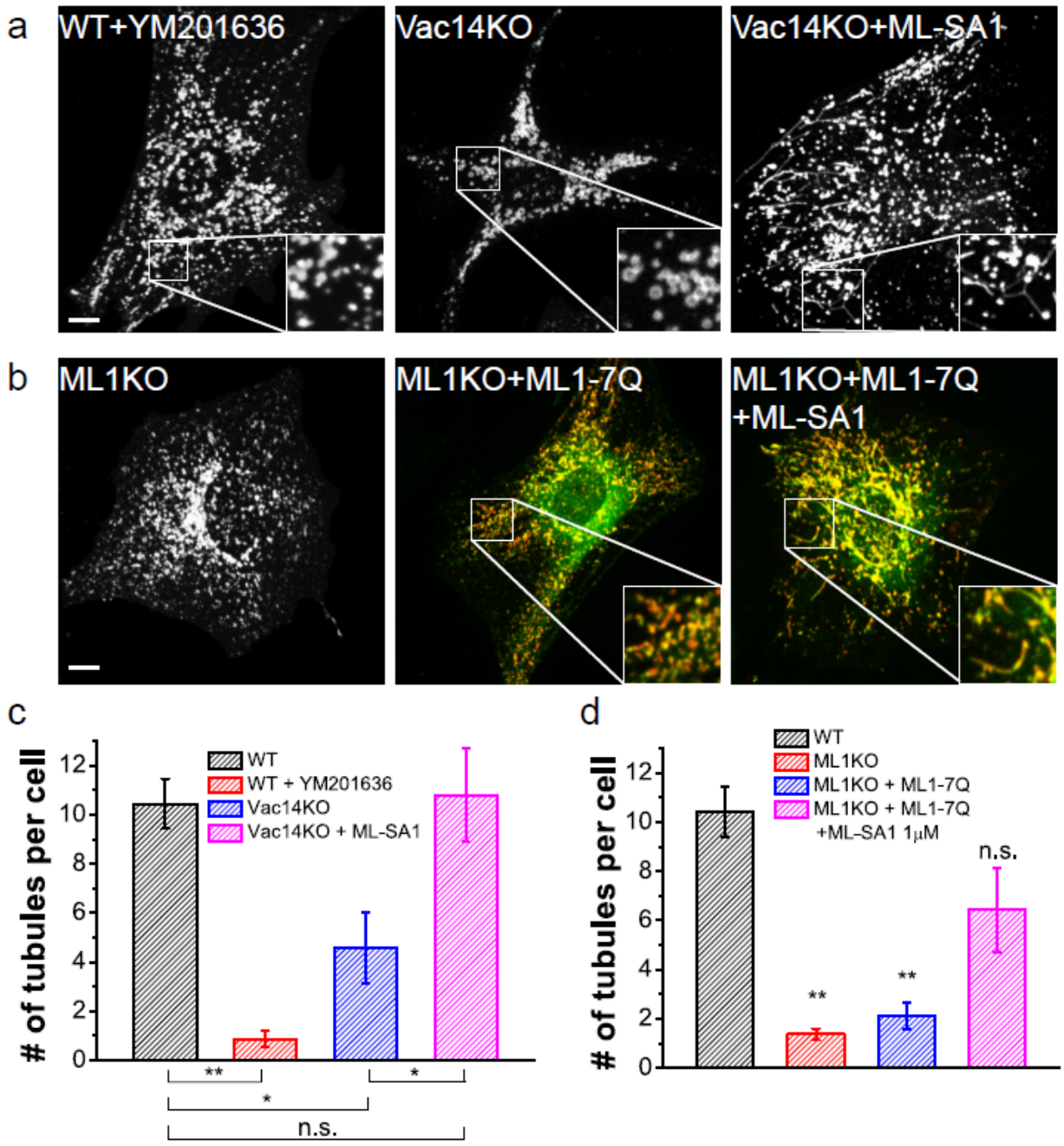

Fig. 4.5 PI(3,5)P_2 is required for lysosome tubulation through activation of TRPML1.

(**a**) Representative WT fibroblasts starved for 24 hours and treated with 1 μM YM 201636 for 30 min (left), Vac14 KO fibroblasts starved for 24 hours (middle), and starved Vac14 KO fibroblasts treated with 10 μM ML-SA1 for 30 min (right). (**b**) Lysosome tubulation after 24 hours starvation of ML1 KO fibroblasts transfected with Lamp1-mCherry alone (left), Lamp1-mCherry together with GFP-TRPML1-7Q with (right) or without (middle) a low dose (1 μM) of ML-SA1 for 1 hour. (**c**) Quantification of the groups shown in (**a**). (**d**) Quantification of the groups shown in (**b**). Graphed data are presented as means ± SEM, number of cells used for quantification are shown in the brackets. *p < .05, **p < .01 in ANOVA. Scale bars = 10 μm.

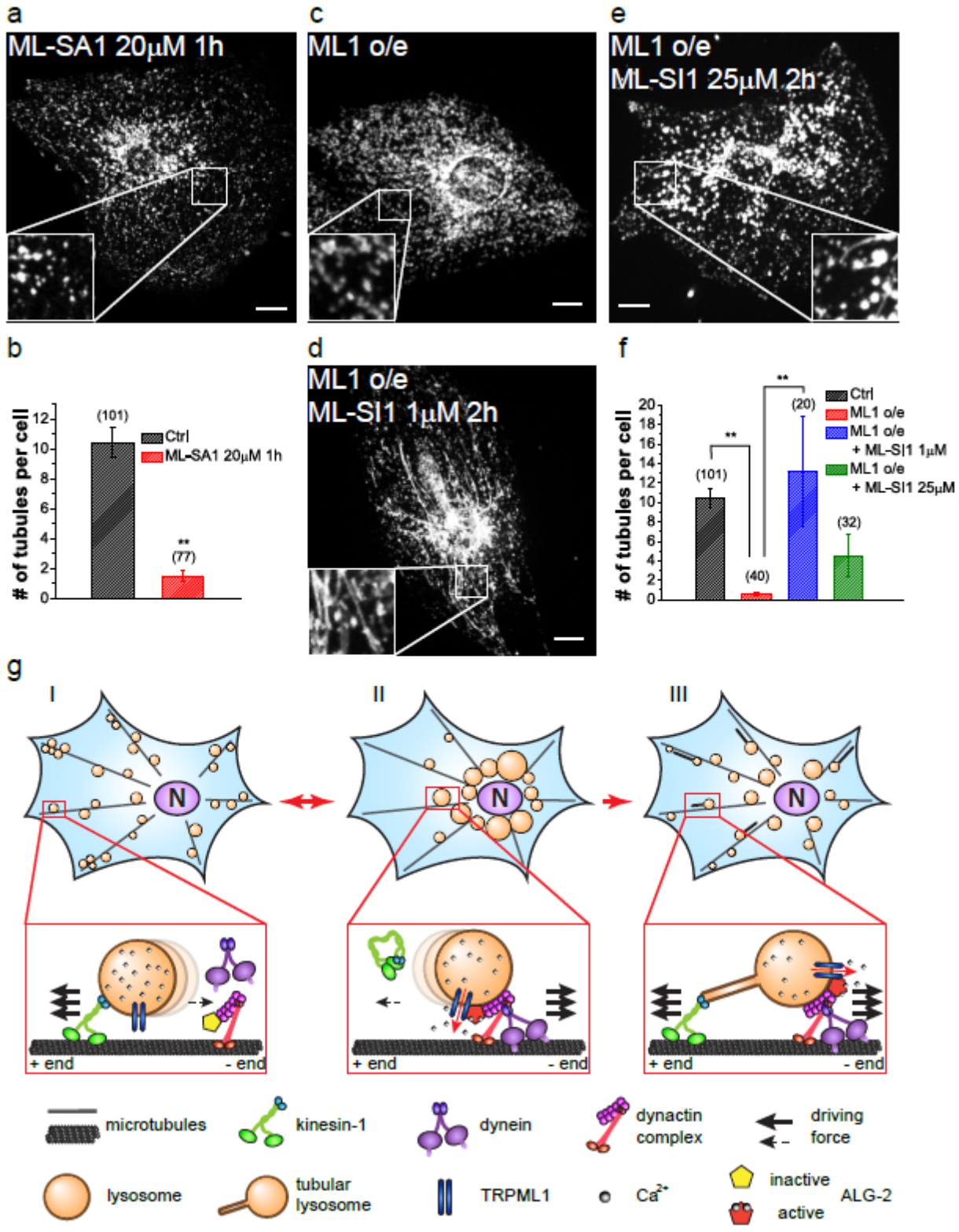

Fig. 4.6 TRPML1 regulates the switch between the plus- and minus-end directed lysosome motility.

(**a, b**) Effect of ML-SA1 (20 μM, 1 hour) on lysosome tubulation in mouse fibroblasts. (**c-e**) Effects of 1 μM (**d**) or 25 μM (**e**) ML-SI1 on lysosome tubulation in TRPML1-overexpressing WT fibroblasts. ML-SIs were applied during the last 2 hours of starvation. (**f**) Quantifications of the groups shown in (**c–e**). (**g**) Model illustrating the proposed role of TRPML1 in the regulation of lysosome motibility and tubulation. Under normal growth conditions (**I**), lysosomes are mostly peripherally distributed. During acute starvation (**II**), the TRPML1-ALG-2 pathway is activated to increase minus-end-directed motility of lysosomes, resulting in rapid redistribution of lysosomes to the juxtanuclear region, thereby facilitating autophagosome-lysosome fusion. After prolonged starvation (**III**), reactivation of mTOR turns on the machinery for lysosome tubulation and reformation. While the TRPML1-ALG-2 pathway remains active, the plus-end motility of lysosomes is increased. Subsequently, the "balanced" driving forces on both directions result in the generation of tubular lysosomes. Graphed data are presented as means ± SEM, number of cells used for quantification are shown in the brackets. *$p < .05$, **$p < .01$ in ANOVA. Scale bars = 10 μm.

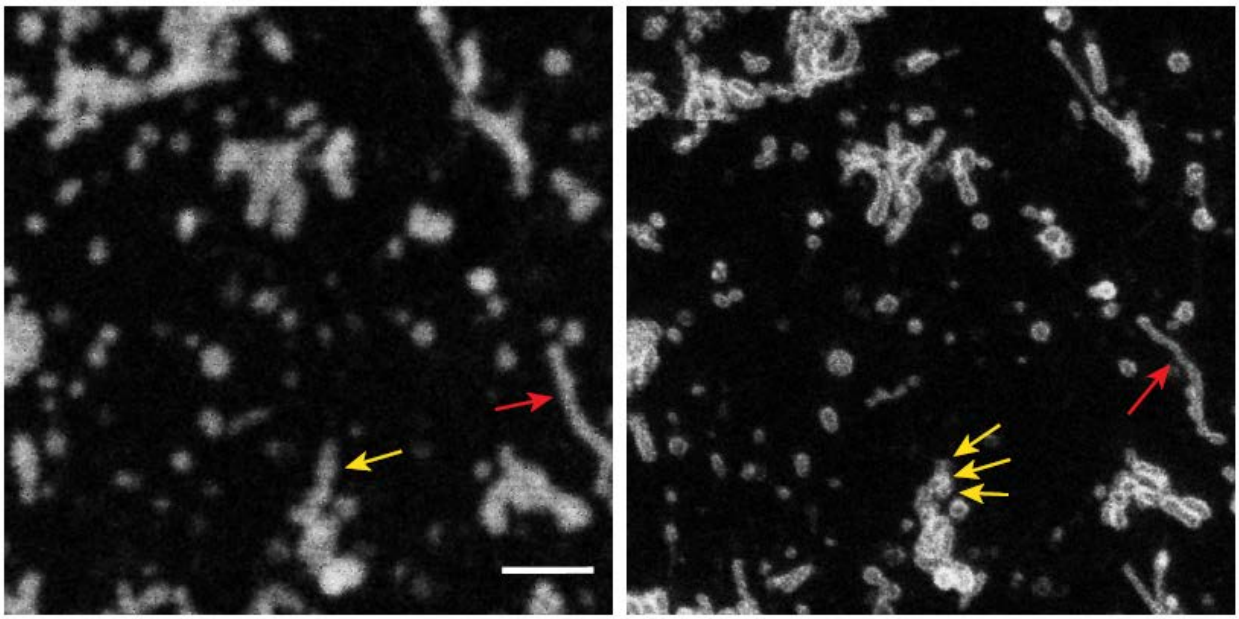

Fig. 4.7 Lysosome tubulation revealed by super-resolution microscopic imaging.

Same region of a Lamp1-GFP-transfected fibroblast starved for 24 hours under conventional (left) or STED super-resolution (right) confocal imaging. The super-resolution image was taken 6 s after the conventional confocal image. Yellow arrows point to several small lysosomes that are lined-up to have a tubular appearance under the conventional confocal images; red arrows point to a genuine tubule. Scale bar = 2 μm.

CHAPTER V

A Genetically Encoded Fluorescent Probe to Visualize Intracellular $PI(3,5)P_2$ Localization and Dynamics[5]

5.1 Abstract

Phosphatidylinositol 3,5-bisphosphate [$PI(3,5)P_2$] is a low-abundance phosphoinositide presumed to be localized to endosomes and lysosomes, where it recruits cytoplasmic peripheral proteins and regulates endolysosome-localized membrane channel activity. Cells lacking $PI(3,5)P_2$ exhibit lysosomal trafficking defects, and human mutations in the $PI(3,5)P_2$-metabolizing enzymes cause lysosome-related diseases. The spatial and temporal dynamics of $PI(3,5)P_2$, however, remain unclear due to the lack of a reliable detection method. Of the seven known phosphoinositides, only $PI(3,5)P_2$ binds, in the low nanomolar range, to a cytoplasmic phosphoinositide-interacting domain (ML1N) to activate LEL-localized TRPML1 channels. Here I show the generation and characterization of a $PI(3,5)P_2$-specific probe, generated by the fusion of fluorescence tags to the tandem repeats of ML1N. The probe was mainly localized to the membranes of Lamp1-positive compartments, and the localization pattern was dynamically altered by either mutations in the probe, or by genetically or pharmacologically manipulating the

[5] Originally published in Proc Natl Acad Sci USA (PNAS). 2013 Dec 24;110(52):21165-70. With authors listed as Xinran Li, Xiang Wang, Xiaoli Zhang, Mingkun Zhao, Wai Lok Tsang, Yangling Zhang, Richard Gar Wai Yau, Lois S. Weisman, and Haoxing Xu.

cellular levels of $PI(3,5)P_2$. Through the use of time-lapse live cell imaging, I found that the localization of the $PI(3,5)P_2$ probe was regulated by serum withdrawal/addition, undergoing rapid changes immediately prior to membrane fusion of two LELs. The development of a $PI(3,5)P_2$-specific probe may facilitate studies of both intracellular signal transduction and membrane trafficking in the endosomes and lysosomes.

5.2 Introduction

Phosphorylated phosphoinositide lipids are produced on the cytosolic side of cellular lipid bilayer membranes, and they mark the identity of intracellular membranes, as well as regulate organelle-specific membrane signaling pathways and trafficking events (Di Paolo and De Camilli 2006, Lemmon 2008). The subcellular localization of the phosphoinositides is, therefore, important information towards understanding the functions of these lipids.

The recent development of specific fluorescent probes has greatly enhanced the understanding of phosphoinositide signaling (Balla 2007, Lemmon 2008). Specific probes were developed against PI(3)P, PI(4)P, $PI(4,5)P_2$, $PI(3,4)P_2$, and $PI(3,4,5)P_3$, through fusion of fluorescent tags with the phosphoinositide binding domains of their effector proteins. For example, GFP or mCherry are fused with the FAPP1-PH domain for PI(4)P, the PLCΔ-PH domain for $PI(4,5)P_2$, the Akt-PH domain for both $PI(3,4)P_2$ and $PI(3,4,5)P_3$, and the Hrs-FYVE and EEA1-FYVE domains for PI(3)P (Halet 2005, Balla 2007). An effective probe for $PI(3,5)P_2$, however, remained lacking.

Due to the lack of specific probes, the subcellular localization and the functions of $PI(3,5)P_2$ are poorly understood. $PI(3,5)P_2$ is proposed to be mainly localized to late endosomes and lysosomes (Dove, Dong et al. 2009), and also to early endosomes (Zhang, McCartney et al. 2012). This is based on the location of its synthesizing enzyme, PIKfyve. Consistent with the LEL localization of $PI(3,5)P_2$, it was recently shown to be an endogenous agonist for TRPML1 and two pore channel 2 (TPC2), which are LEL-localized ion channels (Dong, Shen et al. 2010, Wang, Zhang et al. 2012). Despite these evidences, the localization and dynamics of $PI(3,5)P_2$ remained to be established.

The lack of a probe for $PI(3,5)P_2$ was mainly due to two reasons. First, $PI(3,5)P_2$ is a poorly characterized phosphoinositide, and it has only a few known effectors, most of which exhibit relatively low affinities for $PI(3,5)P_2$ (Tsuruta, Green et al. 2009, Bridges, Ma et al. 2012). Second, intracellular $PI(3,5)P_2$ levels are much lower than other phosphoinositide, reportedly around 1/10 of PI(3)P and less than 1/100 of $PI(4,5)P_2$ (Zhang, Zolov et al. 2007, Lemmon 2008, Zolov, Bridges et al. 2012). Therefore, the lower affinity to a lower abundance phosphoinositide makes it difficult to develop an effective probe using peripheral $PI(3,5)P_2$ binding proteins exhibiting low affinity. The lysosomal ion channel TRPML1, on the other hand, is activated by $PI(3,5)P_2$ in a low nanomolar range (EC_{50} ~ 50 nM) (Dong, Shen et al. 2010). Moreover, the interaction site between TRPML1 and $PI(3,5)P_2$ is known. Therefore, I utilized the N-terminal $PI(3,5)P_2$ binding domain of TRPML1 (ML1N) to generate a genetically encoded $PI(3,5)P_2$ probe.

5.3 Results

5.3.1 A fluorescent $PI(3,5)P_2$ probe based on the $PI(3,5)P_2$-interacting domain of TRPML1 exhibits membrane localization that is dependent on the presence of $PI(3,5)P_2$

$PI(3,5)P_2$ activates TRPML1 with high specificity and affinity, with no other phosphoinositides exhibiting any activation effect (Dong, Shen et al. 2010). Binding assays using GST fusion protein of the N-terminal segment (residues 1-68, ML1N) showed direct interaction between ML1N and $PI(3,5)P_2$ (Dong, Shen et al. 2010). Therefore, fluorescently tagged ML1N might serve as a high affinity $PI(3,5)P_2$ probe. To increase the affinity and specificity, a tandem repeat of ML1N, namely ML1N*2, was fused with GFP or mCherry on its N-terminal (**Fig. 5.1a**).

Fusion protein of GST-GFP-ML1N*2 showed higher specificity towards $PI(3,5)P_2$ *in vitro* in protein-lipid binding assays than GST-ML1N. in liposome binding assay, which mimics the vesicular membrane in living cells, the GST-GFP-ML1N*2 specifically recognized $PI(3,5)P_2$ with a K_d of ~ 5 μM (**Fig. 5.1b**), but not other phosphoinositide tested except for weak binding to PI(5)P (**Fig. 5.2a**). In PIP strip and PIP-beads binding assays, the tandem fusion protein also bound predominantly with $PI(3,5)P_2$, with weak bindings towards $PI(4,5)P_2$, $PI(3,4,5)P_3$ and PI(3)P (**Fig. 5.1c, 5.1d**). Collectively, these results indicated that the tandem probe manifests a high *in vitro* specificity for $PI(3,5)P_2$ over other phosphoinositides.

To determine the intracellular localization of the probe, Cos1 cells were transfected with either GFP- or mCherry-tagged ML1N or ML1N*2. ML1N probe was mainly localized to the cytosol, with limited localization on Lamp1-positive vesicles (**Fig. 5.1e**). In contrast, GFP-ML1N*2 or mCherry-ML1N*2 localized significantly onto Lamp1-positive vesicles (**Fig. 5.2b, 5.3**).

Previous development of other phosphoinositide probes showed that mutations of key residues for phosphoinositide binding could block the localization of the probe to specific membranes (Halet 2005, Balla 2007). Therefore, I generated ML1N-7Q*2 or ML1N-2A*2, corresponding to the mutation of all phosphoinositide-interacting residues to Glu (7Q), or only the two key Arg to Ala (2A), both characterized previously using electrophysiology (Zhang, Li et al. 2012). ML1N-7Q*2 showed a diffused cytosolic pattern in cells, while ML1N-2A*2 showed similar cytosolic localization with very weak co-localization with Lamp1-positive vesicles (**Fig. 5.2d, 5.2e**), possibly due to the incomplete loss of PI(3,5)P2 affinity (**Fig. 5.2c**). Quantification of the co-localization between the probe and Lamp1 (see Methods) showed that ML1N-7Q*2 was completely absent from Lamp1-positive vesicles (3.4 ± 0.5 %, **Fig. 5.2e**), while Ml1N-2A*2 showed very low levels of co-localization (11.8 ± 1.2 %, **Fig. 5.2e**), compared to the high co-localization for the WT ML1N*2 probe (52.3 ± 1.4 %, **Fig. 5.2e**). These results suggest that the localization of ML1N*2 onto Lamp1-positive vesicles correlates with the PI(3,5)P_2 binding affinity of the probe.

To further define the location of the probe, cells were transfected or stained with various organellar markers of the endocytic pathway (**Fig. 5.2f-k**). In Cos1 cells, about half of the Lamp1 signal co-localized with ML1N*2 (**Fig. 5.2b, 5.2e**). A high degree of co-localization between ML1N*2 and Lamp1 was also observed in mouse fibroblasts, Chinese Hamster Ovary cells (CHO), and Human Embryonic Kidney 293T (HEK293T) cells (**Fig. 5.3**). In addition, the probe also co-localized well with lysotracker (**Fig. 5.2g**). No consistent plasma membrane (PM) localization was seen, although patchy regions of PM localization of the probe could be seen in some cells (**Fig. 5.4**). The early endosomal marker EEA1 showed significant co-localization with the probe (31.5 ± 2.4%, **Fig. 5.2h, 5.2k**), consistent with ~40% co-localization of Vac14 and

EEA1 observed previously (Zhang, McCartney et al. 2012). A commonly used PI(3)P probe GFP-FYVE*2 (Gillooly, Morrow et al. 2000) showed a high degree of co-localization with the mCherry-ML1N*2 probe (65.7% ± 3.4%, **Fig. 5.2i, 5.2k**), reflecting the fact that PI(3)P is the precursor and the primary metabolite of $PI(3,5)P_2$. A high degree of co-localization between the $PI(3,5)P_2$ synthesizing enzyme PIKfyve and the probe is also observed (52.1% ± 4.2%, **Fig. 5.2j, 5.2k**).

The results presented above suggest that the probe localize to endolysosomal compartments likely due to its binding to $PI(3,5)P_2$. $PI(3,5)P_2$ levels inside the cells were manipulated to examine this.

YM 201636 inhibits $PI(3,5)P_2$ synthesis through inhibition of PIKfyve, resulting in enlarged vacuoles over longer treatment times (> 1 hour). In Cos1 cells (**Fig. 5.5a, 5.5c**) or NIH 3T3 cells (**Fig. 5.4**), YM 201636 dramatically reduced the co-localization of the probe with Lamp1. The effect of YM 201636 was entirely reversible (**Fig. 5.5c**). The effect of YM 201636 was specific as vesicular localization of PI(3)P probe GFP-FYVE*2 was not affected (**Fig. 5.6**). Under YM 201636 treatment, a small number of vacuoles retained localization of the ML1N*2 probe, raising the possibility that in the absence of $PI(3,5)P_2$, the ML1N*2 probe recognizes another epitope, e.g. a protein or lipid. It is also possible that the incomplete inhibition of PIKfyve through YM 201636 ($PI(3,5)P_2$ levels reportedly reduced to 20% of pre-inhibition levels) resulted in re-distribution of the remnant $PI(3,5)P_2$ pool inside the cells, resulting in concentrated $PI(3,5)P_2$ in critical regions. Interestingly, when purified GST-GFP-ML1N*2 proteins were exogenously applied to the fixed cells, GFP fluorescence exhibited a vesicular localization pattern co-localized with Lamp1, which was abolished by YM 201636 treatment for 30 min (**Fig. 5.7**).

The kinase activity of PIKfyve can also be inhibited by overexpression of dominant negative PIKfyve (Ikonomov, Sbrissa et al. 2009). In Cos1 cells co-transfected with YFP-PIKfyve-DN, mCherry-ML1N*2, and Lamp1-GFP, enlarged vacuoles were seen with profound decrease in the co-localization between Lamp1 and the probe (23.6 ± 2.4 %, **Fig. 5.5b, 5.5c**).

PIKfyve KO mice are embryonic lethal (Ikonomov, Sbrissa et al. 2011), but Vac14 and Fig4 KO, two proteins required for PIKfyve activation, allow the mice to survive postnatally with ~50% reduction of intracellular PI(3,5)P_2 levels (Chow, Zhang et al. 2007, Zhang, Zolov et al. 2007). The co-localization between ML1N*2 and Lamp1 was significantly reduced in both Vac14KO (18.8 ± 1.3%) and Fig4KO (17.7% ± 2.2%) fibroblasts compared to WT fibroblasts (34.3 ± 1.3%) (**Fig. 5.5d-g**). Taken together, the above results suggest that the endolysosomal localization of the probe was dependent on the activity of PIKfyve, and was capable of detecting changes in the intracellular PI(3,5)P_2 levels.

5.3.2 Endolysosmal PI(3,5)P_2 levels are regulated by serum-derived factors

With the establishment of the probe as a sensor to PI(3,5)P_2, I used the probe to track the dynamic and regulatory changes of PI(3,5)P_2 in living cells. In 3T3L1 adipocytes, insulin has been shown to induce a modest increase in PI(3,5)P_2 levels in serum-starved cells (Ikonomov, Sbrissa et al. 2009, Bridges, Ma et al. 2012). Likewise, serum-derived factors such as hormones and growth factors can regulate the levels of PI(3,5)P_2 and other phosphoinositides in other cell types (Zolov, Bridges et al. 2012). Consistent with these findings, serum starvation elicited a striking change in the pattern of the probe localization in Cos1 cells. Under normal conditions, the probe showed co-localization with Lamp1-positive vesicles as intensely bright circles or dots,

depending on the vacuole size (**Fig. 5.2b**). In Cos1 cells serum-starved for 6 hours (**Fig. 5.8a, upper panel**) or overnight for 18 hours (**Fig. 5.8a, middle panel**), the percentage of co-localization between Lamp1 and the ML1N*2 probe was significantly decreased (34.9 ± 3.0% for 6 hours, 22.9 ± 2.5% for 18 hours, **Fig. 5.8b**). It is also noticeable that the relative intensity of the probe on vesicles was reduced compared to serum-replete or normal conditions. When cells were replenished with serum for 2 hours, the co-localization of the probe and Lamp1, as well as the signal intensity returned to normal levels (**Fig. 5.8a, bottom panel, 5.8b**). Thus, intracellular $PI(3,5)P_2$ levels are regulated by serum factors. At this point, it is unclear what are the hormones or growth factors regulating $PI(3,5)P_2$ levels in Cos1 cells, but the identification of such factors can be facilitated by the ML1N*2 probe.

5.3.3 $PI(3,5)P_2$ dynamics in relation to endolysosomal membrane fusion in mammalian cells

$PI(3,5)P_2$ is a key regulator of membrane trafficking in the late endocytic pathway, evidenced by the enlarged vacuoles seen in $PI(3,5)P_2$ deficient cells either through YM 201636 treatment or through Vac14/Fig4 KO. Because $PI(3,5)P_2$ directly activates TRPML1, it was hypothesized that $PI(3,5)P_2$ elevation may induce lysosomal Ca^{2+} release to trigger endolysosomal membrane fusion/fission. In Chapters II, III, and IV I discussed my findings that $PI(3,5)P_2$ is required for TRPML1's function in lysosome retrograde motility, which in turn is required for proper lysosome fission to take place. It remains interesting to test whether $PI(3,5)P_2$ plays a role in membrane fusion using the probe to monitor the dynamics of $PI(3,5)P_2$ in living cells.

To visualize PI(3,5)P_2 dynamics in relation to membrane fusion or fission, I performed time-lapse confocal imaging in Cos1 cells that were dually transfected with GFP-ML1N*2 and Lamp1-mCherry, with Lamp1 revealing the trafficking events and the probe tracking PI(3,5)P_2 dynamics. Due to the small size (100 to 500 nm normally, also see **Fig. 4.6**) of most Lamp1-positive compartments, fusion events were not easy to catch due to the technical limitations of speed vs. resolution/photobleaching. The naturally occurring rate of fusion between larger vesicles (> 1 μm) appeared to be very low (experimental estimation of ~1 event per cell per 100 minutes). Nevertheless, in the few observations made, a rapid and robust increase in the vacuolar GFP fluorescence was detected immediately before fusion of the two Lamp1-positive vesicles (**Fig. 5.9a, 5.9c**). The vacuolar intensity of the probe peaked at the time of fusion, and then gradually decreased over time (**Fig. 5.9b**). In contrast, the intensity of mCherry-Lamp1 and cytoplasmic probe remained relatively constant, suggesting that the increase in the probe intensity was not the consequence of the fusion. These results suggest that PI(3,5)P_2 is rapidly produced on vacuolar membrane right before fusion events.

To facilitate the detection of fusion events between large vacuoles, I treated the cells with Acetate Ringer's solution for 20-30 minutes to acidify cytosolic pH, and then washed out the solution with normal medium to restore the pH, which facilitates fusion between vacuoles. In Cos1 cells dually transfected with GFP-ML1N*2 and Lamp1-mCherry, withdrawal of the Acetate Ringer's solution resulted in an increased rate of fusion between large vacuoles (increasd to ~0.17 events per cell per minute). All vacuoles that underwent fusion had much higher probe intensity on the vacuolar membrane than the cytosolic background at the time of fusion (averaging 164.4 ± 1.5% of cytosolic intensity). Based on the PI(3,5)P_2 dynamics, the fusogenic vacuoles could be classified into two groups. The first group (~ 45% of all events recorded) had

significant increases (>20%) in their membrane probe intensity within 1 min prior to fusion (**Fig. 5.9d, upper panels, 5.9f**), while the second group (~55% of all events) exhibited little or no increase in their probe intensity (**Fig. 5.9e, upper panels, 5.9f**). Interestingly, the basal fluorescence intensity of the probe in the second group was significantly higher than that of the first group (**Fig. 5.9e-f**). These results suggest that the vacuole fusion upon the removal of Acetate Ringer would require high $PI(3,5)P_2$ levels on the vacuolar membranes.

5.4 Discussion

The importance of $PI(3,5)P_2$ in endolysosomal membrane trafficking is well accepted, but the dynamics and localization of $PI(3,5)P_2$ in intact cells remained unclear, largely due to the lack of a method to directly visualize intracellular $PI(3,5)P_2$ pools. In the work presented in this chapter, I characterized a genetically encoded $PI(3,5)P_2$ fluorescent probe that can be used to track $PI(3,5)P_2$ dynamics in living cells. The $PI(3,5)P_2$ probe, consisting of two repeats of the cytosolic N-terminal of TRPML1, responded specifically to changes in the intracellular $PI(3,5)P_2$ levels and localization.

The predominantly-LEL localization of the probe was somewhat unexpected. Although $PI(3,5)P_2$ is the only phosphoinositide that activates TRPML1, it was shown that $PI(4,5)P_2$ and $PI(3,4,5)P_3$ were able to inhibit TRPML1 likely using the same stretch of positively charged residues as $PI(3,5)P_2$ (Zhang, Li et al. 2012). Indeed, though weakly, *in vitro* binding assays showed some binding between the ML1N*2 probe and $PI(4,5)P_2$/$PI(3,4,5)P_3$. No consistent PM localization of the probe, however, was detected in all cell types tested, although patchy PM localization was observed in a small number of cells. One possible explanation is that $PI(3,5)P_2$

binds to TRPML1 with much higher affinity than other phosphoinositides. Alternatively, the overexpression of the probe may have resulted in PI(3,5)P_2 enrichment in the endolysosomes by protecting them from degradation, similar to what observed for the PI(4,5)P_2 probe (Varnai and Balla 1998). It is also possible that ML1N*2 contains additional motifs, either PI(3,5)P_2 dependent or PI(3,5)P_2 independent, that can strengthen the LEL localization of the probe. Similar phenomenon was described for other phosphoinositide probes, such as the PI(4)P probe. Although unidentified, additional recruitment mechanisms may play permissive roles to recruit the probe to the LEL membranes. Nevertheless, mechanisms discussed above will not prevent the use of the probe to detect PI(3,5)P_2 dynamics on LEL membranes.

The weak binding of the probe to PI(5)P might be problematic, as this lipid is also known to be present in late endocytic compartments in mammalian cells, and it is also produced and turned over by the same enzymes as PI(3,5)P_2 (Zolov, Bridges et al. 2012). Because the production of these two phosphoinositides and their turn over are linked, it is likely their biological roles are not so well separated, similar to PI(3,4)P_2 and PI(3,4,5)P_3 on the plasma membrane. In this case, the probe may detect the changes of both phosphoinositides, similar to that of Akt-PH domain in detecting PI(3,4)P_2 and PI(3,4,5)P_3 (Balla 2007).

The lack of effective PI(3,5)P_2 probes have long restricted the measurement of intracellular PI(3,5)P_2 levels to methods like radiolabeled HPLC. Such techniques are lengthy, costly, and most importantly, won't provide any information about subcellular localization and dynamics of PI(3,5)P_2. By using the new probe developed here, I have shown for the first time that PI(3,5)P_2 elevation on vacuolar membranes occur prior to fusion, and the clear correlation between high membrane PI(3,5)P_2 and fusion events. With the aid of high-resolution live

imaging in combination with genetic and pharmacological approaches, the PI(3,5)P_2 probe may prove to be a valuable tool for the study of PI(3,5)P_2 signaling.

5.5 Materials and Methods

Molecular biology

Tandem repeats of the TRPML1 (accession number CCDS22063.1 in NCBI cDNA database) N-terminal segment (residues 1–68) were subcloned from mouse cDNA into a pEGFPC3 (Clontech) plasmid by using the following two pairs of primers: F1: GAAGATCTCA CCATGGCCAC CCCG; R1: CGGAATTCGC AGCATCAGCT TGCAG; F2: CGGAATTCTC ACCATGGCCA CCCC; R2 CGGGATCCAG CATCAGCTTG CAG. For the mCherry-ML1N*2 construct, mCherry was inserted into the GFP-ML1N*2 construct from the pmCherry-C1 plasmid (Clontech) to replace GFP by using the following primers: F: CATCAAGTGT ATCATATGCC; R: GAAGATCTAG TCCGGACTTG TACAG. The ML1N-7Q*2 and ML1N-2A*2 mutants were generated by site-directed mutagenesis with Pfu Turbo polymerase (Stratagene). A GST-fusion construct was made by inserting the GFP-ML1N*2 fragment into the pGEX-4T1 vector (GE Healthcare). The Lamp1-mCherry construct was made by insertion of Lamp1 cDNA into pcDNA3.1 (Invitrogen) followed by fusion of mCherry with the C-terminus of Lamp1. All constructs were confirmed by sequencing.

GST-fusion protein purification

To purify GST-GFP-ML1N*2, E. *Coli* strain BL-21 supplemented with pRareCDF (optimizing for mammalian codon distribution) was transformed with pGEX4T1-GFP-ML1N*2.

Bacteria were inoculated at 37°C in Terrific Broth medium containing Spectinomycin and Ampicillin. Once the O.D. of the culture reached ~2, cells were equilibrated to room temperature and protein expression was induced with 250 μM IPTG for 2 hour. Cells were then pelleted and resuspended with PBS containing 0.5 mM EDTA, 0.1mg/ml lysozyme, and 1% v/v protease inhibitor cocktail (P8849, Sigma). Cells were then lysed by sonication and centrifuged. The GST-fusion proteins in the supernatant were concentrated using glutathione sepharose beads (GE Healthcare). After extensive washes with PBS, purified proteins were eluted with elution buffer (20 mM glutathione, 150 mM NaCl in 50 mM Tris, pH 8.0).

Liposome binding assay

Phosphoinositide-containing liposomes (PIPosomes) from Echelon Biosciences were used for the assay. 20 μL liposomes were diluted in 1 mL binding buffer (150 mM NaCl, 0.05% NP-40 in 50mM Tris, pH 7.5) containing 3 μg GST-GFP-ML1N*2. After 10 min of incubation, liposomes were pelleted at 16,000g for 10 min. Supernatants were carefully removed and liposomes were re-suspended with 1 ml binding buffer. After six washes, the bound fractions were analyzed by western blot using anti-GST antibodies.

To estimate the affinity (K_d) of PI(3,5)P_2-probe binding, liposomes containing 30-3,000 pmol PI(3,5)P_2 or 2 nmol control lipids without PI(3,5)P_2 were incubated with various concentrations of the purified GST-GSP-ML1N*2 proteins in 100 μL of binding buffer. The mixture was incubated for 1 hour with gentle rotation. After 10 μL of the mixture was separated as input, the liposomes were pelleted at 16,000g for 15 min. The supernatant was then carefully separated as the unbound fraction. Protein concentrations from input and unbound fractions were measured by absorbance at 280 nm and western blot analysis.

Lipid strip binding assay

PIP-strip was purchased from Echelon Biosciences (P-6001), containing 15 different lipid species, including all 7 phosphoinositides. The strip was first blocked with PBST (containing 3% BSA) for 1hr, incubated with 0.2 μg/ml GST-GFP-ML1N*2 for 1 hour, and then washed for 6 times with the blocking buffer. Bound proteins were recognized with anti-GST antibodies (Sigma, G1160) and detected with goat-anti-mouse HRP- conjugated secondary antibodies (Invitrogen, 62-6520).

PIP beads binding assay

50 μL of 50% phosphoinositide -containing beads (Echelon Biosciences) were incubated with 1 mL of binding buffer (150 mM NaCl, 0.25% NP-40 in 50mM Tris, pH 7.5) containing 5 μg GST-GFP-ML1N*2. After 2 hours of incubation, beads were pelleted at 500 g for 5 min, and beads were re-suspended with 1 mL binding buffer. After 5 washes, the bound fractions were analyzed by western blot using anti-GST antibodies.

PI(3,5)P_2 detection using purified GST-GFP-ML1N*2 proteins

Lamp1-transfected cells were fixed with 4% PFA, blocked with PBST (containing 3% BSA) for 2 hours, incubated with 5 μg/mL GST-GFP-ML1N*2 in the blocking buffer for 2 hours, and then subjected to fluorescence microscopy.

Mammalian cell culture

Mammalian cells were cultured in a 37°C, 5% CO_2 incubator. MEFs were isolated and cultured as described previously (Di Paolo and De Camilli 2006, Jin, Chow et al. 2008). Cells were cultured with DMEM (Invitrogen) supplemented with 10% FBS (Gemini). All other

mammalian cell types (CHO, COS1, and HEK293T) were cultured with DMEM F12 (Invitrogen) supplemented with 10% FBS. For the delivery of the plasmids into the cells, MEF cells were electroporated by using an Invitrogen Neon electroporation kit; all other mammalian cells were transfected by using Lipofectamine 2000 (Invitrogen). Cells were typically imaged 24 hours post-transfection. Serum starvation was performed with three washes of PBS to completely remove serum. Cells were then incubated with the respective culture medium without serum for the indicated periods. Acetate Ringer's solution contained (in mM): 80 NaCl, 70 CH_3COOH, 5 KCl, 2 $CaCl_2$, 1 $MgCl_2$, 2 NaH_2PO_4, 10 HEPES, 10 MES, and 10 glucose (pH adjusted to 6.9 with NaOH). Standard Ringer's solution contained (in mM): 145 NaCl, 5 KCl, 2 $CaCl_2$, 1 $MgCl_2$, 10 HEPES, 10 MES, and 10 glucose (pH adjusted to 7.4 with NaOH).

Confocal Microscopy

For fixed samples, cells were fixed and immunostained following a standard protocol. Briefly, cells were fixed with 4% PFA for 30 min, blocked with 1% BSA for 2 hours, incubated with primary antibody overnight, and stained with fluorescent secondary antibody for 1 hour. Cells were then imaged with a Leica Confocal microscope. For live samples, cells were washed with DMEM F12 medium without phenol-red (Invitrogen) to reduce background fluorescence. Live imaging was performed with an Olympus Spindisk Confocal microscope with a heated chamber to maintain the temperature at ~37°C during imaging. Wavelengths used for each channel are (excitation/emission in nm): 405/447 (DAPI), 488/525 (GFP), and 561/607 (mCherry).

Imaging analysis

Images were analyzed with ImageJ software. For co-localization analysis, images were first split into separate color channels. The red and green channels were then thresholded on a regional basis, with the threshold being 50% above the average background intensity in the nearby cytosolic regions. Co-localization was performed with the Co-localization Plug-in of ImageJ. The percentage of co-localization was defined as the [total number of pixels that are positive for both channels/total number of pixels that are positive for the channel other than the probe (e.g., Lamp1)] × 100%. For the measurement of the change in the vacuolar fluorescence intensity, the vacuolar membrane area was selected by masking from the Lamp1-mCherry channel. The vacuolar probe intensity was defined as the average intensity of both vacuole membranes (before fusion) or the average intensity on the membrane of the fused vacuole

Endolysosomal electrophysiology

Endolysosomal electrophysiology was performed in isolated enlarged endolysosomes with a modified patch-clamp method as described previously (Dong, Shen et al. 2010, Wang, Zhang et al. 2012, Zhang, Li et al. 2012). Briefly, cells were treated with 1 μM vacuolin-1 for 1–12 hours. Enlarged vacuoles (up to 5 μm) were isolated manually with a patch pipette, and then whole-endolysosome voltage clamp recordings were performed. The vacuolar membrane was ruptured with a series of voltage steps. Whole-endolysosome configuration was verified by the re-appearance of capacitance transients after break-in. Whole-endolysosomal currents were elicited by repeated voltage ramps from -120 to 120 mV (400 ms) with an inter-ramp interval of 2 s. The pipette (luminal) solution was modified Tyrode's, including (in mM) 145 NaCl, 5 KCl, 2 $CaCl_2$, 1 $MgCl_2$, 10 HEPES, 10 MES, 10 glucose (pH adjusted with NaOH to pH 4.6). The bath (internal/cytoplasmic) solution contained (in mM) 140 K-gluconate, 4 NaCl, 1 EGTA, 2 $MgCl_2$, 0.39 $CaCl_2$, 20 HEPES (pH adjusted with KOH to 7.2; free $[Ca^{2+}]_i$ ~ 100 nM estimated

using MaxChelator software). Bath solutions were applied via a perfusion system that allowed a complete solution exchange within a few seconds. Data were collected using an Axopatch 2A patch clamp amplifier, Digidata 1440, and pClamp 10.2 software (Axon Instruments). Whole-endolysosome currents were digitized at 10 kHz and filtered at 2 kHz. All experiments were conducted at RT (21–23 ºC), and all recordings were analyzed with pClamp 10.2, and Origin 8.0 (OriginLab, Northampton, MA)

Chemicals and reagents

The PIKfyve inhibitor YM201636 was purchased from Symansis. Mouse anti-Lamp1 antibody was purchased from the Developmental Studies Hybridoma Bank (1D4B). Monoclonal anti-GST antibody was purchased from Sigma (G1160).

Data analysis

Statistical data are presented as the mean ± standard error of the mean (SEM). The quantifications shown in figures were performed for a total number (n) of individual cells for each group from at least three independent experiments. Statistical comparisons were made with a Student's t-test. Asterisks in the figures generally represent P values $< 1 \times 10^{-5}$. P value < 0.01 was considered statistically significant.

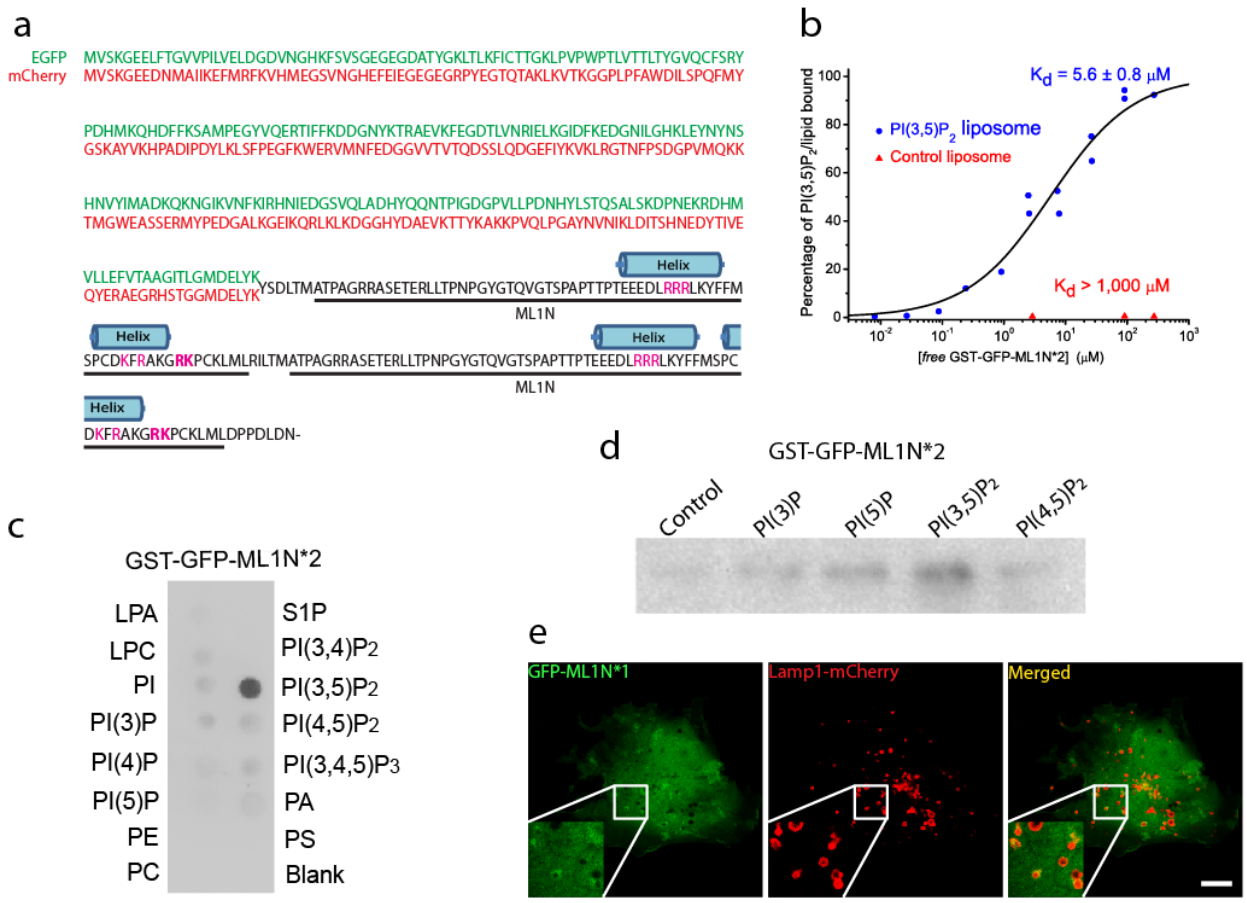

Fig. 5.1 Generation of the ML1N*1 and ML1N*2 probe

(**a**) Two copies of the cytosolic N-terminal segments of TRPML1 (underlined with black color) were fused with either GFP or mCherry. Amino acid residues (R^{42-44}, K^{55}, R^{57}, R^{61}, K^{62}, in magenta) were mutated in the ML1N-7Q*2 construct; R^{61} and K^{62} were mutated in the ML1N-2A*2 construct (magenta bold). Blue columns denote α-helices predicted by the PSIPRED software. (**b**) Purified GST-GFP-ML1N*2 proteins bound to PI(3,5)P_2-containing liposomes (65% PC, 30% PE, and 5% PI(3,5)P_2) with a K_d of 5.6 μM. No significant binding was observed for control liposomes with 70% PC and 30% PE. (**c**) GST-GFP-ML1N*2 selectively binds to PI(3,5)P_2 in a lipid strip assay. The lipid strip contained 15 different types of lipids including all seven phosphoinositides. The purified GST-GFP-ML1N*2 proteins were used to probe the strip. Proteins bound to the strip were detected using anti-GST antibodies. LPA: lysophosphatidic acid; LPC: lysophosphocholine; PI: phosphatidylinositol; PE: phosphatidylethanolamine; PC: phosphatidylcholine; S1P: sphingosine-1-phosphate; PA: phosphatidic acid; PS: phosphatidylserine. (**d**) Purified GST-GFP-ML1N*2 proteins exhibited strong binding to PI(3,5)P_2-conjugated agarose beads, but weak or no binding to beads conjugated with PI(3)P, PI(5)P, or PI(4,5)P_2. Beads were diluted to a final concentration of 500 nM respective phosphoinositide, and incubated with purified GST-GFP-ML1N*2 protien for 2 hours. Proteins bound to beads were washed thoroughly and visualized by western blot with anti-GST antibodies. (**e**) Cos1 cells were co-transfected with GFP-ML1N*1 and Lamp1-mCherry, and images 24 hours after transfection. Scale bar = 10 μm.

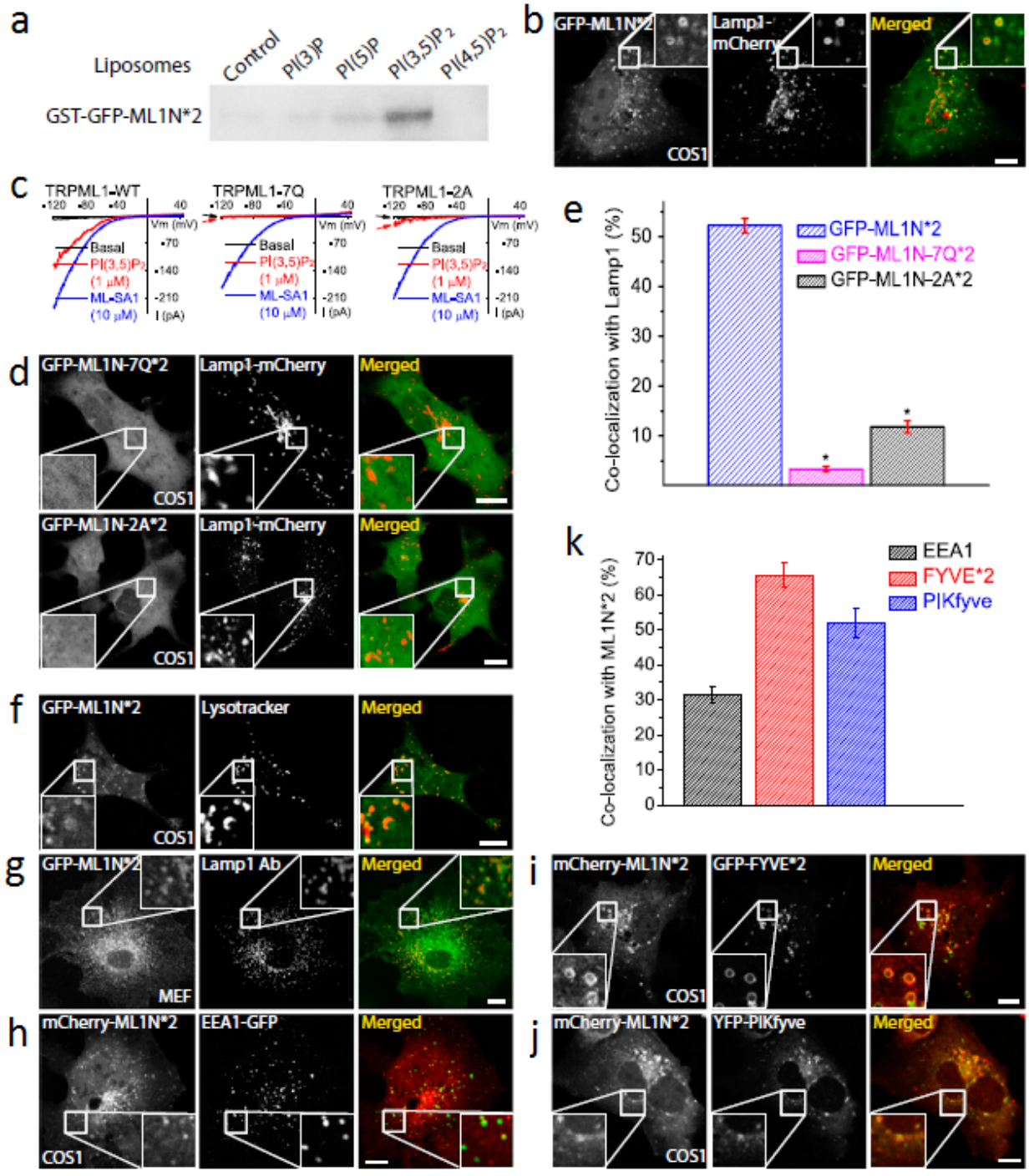

Fig. 5.2 Co-localization of the ML1N-based PI(3,5)P_2 probe with endolysosomal markers.

(**a**) Purified GST-GFP-ML1N*2 proteins bound strongly to PI(3,5)P_2-containing liposomes, but not to liposomes containing PI(3)P, PI(5)P, or PI(4,5)P_2. Liposomes, diluted to a final concentration of 20 μM total lipids with 1 μM tested phosphoinositide, were incubated with purified GST-fusion proteins for 20 min, centrifuged, and visualized by western blot with GST antibodies. (**b**) GFP-ML1N*2 exhibited a vesicular location and significant co-localization with

Lamp1-mCherry. Confocal images were taken 24 hours post-transfection in Cos1 cells that were co-transfected with Lamp1-mCherry and GFP-ML1N*2. (**c**) Charge-neutralizing mutations in the phosphoinositide-interacting domain (TRPML1-7Q and TRPML1-2A) selectively impaired or abolished the activation of TRPML1 by $PI(3,5)P_2$ (1 μM) in the whole-endolysosome configuration. In contrast, ML-SA1 readily activated wild-type (WT) TRPML1, TRPML1-7Q, and TRPML1-2A in the same endolysosomes. (**d**) The localization of the ML1N*2 probe to vacuolar membranes was dependent on the basic residues in its phosphoinositide-interacting domain. Both ML1N-7Q*2 and ML1N-2A*2 displayed a diffuse, cytosolic localization pattern. (**e**) Quantification of the co-localization index between ML1N*2 and Lamp1 (see Methods for the algorithm that was used to analyze the co-localization). (**f**) Co-localization of GFP-ML1N*2 with LysoTracker (red) in Cos1 cells. (**g**) Co-localization of GFP-ML1N*2 with endogenous Lamp1 (recognized by a Lamp1 antibody) in MEF cells. (**h-k**) Co-localization analyses between ML1N*2 and other fluorescently tagged endolysosomal proteins/markers in Cos1 or MEF cells that were transfected with the indicated constructs for 24 hours. (**h**) Co-localization of mCherry-ML1N*2 with the early endosomal marker GFP-EEA1. (**i**) Co-localization of ML1N*2 with the PI(3)P probe GFP-Hrs-FYVE*2. (**j**) Co-localization of ML1N*2 with YFP-PIKfyve. (**k**) Quantitative analyses revealed that ML1N*2 exhibited various degrees of co-localization with YFP-PIKfyve, GFP-FYVE*2, and GFP-EEA1. Error bars represent SEM. The asterisk indicates $P < 10^{-5}$. Scale bars = 10 μm.

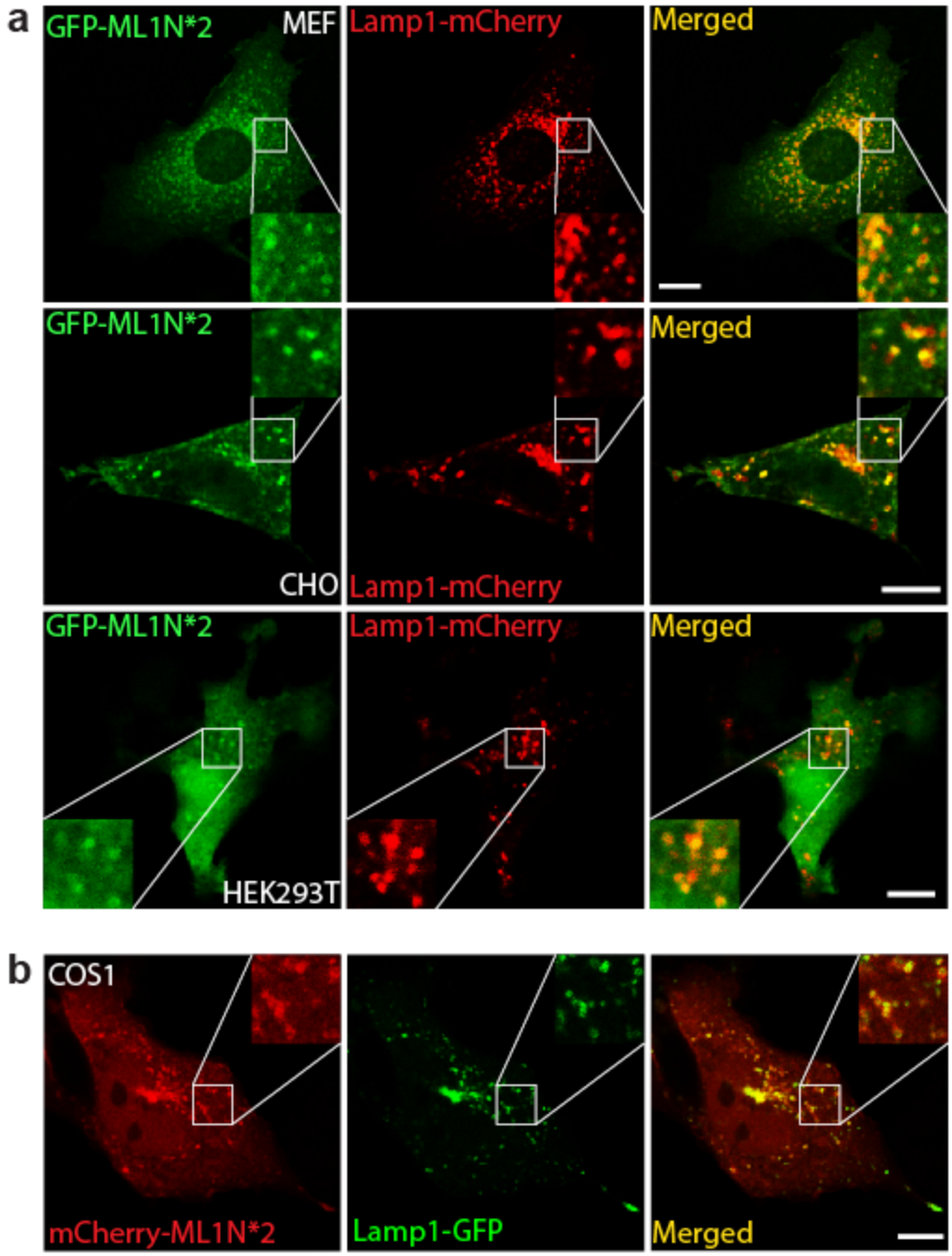

Fig. 5.3 vacuolar localization of the ML1N*2 probe is independent of cell type and fluorescent tag.

(**a**) Significant co-localizations between GFP-ML1N*2 and Lamp1-mCherry were observed in various cell types, including MEF (upper panels), CHO (middle panels), and HEK293T (lower panels). (**b**) Co-localization between mCherry-ML1N*2 and Lamp1-GFP in Cos1 cells. Scale bars = 10 μm.

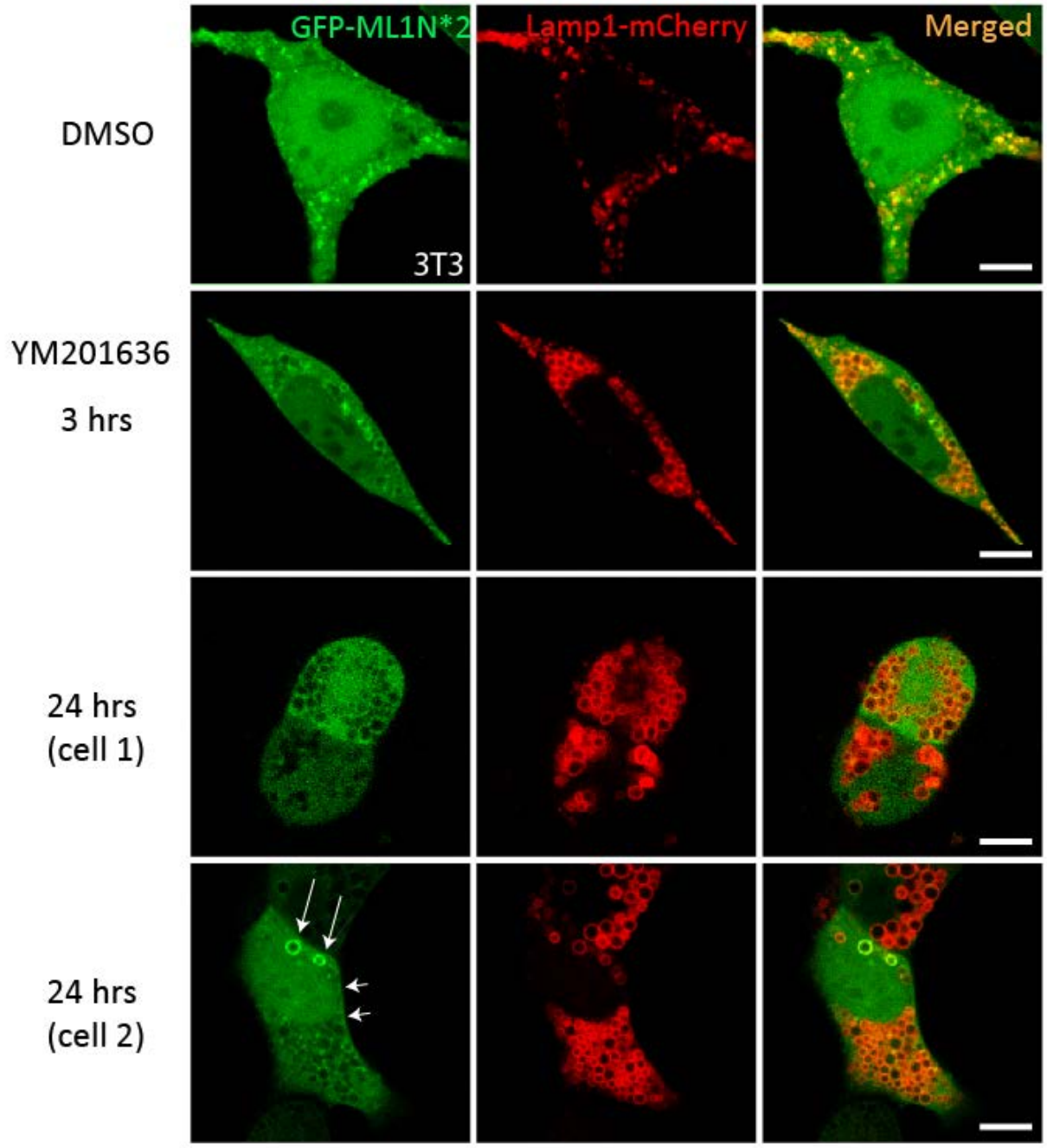

Fig. 5.4 Lysosomal localization of the GFP-ML1N*2 probe is sensitive to YM 201636 treatment in NIH3T3 cells.

NIH3T3 cells were co-transfected with GFP-ML1N*2 and Lamp1-mCherry plasmids. Cells were treated with 1.6 μM YM201636 for the indicated lengths of time or DMSO for 3 hours or 24 horus. GFP-ML1N*2 dissociated from Lamp1-mCherry positive compartments after YM 201636 treatment. In a subset of cells, patchy PM localization (arrow heads) and few GFP-positive vesicles (arrows) were still observed after 24 hours of YM 201636 treatment. Scale bars = 10 μm.

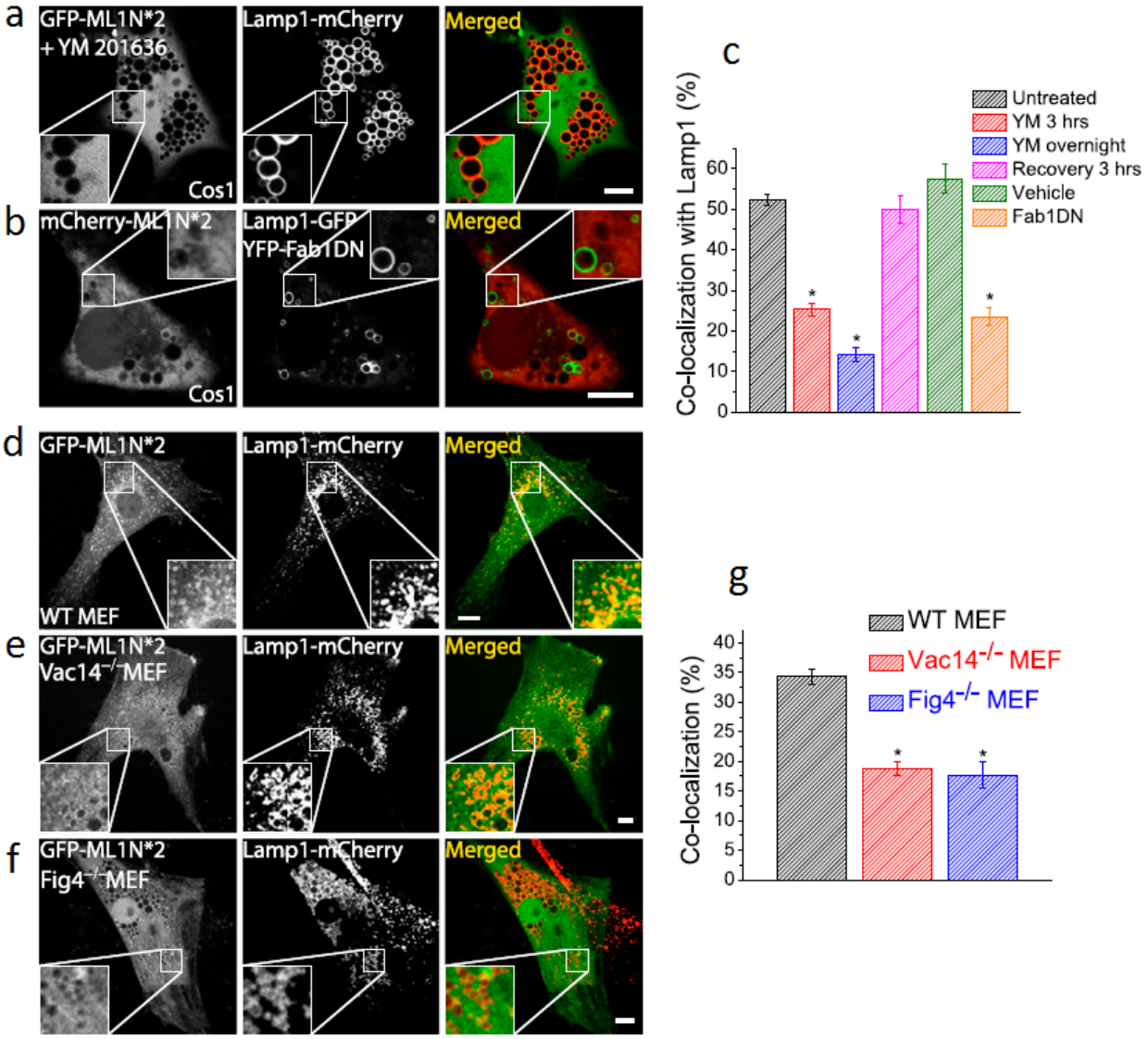

Fig. 5.5 Genetically or pharmacologically induced drops in PI(3,5)P_2 levels diminish or abolish the vesicular localization of the ML1N*2 probe.

(**a**) GFP-ML1N*2- and Lamp1-mCherry-transfected COS1 cells were treated with YM201636 (800 nM) overnight prior to confocal imaging analysis. Though Lamp1-positive compartments were dramatically enlarged, the GFP-ML1N*2 probe was primarily localized to the cytosol, and was not found on enlarged vacuolar membranes. (**b**) The vesicular localization of the mCherry-ML1N*2 probe was significantly reduced in cells co-transfected with the Fab1-DN construct. Images were taken 24 hours post-transfection. (**c**) YM201636 treatment resulted in a progressive decrease in ML1N*2's co-localization with Lamp1. Washout of the drug in the culture medium led to a complete recovery of the co-localization. (**d-f**) The ML1N*2 probe exhibited an apparent vesicular localization pattern in WT (**d**), but not in Vac14$^{-/-}$ (**e**) or Fig4$^{-/-}$ (**f**) MEF cells. (**g**) The colocalization index between ML1N*2 and Lamp1 was significantly reduced in Vac14$^{-/-}$ and Fig4$^{-/-}$ MEFs. Error bars represent SEM. The asterisk indicates $P < 10^{-5}$. Scale bars = 10 μm.

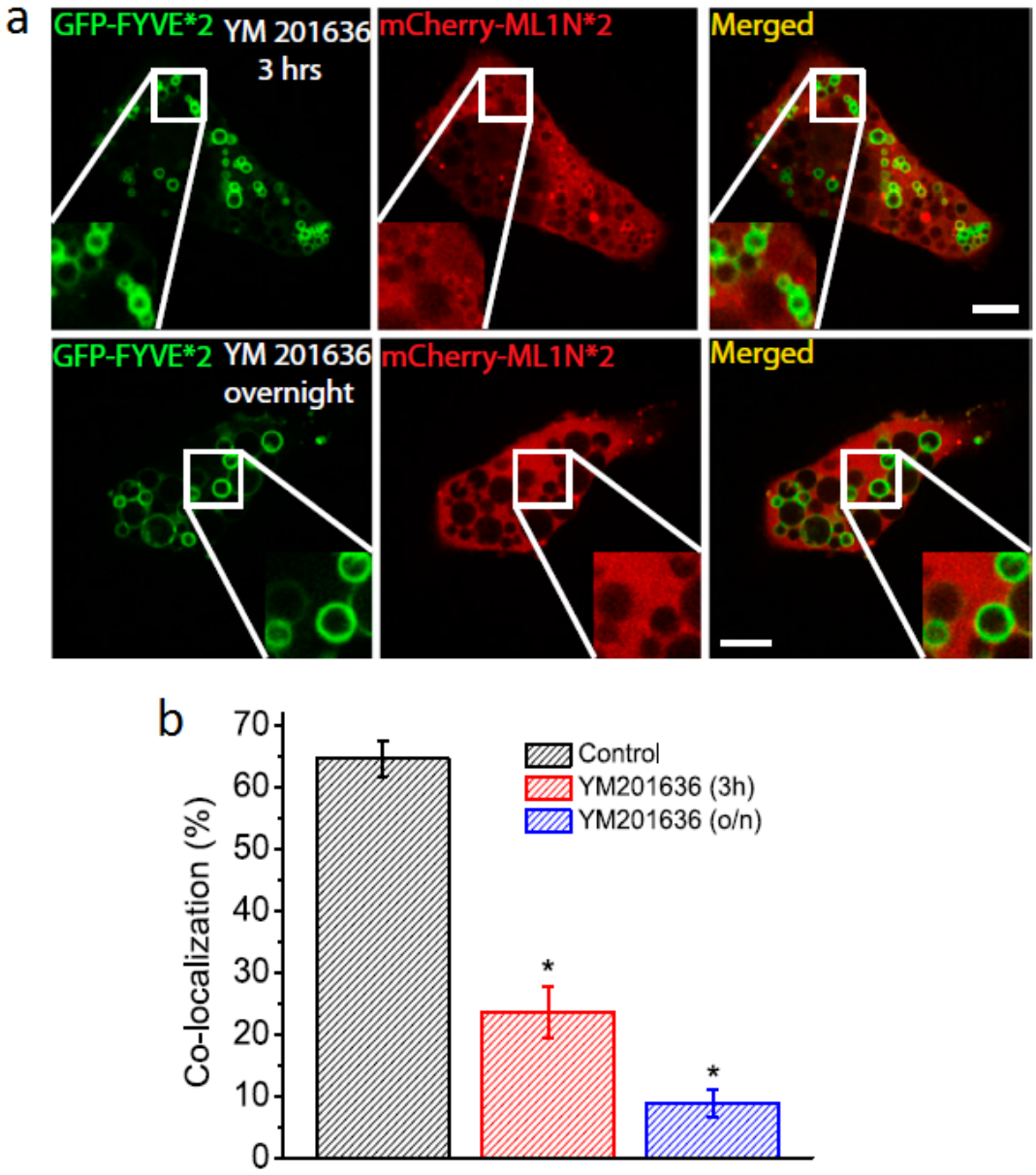

Fig. 5.6 Inhibition of PI(3,5)P_2 synthesis reduces the co-localization between the PI(3)P and PI(3,5)P_2 probes.

(**a**) Cos1 cells were cotransfected with the PI(3)P probe GFP-Hrs-FYVE*2 and mCherry-ML1N*2, and were then treated with YM 201636 for 3 hours (upper panel) or overnight (lower panel). (**b**) The colocalization index between GFP-Hrs-FYVE*2 and mCherry-ML1N*2 was reduced by YM 201636 treatment for 3 hours (23.7% ± 4.2%) or overnight (8.9% ± 2.2%), when compared with non-treated cells (64.6% ± 2.9%). Error bars represent SEM. The asterisk indicates $P < 10^{-5}$. Scale bars = 10 μm.

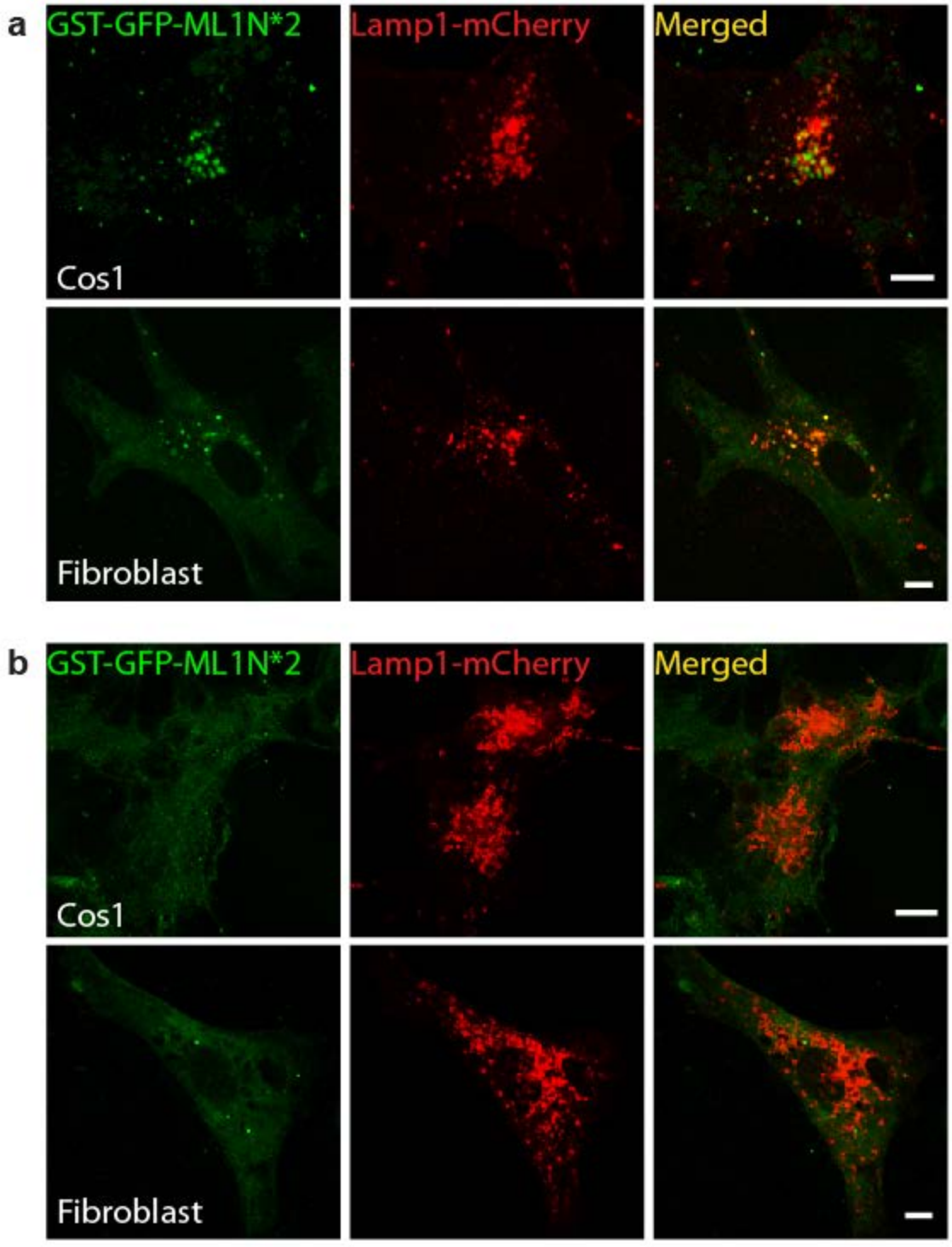

Fig. 5.7 Detection of endogenous PI(3,5)P_2 in fixed cells using exogenously-applied purified GST-GFP-ML1N*2 proteins.

(**a, b**) Lamp1-mCherry-transfected Cos1 cells or fibroblasts were treated without (**a**) or with (**b**) 1 μM YM 201636 for 30 min, fixed, blocked, and then incubated with exogenously-applied purified GST-GFP-ML1N*2 protein (see Methods). GFP fluorescence showed clear co-

localization with Lamp1-mCherry in (**a**). Cells treated with YM 201636 exhibited mostly diffuse or background fluorescence. Scale bars = 10 μm

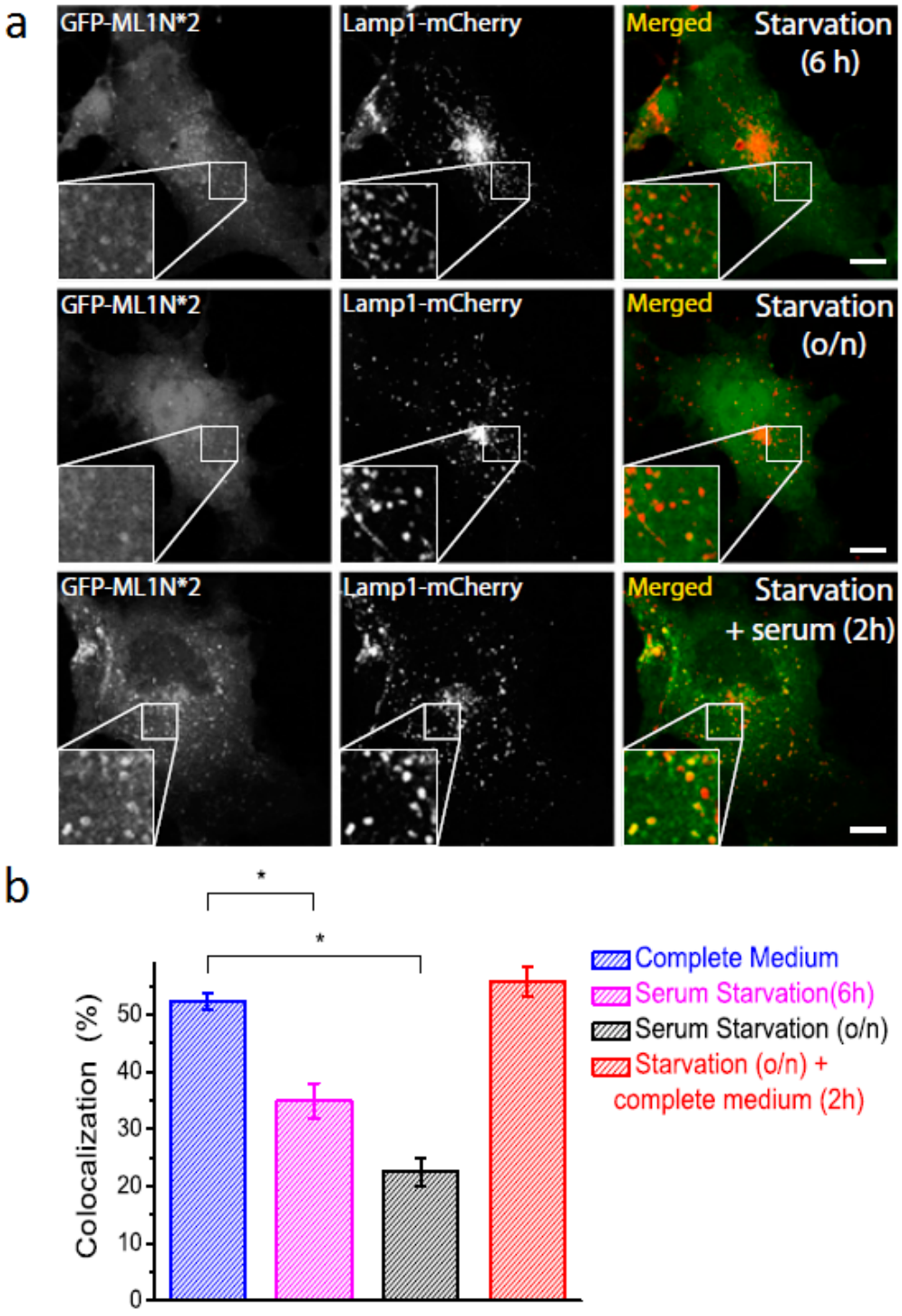

Fig. 5.8 Endolysosomal PI(3,5)P_2 levels are regulated by serum-derived factors.

(**a**) In Cos1 cells dually transfected with GFP-ML1N*2 and Lamp1-mCherry, serum starvation induced a progressive reduction in the co-localization of ML1N*2 and Lamp1. Re-addition of complete medium rapidly (< 2 hours) restored the high degree of co-localization. (**b**) Serum-dependent co-localization of the ML1N*2 probe and Lamp1. Error bars represent SEM. The asterisk indicates $P < 10^{-5}$. Scale bars = 10 μm.

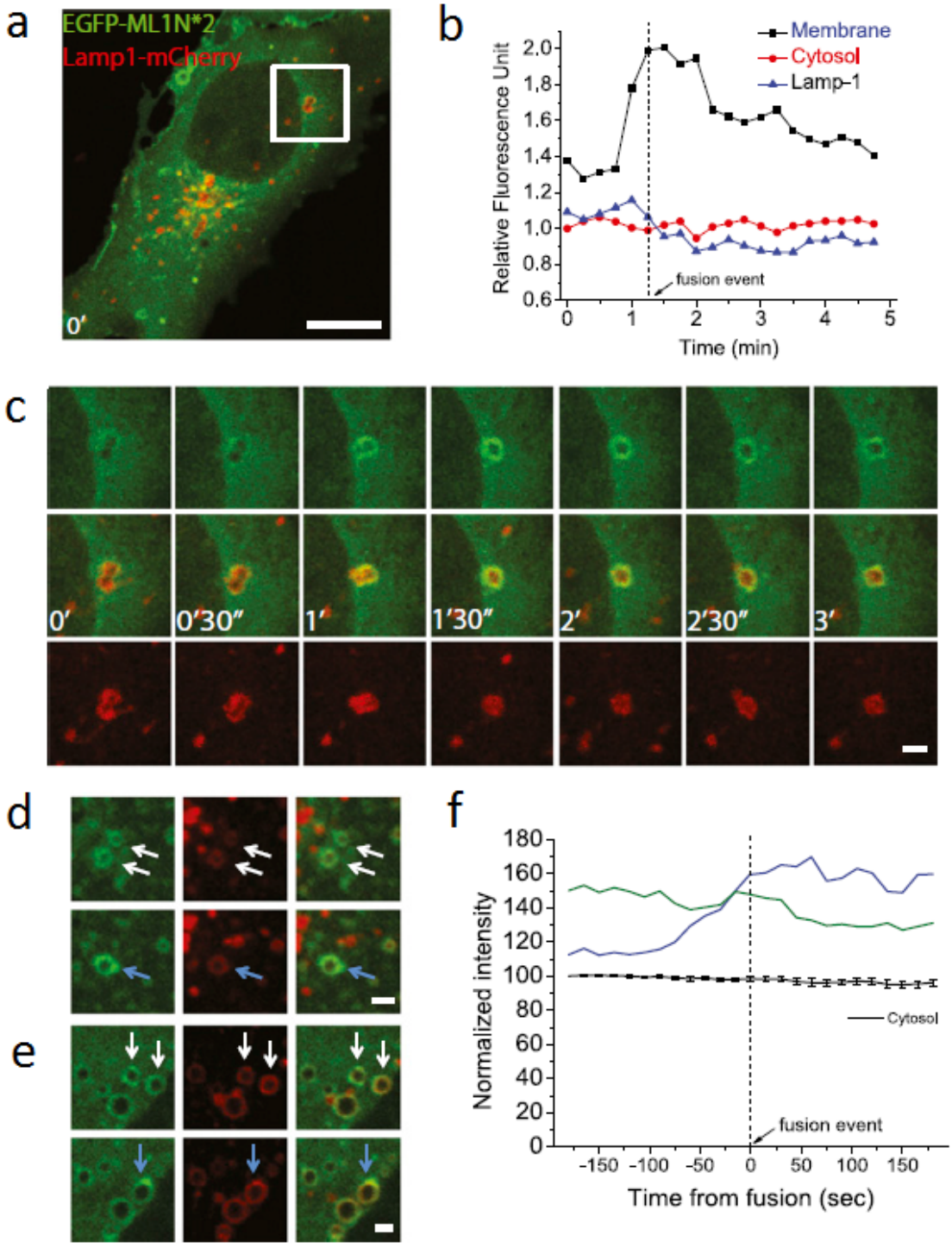

Fig. 5.9 Elevated PI(3,5)P_2 levels in LELs immediately prior to membrane fusion LELs.

(**a-c**) Time-lapse live imaging of Cos1 cells that were dually transfected with GFP-ML1N*2 and Lamp1-mCherry. (**a**) Image of a Cos1 cell immediately before membrane fusion between two Lamp1-positive vacuoles occurred (highlighted in the white box). (**b**) Time-dependent changes in the fluorescence intensities of GFP and mCherry for the selected region (white box, panel **a**). (**c**) Series of images of the selected region at corresponding time points as in (**b**). One fusion

event between two vacuoles occurred between 1 min and 1 min 15 sec. (**d. e**) GFP-ML1N*2 and Lamp1-mCherry dually transfected Cos1 cells were treated with Acetate Ringer's solution for 30 min and then subjected to live imaging for 5-20 minutes after returning to normal medium. Approximately half of the vacuoles (**d**) exhibited a significant increase in their membrane $PI(3,5)P_2$ before fusion, whereas the other half had little or no changes, but had higher membrane $PI(3,5)P_2$ to begin with. The fluorescent intensity of GFP-ML1N*2 was normalized to the cytosolic intensity at time 0, and two representative traces are shown; the vertical dotted line indicates the time when the fusion took place. The cytosolic intensity of the probe remained relatively constant over the time period of the live imaging experiment. Scale bars = 10 μm (for **a**) and 2 μm (for **c, d, e**)

CHAPTER VI

Conclusions and Future Directions

6.1 Conclusions

The goal of the study was to examine the possible roles of TRPML1 in regulating aspects of lysosome membrane trafficking apart from membrane fusion. The main aims focused on two aspects: lysosome motility and lysosome membrane fission (i.e. lysosome reformation).

Results of this study showed clear evidence that TRPML1 regulates the minus-end directed motility of lysosomes under conditions with a demand for the perinuclear recruitment of lysosomes. Additionally, TRPML1 is also involved in the regulation of lysosome tubulation, a process serving as the pre-requisite of lysosome membrane fission (i.e. lysosome reformation). The data suggested that the role of TRPML1 in regulating lysosome tubulation is through its regulation of lysosome motility. Therefore, my investigation concluded that TRPML1 regulates the minus-end directed motility of lysosomes and lysosome tubulation, the latter likely through the regulation of motility.

Results described in Chapters II and III mapped a detailed mechanism of the regulatory pathway. First, these results confirmed that the activity of TRPML1 is necessary to drive the retrograde migration of lysosomes under acute conditions, and that the effects of TRPML1 activation were through its Ca^{2+} release. Second, TRPML1 activation is sufficient to

drive the retrograde migration of lysosomes. Third, it was shown that $PI(3,5)P_2$, the phosphoinositide serving as an endogenous agonist of TRPML1, is required for the function of TRPML1 in retrograde trafficking of lysosomes. Fourth, the calcium-binding and TRPML1-interacting protein ALG-2 was shown to be the direct downstream target of TRPML1, and that its function requires the interaction with TRPML1. Moreover, the function of ALG-2 is to interact with dynamitin, a member of the dynactin complex, to recruit dynein to the lysosomes. Therefore, $PI(3,5)P_2$, TRPML1, ALG-2, and dynactin serve as a complete pathway for lysosomal recruitment of the dynein complex to initiate retrograde transport of lysosomes.

My data also showed that TRPML1 regulates lysosome motility through a different pathway than the previously characterized Rab7-RILP pathway. Why do the cells need two different pathways to regulate the minus-end motility of lysosomes? My results agree with the hypothesis that the Rab7-RILP pathway is required for the constitutive housekeeping retrograde movement of lysosomes for daily functions, while the TRPML1-ALG-2 pathway is required as an emergency plan, being activated under abnormal conditions such as cellular starvation or cytosolic alkalization. This is in accordance with the nature of the key regulators for the two pathways. Two key regulators for the constitutive pathway are Rab7 and cholesterol, one turns on RILP while the other recruits ORP1L. Cholesterol is present on plasma membranes and in liposomes, both of which get into early endosomes, late endosomes and lysosomes through endocytosis. Therefore, the promotion effect of cholesterol on the retrograde transport of lysosomes (probably endosomal vesicles of earlier stages as well) is beneficial for the fate-determination of endocytic vesicles. However, the amount of cholesterol on lysosomal membrane is unlikely able to change rapidly, rendering it unfit for regulations towards acute conditions. Similar problems exist for Rab7, which is a key regulator of late endosome and

lysosome metabolism, and tends to be present on the LEL membrane all the time. Therefore, the cell needs a mechanism to be able to activate and inactivate quickly, and be able to respond to signaling cues in a timely fashion. TRPML1 is a Ca^{2+} permeable, lysosomal TRP channel, and a key feature for TRP channels is their ability to serve as sensors for various conditions, including heat, cold, taste, and so on, all of which are temporally transient signals. Therefore, TRPML1 is well suited for the lysosomal sensing of acute signaling cues.

The FRAP assay suggested that under TRPML1 activation, or starvation, the up-regulation of the retrograde transport of lysosomes is not as dramatic as some well-known channel-regulated processes (e.g. synaptic release), only doubling the amount of the resting state. This may serve biological purposes, as it may not be beneficial to have the movement of lysosomes too synchronized. One reason is that the many lysosomes inside the cells have multiple tasks, and thus would require the position of lysosomes to be more cautiously regulated. Another reason is that transport of additional lysosomes exceeding the needs would be energy-inefficient, as directional transport of vesicles consumes a lot of ATPs. Therefore, it makes sense that the up-regulation of lysosome transport towards any direction would not go crazy under any conditions.

But how does the cell achieve this mild up-regulation of vesicle movement? There are several possibilities. First, motor proteins have a characteristic called processivity, which means a motor protein can only walk along the microtubule for a limited number of strides before it falls off the microtubule due to the random event that both of its heads detach from the microtubule during a stride. Therefore, processive motor proteins, including cytoplasmic dynein, can only walk along a track for a short distance, while non-processive motor proteins such as myosin II detaches from the track after each stride. This nature of motor proteins ensures that a

vesicle won't be carried by a single motor protein for more than a couple of seconds, allowing for more accurate manipulation of the position of vesicles. Second, lysosomes, unlike the extracellular space, have a very limited amount of Ca^{2+} within its lumen. Assuming a 1 mM free Ca^{2+} concentration (Wang, Zhang et al. 2012) in the lumen of a 1 μm^3 lysosome (which is larger than normal lysosomes under fed conditions), this would mean about 600,000 free Ca^{2+} in the lumen of the lysosome. Provided that the single channel conductance of TRPML1 was measured to be tens of pico-Siemens (pS) (Dong, Cheng et al. 2008), and the driving force for Ca^{2+} assuming 1 mM luminal and 100 nM cytosolic Ca^{2+} concentration would be at least 100 mV across the lysosomal membrane, a single channel theoretically can deplete the luminal free Ca^{2+} in less than 0.1 second. Therefore, each Ca^{2+} release event through activated TRPML1 won't last for a long time before it depletes the luminal Ca^{2+}. Thus, the Ca^{2+} release conducted by TRPML1 on the lysosome membrane is most likely only intermittent, allowing moderate up-regulation of the retrograde motility of lysosomes.

The involvement of TRPML1 in the regulation of lysosome reformation appeared to be more complicated, as both inhibition and hyper-activation of TRPML1 lead to the abolishment of lysosome tubulation, a prerequisite and platform for lysosome reformation. This result can be explained by a model in which TRPML1 mediates the retrograde motility of the lysosome, coordinating with the plus-end motility on the other end (i.e. one end on the vesicular part of lysosomes, the other on the tip of the tubular structure) to elongate and maintain the tubular structure. This model is supported by the fact that motor proteins responsible for the motility in both directions, i.e. both dyneins and kinesins, are indispensable for the tubulation process. One experiment to further test this hypothesis is to monitor the lysosome tubulation in ALG-2 KO

cells. If the model is true, ALG-2 KO cells should show abolished tubulation similar to that observed with acute inhibition of TRPML1.

What is the trigger for tubulation under different conditions? It is possible that tubulation has multiple triggers, but a simpler explanation is that the direct trigger can be the same, but different conditions arrive at the same signals to trigger the tubulation. Three things are required for the tubulation: plus-end motility, minus-end motility, and neck restriction, the latter responsible for separating the vesicular domain from the tubular domain. It is possible that lysosome tubulation is an autonomous process. When all three criteria are fulfilled, i.e. balanced plus-end and minus-end directed motor proteins are present on the same lysosome, and they are separated by a neck restriction mechanism. TRPML1 is shown in this study to be responsible for the tubulation in all conditions, likely through the up-regulation of the minus-end motility. Activation of mTORC1 was shown previously to be responsible for the autophagic tubulation (Yu, McPhee et al. 2010). I have also shown that mTOR activity is required for tubulation in activated macrophages (Chapter IV). Provided the previous report that mTOR activity is directly correlated with kinesin-1 activity (Korolchuk, Saiki et al. 2011), it is possible that mTOR activity is required in the tubulation process for proper plus-end directed motility. Sorting nexins are a class of BAR-domain containing proteins that can sense/stabilize membrane curvature, and were shown to participate in the generation and stabilization of tubular structures on early endosomes (Carlton, Bujny et al. 2004, Cullen 2008). Provided the similarities between lysosomal tubulation and early endosomal tubulation, sorting nexins may be responsible for the generation and stabilization of lysosomal tubules.

My data suggest that the effects of TRPML1 activation/inhibition on lysosome distribution and tubulation are very acute, with the FRAP assay showing the up-regulation of

retrograde transport within a couple of minutes, and with treatments of agonists/antagonists all showing significant effects within an hour. Moreover, the identification of ALG-2 and its interaction with the dynactin complex suggest that TRPML1 is indeed able to act directly on the retrograde transport machinery. My data, however, do not eliminate the possibility that apart from the acute effects, TRPML1 may also affect lysosome distribution and tubulation through secondary effects, such as up-regulation of lysosome activity (Wang, Gao et al. 2015), up-regulation of lysosomal gene expression (Medina, Di Paola et al. 2015), etc. Potentially, these secondary effects may affect lysosome distribution and tubulation in a long-term basis.

The similar phenotypes of short-term activation of TRPML1 and the long-term inhibition/loss of TRPML1 on lysosome pattern is something to pay attention to. This, as shown by the results in Chapter II, is most likely caused by the fact that two different pathways promote retrograde transport of lysosomes. One is the TRPML1-ALG-2 pathway, which is activated on-demand. The other is the previously known Rab7-RILP pathway, which is responsible for the routine retrograde trafficking of lysosomes. Under long-term loss of TRPML1 activity, cholesterol accumulation occurs in lysosomes, which boosts up the routine retrograde transport of lysosomes through the Rab7-RILP pathway. It is worth noting that the cholesterol accumulation seems to be independent of the positioning of lysosomes, because dynein inhibition, which dissipated lysosomes to the peripheral regions of the cell, did not rescue the accumulation of cholesterol in ML1KO fibroblasts. Also, overexpression of TRPML1 wild-type and TRPML1-R^{44}/A, the ALG-2 non-interacting mutant channel, both rescued the accumulation of cholesterol, but showed opposite distribution of lysosomes.

Due to the similar effects on lysosome distribution and minus-end motility with short-term TRPML1 activation and long-term inhibition, it is clear that results obtained through

chronic inhibition or loss of TRPML1 must be interpreted with care. For example, it must be considered and tested whether an effect seen with long-term inhibition of TRPML1 is through the loss of TRPML1 activity itself, or through the secondary accumulation of cholesterol, or other substances. One easy way to do this is to use the small molecule inhibitors, which allow acute manipulation of TRPML1 activity to be possible.

In Chapter V, I characterized a genetically-encoded fluorescent probe for the detection of intracellular $PI(3,5)P_2$. The generation of a $PI(3,5)P_2$ specific probe is an important step towards the understanding about this phosphoinositide. Previously, $PI(3,5)P_2$ was proposed to localize to late-endosomes and lysosomes based on its synthesizing enzyme's localization and the localization of most of its identified effectors, but was never proven, as previous methods to measure intracellular $PI(3,5)P_2$ were based on HPLC, without providing any information about the intracellular localization about the lipid. With the development of a fluorescent probe to identify intracellular localization and dynamics, I was able to show for the first time that $PI(3,5)P_2$ is indeed localized on late-endosomes and lysosomes, and that it is important for lysosome fusion.

Several reports from other groups utilizing this probe were already published (Samie, Wang et al. 2013, McCartney, Zolov et al. 2014, Hong, Qi et al. 2015, Vicinanza, Korolchuk et al. 2015), within two years of its generation. It is obvious that the probe showed its unique advantage against the previously-utilized HPLC method. The probe was able to visualize the increased $PI(3,5)P_2$ levels on lysosomes close to phagocytic cup prior to lysosome exocytosis (Samie, Wang et al. 2013), the synaptic activity-dependent increase of $PI(3,5)P_2$ levels in the dendrites (McCartney, Zolov et al. 2014), and the localization of $PI(3,5)P_2$ on autophagosomes

(Vicinanza, Korolchuk et al. 2015), none of which could be determined with conventional methods.

Although powerful, the probe is not yet perfect, mainly due to one existing problem about its apparent slow drop-off rate after PI(3,5)P_2 depletion, which was also pointed out in a recently published Plos One paper (Hammond, Takasuga et al. 2015). The *in vitro* binding assays and the loss of co-localization with the mutant probes all suggested specificity of this probe to PI(3,5)P_2. However, it is noticeable that the probe drops off LEL membranes slower than HPLC data would predict under PI(3,5)P_2 depletion conditions such as YM 201636 treatment and serum starvation, both conditions showed to rapidly reach maximal PI(3,5)P_2 depletion within the first 30 min of treatment (Jefferies, Cooke et al. 2008, Zolov, Bridges et al. 2012). One possibility is that the probe was able to protect PI(3,5)P_2 from hydrolysis through binding to it, making it inaccessible to hydrolytic enzymes. Another possibility is that the binding to PI(3,5)P_2 results in conformational changes in the probe, making it either able to interact with additional binding partners, or able to expose hydrophobic domains facilitating its hydrophobic interaction with the membrane.

6.2 Future directions

A crystal structure of TRPML1 is still unavailable. Therefore, it is unknown to this point how exactly ML1N binds to PI(3,5)P_2. Without such knowledge, it may prove difficult to improve the ML1N-based PI(3,5)P_2 probe. Further utilization of the probe in researches involving PI(3,5)P_2, however, can be expected to increase.

The finding of the regulation of retrograde motility of lysosomes through TRPML1 is a big step towards understanding the functions of TRPML1, as well as understanding the metabolism around the lysosomes.

One immediate follow-up experiment is to find the motif through which ALG-2 interacts with dynamitin. This would enable the generation of mutants with decreased or increased lysosome retrograde trafficking under autophagy induction, or other acute circumstances. It is also worth examining the possible role of ALG-2 in regulating ER-to-Golgi transport, as ALG-2 also interacts with Sec31A, a protein found on the transport vesicle membranes (Shibata, Suzuki et al. 2007, Helm, Bentley et al. 2014).

The hypothesis that TRPML1's regulation on lysosome tubulation is simply through its manipulation of lysosome motility is not directly evidenced at this point. It is clear that manipulation of TRPML1's activity can mess up the balance between the plus-end and the minus-end motility, which apparently is important in the maintenance of the tubular structure, the existence of which naturally would require two opposite forces. It is not tested, however, if TRPML1 is required for the tubulation in more than just affecting motility. For example, it remains to be tested if TRPML1 also participates in the final fission step, as suggested by results from a recent study (Miller, Schafer et al. 2015).

The identification of TRPML1's function in lysosome motility, as well as the identification of the cause of the ML1KO lysosome distribution phenotype, also has important implications in the clinics. It is expected, for example, that pharmacological depletion of cholesterol can rescue some of cellular phenotypes seen with MLIV patients similar to NPC patients. In other circumstances such as aging-related neurodegeneration diseases, temporally-

controlled boosting of TRPML1 activity may help clearing accumulated toxic substances through facilitating autophagic clearance.

References

Akhmanova, A. and J. A. Hammer, 3rd (2010). "Linking molecular motors to membrane cargo." Curr Opin Cell Biol **22**(4): 479-487.

Andrews, N. W. and S. Chakrabarti (2005). "There's more to life than neurotransmission: the regulation of exocytosis by synaptotagmin VII." Trends Cell Biol **15**(11): 626-631.

Babst, M. (2011). "MVB vesicle formation: ESCRT-dependent, ESCRT-independent and everything in between." Curr Opin Cell Biol **23**(4): 452-457.

Bai, J. and E. R. Chapman (2004). "The C2 domains of synaptotagmin--partners in exocytosis." Trends Biochem Sci **29**(3): 143-151.

Balla, T. (2007). "Imaging and manipulating phosphoinositides in living cells." J Physiol **582**(Pt 3): 927-937.

Balla, T. and P. Varnai (2002). "Visualizing cellular phosphoinositide pools with GFP-fused protein-modules." Sci STKE **2002**(125): pl3.

Bargal, R., N. Avidan, E. Ben-Asher, Z. Olender, M. Zeigler, A. Frumkin, A. Raas-Rothschild, G. Glusman, D. Lancet and G. Bach (2000). "Identification of the gene causing mucolipidosis type IV." Nat Genet **26**(1): 118-123.

Bassi, M. T., M. Manzoni, E. Monti, M. T. Pizzo, A. Ballabio and G. Borsani (2000). "Cloning of the gene encoding a novel integral membrane protein, mucolipidin-and identification of the two major founder mutations causing mucolipidosis type IV." Am J Hum Genet **67**(5): 1110-1120.

Blumer, J., J. Rey, L. Dehmelt, T. Mazel, Y. W. Wu, P. Bastiaens, R. S. Goody and A. Itzen (2013). "RabGEFs are a major determinant for specific Rab membrane targeting." J Cell Biol **200**(3): 287-300.

Boll, M., M. Foltz, I. Rubio-Aliaga, G. Kottra and H. Daniel (2002). "Functional characterization of two novel mammalian electrogenic proton-dependent amino acid cotransporters." J Biol Chem **277**(25): 22966-22973.

Braulke, T. and J. S. Bonifacino (2009). "Sorting of lysosomal proteins." Biochim Biophys Acta **1793**(4): 605-614.

Bridges, D., J. T. Ma, S. Park, K. Inoki, L. S. Weisman and A. R. Saltiel (2012). "Phosphatidylinositol 3,5-bisphosphate plays a role in the activation and subcellular localization of mechanistic target of rapamycin 1." Mol Biol Cell **23**(15): 2955-2962.

Brinkley, B. R. (1985). "Microtubule organizing centers." Annu Rev Cell Biol **1**: 145-172.

Bucci, C., P. Thomsen, P. Nicoziani, J. McCarthy and B. van Deurs (2000). "Rab7: a key to lysosome biogenesis." Mol Biol Cell **11**(2): 467-480.

Buerger, C., B. DeVries and V. Stambolic (2006). "Localization of Rheb to the endomembrane is critical for its signaling function." Biochem Biophys Res Commun **344**(3): 869-880.

Cai, X., Y. Xu, A. K. Cheung, R. C. Tomlinson, A. Alcazar-Roman, L. Murphy, A. Billich, B. Zhang, Y. Feng, M. Klumpp, J. M. Rondeau, A. N. Fazal, C. J. Wilson, V. Myer, G. Joberty, T. Bouwmeester, M. A. Labow, P. M. Finan, J. A. Porter, H. L. Ploegh, D. Baird, P. De Camilli, J. A. Tallarico and Q. Huang (2013).

"PIKfyve, a class III PI kinase, is the target of the small molecular IL-12/IL-23 inhibitor apilimod and a player in Toll-like receptor signaling." Chem Biol **20**(7): 912-921.

Cantalupo, G., P. Alifano, V. Roberti, C. B. Bruni and C. Bucci (2001). "Rab-interacting lysosomal protein (RILP): the Rab7 effector required for transport to lysosomes." EMBO J **20**(4): 683-693.

Carlton, J., M. Bujny, B. J. Peter, V. M. Oorschot, A. Rutherford, H. Mellor, J. Klumperman, H. T. McMahon and P. J. Cullen (2004). "Sorting nexin-1 mediates tubular endosome-to-TGN transport through coincidence sensing of high- curvature membranes and 3-phosphoinositides." Curr Biol **14**(20): 1791-1800.

Carter, N. J. and R. A. Cross (2006). "Kinesin's moonwalk." Curr Opin Cell Biol **18**(1): 61-67.

Chen, Y. and L. Yu (2013). "Autophagic lysosome reformation." Exp Cell Res **319**(2): 142-146.

Cheng, X., D. Shen, M. Samie and H. Xu (2010). "Mucolipins: Intracellular TRPML1-3 channels." FEBS Lett **584**(10): 2013-2021.

Cheng, X., X. Zhang, Q. Gao, M. Ali Samie, M. Azar, W. L. Tsang, L. Dong, N. Sahoo, X. Li, Y. Zhuo, A. G. Garrity, X. Wang, M. Ferrer, J. Dowling, L. Xu, R. Han and H. Xu (2014). "The intracellular Ca(2)(+) channel MCOLN1 is required for sarcolemma repair to prevent muscular dystrophy." Nat Med **20**(10): 1187-1192.

Cheng, X., X. Zhang, L. Yu and H. Xu (2015). "Calcium signaling in membrane repair." Semin Cell Dev Biol.

Chow, C. Y., Y. Zhang, J. J. Dowling, N. Jin, M. Adamska, K. Shiga, K. Szigeti, M. E. Shy, J. Li, X. Zhang, J. R. Lupski, L. S. Weisman and M. H. Meisler (2007). "Mutation of FIG4 causes neurodegeneration in the pale tremor mouse and patients with CMT4J." Nature **448**(7149): 68-72.

Chu, B. B., Y. C. Liao, W. Qi, C. Xie, X. Du, J. Wang, H. Yang, H. H. Miao, B. L. Li and B. L. Song (2015). "Cholesterol transport through lysosome-peroxisome membrane contacts." Cell **161**(2): 291-306.

Collins, K. M. and W. T. Wickner (2007). "Trans-SNARE complex assembly and yeast vacuole membrane fusion." Proc Natl Acad Sci U S A **104**(21): 8755-8760.

Colvin, R. A., T. K. Means, T. J. Diefenbach, L. F. Moita, R. P. Friday, S. Sever, G. S. Campanella, T. Abrazinski, L. A. Manice, C. Moita, N. W. Andrews, D. Wu, N. Hacohen and A. D. Luster (2010). "Synaptotagmin-mediated vesicle fusion regulates cell migration." Nat Immunol **11**(6): 495-502.

Cong, L. and F. Zhang (2015). "Genome engineering using CRISPR-Cas9 system." Methods Mol Biol **1239**: 197-217.

Cooper, B. J. (1989). "Animal models of Duchenne and Becker muscular dystrophy." Br Med Bull **45**(3): 703-718.

Cuajungco, M. P., J. Silva, A. Habibi and J. A. Valadez (2015). "The mucolipin-2 (TRPML2) ion channel: a tissue-specific protein crucial to normal cell function." Pflugers Arch.

Cullen, P. J. (2008). "Endosomal sorting and signalling: an emerging role for sorting nexins." Nat Rev Mol Cell Biol **9**(7): 574-582.

Curcio-Morelli, C., F. A. Charles, M. C. Micsenyi, Y. Cao, B. Venugopal, M. F. Browning, K. Dobrenis, S. L. Cotman, S. U. Walkley and S. A. Slaugenhaupt (2010). "Macroautophagy is defective in mucolipin-1-deficient mouse neurons." Neurobiol Dis **40**(2): 370-377.

Czibener, C., N. M. Sherer, S. M. Becker, M. Pypaert, E. Hui, E. R. Chapman, W. Mothes and N. W. Andrews (2006). "Ca2+ and synaptotagmin VII-dependent delivery of lysosomal membrane to nascent phagosomes." J Cell Biol **174**(7): 997-1007.

Dayam, R. M., A. Saric, R. E. Shilliday and R. J. Botelho (2015). "The Phosphoinositide-Gated Lysosomal Ca(2+) Channel, TRPML1, Is Required for Phagosome Maturation." Traffic **16**(9): 1010-1026.

Deutsch, C., J. S. Taylor and D. F. Wilson (1982). "Regulation of intracellular pH by human peripheral blood lymphocytes as measured by 19F NMR." Proc Natl Acad Sci U S A **79**(24): 7944-7948.

Di Palma, F., I. A. Belyantseva, H. J. Kim, T. F. Vogt, B. Kachar and K. Noben-Trauth (2002). "Mutations in Mcoln3 associated with deafness and pigmentation defects in varitint-waddler (Va) mice." Proc Natl Acad Sci U S A **99**(23): 14994-14999.

Di Paolo, G. and P. De Camilli (2006). "Phosphoinositides in cell regulation and membrane dynamics." Nature **443**(7112): 651-657.

Dong, X. P., X. Cheng, E. Mills, M. Delling, F. Wang, T. Kurz and H. Xu (2008). "The type IV mucolipidosis-associated protein TRPML1 is an endolysosomal iron release channel." Nature **455**(7215): 992-996.

Dong, X. P., D. Shen, X. Wang, T. Dawson, X. Li, Q. Zhang, X. Cheng, Y. Zhang, L. S. Weisman, M. Delling and H. Xu (2010). "PI(3,5)P(2) controls membrane trafficking by direct activation of mucolipin Ca(2+) release channels in the endolysosome." Nat Commun **1**: 38.

Dove, S. K., K. Dong, T. Kobayashi, F. K. Williams and R. H. Michell (2009). "Phosphatidylinositol 3,5-bisphosphate and Fab1p/PIKfyve underPPIn endo-lysosome function." Biochem J **419**(1): 1-13.

Durchfort, N., S. Verhoef, M. B. Vaughn, R. Shrestha, D. Adam, J. Kaplan and D. M. Ward (2012). "The enlarged lysosomes in beige j cells result from decreased lysosome fission and not increased lysosome fusion." Traffic **13**(1): 108-119.

Eichelsdoerfer, J. L., J. A. Evans, S. A. Slaugenhaupt and M. P. Cuajungco (2010). "Zinc dyshomeostasis is linked with the loss of mucolipidosis IV-associated TRPML1 ion channel." J Biol Chem **285**(45): 34304-34308.

Erie, C., M. Sacino, L. Houle, M. L. Lu and J. Wei (2015). "Altered lysosomal positioning affects lysosomal functions in a cellular model of Huntington's disease." Eur J Neurosci **42**(3): 1941-1951.

Falkenburger, B. H., J. B. Jensen, E. J. Dickson, B. C. Suh and B. Hille (2010). "Phosphoinositides: lipid regulators of membrane proteins." J Physiol **588**(Pt 17): 3179-3185.

Flannagan, R. S., V. Jaumouille and S. Grinstein (2012). "The cell biology of phagocytosis." Annu Rev Pathol **7**: 61-98.

Follett, J., S. J. Norwood, N. A. Hamilton, M. Mohan, O. Kovtun, S. Tay, Y. Zhe, S. A. Wood, G. D. Mellick, P. A. Silburn, B. M. Collins, A. Bugarcic and R. D. Teasdale (2014). "The Vps35 D620N mutation linked to Parkinson's disease disrupts the cargo sorting function of retromer." Traffic **15**(2): 230-244.

Ford, M. G., B. M. Pearse, M. K. Higgins, Y. Vallis, D. J. Owen, A. Gibson, C. R. Hopkins, P. R. Evans and H. T. McMahon (2001). "Simultaneous binding of PtdIns(4,5)P2 and clathrin by AP180 in the nucleation of clathrin lattices on membranes." Science **291**(5506): 1051-1055.

Gillooly, D. J., I. C. Morrow, M. Lindsay, R. Gould, N. J. Bryant, J. M. Gaullier, R. G. Parton and H. Stenmark (2000). "Localization of phosphatidylinositol 3-phosphate in yeast and mammalian cells." EMBO J **19**(17): 4577-4588.

Grant, B. D. and J. G. Donaldson (2009). "Pathways and mechanisms of endocytic recycling." Nat Rev Mol Cell Biol **10**(9): 597-608.

Grimm, C., S. Jors, S. A. Saldanha, A. G. Obukhov, B. Pan, K. Oshima, M. P. Cuajungco, P. Chase, P. Hodder and S. Heller (2010). "Small molecule activators of TRPML3." Chem Biol **17**(2): 135-148.

Halet, G. (2005). "Imaging phosphoinositide dynamics using GFP-tagged protein domains." Biol Cell **97**(7): 501-518.

Hammond, G. R., S. Takasuga, T. Sasaki and T. Balla (2015). "The ML1Nx2 Phosphatidylinositol 3,5-Bisphosphate Probe Shows Poor Selectivity in Cells." PLoS One **10**(10): e0139957.

Helm, J. R., M. Bentley, K. D. Thorsen, T. Wang, L. Foltz, V. Oorschot, J. Klumperman and J. C. Hay (2014). "Apoptosis-linked gene-2 (ALG-2)/Sec31 interactions regulate endoplasmic reticulum (ER)-to-Golgi transport: a potential effector pathway for luminal calcium." J Biol Chem **289**(34): 23609-23628.

Henley, J. R., H. Cao and M. A. McNiven (1999). "Participation of dynamin in the biogenesis of cytoplasmic vesicles." FASEB J **13 Suppl 2**: S243-247.

Heuser, J. (1989). "Changes in lysosome shape and distribution correlated with changes in cytoplasmic pH." J Cell Biol **108**(3): 855-864.

Higgins, M. K. and H. T. McMahon (2002). "Snap-shots of clathrin-mediated endocytosis." Trends Biochem Sci **27**(5): 257-263.

Hissa, B., B. Pontes, P. M. Roma, A. P. Alves, C. D. Rocha, T. M. Valverde, P. H. Aguiar, F. P. Almeida, A. J. Guimaraes, C. Guatimosim, A. M. Silva, M. C. Fernandes, N. W. Andrews, N. B. Viana, O. N. Mesquita, U. Agero and L. O. Andrade (2013). "Membrane cholesterol removal changes mechanical properties of cells and induces secretion of a specific pool of lysosomes." PLoS One **8**(12): e82988.

Ho, C. Y., C. H. Choy, C. A. Wattson, D. E. Johnson and R. J. Botelho (2015). "The Fab1/PIKfyve Phosphoinositide Phosphate Kinase Is Not Necessary to Maintain the pH of Lysosomes and of the Yeast Vacuole." J Biol Chem **290**(15): 9919-9928.

Hong, N. H., A. Qi and A. M. Weaver (2015). "PI(3,5)P2 controls endosomal branched actin dynamics by regulating cortactin-actin interactions." J Cell Biol **210**(5): 753-769.

Hsu, V. W. and R. Prekeris (2010). "Transport at the recycling endosome." Curr Opin Cell Biol **22**(4): 528-534.

Hurley, J. H. (2010). "The ESCRT complexes." Crit Rev Biochem Mol Biol **45**(6): 463-487.

Ichimura, Y., T. Kirisako, T. Takao, Y. Satomi, Y. Shimonishi, N. Ishihara, N. Mizushima, I. Tanida, E. Kominami, M. Ohsumi, T. Noda and Y. Ohsumi (2000). "A ubiquitin-like system mediates protein lipidation." Nature **408**(6811): 488-492.

Idone, V., C. Tam, J. W. Goss, D. Toomre, M. Pypaert and N. W. Andrews (2008). "Repair of injured plasma membrane by rapid Ca2+-dependent endocytosis." J Cell Biol **180**(5): 905-914.

Ikonomov, O. C., D. Sbrissa, K. Delvecchio, Y. Xie, J. P. Jin, D. Rappolee and A. Shisheva (2011). "The phosphoinositide kinase PIKfyve is vital in early embryonic development: preimplantation lethality of PIKfyve-/- embryos but normality of PIKfyve+/- mice." J Biol Chem **286**(15): 13404-13413.

Ikonomov, O. C., D. Sbrissa and A. Shisheva (2009). "YM201636, an inhibitor of retroviral budding and PIKfyve-catalyzed PtdIns(3,5)P2 synthesis, halts glucose entry by insulin in adipocytes." Biochem Biophys Res Commun **382**(3): 566-570.

Inuzuka, T., H. Suzuki, M. Kawasaki, H. Shibata, S. Wakatsuki and M. Maki (2010). "Molecular basis for defect in Alix-binding by alternatively spliced isoform of ALG-2 (ALG-2DeltaGF122) and structural roles of F122 in target recognition." BMC Struct Biol **10**: 25.

Jefferies, H. B., F. T. Cooke, P. Jat, C. Boucheron, T. Koizumi, M. Hayakawa, H. Kaizawa, T. Ohishi, P. Workman, M. D. Waterfield and P. J. Parker (2008). "A selective PIKfyve inhibitor blocks PtdIns(3,5)P(2) production and disrupts endomembrane transport and retroviral budding." EMBO Rep **9**(2): 164-170.

Jenkins, R. W., D. Canals and Y. A. Hannun (2009). "Roles and regulation of secretory and lysosomal acid sphingomyelinase." Cell Signal **21**(6): 836-846.

Jeppesen, G. M. and J. K. Hoerber (2012). "The mechanical properties of kinesin-1: a holistic approach." Biochem Soc Trans **40**(2): 438-443.

Jin, N., C. Y. Chow, L. Liu, S. N. Zolov, R. Bronson, M. Davisson, J. L. Petersen, Y. Zhang, S. Park, J. E. Duex, D. Goldowitz, M. H. Meisler and L. S. Weisman (2008). "VAC14 nucleates a protein complex essential for the acute interconversion of PI3P and PI(3,5)P(2) in yeast and mouse." EMBO J **27**(24): 3221-3234.

Johansson, M., N. Rocha, W. Zwart, I. Jordens, L. Janssen, C. Kuijl, V. M. Olkkonen and J. Neefjes (2007). "Activation of endosomal dynein motors by stepwise assembly of Rab7-RILP-p150Glued, ORP1L, and the receptor betalll spectrin." J Cell Biol **176**(4): 459-471.

Jordens, I., M. Fernandez-Borja, M. Marsman, S. Dusseljee, L. Janssen, J. Calafat, H. Janssen, R. Wubbolts and J. Neefjes (2001). "The Rab7 effector protein RILP controls lysosomal transport by inducing the recruitment of dynein-dynactin motors." Curr Biol **11**(21): 1680-1685.

Kardon, J. R. and R. D. Vale (2009). "Regulators of the cytoplasmic dynein motor." Nat Rev Mol Cell Biol **10**(12): 854-865.

Kaushik, S. and A. M. Cuervo (2012). "Chaperone-mediated autophagy: a unique way to enter the lysosome world." Trends Cell Biol **22**(8): 407-417.

Kilpatrick, B. S., E. R. Eden, A. H. Schapira, C. E. Futter and S. Patel (2013). "Direct mobilisation of lysosomal Ca2+ triggers complex Ca2+ signals." J Cell Sci **126**(Pt 1): 60-66.

Kim, H. J., Q. Li, S. Tjon-Kon-Sang, I. So, K. Kiselyov and S. Muallem (2007). "Gain-of-function mutation in TRPML3 causes the mouse Varitint-Waddler phenotype." J Biol Chem **282**(50): 36138-36142.

Kim, J., M. Kundu, B. Viollet and K. L. Guan (2011). "AMPK and mTOR regulate autophagy through direct phosphorylation of Ulk1." Nat Cell Biol **13**(2): 132-141.

Kimura, S., T. Noda and T. Yoshimori (2007). "Dissection of the autophagosome maturation process by a novel reporter protein, tandem fluorescent-tagged LC3." Autophagy **3**(5): 452-460.

Kimura, S., T. Noda and T. Yoshimori (2008). "Dynein-dependent movement of autophagosomes mediates efficient encounters with lysosomes." Cell Struct Funct **33**(1): 109-122.

King, S. J., C. L. Brown, K. C. Maier, N. J. Quintyne and T. A. Schroer (2003). "Analysis of the dynein-dynactin interaction in vitro and in vivo." Mol Biol Cell **14**(12): 5089-5097.

King, S. M. (2000). "The dynein microtubule motor." Biochim Biophys Acta **1496**(1): 60-75.

Korolchuk, V. I., S. Saiki, M. Lichtenberg, F. H. Siddiqi, E. A. Roberts, S. Imarisio, L. Jahreiss, S. Sarkar, M. Futter, F. M. Menzies, C. J. O'Kane, V. Deretic and D. C. Rubinsztein (2011). "Lysosomal positioning coordinates cellular nutrient responses." Nat Cell Biol **13**(4): 453-460.

Kwiatkowska, K., E. Marszalek-Sadowska, G. Traczyk, P. Koprowski, M. Musielak, A. Lugowska, M. Kulma, A. Grzelczyk and A. Sobota (2014). "Visualization of cholesterol deposits in lysosomes of Niemann-Pick type C fibroblasts using recombinant perfringolysin O." Orphanet J Rare Dis **9**: 64.

Lee, J. H., W. H. Yu, A. Kumar, S. Lee, P. S. Mohan, C. M. Peterhoff, D. M. Wolfe, M. Martinez-Vicente, A. C. Massey, G. Sovak, Y. Uchiyama, D. Westaway, A. M. Cuervo and R. A. Nixon (2010). "Lysosomal proteolysis and autophagy require presenilin 1 and are disrupted by Alzheimer-related PS1 mutations." Cell **141**(7): 1146-1158.

Lemmon, M. A. (2008). "Membrane recognition by phospholipid-binding domains." Nat Rev Mol Cell Biol **9**(2): 99-111.

Li, X., X. Wang, X. Zhang, M. Zhao, W. L. Tsang, Y. Zhang, R. G. Yau, L. S. Weisman and H. Xu (2013). "Genetically encoded fluorescent probe to visualize intracellular phosphatidylinositol 3,5-bisphosphate localization and dynamics." Proc Natl Acad Sci U S A **110**(52): 21165-21170.

Lim, J. P. and P. A. Gleeson (2011). "Macropinocytosis: an endocytic pathway for internalising large gulps." Immunol Cell Biol **89**(8): 836-843.

Lopez-Sanjurjo, C. I., S. C. Tovey, D. L. Prole and C. W. Taylor (2013). "Lysosomes shape Ins(1,4,5)P3-evoked Ca2+ signals by selectively sequestering Ca2+ released from the endoplasmic reticulum." J Cell Sci **126**(Pt 1): 289-300.

Marsh, M. and H. T. McMahon (1999). "The structural era of endocytosis." Science **285**(5425): 215-220.

Martin, S., C. B. Harper, L. M. May, E. J. Coulson, F. A. Meunier and S. L. Osborne (2013). "Inhibition of PIKfyve by YM-201636 dysregulates autophagy and leads to apoptosis-independent neuronal cell death." PLoS One **8**(3): e60152.

Mauvezin, C. and T. P. Neufeld (2015). "Bafilomycin A1 disrupts autophagic flux by inhibiting both V-ATPase-dependent acidification and Ca-P60A/SERCA-dependent autophagosome-lysosome fusion." Autophagy **11**(8): 1437-1438.

McCartney, A. J., S. N. Zolov, E. J. Kauffman, Y. Zhang, B. S. Strunk, L. S. Weisman and M. A. Sutton (2014). "Activity-dependent PI(3,5)P2 synthesis controls AMPA receptor trafficking during synaptic depression." Proc Natl Acad Sci U S A **111**(45): E4896-4905.

McMahon, H. T. and E. Boucrot (2011). "Molecular mechanism and physiological functions of clathrin-mediated endocytosis." Nat Rev Mol Cell Biol **12**(8): 517-533.

Medina, D. L., S. Di Paola, I. Peluso, A. Armani, D. De Stefani, R. Venditti, S. Montefusco, A. Scotto-Rosato, C. Prezioso, A. Forrester, C. Settembre, W. Wang, Q. Gao, H. Xu, M. Sandri, R. Rizzuto, M. A. De Matteis and A. Ballabio (2015). "Lysosomal calcium signalling regulates autophagy through calcineurin and TFEB." Nat Cell Biol **17**(3): 288-299.

Menon, S., C. C. Dibble, G. Talbott, G. Hoxhaj, A. J. Valvezan, H. Takahashi, L. C. Cantley and B. D. Manning (2014). "Spatial control of the TSC complex integrates insulin and nutrient regulation of mTORC1 at the lysosome." Cell **156**(4): 771-785.

Miller, A., J. Schafer, C. Upchurch, E. Spooner, J. Huynh, S. Hernandez, B. McLaughlin, L. Oden and H. Fares (2015). "Mucolipidosis type IV protein TRPML1-dependent lysosome formation." Traffic **16**(3): 284-297.

Mizuno-Yamasaki, E., F. Rivera-Molina and P. Novick (2012). "GTPase networks in membrane traffic." Annu Rev Biochem **81**: 637-659.

Mizushima, N. and M. Komatsu (2011). "Autophagy: renovation of cells and tissues." Cell **147**(4): 728-741.

Morgan, A. J., F. M. Platt, E. Lloyd-Evans and A. Galione (2011). "Molecular mechanisms of endolysosomal Ca2+ signalling in health and disease." Biochem J **439**(3): 349-374.

Mrakovic, A., J. G. Kay, W. Furuya, J. H. Brumell and R. J. Botelho (2012). "Rab7 and Arl8 GTPases are necessary for lysosome tubulation in macrophages." Traffic **13**(12): 1667-1679.

Navone, F., J. Niclas, N. Hom-Booher, L. Sparks, H. D. Bernstein, G. McCaffrey and R. D. Vale (1992). "Cloning and expression of a human kinesin heavy chain gene: interaction of the COOH-terminal domain with cytoplasmic microtubules in transfected CV-1 cells." J Cell Biol **117**(6): 1263-1275.

Nelson, N. and W. R. Harvey (1999). "Vacuolar and plasma membrane proton-adenosinetriphosphatases." Physiol Rev **79**(2): 361-385.

Nilius, B., G. Owsianik, T. Voets and J. A. Peters (2007). "Transient receptor potential cation channels in disease." Physiol Rev **87**(1): 165-217.

Okumura, M., A. M. Katsuyama, H. Shibata and M. Maki (2013). "VPS37 isoforms differentially modulate the ternary complex formation of ALIX, ALG-2, and ESCRT-I." Biosci Biotechnol Biochem **77**(8): 1715-1721.

Olivier, M., C. Proulx and C. E. Tanner (1989). "Importance of lymphokines in the control of multiplication and dispersion of Leishmania donovani within liver macrophages of resistant and susceptible mice." J Parasitol **75**(5): 720-727.

Onyenwoke, R. U., J. Z. Sexton, F. Yan, M. C. Diaz, L. J. Forsberg, M. B. Major and J. E. Brenman (2015). "The mucolipidosis IV Ca2+ channel TRPML1 (MCOLN1) is regulated by the TOR kinase." Biochem J **470**(3): 331-342.

Pagano, R. E., O. C. Martin, H. C. Kang and R. P. Haugland (1991). "A novel fluorescent ceramide analogue for studying membrane traffic in animal cells: accumulation at the Golgi apparatus results in altered spectral properties of the sphingolipid precursor." J Cell Biol **113**(6): 1267-1279.

Pagano, R. E., V. Puri, M. Dominguez and D. L. Marks (2000). "Membrane traffic in sphingolipid storage diseases." Traffic **1**(11): 807-815.

Parton, R. G. and M. A. del Pozo (2013). "Caveolae as plasma membrane sensors, protectors and organizers." Nat Rev Mol Cell Biol **14**(2): 98-112.

Pearse, B. M. (1976). "Clathrin: a unique protein associated with intracellular transfer of membrane by coated vesicles." Proc Natl Acad Sci U S A **73**(4): 1255-1259.

Pena-Llopis, S., S. Vega-Rubin-de-Celis, J. C. Schwartz, N. C. Wolff, T. A. Tran, L. Zou, X. J. Xie, D. R. Corey and J. Brugarolas (2011). "Regulation of TFEB and V-ATPases by mTORC1." EMBO J **30**(16): 3242-3258.

Peters, C. and A. Mayer (1998). "Ca2+/calmodulin signals the completion of docking and triggers a late step of vacuole fusion." Nature **396**(6711): 575-580.

Pfeffer, S. R. (2013). "Rab GTPase regulation of membrane identity." Curr Opin Cell Biol **25**(4): 414-419.

Poccia, D. and B. Larijani (2009). "Phosphatidylinositol metabolism and membrane fusion." Biochem J **418**(2): 233-246.

Pryor, P. R., F. Reimann, F. M. Gribble and J. P. Luzio (2006). "Mucolipin-1 is a lysosomal membrane protein required for intracellular lactosylceramide traffic." Traffic **7**(10): 1388-1398.

Reid, P. C., S. Sugii and T. Y. Chang (2003). "Trafficking defects in endogenously synthesized cholesterol in fibroblasts, macrophages, hepatocytes, and glial cells from Niemann-Pick type C1 mice." J Lipid Res **44**(5): 1010-1019.

Reilein, A. R., S. L. Rogers, M. C. Tuma and V. I. Gelfand (2001). "Regulation of molecular motor proteins." Int Rev Cytol **204**: 179-238.

Rios, R. M. (2014). "The centrosome-Golgi apparatus nexus." Philos Trans R Soc Lond B Biol Sci **369**(1650).

Rocha, N., C. Kuijl, R. van der Kant, L. Janssen, D. Houben, H. Janssen, W. Zwart and J. Neefjes (2009). "Cholesterol sensor ORP1L contacts the ER protein VAP to control Rab7-RILP-p150 Glued and late endosome positioning." J Cell Biol **185**(7): 1209-1225.

Rojas, A. M., G. Fuentes, A. Rausell and A. Valencia (2012). "The Ras protein superfamily: evolutionary tree and role of conserved amino acids." J Cell Biol **196**(2): 189-201.

Rong, Y., M. Liu, L. Ma, W. Du, H. Zhang, Y. Tian, Z. Cao, Y. Li, H. Ren, C. Zhang, L. Li, S. Chen, J. Xi and L. Yu (2012). "Clathrin and phosphatidylinositol-4,5-bisphosphate regulate autophagic lysosome reformation." Nat Cell Biol **14**(9): 924-934.

Rong, Y., C. K. McPhee, S. Deng, L. Huang, L. Chen, M. Liu, K. Tracy, E. H. Baehrecke, L. Yu and M. J. Lenardo (2011). "Spinster is required for autophagic lysosome reformation and mTOR reactivation following starvation." Proc Natl Acad Sci U S A **108**(19): 7826-7831.

Roostalu, J., C. Hentrich, P. Bieling, I. A. Telley, E. Schiebel and T. Surrey (2011). "Directional switching of the kinesin Cin8 through motor coupling." Science **332**(6025): 94-99.

Rosa-Ferreira, C. and S. Munro (2011). "Arl8 and SKIP act together to link lysosomes to kinesin-1." Dev Cell **21**(6): 1171-1178.

Roux, A., K. Uyhazi, A. Frost and P. De Camilli (2006). "GTP-dependent twisting of dynamin implicates constriction and tension in membrane fission." Nature **441**(7092): 528-531.

Sagne, C., C. Agulhon, P. Ravassard, M. Darmon, M. Hamon, S. El Mestikawy, B. Gasnier and B. Giros (2001). "Identification and characterization of a lysosomal transporter for small neutral amino acids." Proc Natl Acad Sci U S A **98**(13): 7206-7211.

Sainath, R. and G. Gallo (2015). "The dynein inhibitor Ciliobrevin D inhibits the bidirectional transport of organelles along sensory axons and impairs NGF-mediated regulation of growth cones and axon branches." Dev Neurobiol **75**(7): 757-777.

Samie, M., X. Wang, X. Zhang, A. Goschka, X. Li, X. Cheng, E. Gregg, M. Azar, Y. Zhuo, A. G. Garrity, Q. Gao, S. Slaugenhaupt, J. Pickel, S. N. Zolov, L. S. Weisman, G. M. Lenk, S. Titus, M. Bryant-Genevier, N. Southall, M. Juan, M. Ferrer and H. Xu (2013). "A TRP channel in the lysosome regulates large particle phagocytosis via focal exocytosis." Dev Cell **26**(5): 511-524.

Samie, M. A. and H. Xu (2014). "Lysosomal exocytosis and lipid storage disorders." J Lipid Res **55**(6): 995-1009.

Sancak, Y., L. Bar-Peled, R. Zoncu, A. L. Markhard, S. Nada and D. M. Sabatini (2010). "Ragulator-Rag complex targets mTORC1 to the lysosomal surface and is necessary for its activation by amino acids." Cell **141**(2): 290-303.

Santiago-Tirado, F. H. and A. Bretscher (2011). "Membrane-trafficking sorting hubs: cooperation between PI4P and small GTPases at the trans-Golgi network." Trends Cell Biol **21**(9): 515-525.

Sbrissa, D., O. C. Ikonomov and A. Shisheva (2002). "Phosphatidylinositol 3-phosphate-interacting domains in PIKfyve. Binding specificity and role in PIKfyve. Endomenbrane localization." J Biol Chem **277**(8): 6073-6079.

Scheffer, L. L., S. C. Sreetama, N. Sharma, S. Medikayala, K. J. Brown, A. Defour and J. K. Jaiswal (2014). "Mechanism of Ca(2)(+)-triggered ESCRT assembly and regulation of cell membrane repair." Nat Commun **5**: 5646.

Schiavo, G., L. Greensmith, M. Hafezparast and E. M. Fisher (2013). "Cytoplasmic dynein heavy chain: the servant of many masters." Trends Neurosci **36**(11): 641-651.

Schmidt, O. and D. Teis (2012). "The ESCRT machinery." Curr Biol **22**(4): R116-120.

Schroer, T. A. (2004). "Dynactin." Annu Rev Cell Dev Biol **20**: 759-779.

Schuchman, E. H. (2010). "Acid sphingomyelinase, cell membranes and human disease: lessons from Niemann-Pick disease." FEBS Lett **584**(9): 1895-1900.

Shen, D., X. Wang, X. Li, X. Zhang, Z. Yao, S. Dibble, X. P. Dong, T. Yu, A. P. Lieberman, H. D. Showalter and H. Xu (2012). "Lipid storage disorders block lysosomal trafficking by inhibiting a TRP channel and lysosomal calcium release." Nat Commun **3**: 731.

Shibata, H., H. Suzuki, H. Yoshida and M. Maki (2007). "ALG-2 directly binds Sec31A and localizes at endoplasmic reticulum exit sites in a Ca2+-dependent manner." Biochem Biophys Res Commun **353**(3): 756-763.

Shin, Y. H., S. J. Lee and J. Jung (2012). "Secretion of ATP from Schwann cells through lysosomal exocytosis during Wallerian degeneration." Biochem Biophys Res Commun **429**(3-4): 163-167.

Silver, K. E. and R. E. Harrison (2011). "Kinesin 5B is necessary for delivery of membrane and receptors during FcgammaR-mediated phagocytosis." J Immunol **186**(2): 816-825.

Simonsen, A., R. Lippe, S. Christoforidis, J. M. Gaullier, A. Brech, J. Callaghan, B. H. Toh, C. Murphy, M. Zerial and H. Stenmark (1998). "EEA1 links PI(3)K function to Rab5 regulation of endosome fusion." Nature **394**(6692): 494-498.

Sivaramakrishnan, V., S. Bidula, H. Campwala, D. Katikaneni and S. J. Fountain (2012). "Constitutive lysosome exocytosis releases ATP and engages P2Y receptors in human monocytes." J Cell Sci **125**(Pt 19): 4567-4575.

Solinger, J. A. and A. Spang (2013). "Tethering complexes in the endocytic pathway: CORVET and HOPS." FEBS J **280**(12): 2743-2757.

Soyombo, A. A., S. Tjon-Kon-Sang, Y. Rbaibi, E. Bashllari, J. Bisceglia, S. Muallem and K. Kiselyov (2006). "TRP-ML1 regulates lysosomal pH and acidic lysosomal lipid hydrolytic activity." J Biol Chem **281**(11): 7294-7301.

Spinosa, M. R., C. Progida, A. De Luca, A. M. Colucci, P. Alifano and C. Bucci (2008). "Functional characterization of Rab7 mutant proteins associated with Charcot-Marie-Tooth type 2B disease." J Neurosci **28**(7): 1640-1648.

Sridhar, S., B. Patel, D. Aphkhazava, F. Macian, L. Santambrogio, D. Shields and A. M. Cuervo (2013). "The lipid kinase PI4KIIIbeta preserves lysosomal identity." EMBO J **32**(3): 324-339.

Starai, V. J., C. M. Hickey and W. Wickner (2008). "HOPS proofreads the trans-SNARE complex for yeast vacuole fusion." Mol Biol Cell **19**(6): 2500-2508.

Stenmark, H. (2009). "Rab GTPases as coordinators of vesicle traffic." Nat Rev Mol Cell Biol **10**(8): 513-525.

Sun, M., E. Goldin, S. Stahl, J. L. Falardeau, J. C. Kennedy, J. S. Acierno, Jr., C. Bove, C. R. Kaneski, J. Nagle, M. C. Bromley, M. Colman, R. Schiffmann and S. A. Slaugenhaupt (2000). "Mucolipidosis type IV is caused by mutations in a gene encoding a novel transient receptor potential channel." Hum Mol Genet **9**(17): 2471-2478.

Sun, W., Q. Yan, T. A. Vida and A. J. Bean (2003). "Hrs regulates early endosome fusion by inhibiting formation of an endosomal SNARE complex." J Cell Biol **162**(1): 125-137.

Swanson, J., A. Bushnell and S. C. Silverstein (1987). "Tubular lysosome morphology and distribution within macrophages depend on the integrity of cytoplasmic microtubules." Proc Natl Acad Sci U S A **84**(7): 1921-1925.

Tan, S. C., J. Scherer and R. B. Vallee (2011). "Recruitment of dynein to late endosomes and lysosomes through light intermediate chains." Mol Biol Cell **22**(4): 467-477.

Tanaka, Y., Y. Kanai, Y. Okada, S. Nonaka, S. Takeda, A. Harada and N. Hirokawa (1998). "Targeted disruption of mouse conventional kinesin heavy chain, kif5B, results in abnormal perinuclear clustering of mitochondria." Cell **93**(7): 1147-1158.

Thoreen, C. C., S. A. Kang, J. W. Chang, Q. Liu, J. Zhang, Y. Gao, L. J. Reichling, T. Sim, D. M. Sabatini and N. S. Gray (2009). "An ATP-competitive mammalian target of rapamycin inhibitor reveals rapamycin-resistant functions of mTORC1." J Biol Chem **284**(12): 8023-8032.

Tsuruta, F., E. M. Green, M. Rousset and R. E. Dolmetsch (2009). "PIKfyve regulates CaV1.2 degradation and prevents excitotoxic cell death." J Cell Biol **187**(2): 279-294.

van der Kant, R., A. Fish, L. Janssen, H. Janssen, S. Krom, N. Ho, T. Brummelkamp, J. Carette, N. Rocha and J. Neefjes (2013). "Late endosomal transport and tethering are coupled processes controlled by RILP and the cholesterol sensor ORP1L." J Cell Sci **126**(Pt 15): 3462-3474.

Varnai, P. and T. Balla (1998). "Visualization of phosphoinositides that bind pleckstrin homology domains: calcium- and agonist-induced dynamic changes and relationship to myo-[3H]inositol-labeled phosphoinositide pools." J Cell Biol **143**(2): 501-510.

Venugopal, B., M. F. Browning, C. Curcio-Morelli, A. Varro, N. Michaud, N. Nanthakumar, S. U. Walkley, J. Pickel and S. A. Slaugenhaupt (2007). "Neurologic, gastric, and opthalmologic pathologies in a murine model of mucolipidosis type IV." Am J Hum Genet **81**(5): 1070-1083.

Vergarajauregui, S., J. A. Martina and R. Puertollano (2009). "Identification of the penta-EF-hand protein ALG-2 as a Ca2+-dependent interactor of mucolipin-1." J Biol Chem **284**(52): 36357-36366.

Verhey, K. J. and J. W. Hammond (2009). "Traffic control: regulation of kinesin motors." Nat Rev Mol Cell Biol **10**(11): 765-777.

Vicinanza, M., V. I. Korolchuk, A. Ashkenazi, C. Puri, F. M. Menzies, J. H. Clarke and D. C. Rubinsztein (2015). "PI(5)P regulates autophagosome biogenesis." Mol Cell **57**(2): 219-234.

Wakabayashi, K., A. M. Gustafson, E. Sidransky and E. Goldin (2011). "Mucolipidosis type IV: an update." Mol Genet Metab **104**(3): 206-213.

Wang, W., Q. Gao, M. Yang, X. Zhang, L. Yu, M. Lawas, X. Li, M. Bryant-Genevier, N. T. Southall, J. Marugan, M. Ferrer and H. Xu (2015). "Up-regulation of lysosomal TRPML1 channels is essential for lysosomal adaptation to nutrient starvation." Proc Natl Acad Sci U S A **112**(11): E1373-1381.

Wang, X., X. Zhang, X. P. Dong, M. Samie, X. Li, X. Cheng, A. Goschka, D. Shen, Y. Zhou, J. Harlow, M. X. Zhu, D. E. Clapham, D. Ren and H. Xu (2012). "TPC proteins are phosphoinositide- activated sodium-selective ion channels in endosomes and lysosomes." Cell **151**(2): 372-383.

Whitley, P., B. J. Reaves, M. Hashimoto, A. M. Riley, B. V. Potter and G. D. Holman (2003). "Identification of mammalian Vps24p as an effector of phosphatidylinositol 3,5-bisphosphate-dependent endosome compartmentalization." J Biol Chem **278**(40): 38786-38795.

Wickner, W. (2010). "Membrane fusion: five lipids, four SNAREs, three chaperones, two nucleotides, and a Rab, all dancing in a ring on yeast vacuoles." Annu Rev Cell Dev Biol **26**: 115-136.

Wong, C. O., R. Li, C. Montell and K. Venkatachalam (2012). "Drosophila TRPML is required for TORC1 activation." Curr Biol **22**(17): 1616-1621.

Xu, H. and D. Ren (2015). "Lysosomal physiology." Annu Rev Physiol **77**: 57-80.

Xu, M., X. X. Li, J. Xiong, M. Xia, E. Gulbins, Y. Zhang and P. L. Li (2013). "Regulation of autophagic flux by dynein-mediated autophagosomes trafficking in mouse coronary arterial myocytes." Biochim Biophys Acta **1833**(12): 3228-3236.

Yanagawa, M., T. Tsukuba, T. Nishioku, Y. Okamoto, K. Okamoto, R. Takii, Y. Terada, K. I. Nakayama, T. Kadowaki and K. Yamamoto (2007). "Cathepsin E deficiency induces a novel form of lysosomal storage disorder showing the accumulation of lysosomal membrane sialoglycoproteins and the elevation of lysosomal pH in macrophages." J Biol Chem **282**(3): 1851-1862.

Yu, I. M. and F. M. Hughson (2010). "Tethering factors as organizers of intracellular vesicular traffic." Annu Rev Cell Dev Biol **26**: 137-156.

Yu, L., C. K. McPhee, L. Zheng, G. A. Mardones, Y. Rong, J. Peng, N. Mi, Y. Zhao, Z. Liu, F. Wan, D. W. Hailey, V. Oorschot, J. Klumperman, E. H. Baehrecke and M. J. Lenardo (2010). "Termination of autophagy and reformation of lysosomes regulated by mTOR." Nature **465**(7300): 942-946.

Zhang, X., X. Li and H. Xu (2012). "Phosphoinositide isoforms determine compartment-specific ion channel activity." Proc Natl Acad Sci U S A **109**(28): 11384-11389.

Zhang, Y., A. J. McCartney, S. N. Zolov, C. J. Ferguson, M. H. Meisler, M. A. Sutton and L. S. Weisman (2012). "Modulation of synaptic function by VAC14, a protein that regulates the phosphoinositides PI(3,5)P(2) and PI(5)P." EMBO J **31**(16): 3442-3456.

Zhang, Y., S. N. Zolov, C. Y. Chow, S. G. Slutsky, S. C. Richardson, R. C. Piper, B. Yang, J. J. Nau, R. J. Westrick, S. J. Morrison, M. H. Meisler and L. S. Weisman (2007). "Loss of Vac14, a regulator of the signaling lipid phosphatidylinositol 3,5-bisphosphate, results in neurodegeneration in mice." Proc Natl Acad Sci U S A **104**(44): 17518-17523.

Zolov, S. N., D. Bridges, Y. Zhang, W. W. Lee, E. Riehle, R. Verma, G. M. Lenk, K. Converso-Baran, T. Weide, R. L. Albin, A. R. Saltiel, M. H. Meisler, M. W. Russell and L. S. Weisman (2012). "In vivo, Pikfyve generates PI(3,5)P2, which serves as both a signaling lipid and the major precursor for PI5P." Proc Natl Acad Sci U S A **109**(43): 17472-17477.

Zoncu, R., L. Bar-Peled, A. Efeyan, S. Wang, Y. Sancak and D. M. Sabatini (2011). "mTORC1 senses lysosomal amino acids through an inside-out mechanism that requires the vacuolar H(+)-ATPase." Science **334**(6056): 678-683.